A Technique for Examining Longitudinal and Cross Sections of Teased Nerve Fibres and Its Application to Human and Experimental Neuropathy

A Thesis Submitted By

Zhao Cai

For the Degree of Doctor of Philosophy

Department of Medicine, University of Adelaide

Department of Neurology, Royal Adelaide Hospital

and

Neuropathology Laboratory, Division of Tissue Pathology

Institute of Medical and Veterinary Science, Adelaide, Australia

8 January 2002

CONTENTS

Declaration i

Acknowledgments ii

Publications iv

Abbreviations vi

Summary viii

CHAPTER 1: Myelinated nerve fibres 1

1.1 Introduction 2

1.2 Normal structure of myelinated nerve fibres (MFs) 3

1.3 Myelin-associated glycoprotein 21

1.4 Schwann cell–axon interactions 32

CHAPTER 2: Development of a new method for the correlation of external and internal structure at specific points of teased nerve fibres 42

2.1 Introduction 43

2.2 Previous methods of studying transverse and longitudinal sections of teased nerve fibres 49

2.3 Development of new technique 53

2.4 Examples of application of new technique in the interpretation of teased nerve fibre abnormalities 67

2.5 Discussion 97

CHAPTER 3: Teased nerve fibre studies in human IgM anti-MAG paraproteinaemic neuropathy 104

3.1 Introduction 105

3.2 Materials and Methods 125

3.3 Results 126

3.4 Discussion 140

3.5 Conclusion 146

CHAPTER 4: Teased nerve fibre studies in MAG deficient mice 147

4.1 Introduction 148

4.2 MAG knockout mice and tomacula in experimental models 149

4.3 Materials and Methods 159

4.4 Results 160

4.5 Discussion 181

4.6 Conclusions 190

CHAPTER 5: Future directions 191

Bibliography 194

Appendix A i

Appendix B vi

Appendix C vii

DECLARATION

This work contains no material which has been accepted for the award of any other degree or diploma in any university or other tertiary institution and, to the best of my knowledge and belief, contains no material previously published or written by another person, except where due reference has been made in the text.

I give consent to this copy of my thesis, when deposited in the University Library, being available for loan and photocopying.

Zhao Cai

January, 2001

ACKNOWLEDGMENTS

This study was supported by the Overseas Postgraduate Research Scholarship and Research Abroad Scholarship from the University of Adelaide. Funding was also obtained through the Medical Specialist Staff Fund from the Institute of Medical and Veterinary Science, Adelaide. I am indebted to the Australian Brain Foundation (SA), Australia, for awarding me the Elizabeth Penfold Simpson Prize in June 2001.

I would like to express my sincere gratitude to Professor Philip D Thompson and Professor Peter C Blumbergs for allowing me to undertake my PhD in the Department of Medicine, the University of Adelaide and Royal Adelaide Hospital, and in the Division of Tissue Pathology, the Institute of Medical and Veterinary Science, Adelaide. Thanks to Professor Thompson for your constant support, intellectual supervision and guidance throughout this enduring journey of scientific experience. To Professor Blumbergs, your expert guidance, constant enthusiasm and positive reinforcement throughout the last 5 years have made this journey smoother. Your tireless effort, insight, and patient direction during this project were principal elements in its progression and completion. Especially, you have taught me how to think like a scientist. It has been a privilege to work with you. To Dr Peter Sutton-Smith, I thank you for your supervision and for teaching me many valuable technical and scientific skills. Your suggestions played an important role in developing the new teased nerve fibre technique.

I am grateful to Professor PK Thomas for his scientific critiques in developing the new teased fibre technique and its applications. Special thanks to Professor John Pollard for his kind support in this study.

Thank you to Dr Grace Scott, Dr Barbara Koszyca, and Dr Corinna Van Den Heuvel for their kind help. I also acknowledge Dr Martin Robinson, Dr Simon Koblar, Dr Chris Burke, Dr Tom Kimber, Dr Jason Warren and Dr Jane Rice for their helpful support.

I am grateful for Dr John Finnie and Dr Anne Turnley for their kind support in the animal experiments. Thanks John for all of your help.

Special thanks to Mr. Jeffery Swift and Ms. Kathy Cash for teaching me many valuable technical skills and helping with the technical work. Thanks to Dr Nick Fazzalari and Mr. Ian Parkinson for their considerable support of the morphometric studies.

To the entire Neuropathology Laboratory including Jim Manavis, Helen Wainwright, Penny Leaney, Bernice Gutschmidt and, of course, Margaret Elemer for making my life easier with their brilliant technical skills and support. You have created a marvellous working environment. I have really enjoyed working with you.

Special thanks to Mark Fitz-Gerald, Peta Grant and Peter Dent for their endless technical support in photography.

I would like to express my special thanks and deepest gratitude to my family for their boundless love, encouragement and support. Mum and Dad, your guidance and tireless support got me here.

Last but not least I wish to thank my wife especially for putting up with me through the stressful times and for her tireless love and support. I love you forever!

PUBLICATIONS

The following publications and Platform presentations and Posters at National and International Meetings have arisen from this thesis.

Publications

Cai Z, Cash K, Swift J, Sutton-Smith P, Robinson M, Thompson PD, Blumbergs PC. Focal myelin swellings and tomacula in anti-MAG IgM paraproteinaemic neuropathy: novel teased nerve fibre studies. *Journal of Peripheral Nervous System* 2001; 6:95-101

Cai Z, Cash K, Swift J, Sutton-Smith P, Thompson PD, Blumbergs PC. A novel method for correlating internal and external structure of individual myelinated nerve fibres. *J Neurosci Methods* 2001; 105:39-43

Cai Z, Cash K, Thompson PD, Blumbergs PC. Accuracy of sampling methods in morphometric studies of human sural nerves. *Journal of Clinical Neuroscience* 2002; 9:181-6

Cai Z, Smith P, Swift J, Cash K, Turnley A, Finnie J, Thompson PD, Blumbergs PC. Teased nerve fibre studies in aged myelin-associated glycoprotein (MAG) knockout mice. *Brain Pathology* 2000; 10:547

Cai Z, Sutton-Smith P, Swift, J, Cash K, Finnie J, Turnley A, Thompson PD, Blumbergs PC. Tomacula in MAG-deficient mice. *Submitted to Journal of Peripheral Nervous System*

Platform presentations and Posters at National and International Meetings

Tomacula in MAG knockout mice. Annual Scientific Meeting, Australian and New Zealand Society of Neuropathology, May 2001, Adelaide.

Teased nerve fibre studies in aged myelin-associated glycoprotein (MAG) knockout mice. XIVth International Congress of Neuropathology. Birmingham, UK, September 2000.

Myelin abnormalities in teased nerve fibres from a case of IgM paraproteinaemic neuropathy. Annual Scientific Meeting, Australian Association of Neurologists. Melbourne, May 2000.

Modified teased nerve fibre technique for correlative cross-sectional studies at multiple specified sites of individual teased nerve fibres. Annual Scientific Meeting, Australian and New Zealand Society of Neuropathology, May 2000, Melbourne.

Accuracy of sampling methods in morphometric studies of human sural nerves. IXth International Congress on Neuromuscular Diseases. Adelaide, September, 1998.

ABBREVIATIONS

C	complement
CAM	cell adhesion molecule
Caspr	contactin-associated protein
CIDP	chronic inflammatory demyelinating polyneuropathy
CMT	Charcot-Marie-Tooth disease
CNS	central nervous system
CON	constricted axon segment
CSF	cerebrospinal fluid
Cx32	connexin 32
DMAE	dimethylaminoethanol
DRG	dorsal root ganglion
EAE	experimental allergic encephalomyelitis
EAN	experimental allergic neuritis
EM	electron microscopy
HMSN	hereditary motor and sensory neuropathy
HNPP	hereditary neuropathy with liability to pressure palsies
Ig	immunoglobulin
L-MAG	large isoform of myelin-associated glycoprotein (large MAG)
LM	light microscopy
MAG	myelin-associated glycoprotein
MBP	myelin basic protein
MF	myelinated nerve fibre
MGUS	monoclonal gammopathy of unknown significance
MT	microtubule
MYSA	myelin sheath attachment axon segment

N-CAM	neural cell adhesion molecule
NF	neurofilament
NF155	155kD isoform of neurofascin
NF186	186kD isoform of neurofascin
NFH	NF heavy
NFL	NF light
NFM	NF medium
Ng	neuron-glia
NrCAM	NgCAM-related CAM
P_0	protein zero
PLP	proteolipid protein
PMD	Pelizaeus-Merzbacher disease
PMP22	peripheral myelin protein 22
PNP region	paranodal-nodal-paranodal region
PNS	peripheral nervous system
RGD	arginine-glycine-asparatic acid
S-MAG	small isoform of myelin-associated glycoprotein (small MAG)
SGLPG	sulfated glucuronic acid containing lactosaminyl paragloboside
SGPG	sulfated-3-glucuronyl paragloboside
Siglec	sialic acid binding lectin
SLC	Schmidt-Lanterman cleft
SLI	Schmidt-Lanterman incisure
STIN region	stereotyped internodal region
TCC	terminal complement complex
WM	Waldenström's macroglobulinaemia
WML	widening of myelin lamellae

SUMMARY

A new method is described that enables longitudinal and cross sections of an individual nerve fibre to be cut at multiple specified sites along the fibre by the use of a unique marker system. In this way the internal structure of the fibre can be correlated with the external appearance. Individual myelinated nerve fibres were teased apart in epoxy resin and mounted onto a carbon-coated slide, and after orientation and marking of specific sites of interest are snap frozen to liberate the orientated and marked fibres for embedding on the surface of an epoxy resin block for subsequent longitudinal or transverse sectioning. This method is particularly useful for the correlative study of myelin-axon relationships.

One hundred and six teased nerve fibres from sural nerve biopsies of cases of sensory neuropathy with mitochondrial abnormalities, uraemic neuropathy, IgM anti-GM1 neuropathy and a normal sural nerve were examined using this technique. Correlation of the findings on cross and longitudinal sections with the external appearance of teased fibres has yielded new insights in the interpretation and classification of pathological changes affecting peripheral nerves.

Focal myelin swellings and tomacula in teased nerve fibres from a case of IgM anti-myelin-associated glycoprotein (MAG) paraproteinaemic neuropathy were examined using this novel technique. Five different morphologic abnormalities were identified consisting of myelin sheath outfolding, myelin sheath infolding, enlargement of the adaxonal space, myelin degeneration, multiple increased concentric loops, and a combination of these structural abnormalities often in association with myelin degeneration. Similar structural changes were found in externally normal segments of teased fibres without evidence of myelin swelling or tomacula from the same case. These structural abnormalities were

consistent with a disturbance of the normal adhesion functions of MAG in the maintenance of axon-myelin relationships.

The pathogenesis of tomacula in mice with a null mutation of the myelin-associated glycoprotein (MAG) gene is not well understood. Using this technique it was demonstrated that tomacula in MAG-deficient mice were formed by redundant myelin infoldings and outfoldings in the paranodal regions as early as 4 weeks after birth and that these increased in size and frequency with age. Although tomacula showed degenerative changes with increasing age, there was no evidence of demyelination/remyelination. Longitudinal sections of teased nerve fibers also showed early redundant myelin foldings in externally normal paranodal regions. These data and the absence of internodal tomacula support a role for MAG in the maintenance of myelin at the paranodal regions.

CHAPTER 1: Myelinated Nerve Fibres

1.1 Introduction **2**

1.2 Normal structure of myelinated nerve fibres (MFs) **3**

1.2.1 Myelin 5

1.2.2 Axons 12

1.2.3 Nodes of Ranvier 14

1.2.4 Paranodal-nodal-paranodal regions 16

1.2.5 Juxtaparanodes 19

1.3 Myelin-associated glycoprotein **21**

1.3.1 Biochemistry of MAG 21

1.3.2 Human MAG 24

1.3.3 MAG belongs to the immunoglobulin superfamily 24

1.3.4 MAG belongs to the siglec family 25

1.3.5 MAG carries L2/HNK-1 epitope 25

1.3.6 The MAG gene 26

1.3.7 Subcellular location of MAG 27

1.3.8 Function of MAG 28

1.4 Schwann cell–axon interactions **32**

1.4.1 Development of Schwann cells 33

1.4.2 Survival of Schwann cell precursors depends on signals from the axon 35

1.4.3 Developing Schwann cells acquire the ability to survive without axons 36

1.4.4 Schwann cells modify axon cytoskeletal architecture 37

1.4.5 Schwann cells organize molecular domains of the axons 39

1.4.6 Abnormal Schwann cells induce pathologic changes in axons 39

1.1 INTRODUCTION

The discovery of myelinated nerve fibres (MFs) is credited by Cajal (1909) to Ehrenberg, who in 1833 described nerve fibres in teased preparations as consisting of cylindrical tubes (Rosenbluth, 1999). The morphology of peripheral nerves was examined in teased fibre studies by Ranvier in 1871, who demonstrated the node of Ranvier for the first time. In the second half of 19th century, Remak, Ranvier, Kolliker, Renaut, Gombault, Retzius and Cajal described the normal and pathologic features of teased nerve fibres including unfixed fresh material using various teasing methods (cited in Dyck and Lofgren 1968; Dyck *et al.*, 1984). However, poor tissue fixation and the technical difficulty in teasing often resulted in short preparations (limited to only one or part of an internode) and numerous artefacts (Hiscoe, 1947; Lubinska, 1956). In the middle of the 20th century, the technique for preparing single nerve fibres was refined further (Dyck and Lofgren, 1966, 1968; Thomas and Young, 1949; Vizoso and Young, 1948). The current method for preparing teased fibres and the criteria for classifying pathological abnormalities of teased nerve fibres are based on these descriptions (Dyck *et al.*, 1984, 1993*a*; Thomas *et al.*, 1997).

The teased fibre technique is the best approach to study peripheral MFs in their continuity. The examination of teased fibres has proved particular value in studying the dimensions of the nodes of Ranvier (Cavanagh and Jacobs, 1964), in measuring internodal length (Hiscoe, 1947; Lascelles and Thomas, 1966), in detecting segmental demyelination (Dyck and Lofgren, 1968; Lubinska, 1961), in differentiating axonal from myelin changes (Dyck *et al.*, 1971*b*), and in precisely localizing molecules along MFs (Sheikh *et al.*, 1999*a*). This procedure permits evaluation of consecutive internodes or segments of the same myelinated nerve fibre and may be used to detect and establish the frequency of certain neuropathologic abnormalities with more sensitivity than by using fixed sections (Dyck *et al.*, 1993*a*).

1.2 NORMAL STRUCTURE OF MYELINATED NERVE FIBRES (MFs)

The morphology of normal MFs has been reviewed by Thomas *et al.* (1993) and Berthold and Rydmark (1995) and the molecular biology by Scherer (1996), Arroyo *et al.* (1999), Arroyo and Scherer (2000), and Peles and Salzer (2000). The MF consists of an axon which is a single continuous neuronal process, surrounded by Schwann cells arranged serially outside of the axon. Each Schwann cell enwraps the axon segment in a myelin sheath, a specialized multilayered cell membrane. Myelinated axons are completely covered by myelin sheaths except at the initial segments (the small segment adjoining the neuron cell body) and the nodes of Ranvier at the junction of consecutive Schwann cells where the axon is directly exposed to the extracellular milieu. The axonal segment between two neighbouring nodes of Ranvier and its myelin sheath, corresponding to the extension of one Schwann cell, constitute an internode. In adult human nerves, internodal length ranges from about 200 μm to 1800 μm (Thomas *et al.*, 1993). Longitudinally, an internode can be separated into three main parts: a central stereotyped internodal (STIN) region forming about 95% of the whole internodal length and proximal and distal paranodes, each corresponding 2 to 3 percent of the whole internodal length (Fig. 1-1).

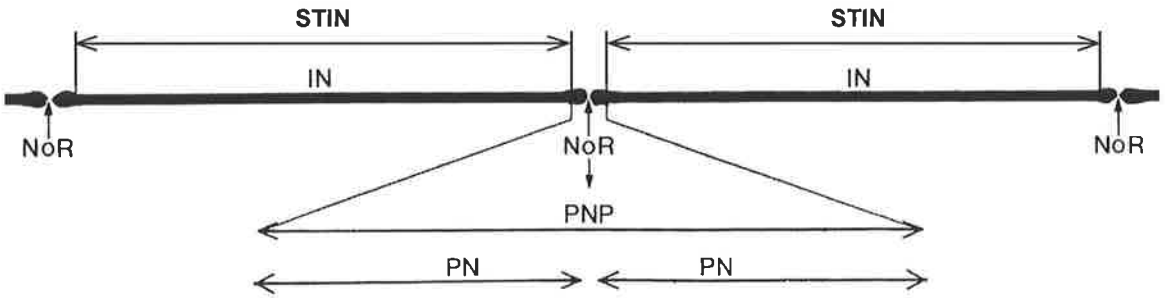

Figure 1-1. Diagram to show the terminology used. IN = internode; NoR = the node of Ranvier; PNP = paranodal-nodal-paranodal region; PN = paranode; STIN = stereotyped internodal region. Modified from Thomas *et al.* (1993).

On transverse section, a MF consists of two main concentric zones: an outer Schwann cell zone and an inner axon zone. In the internodal region the Schwann cell zone consists of concentric layers: the outer (abaxonal) and inner (adaxonal) cytoplasmic compartments and

the myelin compartment in between. The Schwann cell generates the myelin during development in a process of continuous spiral wrapping, close packing, and cell membrane condensation. The inner and outer parts of the Schwann cell membrane, which contact the adjacent layer of the myelin sheath, are called the inner and outer mesaxon, respectively. The innermost turn of the Schwann cell spiral corresponds to the inner cytoplasmic layer and the outermost to the outer layer. Intervening turns form the compact myelin lamellae. A large number of thin cytoplasmic cords (Golgi-Rezzonico spirals) spiral through the compact myelin layer connecting the outer and inner Schwann cell cytoplasmic compartments creating a funnel shaped cleft through the compact myelin, the Schmidt-Lanterman incisure (SLI). The axon is separated from the adaxonal Schwann cell membrane by a narrow extracellular gap (a few to 30 nm in standard electron microscopy (EM) preparations), the adaxonal or periaxonal space (Berthold and Rydmark, 1995; Thomas *et al.*, 1993).

The size of a MF is conventionally measured in the STIN region, avoiding the Schwann cell perikaryon and ranges from 1 to 20 μm in diameter in mammals. The length and the thickness of MFs increase with age during development, and on maturation the fibre diameter is positively related to the internodal length (Gutrecht and Dyck *et al.*, 1970; Lascelles and Thomas, 1966). An abnormally short internodal length usually results from remyelination after segmental demyelination or regeneration after complete degeneration of the fibre (Chopra and Hurwitz, 1967; Dyck and Lambert, 1968; Fullerton *et al.*, 1965; Lascelles and Thomas *et al.*, 1966). The axonal circumference is linearly related to the length of the myelin spiral (Dyck *et al.*, 1993*a*).

1.2.1 Myelin

In the peripheral nervous system (PNS), myelin is the multilamellar spiral of specialized Schwann cell membrane that ensheaths axons larger than 1 μm in diameter and its function is to increase axonal conduction velocity by restricting the depolarizing ionic fluxes that generate action potentials to nodes of Ranvier (Salzer, 1997; Thomas *et al.*, 1993). Lipids and proteins are the two principal components of myelin. Cholesterol and sphingolipids (cerebroside and sulfatide) are the main myelin lipids (Hudson, 1990; Suter and Snipes, 1995). Proteins represent 20~30% of the PNS myelin dry weight. Glycoproteins account for at least 60% of the total proteins, basic proteins for 20~30% and diverse proteins for the remaining 10~20% (Garbay *et al.*, 2000; Mezei, 1993; Thomas *et al.*, 1997). The myelin sheath itself can be divided into compact and non-compact myelin.

Compact myelin

Compact myelin is found in the internodal regions and forms the bulk of the myelin sheath. In EM, the myelin sheath is characterized by a highly regular construction composed of spirally arranged lamellae that are alternately dark (the major dense lines) and light (the intermediate or intraperiod lines), which have a radial periodicity of about 14 nm following conventional preparation for EM and 18 nm in fresh nerves by X-ray diffraction. The major dense line is derived by extrusion of Schwann cell cytoplasm and the fusion of apposed inner cytoplasmic surfaces of the spiral Schwann cell membrane. The intermediate line is derived by approximation of the external surfaces of the Schwann cell membrane. An extracellular space of approximately 5 nm remains between the two membranes so that the intermediate line consists of a pair of lines with an intervening lucent gap under high magnification of EM.

Compact myelin proteins

The major proteins of compact myelin include protein zero (P_0), peripheral myelin protein 22 (PMP22) and myelin basic protein (MBP).

P_0, a glycoprotein of 30 kD molecular weight, is specific to PNS myelin and accounts for over 50% of the total myelin protein. It is a member of the immunoglobulin superfamily and consists of a single extracellular immunoglobulin-like domain, one transmembrane domain and a basic cytoplasmic domain (Lemke, 1986, 1993; Lemke and Axel, 1985). The single Ig-like domain contains one glycosylation site, which contains the HNK-1 carbohydrate epitope (Bollensen and Schachner, 1987). P_0 mediates cell-cell interactions (D'Urso *et al.*, 1990; Filbin *et al.*, 1990; Schneider-Schaulies *et al.*, 1990). The extracellular domain of P_0 forms tetramers, with four molecules arranged around a central hole (Shapiro *et al.*, 1996). These tetramers may interact with their counterparts on the apposing cell membrane, forming a lattice that holds the apposed extracellular surfaces together to stabilize the intermediate line of compact myelin. In addition, direct membrane intercalation of the molecule via a tryptophan side chain has been proposed to mediate the exact membrane spacing in the myelin (Shapiro *et al.*, 1996). The positively charged cytoplasmic domain of P_0 has been suggested to interact with negatively charged phospholipids of the adjacent cytoplasmic parts of the Schwann cell membrane leading to the formation of the major dense line (Ding and Brunden 1994). Therefore, P_0 protein plays an important role in myelin compaction and stabilization and is an integral component of normal myelin. During development, P_0 is expressed on Schwann cells at the initial stage of myelination, down-regulated in non-compacted myelin at maturation, and confined to compacted myelin (Martini, 1994b; Trapp *et al.*, 1986). P_0 gene maps on human chromosome 1q22-q23, spans approximately 7 kb and consists of six coding exons corresponding to the functional domains (Bird *et al.*, 1982; Hayasaka *et al.*, 1993).

Mutations in human P_0 gene cause a demyelinating neuropathy (Nelis *et al.*, 1999; Scherer, 1997*b*). Analysis of P_0 null mice confirms that P_0 is involved in the spiral formation of the Schwann cell membrane around the axon, myelin compaction, formation of the major dense line and in determining the appropriate thickness of myelin (in collaboration with MBP), and maintenance of normal myelin (Martini and Schachner, 1997). Mice homozygously deficient for P_0 show hypomyelination as early as postnatal 4 days and subsequent demyelination and impaired nerve conduction, resembling Dejerine-Sottas Syndrome (DSS). Mice heterozygously deficient for P_0 show normal myelination, but develop progressive demyelination after four months of age, resembling the demyelinating neuropathy accompanying P_0 mutation in man (Charcot-Marie-Tooth (CMT) disease type 1B) (Martini, 1999; Martini *et al.*, 1995*a*). Additionally, Shy *et al.* (1997) reported heterozygous P_0 knockout ($P_0^{+/-}$) mice develop a neuropathy that resembles chronic inflammatory demyelinating polyneuropathy (CIDP).

PMP22 is a 22 kD hydrophobic intrinsic membrane protein of unknown function and accounts for 2-5% of PNS myelin protein (Welcher *et al.*, 1991; Snipes and Suter, 1995). It is also present in the plasma membrane of Schwann cells of unmyelinated fibres and onion bulbs (Haney *et al.*, 1996*a*). PMP22 consists of 160 amino acids including four transmembrane domains, two extracellular loops, one intracellular loop and two short intracellular tails (D'Urso and Müller, 1997; Quarles 1997). Low levels of PMP22 are also expressed in other tissues, including lung, gut, ovary, heart, spinal cord and brain (Baechner *et al.*, 1995; Parmantier *et al.*, 1995; Taylor *et al.*, 1995; Taylor and Suter, 1996). It structurally resembles an ion channel, and also carries a consensus sequence for asparagine-linked glycosylation on which the L2/HNK-1 carbohydrate epitope is present (Hammer *et al.*, 1993; Schachner and Martini, 1995; Snipes *et al.*; 1993). The PMP22 gene maps to human chromosome 17p11.2-p12. It spans approximately 40 kb and contains four coding

exons and two 5'-untranslated exons (Suter *et al.*, 1994). Mutations affecting the PMP22 gene including duplications, deletions, and point mutations are responsible for the most common forms of hereditary peripheral neuropathies in man including CMT1A, hereditary neuropathy with liability to pressure palsies (HNPP), and a subtype of DSS (Naef and Suter, 1998). The complete absence of PMP22, which has been created in *Pmp* null mice but not described in humans, leads to a severe demyelinating neuropathy in mice (Adlkofer *et al.*, 1995). Heterozygous *Pmp* deficient mice have a mild demyelinating neuropathy with the structural abnormalities found in HNPP (Adlkofer *et al.*, 1997). Mutations in the murine PMP22 gene are responsible for the naturally occurring CMT mouse models *Trembler* (*Tr*) and *Trembler-Jackson* (Tr^J) (Suter *et al.*, 1992*ab*). Myelin in *Tr* and Tr^J animals is inappropriately thin for the size of the axon and has a tendency to be uncompacted, especially near the nodes of Ranvier (Ayers and Anderson, 1973, 1975; Low, 1976*ab*).

MBP accounts for 5-15% of PNS myelin and is a cytoplasmic protein, which together with P_0, contributes to the formation of the major dense line. The *Shiverer* mouse, a naturally occurring null-mutant for MBP, is characterized by hypomyelination in the CNS (Rosenbluth, 1980*a*). The PNS myelin is relatively spared (Kirschner and Ganser, 1980; Rosenbluth, 1980*b*), probably because the basic cytoplasmic domain of P_0 may effectively substitute for MBP (Ding and Brunden, 1994; Martini *et al.*, 1995*a*). Subtle pathological changes in the shape and number of Schmidt-Lanterman clefts in shiverer mice (Gould *et al.*, 1995) may suggest MBP regulates other myelin proteins (Connexin 32 (Cx32) and myelin-associated glycoprotein (MAG)) at these sites (Smith-Slatas and Barbarese, 2000).

Noncompact myelin

In some regions of the myelin, the apposed inner cytoplasmic surfaces of the spiral Schwann cell membrane do not fuse to form major dense line, but contain Schwann cell cytoplasm.

Myelin in these regions is called noncompact myelin. Noncompact myelin is found in Schmidt-Lanterman incisures (SCIs) and paranodes. The structure of paranodes will be discussed in section 1.2.4.

Schmidt-Lanterman incisures (SCIs)

Schmidt (1874) and Lanterman (1877) first described these funnel-shaped clefts in the myelin sheath. SLIs, also called Schmidt-Lanterman clefts (SLCs) are part of the normal structure of MFs (Thomas *et al.*, 1993) although they were previously regarded as histological artefacts (Young, 1944). Myelin is interrupted at irregular intervals by SLCs at an angle of about 9° to the long axis of the sheath (Friede and Samorajski, 1969; Hall and Williams 1970). The orientation of SLCs is not regularly in one direction or another along the internode, but in those near to nodes of Ranvier, the narrow ends tend to be directed away from the node (Hiscoe, 1947). SLCs tend not to be present in the paranodal regions and perinuclear regions (Hiscoe, 1947; Webster, 1965). In cross sections, the region of a fibre which contains a SLC is characterized by a gap between two concentric rings of tightly spaced myelin lamellae (Fig. 1-2). The major proteins of the myelin in SLCs include Cx32 and MAG.

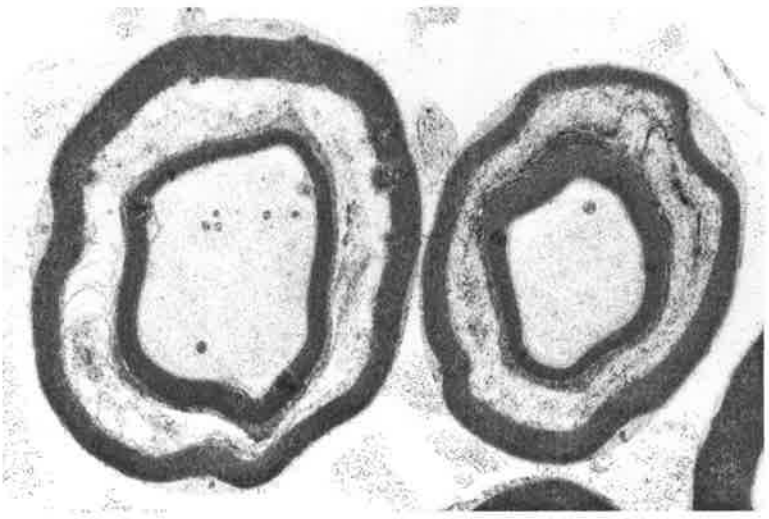

Figure 1-2. Electron micrograph (× 2000). A transverse section of 2 myelinated nerve fibres from a human sural nerve shows SLCs, which are characterized by a gap between two concentric regions of tightly spaced myelin lamellae.

At SLCs the major dense lines of myelin separate to enclose the cytoplasmic spirals of Golgi-Rezzonico that follow a helical course to connect the outer and inner belts of Schwann cell cytoplasm. They may extend through the whole width of the myelin layer or involve only a section of the myelin circumference (Ghabriel and Allt, 1981; Thomas *et al.*, 1993). The cytoplasmic spiral of Golgi-Rezzonico usually contains a single helical microtubule, which may have a mechanical supportive function stabilizing the cytoplasmic spiral (Ghabriel and Allt, 1981). Membrane-bound dense bodies, multivesicular bodies and lysosomes are also observed in the SLCs of the PNS (Hall and Williams, 1970). Adherens junctions (previously referred to as "desmosome-like" junctions) commonly transverse the outer portion of SLCs (Hall and Williams, 1970; Arroyo and Scherer, 2000). Organelles, which were approximately the size of mitochondria, have been observed in SLCs, but could not be identified with certainty (Ghabriel and Allt, 1981). In freeze-fracture studies, tight junctions run in a spiral through the SLCs at both the adaxonal and the abaxonal ends and are continuous with the inner and outer mesaxonal tight junctions. These tight junctions are composed of linear arrays of particles (Sandri *et al.*, 1977; Stolinski *et al.*, 1985).

Hall and Williams (1970) reported SLCs in myelin sheaths composed of only five lamellae although Friede and Samorajski (1969) did not find them in fibres with less than 20 myelin lamellae. SLCs may be detected in remyelinating fibres with 2 to 3 lamellae (Thomas *et al.*, 1993). The number of SLCs per internode is directly related to the thickness of the myelin sheath and fibre diameter in normal adult (Buchthal *et al.*, 1987; Hiscoe, 1947; Friede and Samorajski, 1969; Ghabriel and Allt, 1979*ab*, 1980), developing (Hiscoe, 1947; Friede and Samorajski, 1969), regenerated (Hiscoe, 1947) and remyelinated (Ghabriel and Allt, 1980) peripheral nerve fibres. Buchthal *et al.* (1987) reported that large MFs (9.7–12.4 μm in diameter) of human sural nerve contained 35 SLCs per mm and small MFs (3.6–6 μm in diameter) contained 8 SLCs per mm. In large MFs, the SLCs extended over 13 μm and the

total length of all SLCs amounted to nearly 50% of the internodal length. In small MFs, the SLCs extended over 9 μm and the total length of all SLCs amounted to 6% of the internodal length in small fibres.

The role of SLCs remains unclear. Several functions have been suggested including, elongation of the myelinated fibres in response to physiologic stresses, transport of metabolic substances across the myelin sheath, metabolic maintenance of the myelin sheath and longitudinal growth of the myelin sheath (Balice-Gordon *et al.*, 1998; Ghabriel and Allt, 1981; Scherer, 1999; Thomas *et al.*, 1993).

Morphologic alterations of SLCs have been described experimentally. During Wallerian degeneration, dilation and increased cytoplasmic density have been noted in SLCs (Ghabriel and Allt, 1979*ab*). Immersion of nerve fibres in hypotonic solutions leads to dilation of SLCs and immersion in hypertonic solutions leads to closure of SLCs (Hall and Williams, 1970). Dilation of SLCs has also been noted following exposure to vibration (Ho and Yu, 1989), toxic agents (Vuorinen and Röyttä, 1990*ab*) and electrical stimulation (Hall and Williams, 1970). Disorganization and degeneration of myelin were observed at SLCs in experimental allergic neuritis and experimental allergic encephalomyelitis (Allt *et al.*, 1988; Saida *et al.*, 1979; Saida *et al.*, 1980, Westland and Pollard, 1987). SLCs may be the principal target of autoimmune attack in human demyelinating and axonal neuropathies (Gortzen *et al.*, 1999; Quattrini *et al.*, 1991). Disorganization of SLCs and invagination of membranes seemingly arising from SLCs were also commonly seen in xenografts from CMT1A and X-linked CMT (CMTX) (Sahenk and Mendell, 1999). In a large series of human sural nerve biopsies, structural alterations of SLCs were classified into three groups based on changes in shape and dimension, modes of disintegration and the presence of inclusions (Schröder and Himmelmann, 1992). Abnormal inclusions comprised

membranous whorls, uniform and pleomorphic lysosome-like bodies, accumulation of granular substances at major dense and intraperiod lines of the myelin sheath. Membranous whorls, detected in 89 biopsies, were the most frequent type of inclusion and most prominent in chloroquine neuropathy where they also occurred in adaxonal and abaxonal cytoplasm of Schwann cells (Schröder and Himmelmann, 1992). Variations in the shape and dimension of SLCs included folding, dilation, and pocket formation (compartmentalization). Compartmentalization of the myelin sheath at incisures associated with formation of myelin loops was a frequent feature in myotonic dystrophy. Disintegration at incisures comprised a fine vesicular and a gross vacuolar type. The authors suggested that the ultrastructural changes in SLCs are sensitive indicators of human neuropathies offering clues to the type of the underlying pathomechanism (Schröder and Himmelmann, 1992).

A comprehensive analysis by Ghabriel and Allt (1981) indicated that there was no significant increase of the number of SLCs in degenerating or demyelinating fibres. However, the frequency of SLCs per unit length was greater in regenerated and remyelinated fibres than in normal fibres (Hiscoe, 1947; Ghabriel and Allt, 1980, 1981). Gould *et al.* (1995) reported that the number of SLCs was more than doubled in homozygous MBP deficient mice. An increased number of SLCs was also observed in the xenografts from CMT1A and CMTX (Sahenk and Mendell, 1999).

1.2.2 Axons

An axon consists of a relatively firm gelatinous cord of neuronal cytoplasm, the axoplasm, which is enclosed by the axonal part of the neuronal cell membrane, the axolemma (Berthold and Rydmark, 1995; Thomas *et al.*, 1993).

Axolemma

In conventional EM preparations, the axolemma appears as an 8 nm thick, asymmetric, triple-layered membrane. Freeze-fracture preparations have shown that the outer aspect of the inner leaflet of the axolemma, the P-face, is rich in intramembranous particles (IMPs). The inner aspect of the outer leaflet, the E-face displays relatively few IMPs, except at nodes of Ranvier. These IMPs are about 10 nm in diameter and may represent voltage-sensitive Na^+ channels (Stolinski *et al.*, 1985; Tao-Cheng and Rosenbluth, 1980).

Axoplasm

The axoplasm consists of a fluid, cytosol, and formed elements. The latter consists of axoplasmic organelles and granular material (Berthold and Rydmark, 1995; LoPachin *et al.*, 1993; Thomas *et al.*, 1993). The axoplasmic organelles include mitochondria, the axoplasmic–smooth endoplasmic reticulum (AR), the cytoskeleton, vesiculotubular membranous profiles, dense lamellar bodies, multivesicular bodies (MVBs), and membranous cisterns. Ribosomes and Golgi apparatus are absent in axoplasm. The cytoskeleton is the most conspicuous of the axoplasmic components and consists of microtubules (MTs), neurofilaments (NFs), and the microtrabecular matrix (Ellisman and Porter, 1980; Tsukita *et al.*, 1980). It determines the growth pattern and morphology of the axon, stabilizes the axolemma, and contains the machinery necessary for interaction with the anterograde transport "motor" (kinesin) and the retrograde "motor" (dynein) (Brandt, 1998; Sheetz and Martenson, 1991).

Microtubules

MTs are about 25 nm thick, are unbranched, and vary from a few to more than 1000 μm in length (Bray and Bunge, 1981; Tsukita and Ishkawa, 1981). In axons, MTs are uniformly oriented with their fast growing ends pointing toward distal (Baas *et al.*, 1988). The number

of MTs varies inversely with axon size with about 100/μm^2 in small axons and 10/μm^2 in the largest ones (Berthold, 1978). MTs form the tracks along which fast axoplasmic transport of membranous organelles takes place (Pfister, 1999; Weiss *et al.*, 1987). Recent studies suggest that microtubule-associated proteins (MAPs) play critical roles in the development and maturation of neurites (Garcia and Cleveland, 2001).

Neurofilaments

NFs are 10 nm in diameter and unbranched (Thomas *et al.*, 1993). They are the most abundant cytoskeletal components in myelinated axons and form diffuse bundles running longitudinally in the axon often with a spiralling course. The density of NFs is about 150 to 300/μm^2 in cross-sectioned axoplasm and normally is not affected by the size of the axon (Berthold and Rydmark, 1995). NFs consist of three subunits with molecular weights of 68, 150 and 200 kDa that are referred to as neurofilament light (NFL), neurofilament medium (NFM) and neurofilament heavy (NFH), respectively (Nixon and Sihag, 1991). All subunits share a highly conserved central rod domain but differ in their C-terminal region. NFL forms the core of the 10 nm neurofilaments, and the C-terminal regions of NFM and NFH include sidearms that extend from the core filament. The C-terminal regions of NFM and NFH contain lysine-serine-proline (KSP) repeats, which are the major phosphorylation sites (Geisler *et al.*, 1987). It has been proposed that phosphorylation of NFM and NFH increases the total negative charge and the lateral extension of NF sidearms and that sidearm extension, in turn increases NF spacing and axonal calibre (Berthold and Rydmark, 1995; Hirokawa *et al.*, 1984; Lee and Cleveland, 1996; Nakagawa *et al.*, 1995).

1.2.3 Nodes of Ranvier

Nodes of Ranvier are the only sites along MFs that can support fast depolarization and repolarization necessary for generation of action potentials. This ability is mainly due to the

high concentration of voltage-sensitive Na+ channels in the nodal axolemma, where it is free of myelin insulation (Berthold and Rydmark, 1995). At nodes, the basal lamina that surrounds one Schwann cell continues uninterrupted to the adjacent Schwann cell. The Schwann cell basal lamina contains laminin 2 (comprising α2, β1 and γ1 laminin chains), type IV collagens, entactin/nidogen, fibronectin, N-syndecan and glypican (Bunge 1993; Scherer, 1996). All these molecules are found throughout the longitudinal extent of the basal lamellae. The coexistence of cell adhesion molecules (CAMs) of both neuron-glia (Ng) and neural types (N) in association with the nodal basal lamina emphasizes their importance to nodal structural integrity (Scherer, 1996; Thomas *et al.*, 1993). Like other parts of a MF, a node of Ranvier can be considered to consist of two concentrically arranged compartments: an outer Schwann cell compartment (here without myelin) and an inner axonal compartment (Scherer, 1996; Thomas *et al.*, 1993). The outer boundary of the node of Ranvier is defined by more or less overlapping extensions of the outer cytoplasmic compartments of the two adjoining internodes. The extensions are referred to as Schwann cell collars, which send a brush border of radially arranged microvilli into the nodal gap (Fig. 1-3). The nodal microvilli come close to the axolemma, and contain a high density of Na+ channels (Berthold and Rydmark, 1995; Scherer, 1996; Thomas *et al.*, 1993). Na+ channels are located in microvilli in high density (Scherer, 1996; Thomas *et al.*, 1993). The nodal gap is the space of about 1 μm in length under the basal lamina and between the two adjacent Schwann cells and contains extracellular matrix and the Schwann cell microvilli (Scherer, 1996; Thomas *et al.*, 1993). The constricted axon at the node of Ranvier is usually about 1 to 1.5 μm in length regardless of the fibre size (Rydmark and Berthold, 1983).

Several specific proteins, including Na^+ channels, ankyrin G, cell adhesion molecules (CAMs), NgCAM-related CAM (Nr-CAM), a 186kD isoform of neurofascin (NF186) and the Na^+/K^+ATPase are present at the nodes (Peles and Salzer, 2000; Scherer, 1996). The

presence of specific gangliosides, such as GM1 and GD1b, at the nodes may be relevant to the pathogenesis of some acquired demyelinating peripheral neuropathies (Peles and Salzer, 2000; Scherer, 1996; Sheikh *et al.*, 1999*a*).

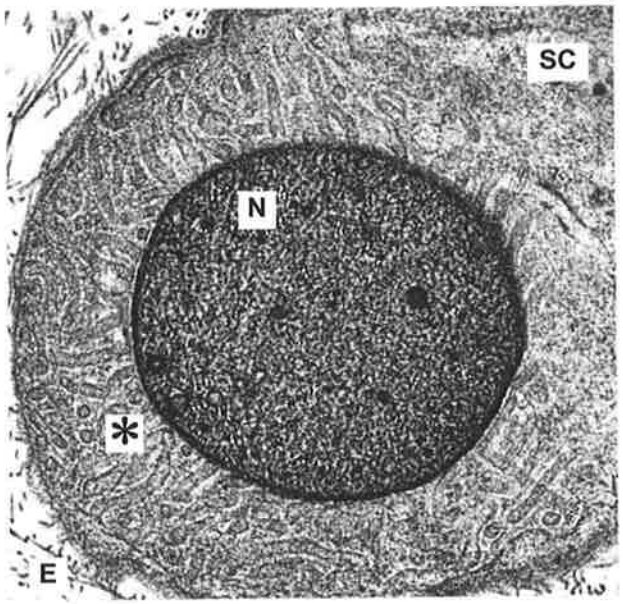

Figure 1-3. Node of Ranvier (×10000) from a mouse sciatic nerve. N, nodal axon segment; Sc, Schwann cell collar surrounding the axon; asterisks, finger-like processes extending through the node gap brush border; E, endoneurial space.

1.2.4 Paranodal-nodal-paranodal (PNP) regions

A PNP (Fig. 1-1) region includes a central node of Ranvier flanked by two paranodes. The paranodal region generates action potentials at comparatively high frequencies and maintains axoplasmic transport in spite of a reduction in axon diameter (Berthold and Rydmark, 1995; Thomas *et al.*, 1993), and functions as a hub to transport waste material from the axon to the Schwann cell (Gatzinsky, 1996; Gatzinsky *et al.*, 1997).

Paranodes

A paranode can be subdivided into two segments, a main and an end segment. The latter is the region in which myelin lamellae terminate on the axolemma as a series of loops (paranodal terminal loops), each containing a small pocket of Schwann cell cytoplasm. The

outermost lamellae terminate nearest to the node of Ranvier. Fig. 1-4 shows a normal paranode of a small MF in longitudinal section. In large MFs, not all of the lamellae terminate on the axolemma but are stacked on each other. The paranodal terminal loops spiral around, closely appose and form septate-like junctions with the axon (Thomas *et al.*, 1993), which anchor myelin loops to the axon and form a partial diffusion barrier into the periaxonal space (Peles and Salzer, 2000).

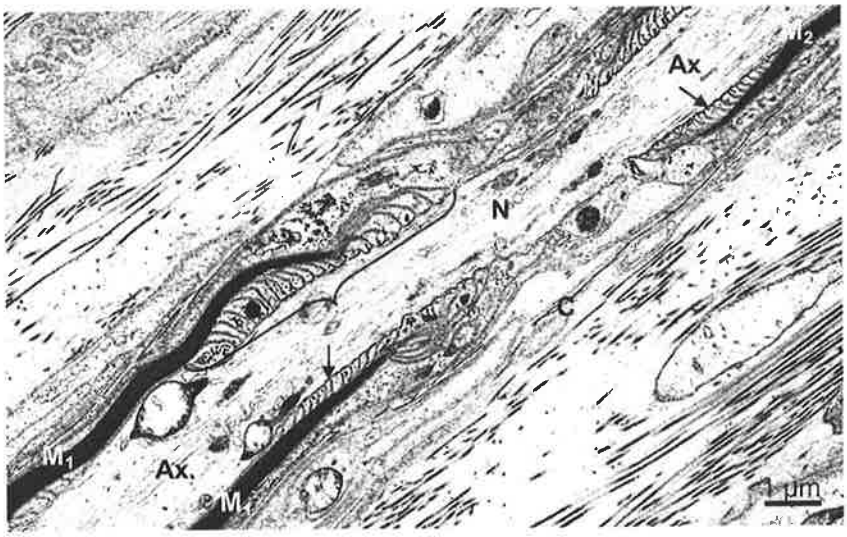

Figure 1-4. Longitudinal section of a myelinated axon (Ax) under EM illustrating a node of Ranvier. At this node, two myelinating Schwann cells (M1 and M2) meet, leaving the axonal membrane in the nodal region (N) relatively exposed. The myelin sheaths become thinner as they approach the nodal region and each layer of myelin forms a paranodal loop containing Schwann-cell cytoplasm. The loops (for example, arrows) lie tightly together, forming intimate contacts with the underlying axonal membrane. The myelin loops define the end segment of the paranodal region. C, collagen in the surrounding extracellular space.

The axonal diameter in the paranodal end segment is one half to one third of that in the STIN region (Rydmark, 1981). This section of the axon is referred to as the myelin sheath attachment (MYSA) segment (Fig. 1-5). The two MYSA axon segments and the intervening nodal axon segment constitute the constricted (CON) axon segment (Fig. 1-6), which is 6 to 10 µm in length regardless of the size of the fibre (Rydmark, 1981). The axon in the paranodal main segment is characterized by a fluted shape (Fig. 1-5). The slender longitudinal axonal ridges and grooves cease at the level of the end segment, where the

myelin sheath terminates and attaches to the axon core. There is a gradual reduction of the transverse axonal area from the main paranodal segment toward the node with the increasing delicacy and final disappearance of the axon ridges. In many paranodes the axon ridges close to the node become thin, winding, irregularly shaped processes embedded in the adaxonal Schwann cell compartment. This complex of interwoven axonal and Schwann profiles is the axon-Schwann cell network (Fig. 1-5) (Berthold and Rydmark, 1995; Thomas *et al.*, 1993).

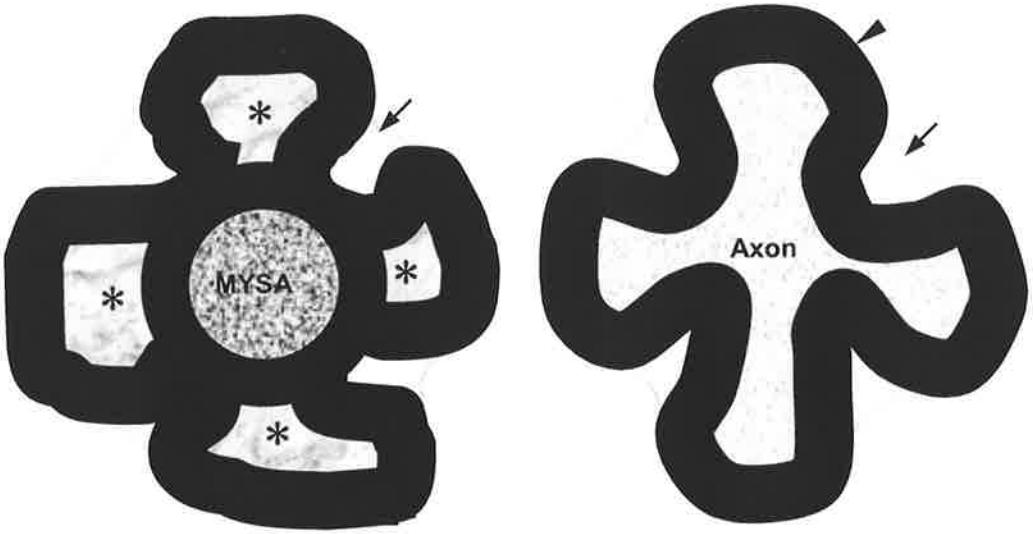

Figure 1-5. Diagrams to show cross sections through a paranodal end segment (left) and paranodal main segment (right). In the paranodal end segment (left) the MYSA part of the constricted axon is circular in outline. The axon of the paranodal main segment (right) is fluted in shape. Asterisk, axon-Schwann cell network inside myelin crests; arrow, mitochondrial bag in outer cytoplasmic Schwann cell compartment; Arrowhead, myelin crest.

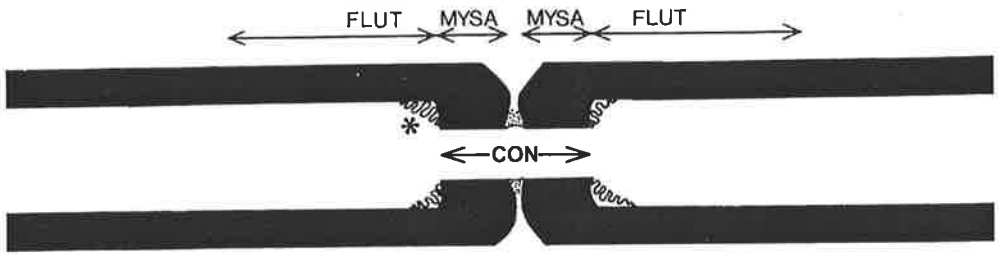

Figure 1-6. Diagram of a PNP region. CON = constricted axon segment; Flut = fluted paranodal axon segment (main paranodal segment); MYSA = myelin sheath attachment axon segment (paranodal end segment); asterisk, the axon-Schwann cell network. Modified from Thomas *et al.* (1993).

The contour of the paranodal myelin sheath is irregular and the outer cytoplasmic Schwann cell compartment forms longitudinal cords that are rich in mitochondria (mitochondrial bags). These compartments increase in volume towards the node of Ranvier and indent the contours of both the myelin sheath and the axon (Fig 1-5).

Contactin, contactin-associated protein (Caspr/Paranodin) and a 155kD isoform of neurofascin (NF155) are concentrated in the paranodal axons (Fig. 1-6, Peles and Salzer, 2000). Caspr is a component of the septate-like junctions. Adherens junctions are found in paranodes as well as in inner and outer mesaxons and SLCs (Fannon *et al.*, 1995). Adherens junctions contain E-cadherin, a Ca^{+} dependent cell adhesion molecule that forms "strand dimers", which bind homophilically in *trans* with those of the apposing membrane (Shapiro *et al.*, 1995). The cytoplasmic domain of E-cadherin binds α-catenin and β-catenin (Fannon *et al.*, 1995), which link E-cadherin to the actin cytoskeleton (Nagafuchi *et al.*, 1993). Gap junctions are also noted in paranodes. One gap junction protein, Cx32, is localized to the paranodes in the PNS (Bergoffen *et al.*, 1993). Cx32 consists of 283 amino acids, containing 4 hydrophobic transmembrane domains, 2 extracellular loops, 1 cytoplasmic loop, and intracellular N- and C-termini (Nelis *et al.*, 1999) and is also expressed in liver, kidney, gut, secretory epithelium, and neurons and glia in the CNS (Fischbeck *et al.*, 1999). The Cx32 gene maps to human chromosome Xq13.1 (Gal *et al.*, 1985). Mutations of Cx32 are related to CMTX in man (Bergoffen *et al.*, 1993).

1.2.5 Juxtaparanodes

Juxtaparanodal region lies at the paranodal-internodal junction. Since it is covered by the compact myelin (Fig. 1-7), it may be considered a specific portion of the internode (Peles and Salzer, 2000). The delayed-rectifier K^{+} channels Kv1.1, Kv1.2 and their Kvβ subunits are enriched in the juxtaparanodal axolemma. Caspr2, a second member of the Caspr

family, colocalizes and interacts with these channels (Poliak *et al.*, 1999; Peles and Salzer, 2000).

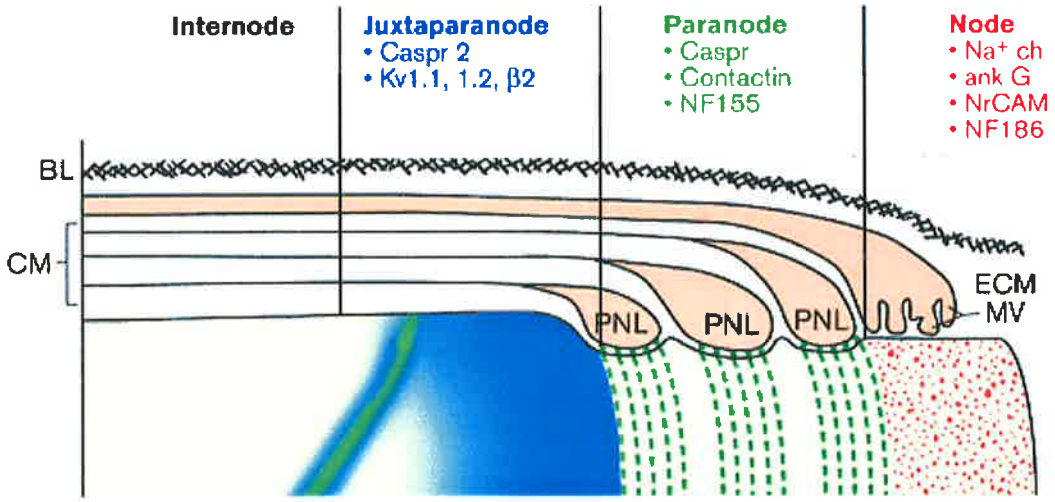

Figure 1-6. A diagram showing a longitudinal section through the nodal region illustrating the organization and composition of axonal domains in relation to their glial ensheathment in the PNS. The axon is myelinated by a Schwann cell that is surrounded by a basal lamina (BL). A spiral of paranodal and juxtaparanodal proteins extends into the internode. This spiral is apposed to the inner mesaxon of the myelin sheath (not shown). K^+ channels and Caspr2 are concentrated in the juxtaparanodal region. In the paranodal region, the compact myelin sheath opens up into a series of paranodal cytoplasmic loops (PNL) that invaginate and closely appose the axon, forming a series of septate-like junctions that spiral around the axon. Caspr, contactin and NF155 are concentrated here. At the node, numerous microvilli (MV) project from the outer collar of the Schwann cell to contact the axolemma. Modified from Peles and Salzer (2000).

1.3 MYELIN-ASSOCIATED GLYCOPROTEIN

Myelin-associated glycoprotein (MAG) was first found in rat central nervous system (CNS) in 1973 (Quarles *et al.*, 1973*a*) and later in the peripheral nervous system (PNS) by Quarles and colleagues (Figlewicz *et al.*, 1981; Sternberger *et al.*, 1979). Although it is quantitatively a minor constituent of the myelin sheath, comprising only 1% of the total protein content of the CNS myelin and less than 0.1% of PNS myelin (Quarles *et al.*, 1973*ab*; Figlewicz *et al.*, 1981), it is generally accepted that MAG plays an important role in membrane-membrane interaction as an adhesion molecule (Trapp, 1990). This section will review the biochemistry and subcellular localization of MAG and its functions.

1.3.1 Biochemistry of MAG

MAG is a nervous system specific protein of 100-kDa that contains about 30% carbohydrate by weight (Quarles *et al.*, 1983). The complete amino acid sequence of rat MAG deduced from the sequences of full length cDNA clones of the corresponding mRNA (Arquint *et al.*, 1987; Lai *et al.*, 1987*a*; Salzer *et al.*, 1987) includes a large extracellular portion, a single transmembrane region, and a cytoplasmic domain. MAG exists as two isoforms with polypeptide molecular masses of 72 and 67 kDa, designated as large MAG (L-MAG) and small MAG (S-MAG) respectively, generated by alternative mRNA splicing of exon 12. Both isoforms have identical extracellular and transmembrane regions, but are distinct at their cytoplasmic carboxy terminals (Fig. 1-7). The 67 kDa polypeptide of S-MAG has 10 different amino acids and lacks 54 amino acids that are present in the 72 kDa polypeptide of L-MAG (90 amino acids for L-MAG and 46 amino acids for S-MAG) (Arquint *et al.*, 1987; Lai *et al.*, 1987*a*; Salzer *et al.*, 1987). Sequencing of cDNA clones predicts the existence of two classes of MAG mRNAs, which differ in the presence or absence of a 45 nucleotide insert near the 3' end (Lai *et al.*, 1987*a*; Salzer *et al.*, 1987). During development L-MAG is the principle isoform during early and active stages of CNS myelination, whereas S-MAG

is present in the mature CNS (Frail *et al.*, 1985; Ishiguro *et al.*, 1991; Quarles *et al.*, 1973*b*). In the PNS, S-MAG represents at least 95% of the total MAG at all stages of development (Frail *et al.*, 1985; Tropak *et al.*, 1988). The MAG polypeptides undergo a number of post-translational modifications. The most extensive of these are glycosylation and phosphorylation, which play critical roles in the processes of cell recognition and signal transduction.

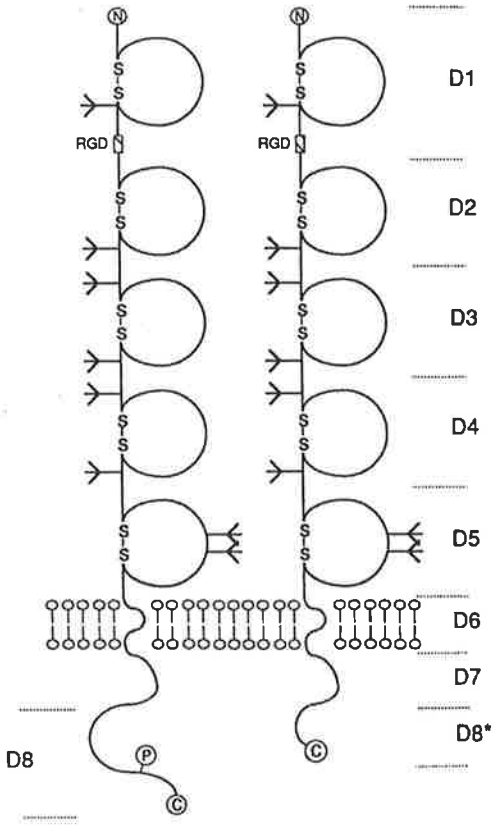

Figure 1-7. Models of the L-MAG and S-MAG polypeptides. Five Ig-like domains are represented by disulfide-bonded loops and oligosaccharide side chains as branched structures. The transmembrane domain D6 anchors the protein in the membrane. The two forms are generated by alternative splicing of mRNA and differ in the C-terminal, cytoplasmic domain D8 or D8*. A potential site for tyrosine kinase phosphorylation on the L-MAG is indicated by the P (modified from Lai *et al.*, 1987a).

MAG is phosphorylated in both the PNS and CNS, and the phosphorylation state of MAG modulates its adhesion and spatial properties (Attia *et al.*, 1989). Early studies reported that MAG phosphorylation only occurred in the cytoplasmic domain of L-MAG *in vitro* and *in*

vivo in the normal CNS (Braun *et al.*, 1990; Edwards *et al.*, 1989) and in the CNS of the quaking mutant (Braun *et al.*, 1990). Further investigations proved that both L-MAG and S-MAG in the CNS are phosphorylated (Kirchhoff *et al.*, 1993; Yim *et al.*, 1995), and that the cytoplasmic domain of L-MAG is much more heavily phosphorylated (Yim *et al.*, 1995), probably due to more potential phosphorylation sites on the 72 kDa polypeptide (Salzer *et al.*, 1990). The S-MAG in the PNS is also phosphorylated (Agrawal *et al.*, 1990; Yim *et al.*, 1995). The phosphorylation of MAG is catalyzed by protein kinase C and possibly other calcium-activated kinases (Kirchhoff *et al.*, 1993; Yim *et al.*, 1995). The principle phosphorylated amino acid in MAG is serine in both the PNS and CNS (Agrawal *et al.*, 1990; Kirchhoff *et al.*, 1993; Yim *et al.*, 1995). Threonine and tyrosine are also sites for phosphorylation in the MAG from oligodendrocytes (Yim *et al.*, 1995). In Schwann cells, there is less phosphorylation of threonine and labeled phosphotyrosine is not detected (Yim *et al.*, 1995).

Carbohydrate analysis of rat brain MAG reveals *N*-linked glycoproteins with *N*-acetylglycosamine, mannose, galactose, fucose, and sialic acid (Quarles *et al.*, 1983). There are eight extracellular consensus sites for N-linked glycosylation in rat MAG (Arquint *et al.*, 1987; Lai *et al.*, 1987*a*; Salzer *et al.*, 1987). All MAG glycosylated sequons might bear the L2/HNK-1 epitope (Burger *et al.*, 1993). Abnormal glycosylation of MAG may contribute to myelin pathology in the quaking mutants (Bartoszewicz *et al.*, 1995).

Of potential interest for the role of MAG in cell adhesion is the tripeptide sequence arginine-glycine-asparatic acid (Arg-Gly-Asp, RGD) which is present in the extracellular portion (Salzer *et al.*, 1990). RGD and related sequences in other cell recognition and extracellular matrix molecules are frequently important elements of the binding sites recognized by specific cell surface receptors, which form a closely related receptor family,

termed the integrins. Integrins are heterodimeric receptors that recognize RGD containing ligands extracellularly and cytoskeletal elements intracellularly (Hynes, 1987; Ruoslahti and Pierschbacher, 1987). Therefore, determination of whether the RGD sequence of MAG is an important functional element has clear implications for whether its axonal receptor is an integrin or whether, like many immunoglobulin gene superfamily members, its axonal receptor is immunoglobulin related (Salzer *et al.*, 1990).

1.3.2 Human MAG

The peptide of human MAG consists of 626 amino acids with a calculated molecular weight of 69.1 kD. It is 89% homologous in nucleotide sequence to the large isoform of rat MAG, with 95% homology in the amino acid sequence. It contains 9 potential *N*-glycosylation sites, one more than in rat, and shares other key features with rat MAG, including 5 Ig-like domains of internal homology and a RGD sequence (Sato *et al.*, 1989; Spagnol *et al.*, 1989). Of the 9 potential glycosylation sites, Burger *et al.* (1993) proved that 7 are glycosylated and 1 partially glycosylated at Asn^{106} (asparagine). Asn^{332}, which is not recovered in the glycopeptide fractions, is probably not glycosylated (Burger *et al.*, 1993).

1.3.3 MAG belongs to the immunoglobulin superfamily

The N-terminal region of MAG can be divided into five domains, each approximately 80-90 amino acid residues. All the domains have the characteristic structural features of immunoglobulin (Ig) domains: a pair of cysteines separated by 43-62 residues. Each of the domains has significant sequence identity with known Ig domains or with other proteins belonging to the Ig superfamily (Lai *et al.*, 1987*ab*; Salzer *et al.*, 1987; Williams and Barclay, 1988). The first domain contains a "RGD" sequence, which has been shown to be critical for binding between the extracellular matrix protein fibronectin and its cellular integrin receptor (Ruoslahti and Pierschbacher, 1987). In the Ig superfamily, MAG appears

to be most closely related to the neural cell adhesion molecules N-CAM (Cunningham *et al.*, 1987) and L1 (Moos *et al.*, 1988) and the neural glycoprotein contactin (Ranscht, 1988). The Ig-like domains of these proteins are structurally distinct and form a subset of the Ig superfamily, which has been termed the C2 set (William and Barclay, 1988). The fact that the majority of cell adhesion molecules possess C2-type domains suggests that this may have been the primordial Ig structure (Milner *et al.*, 1990)

1.3.4 MAG belongs to the Siglec family

Cell-surface carbohydrates are often terminated by sialic acids, a family of nine-carbon acidic sugars, all of which are derivatives of neuraminic acid (Schauer, 1982). Siglecs are sialic acid binding lectins of the Ig superfamily. Siglecs selectively recognize different types and linkages of sialic acid which are major components of cell surface and secreted glycoconjugates (Crocker *et al.*, 1998). Structurally, they have a characteristic N-terminal V-set Ig-like domain containing the sialic acid-binding site (May *et al.*, 1998) followed by varying numbers of C2-set Ig domains, which display distinct functional roles in the immune system or the nervous system (Kelm and Schauer, 1997). At least 10 siglecs have been defined, including sialoadhesin (siglec-1), CD22 (siglec-2), CD33 (siglec-3), MAG (siglec-4), Schwann cell myelin protein (siglec-4b), siglec-5, siglec-6 siglec-7, siglec-8, siglec-9 and siglec-10 (Angata and Varki *et al.*, 2000*ab*; Cornish *et al.*, 1998; Crocker *et al.*, 1998; Floyd *et al.*, 2000; Kelm *et al.*, 1994; Kikly *et al.*, 2000; Munday *et al.*, 2001; Nicoll *et al.*, 1999; Patel *et al.*, 1999; Zhang *et al.*, 2000).

1.3.5 MAG carries L2/HNK-1 epitopes

The extracellular portion of MAG carries the L2/HNK-1 carbohydrate adhesion epitope important in intercellular functions (Kruse *et al.*, 1984). The HNK-1 epitope was originally identified by a monoclonal mouse IgM antibody (HNK-1) that recognized the majority of

natural killer cells in peripheral blood (Abo and Balch, 1981). Subsequently, it was shown that a wide variety of putative and proven neural adhesion molecules, as well as, some glycolipids also carry the HNK-1 epitope (Jungalwala, 1994). Other monoclonal antibodies directed against the HNK-1 epitope have been described and the best characterized of these antibodies, the rat monoclonal L2/HNK-1, is capable of functionally blocking cell-cell and cell-substrate interactions mediated through the L2/HNK-1 carbohydrate epitope (Kunemund *et al.*, 1988). The L2/HNK-1 carbohydrate epitope, a sulphate-3-glucuronyl moiety shared by MAG together with other myelin components in the PNS, including N-CAM, L1, P_0 and PMP22, and sulfoglucuronyl glycosphingolipids, is recognized by the human monoclonal IgM antibodies that are found in patients with peripheral demyelinating neuropathy associated with gammopathy (Ariga *et al.*, 1987; Bollensen and Schachner, 1987; Bollensen *et al.*, 1988; Burger *et al.*, 1990, 1992; Chou *et al.*, 1986; Hammer *et al.*, 1993; Ilyas *et al.*, 1990; Kruse *et al.*, 1984; McGarry *et al.*, 1983; Schuller-Petrovic *et al.*, 1983; Snipes *et al.*, 1993; Steck *et al.*, 1983).

1.3.6 The MAG gene

The *Mag* gene in mouse and rat has been localized to chromosome 7 (Barton *et al.*, 1987; Blatt *et al.*, 1985; D'Eustachio *et al.*, 1988), and the human gene to the proximal long arm of chromosome 19 (19q12-q13.2) (Barton *et al.*, 1987; Spagnol *et al.*, 1989). In rats the MAG gene encompasses approximately 16kb, and the main product is a family of mRNAs of approximately 2,500 nucleotides that are first expressed in brain after birth (Lenoir *et al.*, 1986). The different mRNAs are generated by alternative RNA splicing as well as by utilization of at least two alternative sites for polyadenylation within exon 13 which are separated by 85 bases (Lai *et al.*, 1987*a*). In mice, exon 13 encodes the C-terminal portion of L-MAG, whereas the C-terminal part of S-MAG is encoded by the alternative splicing of

exon 12. So far there has been no evidence that a neurological disease in humans maps to the *Mag* gene.

1.3.7 Subcellular location of MAG

Localization of MAG during development

During development, MAG is first detectable intracellularly in oligodendrocytes, associated with the endoplasmic reticulum and Golgi apparatus, before the beginning of myelination (Bartsch *et al.*, 1989; Sternberger *et al.*, 1979; Trapp *et al.*, 1984*a*, 1989). The surface of the oligodendrocyte processes are already immunoactive when axons are being ensheathed (Bartsch *et al.*, 1989; Trapp *et al.*, 1989), suggesting a potential role of MAG in the initiation of myelination. In the PNS, MAG is found on the turning loops of myelinating Schwann cell membrane as early as post natal 8 days in mouse at the time when L1 expression ceases (Martini and Schachner, 1986). MAG is expressed at sites of axon-myelinating Schwann cell apposition and non-compacted loops of developing myelin (Martini and Schachner, 1986). When compaction of myelin occurs, MAG remains present only at the axon-Schwann cell interface, Schmidt-Lanterman incisures, inner and outer mesaxons, and paranodal loops, but not at finger-like processes of Schwann cells at nodes of Ranvier or compact myelin (Martini and Schachner, 1986).

Localization of MAG in the mature CNS and PNS

MAG is absent from the compact myelin sheath. It is selectively localized in the periaxonal membranes of myelin-forming Schwann cells and oligodendrocytes (Trapp, 1990). In PNS, it is also located in paranodal regions, Schmidt-Lantermann incisures, and outer mesaxons (Martini and Schachner, 1986; Trapp and Quarles, 1982, 1984; Trapp *et al.*, 1984*ab*). MAG is not detectable in perikaryal myelin of spiral ganglion neurons (Martini, 1994*a*).

1.3.8 Functions of MAG

On the basis of its location and biochemistry, MAG is supposed to function in: (1) initiation of myelination (2) forming and maintaining contact between myelinating Schwann cells and the axon; (3) maintaining the Schwann cell periaxonal cytoplasmic collar of myelinated fibers; (4) membrane movement (Griffin *et al.*, 1993; Martini, 1994*b*; Trapp, 1990).

Initiation of myelination

Localization of MAG at the tip of the Schwann cell spiralling membrane during development suggests that it may function in the early stages of myelination (Martini and Schachner, 1986). This view is supported by *in vitro* studies (Owens and Bunge, 1989; 1991), but challenged by recent studies in MAG null mutants (Li *et al.*, 1994; Montag *et al.*, 1994; reviewed in Chapter 5). Schwann cells, in which the expression of MAG is blocked by transfected antisense MAG RNA, failed to segregate large calibre neurites of co-cultured dorsal root ganglion (DRG) neurons and did not form myelin (Owens and Bunge, 1991). Conversely, expression of recombinant MAG in Schwann cells accelerated the initial investment of axons by myelinating Schwann cells (Owens *et al.*, 1990). *In vivo* studies of axonal regeneration also support MAG involvement in the initiation of myelin assembly. The steady levels of MAG mRNA in Schwann cells decreased to undetectable levels 4 days after injury in the permanently transected nerve. After crush injury, re-expression of MAG preceded that of P2 by 2 days and that of P_0 and MBP by 3 weeks during axonal regeneration and remyelination (LeBlanc and Poduslo, 1990). Mice deficient in MAG due to targeted disruption of the MAG gene show normal myelination in the PNS but delayed myelination in the CNS (Li *et al.*, 1994, 1998; Montag *et al.*, 1994).

Role in the maintenance of the Schwann cell periaxonal cytoplasmic collar

A unifying ultrastructural feature of all membranes enriched in MAG is that their extracellular surfaces appose other membranes by a 12-14 nm gap (Trapp, 1988; Trapp and Quarles, 1982). The location of MAG in periaxonal Schwann cell membranes is associated with the presence of 12-14 nm wide periaxonal space (Trapp and Quarles, 1982). MAG is absent from the periaxonal Schwann cell membrane if the space is larger than 12 to 14 nm or fused (Trapp *et al.*, 1984*ab*). Thus it is reasonable to speculate that MAG functions as both a membrane spacer and an adhesion molecule in the periaxonal space (Trapp and Quarles, 1982) and may be involved in the formation and maintenance of this space. The bulk and polarity of the extracellular domain of MAG are sufficient to spatially maintain this distance.

Membrane movement

MAG-enriched membranes have the ability to move (Trapp, 1990). Both the migration of periaxonal membrane along the axolemma during initial axonal ensheathment and the increase in the number of myelin lamellae due to the spiral rotation of outer mesaxon are examples showing the motility of MAG-containing membrane (Trapp, 1990). *In vitro* studies also showed the spiral rotation of the inner mesaxon during myelination (Bunge, *et al.*, 1989; Owens and Bunge, 1989). The possibility that Schmidt-Lantermann incisures migrate along the myelin internode has also been raised (Mugnaini *et al.*, 1977). In experimental beta,beta'-iminodipropionitrile neuropathy, interruption of axonal transport leads to the accumulation of neurofilament and axon swelling. Swelling of the axon in the paranodal region displaces the paranodal myelin sheath which retracts to the internodal region (Griffin *et al.*, 1987). Membrane motility and adhesion are mediated in part by interaction between microfilaments and the carboxy terminals of transmembrane proteins. A dynamic interaction between actin microfilaments and the carboxy terminal of MAG

could explain how MAG-containing membranes, on the one hand, are characterized by stable membrane-membrane interactions and, on the other, have the ability to move or expand. Here, MAG might function as part of a "motor" or as a "membrane anchor" that is essential for membrane migration (Trapp, 1990).

MAG functions in Schwann cell-axon interactions

Based on the observation that the Schwann cell can modulate axonal properties, it was postulated that myelin-related proteins at the inner axonal aspect of the Schwann cell may mediate myelin-axon communication, possibly by regulating a kinase-phosphatase system within the axon (de Waegh Brady, 1990). The localization of MAG at the Schwann cell–axon interface of MFs (Martini and Schachner, 1986) supports the notion that MAG is a candidate to mediate Schwann cell-axon interactions. Various degrees of axonal loss and axonal degeneration have been found in IgM anti-MAG neuropathy as will be described. Onion bulbs, focal myelin thickenings, increased frequency of MFs showing axonal degeneration compared to the age-matched controls and decreased axonal diameters were found in MAG deficient mice (Fruttiger *et al.*, 1995; Yin *et al.*, 1998). The decreased axonal calibre was associated with reduced phosphorylation of neurofilaments (Yin *et al.*, 1998). Identification of specific receptors for MAG, especially on the axonal membrane, is important in the investigation of the function of MAG in myelin-axon relationships. The extracellular domain of MAG has been shown to bind to neurons (Sadoul *et al.*, 1990), oligodendrocytes (Poltorak *et al.*, 1987), and constituents of the extracellular matrix (Fahrig *et al.*, 1987; Probstmeier *et al.*, 1992; Yang *et al.*, 1999). Gangliosides and glycoproteins present on the axolemma were shown to specifically bind to the MAG extracellular domain, and it was proposed that these glycoconjugates participate in the MAG-mediated adhesion of the myelinating glial cell to the axon (Collins *et al.*, 1997; De Bellard and Filbin, 1999; Strenge *et al.*, 1999; Yang *et al.*, 1996). In accordance with this view, it was found that

mice lacking complex gangliosides displayed similarly altered axon-Schwann cell units as MAG deficient mice (Sheikh *et al.*, 1999*b*). Recently, Kursula and co-workers have shown that the L-MAG cytoplasmic domain interacts with the S100β protein (Kursula *et al.*, 1999, 2000), while the S-MAG cytoplasmic domain binds directly to tubulin, the core component of the cellular microtubules (Kursula *et al.*, 2001). The characterization of S-MAG as a microtubule-associated protein (MAP) places it in a dynamic macromolecular complex, potentially linking the axon and the myelinating Schwann cell cytoskeleton (Kursula *et al.*, 2001).

1.4 SCHWANN CELL-AXON INTERACTIONS

The relationship between myelin sheath thickness and axonal calibre has been extensively studied during development (Fraher, 1972, 1976, 1978; Friede, 1972; Friede and Samorajski, 1967, 1968; Friede and Beuche, 1995; Kaar and Fraher, 1985; Low, 1976*ab*; Schröder *et al.*, 1978; Williams and Wendell-Smith, 1971) and at maturity (Fraher, 1989, 1992; Friede and Samorajski, 1967; Hildebrand and Hahn, 1978; Williams and Wendell-Smith, 1971). In general, there is a linear relationship between myelin sheath thickness and axonal diameter. However, the molecular basis of myelinogenesis is not fully understood. Evidence is accumulating that axon-glia recognition and mutual signalling may underlie these processes. All peripheral axons are surrounded by myelinating or non-myelinating Schwann cells. In normal nerves, Schwann cells not associated with an axon are rarely found. The axons influence the total number of Schwann cells in a nerve. Every Schwann cell has the potential to form a myelin sheath, but will only do so if it comes into contact with certain types of axons (Weinberg and Spencer, 1976; Aguayo *et al.*, 1976; Bray *et al.*, 1981). Axonal contact has been found to be essential in signalling myelination (Bunge, 1987; Bunge *et al.*, 1982; Gupta *et al.*, 1993; Jessen and Mirsky, 1992). The presence of axons is not only required for the expression of the myelin genes during development (Frail and Braun, 1984; Sternberger *et al.*, 1979; Uyemura *et al.*, 1979; Wood and Engel, 1976), but also for the maintenance of a myelinating phenotype. Loss of axonal contact, as occurs after nerve injury, leads to the down-regulation of myelin gene expression (Brockes *et al.*, 1980, 1981; Brunden *et al.*, 1990; Gupta *et al.*, 1988, 1990, 1993; LeBlanc and Poduslo, 1990; LeBlanc *et al.*, 1987; Poduslo, 1984; Poduslo and Windebank, 1985; Trapp *et al.*, 1988). Schwann cell or myelin disorders also result in axonal damage (Bjartmar *et al.*, 1999; Scherer, 1999). Therefore, the axon and Schwann cell form a mutually interdependent unit. The close relationship between neurites and Schwann cells seems to be of greatest importance during Schwann cell maturation and myelin formation.

1.4.1 Development of Schwann cells

Schwann cells are the principal glial cell type in the PNS, and their development in rodents has been well described (Mirsky and Jessen, 1996, 1999; Webster, 1993; Scherer, 1997*a*; Zorick and Lemke, 1996) and is shown in Fig. 1-8. In adults, they appear as two quite different types, the non-myelinating and myelinating Schwann cells. During the development of the PNS, Schwann cells arise from the neural crest and migrate out to the developing peripheral axons (Le Douarin and Dupin, 1993). The generation of Schwann cells from neural crest cells involves the formation of two main intermediates, the Schwann cell precursor, which is typically found in rat nerves at embryonic day 14 (E14) and E15 (mouse E12 and 13) and immature Schwann cells, present from E17 (mouse E15) to the time of birth (Jessen *et al.*, 1994; Jessen and Mirsky, 1999). At this time the cells start to differentiate in two ways. Some cells establish a one-to-one relationship with an axon, the so-called promyelinating Schwann cells (Scherer, 1997*a*; Webster, 1993; Zorick *et al.*, 1996). They then initiate the program of myelin-specific gene expression, turning on the set of genes encoding the major myelin proteins and turning off a subset of genes already expressed, and finally become myelinating Schwann cells to generate multiple myelin lamellae spirally around the axon (Jessen and Mirsky, 1999; Scherer, 1997a). In contrast, immature Schwann cells that do not establish a one-to-one relationship with an axon segregate small, unmyelinated axons into separate troughs and become nonmyelinating Schwann cells (Mirsky and Jessen, 1990; Webster *et al.*, 1983). The lineage, therefore, involves three main transition points, that is, the transition of crest cells to precursors, of precursors to immature Schwann cells and finally the formation of the two mature Schwann cell types. The survival and differentiation of Schwann cell precursors and immature Schwann cell depends, at least in part, on signals from the axon. The differentiation of nonmyelinating Schwann cells also depends on continuing interactions with axons (Jessen *et*

al., 1987), and Schwann cells from unmyelinated fibres are able to differentiate into myelin producing cells in a suitable environment (Aguayo *et al.*, 1976).

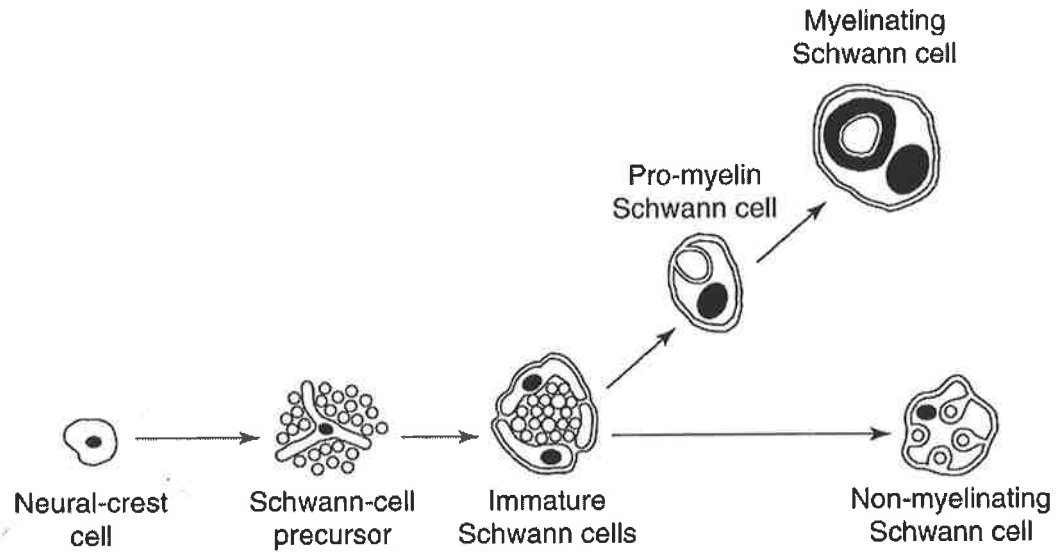

Figure 1-8. Schematic representation of the stages of Schwann cell differentiation in rat and mouse (Modified from Jessen and Mirsky, 1999).

The morphological changes of Schwann cells are accompanied by changes in gene expression (Mirsky and Jessen, 1996; Jessen and Mirsky, 1999). Immature and nonmyelinating Schwann cells have a similar phenotype. Both express neural cell adhesion molecule (NCMA), L1, the low affinity neurotrophin receptor/p75 ($p75^{NTR}$), growth-associated protein of 43 kD (GAP-43), and glial fibrillary acidic protein (GFAP). Myelinating Schwann cells, on the other hand, do not express these proteins but express a set of proteins that are components of the myelin sheath, such as P_0, PMP22, MBP, MAG, and periaxin (Mirsky and Jessen, 1996; Jessen and Mirsky, 1999). The expression of these myelin-related proteins and their cognate mRNAs increases substantially as Schwann cells form myelin sheaths (Lee *et al.*, 1997; Stahl *et al.*, 1990), and this upregulation requires continuous axon-Schwann cell interactions both in developing and in regenerating nerves (Gupta *et al.*, 1993; Scherer *et al.*, 1994).

1.4.2 Survival of Schwann cell precursors depends on signals from axons

Schwann cell precursors undergo apoptosis when they are removed from embryonic nerves and placed in neuron-free cultures (Jessen *et al.*, 1994). Dorsal root ganglion (DRG) neurons secrete protein(s) that prevent this death, and isolated axonal membranes also possess activity that supports precursor survival (Jessen and Mirsky, 1999). Therefore, it is likely that the survival of Schwann cell precursors *in vivo* is regulated by signals from the axons with which they associate. These signals also drive, or permit, the next step in the development of the lineage, since the precursors mature to generate Schwann cells *in vitro* in the presence of the neuron-derived proteins. A key signal is the β form of neuregulin (NRG-β) (Jessen and Mirsky, 1999). NRG-β supports Schwann cell precursor survival *in vitro* for several days and during this period, the cells alter their phenotype from that of precursors to that of Schwann cells. The time course of this Schwann cell generation *in vitro* is similar to that with which the glial population of developing nerves switches from the precursor phenotype to the Schwann cell phenotype *in vivo* (Jessen and Mirsky, 1999). Most importantly, the action of the signal from DRG neurons that supports precursor survival and differentiation is blocked by a soluble hybrid protein containing the extracellular domain of the ErbB4 NRG-β receptor, a receptor that is not known to bind to any other growth factor (Dong *et al.*, 1995). NRG-β is also present at the appropriate time and place in rat and mouse embryos: strikingly high expression of NRG mRNA is seen in motor neurons of the ventral horn in the spinal cord and over DRG neurons, the two major sources of axons in embryonic peripheral nerves (Marchionni *et al.*, 1993; Meyer and Birchmeier, 1994; Orr-Urtreger *et al.*, 1993). Taken together, these results strongly suggest that neuronally derived NRG-β is likely to act as a survival/maturation factor for Schwann cell precursors. Recent studies on knockout mice also support to this conclusion, since they indicate a central role for neuronal NRG signaling in the development of Schwann cell precursors. NRG deficient mice that die between E10 and 11 from heart defects have very

few Schwann cell precursors in dorsal and ventral roots at E10 (Meyer and Birchmeier, 1995). Mice deficient in the major NRG receptor ErbB3, lack Schwann cell precursors and subsequently fail to develop Schwann cells in their peripheral nerves (Riethmacher *et al.*, 1997), showing that NRG signaling through the ErbB3 receptor is needed for precursor development/survival. Examination of transgenic mice that express type III NRG such as SMDF, but do not express NRG that contain an Ig domain in their extracellular domain (Type I and II), has shown that the presence of type III NRG in DRG and motor neurons is sufficient to support the development of Schwann cell precursors and Schwann cells (Meyer *et al.*, 1997). The data discussed above support a paracrine model of precursor survival, in which the survival of precursors depends on its next-door neighbour, the axon. In the embryonic nerve, it is likely that the acute dependence of precursors on axons for survival contributes, together with proliferation factors, to the attainment of the right numerical ratio between axons and precursors and eventually between axons and Schwann cells.

1.4.3 Developing Schwann cells acquire the ability to survive without axons

Apoptotic Schwann cells are present in nerves from newborn rats, and transection of neonatal nerves increases the amount of apoptosis (Jessen *et al.*, 1994). Neuregulin can prevent this apoptosis (Jessen and Mirsky, 1999). However, in 20 day old rats, most Schwann cells survive nerve transection related loss of axonal contact, and in adult nerves no significant Schwann cell death follows denervation (Grinspan *et al.*, 1996; Syroid *et al.*, 1996; Trachtenberg and Thompson, 1996). This raises the question of how Schwann cells survive in the absence of axons. Cell culture studies found that Schwann cell survival is density dependent while the Schwann cell precursors die equally readily even at extremely high plating density; and Schwann cells in sparse cultures, which die by apoptosis in routine media, can be rescued by medium conditioned by dense Schwann cell cultures (Jessen and

Mirsky, 1999). These findings support the view of an autocrine loop in which Schwann cells sustain their own survival by secretion of factors that block Schwann cell apoptosis. Further studies indicate that the autocrine survival activity resides in a cocktail of growth factors, including insulin-like growth factors (IGF), platelet-derived growth factor-BB (PDGF-BB) and neurotrophin-3 (NT-3) (Meier *et al.*, 1999). These factors act synergistically to block Schwann cell death (Jessen and Mirsky, 1999). However, the findings that neither the Schwann cell derived survival factors in conditioned media nor the minimal IgF-2/NT-3/PDGF-BB combination supported survival beyond two days indicate that the autocrine survival loops alone may not be sufficient to guarantee Schwann cell survival and point to the presence of a second survival signals in cut nerves (Jessen and Mirsky, 1999). It is suggested that laminin, a main component if the Schwann cell basal lamina and a molecule implicated in the regulation of Schwann cell development , may be involved in supporting the long term survival of Schwann cells following loss of axonal contact (Bunge, 1993; Martini, 1994*b*). Laminin alone is ineffective in maintaining Schwann cell survival. But, laminin together with the minimal cocktail of IGF-2NT-3/PDGF-BB or Schwann cell conditioned media can maintain the survival of Schwann cell for at least 6 days *in vitro* (Jessen and Mirsky, 1999).

1.4.4 Schwann cells modify axon cytoskeletal architecture

Axonal calibre is influenced by intrinsic and extrinsic factors. Of the extrinsic factors, the extent of Schwann cell ensheathment and myelination is the most important in normal nerves (Hoffman and Griffin, 1993). In primary cultures of peripheral nerve tissue, myelination of segments of axonal processes results in local increases in axonal calibre (Pannese *et al.*, 1988; Windebank *et al.*, 1985). In normal myelinated axons, only the initial segments (stem processes), the nodes of Ranvier and the terminals are not covered by myelin, and the axonal calibre in these areas is substantially smaller than that of myelinated

internodes (Mata *et al.*, 1992; Hsieh *et al.*, 1994). The number of neurofilaments and NF spacing are the principal intrinsic factors that control the axonal calibre (deWaegh *et al.*, 1992). Highly phosphorylated sidearms of NFs are repelled from the filamentous cores by negative charges, resulting in an increase in space between the NFs (Fig. 1-9). This is in accordance with the finding that, in myelinated large-calibre processes of the dorsal root ganglion, NFs are highly phosphorylated and display an increased distance to their neighbours, whereas the small calibre, nonmyelinated initial segments of the axons are associated with less phosphorylated and more densely packed NFs (Hsieh *et al.*, 1994).

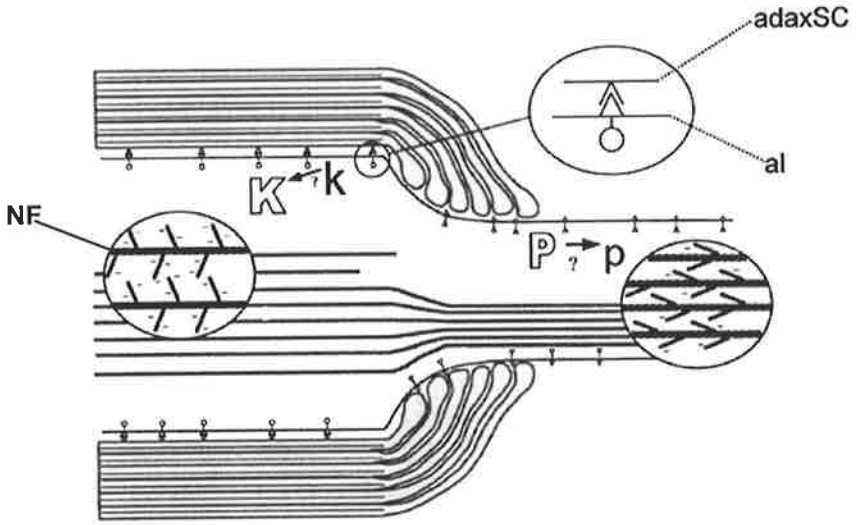

Figure 1-9. Diagram showing modulation of axonal properties by myelinating Schwann cells. Myelination appears to determine the status of activity of a kinase (K, k)-phosphatase (P, p) system. Schwann cell-axon interactions, i.e. binding of a Schwann cell ligand such as myelin-associated glycoprotein to the axonal receptor communication (see symbols at the axon-Schwann cell apposition and enlarged inset) may mediate this system. In the myelinated part of the axon (left), more neurofilaments (NF) are present and they show a higher phosphorylation state (P) leading to repulsion of the highly phosphorylated side arms from the filamentous cores by negative charges. This leads to an increase in space between the neurofilaments and, eventually, to an increase in axon calibre. In the nonmyelinated part of the axon (or at the node of Ranvier), fewer neurofilaments are present and their phosphorylation state is reduced (p), leading to a smaller axon calibre. AdaxSc, adaxonal Schwann cell membrane; al, axolemma. Modified from Martini (2001).

1.4.5 Schwann cells organize molecular domains of the axon

The molecular domains of myelinated axons have been reviewed in **section 1.2**. The spatial distributions of cell adhesion molecules and ion channels on the axolemma are affected by myelinated Schwann cells (Arroyo and Scherer, 2000; Arroyo *et al.*, 1999; Peles and Salzer, 2000; Scherer, 1996). The Schwann cell influence on the distribution of these molecules is best demonstrated in the case of Na^+ channels (Fig. 1-10). During the process of development or remyelination, the longitudinal extension of the Schwann cells along the axon leads to the Na^+ channels being pushed ahead of the leading edges and eventually "fusing" to form the mature channel cluster at the node of Ranvier (Martini, 2001).

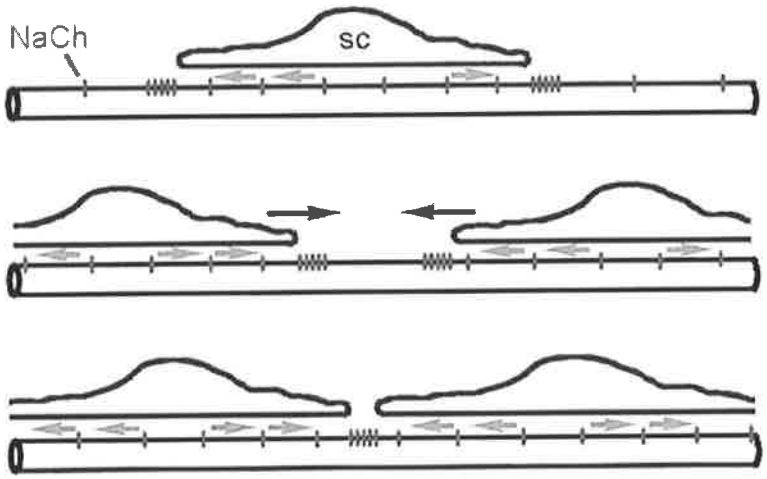

Figure 1-10. Diagram to show the functional roles of myelinating Schwann cells (SC) on the distribution of Na+ channels (NaCh). The Na+ channels are present at low density all along the axon before myelination. During myelination, the Na+ channels are excluded from the regions of contact between the axon and SC and accumulate just beyond the edges of the SC (top). As SC processes grow, the clusters also move and form the transient binary clusters (middle), and eventually fuse to become a node (below). Copied from Martini (2001).

1.4.6 Abnormal Schwann cells induce pathologic changes in axons

Because myelinating Schwann cells can modify axonal properties in the normal nervous system, it is not surprising that abnormal Schwann cells lead to pathologic changes in the axon. Mutations of P_0, PMP22 and Cx32, cause myelin diseases, such as CMT1, HNPP,

DSS and congenital hypomyelinating (CH) neuropathy (Dyck et al., 1993*b*; Nelis *et al.*, 1999; Thomas et al., 1997). A striking feature common to these primary myelin disorders is not only the obvious impairment of myelination or myelin maintenance but also the change in axons. The progressive clinical manifestations, such as muscle atrophy and sensory dysfunction, and the electrophysiological abnormalities in these disorders correlate more with secondary axonal damage (Dyck *et al.*, 1989; Krajewski *et al.*, 1999, 2000). Abnormalities of axonal properties are also found in *Tr* and Tr^J mice (deWaegh and Brady, 1990; Robertson *et al.*, 1997)), PMP duplicated or deficient mice (Sancho *et al.*, 1999), P_0 deficient mice (Giese *et al.*, 1992; Zielasek *et al.*, 1996), Cx32 deficient mice (Anzini *et al.*, 1997; Martini and Carenini, 1998; Scherer *et al.*, 1998) and MAG deficient mice (Yin *et al.*, 1998). The most common axonal abnormalities in these human and animal neuropathies are the reduction of axonal calibre and axonal loss. Reduced axonal calibre probably results from the dephosphorylation of NFs (Cole *et al.*, 1994; deWaegh and Brady *et al.*, 1990; Waston *et al.*, 1994; Yin *et al.*, 1998). Axonal loss and distal axonal degeneration may be related to the disruption of slow axonal transport (deWaegh and Brady, 1990; Frei *et al.*, 1999; Sancho *et al.*, 1999).

The impact of abnormal Schwann cells on axonal properties is further demonstrated by the transplantation experiments using allografts from Tr mice (deWaegh and Brady, 1991; deWaegh *et al.*, 1992) and xenografts from CMT1A, CMTX and HNPP patients (Sahenk and Chen, 1998; Sahenk *et al.*, 1999) as bridges connecting the proximal and distal stumps of transected nerves from normal mice. When axons regenerate through the allografts, they are contacted and eventually ensheathed by the mutant Schwann cells mice (deWaegh and Brady, 1991; deWaegh *et al.*, 1992). The properties of the initially healthy axons are altered by the mutant Schwann cells. Similar to the situations in the stem process of dorsal root ganglion neurons and in the node of Ranvier, where myelin is focally missing, characteristic

axonal features in the allografts include reduction in calibre, higher NF density, and a low NFs phosphorylation state mice (deWaegh and Brady, 1990, 1991; deWaegh *et al.*, 1992). In addition, reduced anterograde transport of NFs in the axons has been found. In the distal, host-derived part of the nerve containing wild-type Schwann cells, axonal properties of normal myelinated fibres are restored (deWaegh and Brady, 1991; deWaegh *et al.*, 1992). Eight to sixteen weeks after the transplantation, the proximal part of the diseased xenograft showed an increased NF density accompanied by an enlarged axonal diameter, suggesting an impaired axonal transport of NFs (Sahenk and Chen, 1998; Sahenk *et al.*, 1999). Reduced axonal calibre and increased NF density were observed at distal end of the diseased xenografts, mimicking some of the alterations seen in nerve biopsies from CMT1A patients (Waston *et al.*, 1994). Preferential distal axonal loss and degeneration were observed in the xenografts and might reflect the well-known phenomenon that distal aspects of limbs are more susceptible to the muscle wasting and sensory dysfunction than proximal parts in peripheral neuropathies (Dyck *et al.*, 1993*a*). Reduced axonal calibre, fibre loss and degeneration were also found in the distal host segment indicating that the pathway through the diseased xenografts had irreversibly injured the host axon (Sahenk and Chen, 1998; Sahenk *et al.*, 1999). Additionally, the onset of regeneration-associated myelination was delayed in the CMT1A and HNPP grafts (Sahenk and Chen, 1998; Sahenk *et al.*, 1999).

Axonal involvement has also been found in inflammatory neuropathies, such as acute and chronic inflammatory demyelinating neuropathies (Bjartmar *et al.*, 1999; Hartung *et al.*, 1995*ab*; Ho *et al.*, 1998). However, in these disorders, it is difficult to determine whether the axonal damage is primary or secondary to the myelin damage.

CHAPTER 2: Development of A New Method for the Correlation of External and Internal Structure at Specific Points of Teased Nerve Fibres

2.1 Introduction **43**

2.2 Previous methods of studying transverse and longitudinal sections of teased nerve fibres **49**

2.3 Development of new technique **53**

2.3.1 Description of the technique 53

2.3.2 Key points about the technique 60

2.4 Examples of application of new technique in the interpretation of teased nerve fibre abnormalities **67**

2.4.1 Condition A 68

2.4.2 Condition B 72

2.4.3 Condition C 79

2.4.4 Condition E 85

2.4.5 Condition F 87

2.4.6 Non-specific change 94

2.5 Discussion **97**

2.5.1 Advantages of the new technique 97

2.5.2 Correlation of external and internal structure of teased fibres 98

2.1 INTRODUCTION

The limitations in the interpretation of teased fibre abnormalities based on their external appearance under LM have long been recognized (Dyck and Lais, 1970; Lascelles and Thomas, 1966; Lubinska, 1961; Ochoa *et al.*, 1971; Spencer and Thomas, 1970; Weiss and Hiscoe, 1948).

Although techniques for cross and longitudinally sectioning single teased fibres were first described almost thirty years ago, they have not attracted much attention probably due to their time-consuming nature and technical difficulty. There is only limited information on this subject (Dyck and Lais, 1970; Dyck *et al.*, 1971*ab*; Ochoa, 1972; Smith *et al.*, 1982; Spencer and Thomas, 1970). Systematic serial transverse sections at multiple levels of a single fibre, and correlation of the internal findings with the external appearance of the fibre, classified according to Dyck's criteria (Dyck *et al.*, 1993*a*), has not been previously undertaken.

In order to address this problem I developed a teased nerve fibre technique that enabled the correlation of the external and internal structural appearance at specified points along the length of individual teased myelinated nerve fibres.

Teased fibre classifications according to the external appearance

Teased fibre analysis is a difficult and time-consuming procedure. It requires perfect tissue preparation, utmost attention during teasing to avoid artefacts, and systematic sampling of single MFs (Dyck *et al.*, 1993*a*; Sima and Blaivas, 1997). Most importantly, the examiner must be aware of the normal structure and possible variations of MFs.

The most commonly adopted criteria for classifying normal and pathological teased nerve fibres are those of Dyck *et al.* (1993*a*) and the different categories or conditions (A to I) are outlined below.

A. Teased fibre of normal appearance. The internodal myelin is regular similar to that of most MF internodes of the control. The average thickness of myelin of the internode with the thinnest myelin is at least 50% of that of the internode with the thickest myelin. No paranodal or internodal segmental demyelination is seen. This judgement assumes the observer is aware that myelin irregularity varies with the preparation used, the species, the nerve assessed, and age. Myelin is more regular in the young than in the old.

B. Teased fibre with excessive irregularity, wrinkling, and folding of myelin but with the other features of condition **A**. This judgement assumes that the observer is familiar with the degree of myelin regularity considering species, nerve, site, and age.

C. Teased fibre with a region or regions of paranodal or internodal segmental demyelination with or without myelin ovoids or balls in the cytoplasm of the associated Schwann cells. Thickness of myelin of the internode with the thinnest myelin is 50 percent or more of that of the internode with the thickest myelin. Myelin of internodes may be regular or irregular. In demyelination, as judged by the high-dry objective of the light microscope, no myelin can be recognized. In paranodal demyelination the

nodal gap is increased beyond that seen in normal fibres. In internodal demyelination the entire internode is demyelinated.

D. Teased fibre with a region or regions of paranodal or internodal segmental demyelination with or without myelin ovoids in the cytoplasm of the associated Schwann cells. Thickness of myelin of the internode with the thinnest myelin is less than 50 percent of that of the internode with the thickest myelin. Myelin of internodes may be regular or irregular.

E. Teased strand of nerve tissue with linear rows of myelin ovoids and balls at the same stage of degeneration.

F. Teased fibre without region or regions of segmental demyelination but with excessive variability of myelin thickness among internodes. Thickness of myelin of the internodes with the thinnest myelin is less than 50 percent of that of the internode with the thickest myelin. Myelin of internodes may be regular or irregular. The internode of thin myelin sheath with an internodal length less than 50 percent of neighbouring normal internodes is designated as an intercalated internode. It results from a demyelinated internode remyelinated by two or more Schwann cells.

G. Teased fibre with excessive variability of myelin thickness within internodes to form "globules" or "sausages".

H. Teased fibre of normal appearance as described in **A**, but in which there are myelin ovoids or balls contiguous to two or more internodes.

I. Teased fibre having several proximal internodes or parts of internodes with or without paranodal or internodal segmental demyelination and, distal to these, a linear row of myelin ovoids or balls.

Condition A and B fibres are classified as normal, condition C and D as demyelination, F and G as remyelination, E as axonal degeneration, and H as axonal regeneration. Condition I is seen typically several days after and at the site of crush, and may represent a dying-back

change. Because these abnormalities can also been seen in normal control nerves at low frequency (Table 1.1), when assessing the pathological changes of teased nerve fibres, the percentage of different pathologic changes should be compared to the findings in control nerves.

Table 2.1. Graded pathologic conditions of teased fibres (%) from sural nerve of healthy volunteers (Dyck *et al.*, 1993*a*)

	A Normal Appearance	B Myelin Irregularity	C, D, F, G Segmental De- and Remyelination	E, H Axonal degeneration and regeneration
Age		*15–<30 years*		
Mean	95.0	0.2	3.9	1.0
Median	94.9	0	3.1	0
SD	3.1	0.5	2.7	1.8
Range	90.2–100.0	0–2.3	0–8.6	0–7.6
Age		*30–<45 years*		
Mean	95.0	0.5	4.0	0
Median	96.5	0	2.9	0
SD	3.6	1.0	4.4	0
Range	89.8–98.1	0–2.0	0–10.2	0–0
Age		*45–<60 years*		
Mean	81.5	1.8	14.5	1.9
Median	83.0	0.6	15.9	1.1
SD	11.0	2.8	9.3	2.3
Range	67.3–92.6	0–59	2.2–23.8	0–5.3

Sima and Blaivas (1997) classified teased nerve fibres into the following nine categories.

1. **Normal**: Consecutive, approximately equally long internodal segments of similar diameter. Within one internode the largest diameter should not exceed 150% of the smallest diameter.

2. **Paranodal Swelling**: Paranodal expansion of the axonal diameter exceeding 150% of the average internodal diameter. It may be present on one or both sides of the nodal gap.
3. **Paranodal Demyelination**: A nodal gap distance, devoid of any myelin, that exceeds the internodal mean diameter of the same fibre.
4. **Excessive Myelin wrinkling**: The internodal area shows irregular infoldings and superimposed myelin folds, involving one third or more of the internodal length and the greatest diameter is equal to or exceeds 150% of the smallest diameter.
5. **Intercalated Internode**: A fibre shows one remyelinated internode surrounded on both sides by normally myelinated internodes. It is regarded as a product of the repair process that follows paranodal demyelination.
6. **Segmental Demyelination**: Active demyelination with myelin fragmentation and ovoids within one internode that is surrounded by normally myelinated internodes.
7. **Segmental Remyelination**: A fibre shows two or more remyelinated intercalated internodes surrounded by normally myelinated internodes.
8. **Regenerated Fibres**: A sequence of short, thinly myelinated internodes less than 50% of normal internode length of the same fibre diameter.
9. **Wallerian Degeneration**: Irregular myelin ovoids over or balls spread over several internodes. These fibres often show a gradient from undulating calibre changes to progressively smaller myelin fragments.

Kalichman *et al.* (1999) classified teased fibres into the following six groups

1. **Unclassifiable**: Except for Wallerian degeneration, a MF is unclassifiable if it is: (1) inadequately osmicated (i.e., nodes of Ranvier cannot be reliably identified along the length of the fibre), (2) too short (i.e., less than 4 consecutive nodes of Ranvier or 3 internodes, or (3) part of an intertwined bundle (i.e., interweaving of 2 or more fibres).

2. **Wallerian Degeneration**: Fragmentation of MF into myelin ovoids and balls (cluster of at least 3 balls or ovoids along the axis of the degeneration axon).
3. **Demyelination**: Absence of myelin along part of or an entire internode, regardless of internodal length, with preservation of the axon (no myelin sheath visible with the high dry objective; fragments of myelin may be seen along the internode). The length of demyelinated segment may be of normal internodal length or short.
4. **Hypomyelination**: Thinly myelinated internode of normal length (myelin thickness <50% neighbouring internodes and internodal length ≥60% of the longest internode).
5. **Remyelination**: At least one abnormally short internode (length <60% of longest internode); myelin thickness may be normal or decreased.
6. **Abnormal Paranodal Myelination**: A mechanically undamaged node in which (1) the nodal gap is widened, or (2) the paranodal myelin is thin (<50% of the rest of the internode). In either case, the region of decreased myelination should be at least twice the nodal axonal diameter.

Dyck's criteria and classification of teased nerve fibre abnormalities are generally used in research and diagnostic practice. They described and classified the common external features of teased fibres (Dyck *et al.*, 1993*a*). Sima and Blaivas (1997) highlighted the importance of internodal length in classifying teased fibres and provided a clear definition of paranodal demyelination. Kalichman *et al.* (1999) added two further categories of fibres with unclassifiable abnormalities and hypomyelination. All of these criteria are based on the external appearance of teased nerve fibres under LM although the inadequacies of this type of examination have long been recognized (Dyck and Lais, 1970; Lascelles and Thomas, 1966; Lubinska, 1961; Ochoa *et al.*, 1971; Spencer and Thomas, 1970; Weiss and Hiscoe, 1948).

2.2 PREVIOUS METHODS OF STUDYING TRANSVERSE AND LONGITUDINAL SECTIONS OF TEASED NERVE FIBRES

Method described by Spencer and Thomas (1970)

Spencer and Thomas (1970) developed a technique to examine ultrathin transverse sections of teased nerve fibres at selected sites to localize focal abnormalities for EM study.

The specimens were first fixed in 2.5% glutaraldehyde for 3 hours, postfixed in 1% osmium tetroxide for 5 hours, dehydrated in graded concentrations of methanol, transferred to toluene (two changes) for 1 hour, and immersed in equal parts of toluene and Araldite for 24 hours. Then single MFs up to 1.5 cm in length were isolated in Araldite embedding medium with fine mounted needles under a dissecting microscope. Fibres of especial interest were transferred to a toluene-cleaned glass slide, straightened, examined by light microscopy, and photographed. Regions of interest were measured from one end of the fibre. The fibres were then transferred with a drop of Araldite to small moulds and hardened in Araldite for 7 days at 60°C. Transverse ultrathin sections were then cut from one end of the fibre, stained with 2% uranyl acetate in methanol for 5 minutes, followed by lead citrate for 2 minutes, and examined under a electron microscope. The fibre was then trimmed to the next position of interest and cross sections repeated.

This technique was applied to study nerve fibres in a traumatic neuroma (Spencer and Thomas, 1970). One remyelinated fibre with multiple "myelin bubbles" proximal to the site of nerve transection was transversely sectioned. Transverse sections through the externally normal segments showed no abnormality. A cross section through a thinly myelinated segment proximal to the focal swellings showed an axon of normal appearance enclosed by a disproportionately thin myelin sheath. Cross sections through the "myelin bubbles" confirmed that the walls of the focal swellings were composed of myelin to form

intramyelinic spaces containing myelin debris. A macrophage containing myelin remnants was found on cross section through a focal swelling.

Method described by Dyck and Lais (1970)

Dyck and Lais (1970) also developed a technique to examine ultrathin transverse sections at selected sites of interest along the length for subsequent electron microscopic study.

A 1 cm fascicle of sural nerve was first fixed in 2% glutaraldehyde for 30 minutes and postfixed in 1% osmium tetroxide for 2 hours. Then small strands of approximately 50 fibres were teased from the fascicle with fine curved forceps in cacodylate buffer on a glass slide under a dissecting microscope. The strands were dehydrated and infiltrated with a mixture of propylene oxide and medium-hard epoxy. Single MFs were then isolated in epoxy on a glass slide and transferred into a dish of 1.25 to 1.5 mm depth. After the epoxy was cured, the flat epoxy dishes were trimmed, the fibres were viewed directly, and areas of interest were photographed under the light microscope. The region of the fibre to be studied was cut with a coping saw and attached with rapidly drying epoxy cement to a blank epoxy block previously prepared in hard rubber molds. Then the block was trimmed to a point close to the area to be studied. Thick transverse sections were cut and viewed under a phase-contrast microscope, and thin sections were stained with uranyl acetate and lead citrate and viewed under an electron microscope.

Transverse sections at 10 sites along the length of a myelinated fibre from the sural nerve of a 2-year-old girl with hypertrophic neuropathy of the Charcot-Marie-Tooth type were examined (Dyck and Lais, 1970). The axonal calibre was small at sites that were demyelinated, intermediate in the region thinly myelinated, and large at the sites having a thicker myelin sheath. The areas of the fibre which were considered to be demyelinated or

remyelinated on the basis of examination of teased fibres under the light microscope were found, on electron microscopy, to have none or only a few (9-18) myelin lamellae, respectively (Dyck and Lais, 1970).

This technique was also applied in a study of uraemic neuropathy (Dyck *et al.*, 1971*b*). Two strands of nerve fibres including linear rows of myelin ovoids and two single MFs showing segmental demyelination were transversely sectioned from the sural nerve of a patient with uraemic neuropathy (Dyck *et al.*, 1971*b*). Both strands of nerve fibres with myelin ovoids in linear rows also showed several clusters of unmyelinated fibres. Both of the single fibres showing segmental demyelination appeared to have atrophic axis cylinders. In internodes with retained myelin, there was extreme distortion of the myelin sheaths and considerable variation of the number of myelin lamellae (Dyck *et al.*, 1971*b*).

Method described by Ochoa (1972)

Ochoa (1972) developed a technique to examine longitudinal sections of single teased nerve fibres for the EM study of paranodes and nodes of Ranvier.

Nerves were first fixed in glutaraldehyde and postfixed in Dalton's fluid, dehydrated and impregnated with epon. Nerve fibres were teased in epon, transported on a hair, and placed on the flat surface of a resin block, which was pre-polymerized. The fibre was hardened on the resin block in an oven overnight, and then covered with a drop of epon and hardened. Longitudinal sections of up to 150–200 μm in length were obtained from the resin block (Ochoa, 1972).

Ochoa (1972) only provided 2 examples of application of this technique. One was a MF from a baboon sciatic nerve showing tapering of the paranodal myelin towards the node of

Ranvier. Longitudinal sections revealed that there was no myelin sheath at the node of Ranvier which was covered by Schwann cell basement membrane. The second example was a study of an intercalated segment in a nerve fibre from a baboon sciatic nerve.

Method described by Smith *et al.* (1982)

Smith *et al.* (1982) examined the transverse sections of teased nerve fibres to measure the internodal length, myelin thickness and circumference and axonal area to study relationships between myelin volume and internodal axonal size and shape.

After perfusion fixation with 4% glutaraldehyde in 0.1 M phosphate buffer, the spinal roots and sciatic nerves of rats were removed. The nerves were then postfixed in osmium tetroxide for 2 hours, dehydrated with graded ethanol and infiltrated with epoxy resin following changes in propylene oxide. The tissues were left in epoxy without accelerator for 24 hours and then placed in epoxy resin plus accelerator. In this medium, individual nerve fibres or small numbers of fibres were teased apart using fine needles and transferred to flat embedding discs. The resin was hardened (56°C) and the individual nerve fibres were numbered and drawn. The individual fibres were then cut out of the embedding disc and held in a flat chuck in an LKB ultramicrotome for transverse sectioning.

Quantitative studies of transverse sections of normal, remyelinated and regenerated nerve fibres revealed a close relationship between the volume of myelin and the surface area of the axolemma beneath the internodal myelin sheath, suggesting that the regulation of myelin volume, and thereby of myelin thickness, may be mediated via the area of the axolemma or of the Schwann cell membrane beneath the myelin sheaths (Smith *et al.*, 1982). However, the authors didn't provide any illustrations to support these concepts.

2.3 DEVELOPMENT OF NEW TECHNIQUE

2.3.1 Description of technique

Step 1: Tissue fixation and dehydration

The method of tissue fixation is the same as for conventional glycerinated teased nerve fibre studies (Cash and Blumbergs, 1995; Dyck *et al.*, 1993*a*), and the method for dehydration is similar to the methods previously described (Dyck and Lais, 1970; Spencer and Thomas, 1970). Nerve tissue was first fixed in 2.5% glutaraldehyde in 0.05 *M* cacodylate buffer at pH 7.4 for 1.5 hours. Then the nerve was separated into single fascicles and further fixed in 2.5% glutaraldehyde for 0.5 hour. The specimens were then washed in 0.05 *M* cacodylate buffer at pH 7.4 on a rotator for at least 30 minutes with at least 5 changes of the buffer, and post-fixed in 1% osmium tetroxide for 2 hours. After further washing in buffer solution for at least 30 minutes with at lest 5 changes of the buffer, the specimens were dehydrated in 70% ethanol for 30 minutes, 95% ethanol for 30 minutes, absolute ethanol for 1 and half hours with 2 changes of ethanol, and transferred to propylene oxide for 30 minutes on a rotator. Tissue dehydration was performed at room temperature.

Step 2: Tissue softening

Following dehydration, specimens were immersed in equal parts of propylene oxide and Spurr resin without accelerator (Dimethylaminoethanol, DMAE) for 30 minutes, transferred to a mixture of propylene oxide and Spurr resin without accelerator (volume : volume = 1 : 3) for 30 minutes, and immersed in Spurr resin without accelerator for three days with a change of fresh resin every day. Then the specimens were immersed in fresh Spurr resin with accelerator for 1 day, and transferred to fresh Spurr resin ready for the teasing of single fibres. The steps for tissue softening were performed on a rotator at room temperature. If there is insufficient time for the operator to complete this procedure in a single sitting, the specimens can be stored in fresh resin (with or without accelerator) after dehydration in a

fridge at –20C°. Some of our tissues have been stored in resin with or without accelerator at –20C° for over 2 years without change of resin, and they are still suitable for successfully teasing single fibres.

The procedures for tissue fixation, dehydration, softening and storing are summarized in table 2-2.

Table 2-2. Processing schedule for resin teased fibre preparations

Step	Solution required	Time	Conditions
1	70% ethanol	30 minutes	room temperature, on a rotator
2	95% ethanol	30 minutes	room temperature, on a rotator
3	100% ethanol	30 minutes	room temperature, on a rotator
4	100% ethanol	30 minutes	room temperature, on a rotator
5	100% ethanol	30 minutes	room temperature, on a rotator
6	Propylene oxide: Spurr resin (1:1) (no DMAE)	30 minutes	room temperature, on a rotator
7	Propylene oxide: Spurr resin (1:3) (no DMAE)	30 minutes	room temperature, on a rotator
8	Spurr resin without DMAE	overnight	room temperature, on a rotator
9	Spurr resin without DMAE	overnight	room temperature, on a rotator
10	Spurr resin without DMAE	overnight	room temperature, on a rotator
11	Spurr resin with DMAE	overnight	room temperature, on a rotator
12	teasing or stored in resin at 20°C		

Step 3: Teasing single myelinated nerve fibres in resin

The method of preparing teased nerve fibres in resin is similar to that for teasing in glycerol (Dyck *et al.*, 1993*a*). Teasing is performed in fresh Spurr resin at room temperature. With two pointed forceps and using a dissecting microscope, epineurium and perineurium are stripped away from endoneurium on a plain glass "teasing" slide. Small strands of nerve fibres are torn from the endoneurium. From these strands, a single fiber or a bundle of a small group of fibres is teased away from the main strand. During this process, the left

forceps grasps one end of the main strand and remains motionless while the right one grasps another end of the main strand to trace an inverted U-pathway. The tip of the forceps is kept in constant contact with the glass slide to prevent the fibre from curling up around it. A carbon-coated "mounting" slide is laid adjacent to the top of the slide on which the teasing has been done. One end of each separated fibre is grasped with forceps and slid onto the carbon-coated slide through a minute drop of resin on the teasing slide near the edge adjacent to the mounting slide (Fig. 2-1). The teased fibre is dragged onto the carbon-coated slide for a short distance in order to straighten the fibre and remove extra resin. Two to eight fibres are placed side by side in close proximity (about 0.2 mm apart) (Fig. 2-2A). The rest of the tissue is restored in fresh resin with accelerator at –20°.

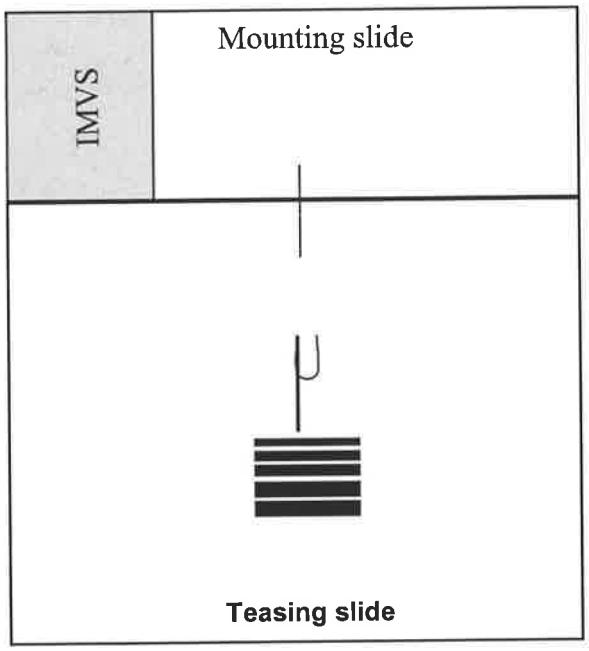

Figure 2-1. Teasing single myelinated fibres in resin. After fixation in glutaraldehyde and osmium and softening in resin, the epineurium and perineurium of a nerve fascicle are stripped off, the fascicle is teased into separate small strands on a plain glass "teasing" slide. Single fibres are isolated from these small strands using forceps. A carbon-coated "mounting" slide is placed at the top of the teasing slide. One end of a teased fibre is grasped by a pair of forceps and slid onto the mounting slide through a small drop of resin near the top edge of the teasing slide.

Step 4: Hardening resin teased nerve fibres

Individual teased fibres mounted on carbon coated slides are hardened in a 73°C oven for 3 days or in a 45°C oven for 1 week.

Step 5: Photographing the individual teased nerve fibres

Teased fibres are digitized using a Quantimet 500MC Image System (Leica-Cambridge, UK) or an Olympus DP11 Microscope Digital Camera System (Japan), and the images stored in the computer. The number of internodes in every fibre is counted, and the length of internodes and the size of any abnormalities, such as focal myelin swellings, are measured.

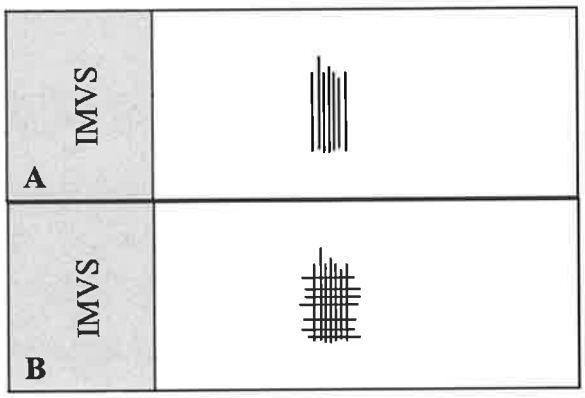

Figure 2-2. Seven vertical resin teased fibres are placed side by side in close proximity on a carbon-coated glass slide (A). Seven short horizontal resin teased fibres are placed perpendicularly to the 7 vertical fibres to mark specific sites or at regular intervals (B).

Step 6: Marking specific sites on the teased fibres

Short single myelinated nerve fibres teased in resin are placed perpendicular to the original teased fibres to mark specific sites of interest or at regular intervals (Fig. 2-2B). The slide is then left in a 73°C oven for a further 3 days or in a 45°C oven for a further one week. Then the original teased fibres together with the marker fibres are digitized using the image system, and the images stored in the computer. The distance between marker fibres or between a marker fibre and a specific site of interest is measured using the image system.

Step 7: Embedding single teased fibres in a resin block for longitudinal sectioning

A small capsule (as used for routine electron microscopy resin embedding with a calibre of 8mm) is filled with fresh Spurr resin with accelerator and placed upside down onto the carbon-coated slide, covering the area that contains the teased fibres (Fig. 2-3A). The slide together with the capsule is left in a 73°C oven for 5 hours or in a 45°C oven for 3 days. Then the flat side of the carbon-coated slide, opposite to the side with the adherent resin capsule, is placed on the top of a solid metal block, which is pre-cooled in liquid nitrogen (Fig. 2-3B). Due to the temperature change in the slide, the resin block separates from the slide along the line of the carbon coat. After separation, the fibres of interest and the marker teased fibres, keeping their original shape on the carbon-coated slide, are left on the surface of the resin block (Fig. 2-3C), visible to the naked eye (Fig. 2-3D) and are ready for longitudinal sectioning. Because the fibres keep the original flat shape they had on the mounting slide and are located at the surface of the resin block, longitudinal sections of single nerve fibres can be cut by keeping the block surface parallel to the knife blade.

Step 8: Embedding single teased fibres in the resin block for transverse sectioning

The resin block (Fig. 2-3D) is trimmed of excess resin with a coping saw then placed in a capsule filled with fresh Spurr resin. The original teased fibres are aligned parallel to the long axis of the capsule so they can be cut in cross section. The capsule is left in a 73°C oven for 5 hours or in a 45°C oven for 3 days, following which the teased fibres, together with marker fibres, are clearly visible in the block (Fig. 2-3E), and can be examined under a dissecting microscope or the binocular magnifier of an ultramicrotome.

Step 9: Sectioning and localizing individual teased fibres embedded in resin

Transverse and longitudinal sections of 0.5 μm thickness are cut using a SORVALL JB4 (Porter-Blum) microtome with glass knives, and thin sections are cut at 60-100nm using SORVALL MT2-B Ultra-microtome (Porter-Blum) or LKB Bromma 8800 Ultrotome®III

with diamond knives. The exact position of each cross section is determined using a combination of visual inspection, a binocular magnifier and counting the number of sections of known thickness in relation to the transverse marker fibres. Keeping the original teased fibres perpendicular to the knife blade under the binocular magnifier of the microtome enables transverse sections to be cut. When sectioning longitudinal sections, keeping the surface of the resin block parallel to the knife blade ensures "true" longitudinal sections of single myelinated fibres.

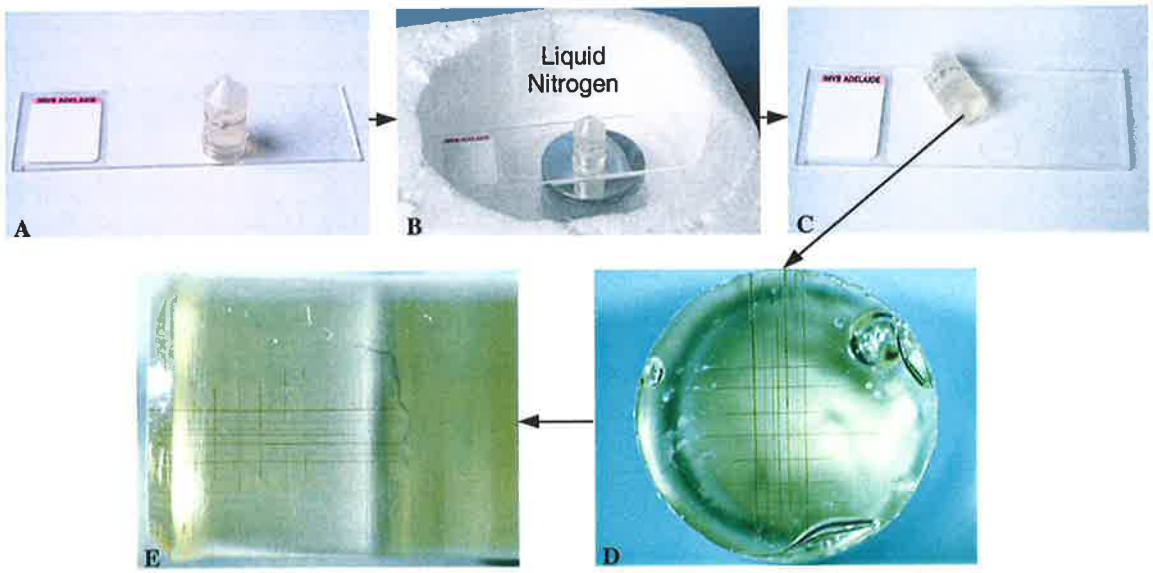

Figure 2-3. Preparation of myelinated nerve fibres for transverse and longitudinal sectional studies. After hardening of the teased fibres and the marker fibres on a carbon-coated glass slide, a small capsule (as used for routine electron microscopy resin embedding) filled with Spurr resin is placed upside down onto the slide, covering the area that contains the teased fibres (A). The slide together with the capsule is left in a 73°C oven for 5 hours or in a 45°C oven for 3 days. After resin polymerization, the slide is placed on a metal block, which is pre-cooled in liquid nitrogen (B). The temperature difference helps to separate the resin block from the glass slide along the line of the carbon coat (C). Seven vertical myelinated fibres and seven horizontal marker fibres are left in the resin block, keeping their original shape as they are on the carbon-coated slide (D). Longitudinal sections of individual myelinated nerve fibres can be sectioned from this resin block, or this block can be trimmed of excess resin with a coping saw and re-embedded in another resin block, keeping the original teased fibres parallel to the long axis of the second resin block (E). Seven horizontal original fibres and seven vertical marker fibres can be seen from the surface of the resin block. Transverse sections can be cut from this block for LM and EM.

Step 10: Staining of plastic sections

Semithin transverse sections are stained with toluidine blue for 10 minutes at 98°C and semithin longitudinal sections are stained with toluidine blue for 8 minutes at 98°C or for 5 minutes at 120°C for light microscopy. At 55-60°C, ultrathin sections are first stained with uranyl acetate for 4 minutes and secondly stained with lead citrate for 1 minute for electron microscopy.

Step 11: Morphometric studies of cross section of individual teased fibres

The profiles of transverse sections of individual myelinated fibres are digitized using the Quantimet 500MC Image System (Leica-Cambridge, UK), and are finally magnified 3017 times on a computer monitor. The axonal area on transverse sections (Aa) is measured by tracing the inner edge of the myelin sheath using a mouse and the total fibre area on transverse sections is measured by tracing the outer edge of myelin sheath. The contour of the fibre is converted to an axonal area equivalent and total fibre area on transverse section equivalent circular shape (Fig. 2-4). The axonal diameter (Da) and fibre diameter (Ds) are mathematically calculated from Aa and As.

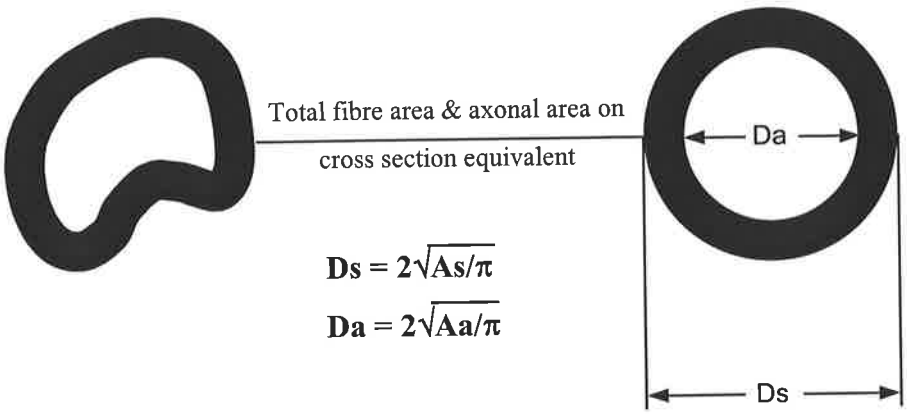

Figure 2-4. Transformation of the shape of MF on cross section of single teased fibres. The contour of the fibre on cross section (left) is transformed to total fibre area and axonal area equivalent circular shape (right). The fibre diameter (Ds) and axonal diameter (Da) are assumed to be equivalent to the outer and inner diameter of the myelin sheath respectively.

2.3.2 Key points about the technique

Tissue softening

Fixed specimens are rigid and not suitable for teasing fibres directly. Conventionally specimens are softened in glycerol (Dyck *et al.*, 1993*a*), but glycerinated teased fibres are not suitable for embedding in resin blocks for further sectioning studies (Dyck and Lais, 1970). Spencer and Thomas (1970) immersed the specimens in Araldite for 24 hours before teasing. Before teasing, Dyck and Lais (1970) immersed the specimens in epoxy resin, but the exact length of time and type of the epoxy resin were not described. Smith *et al.* (1982) immersed the specimens in epoxy resin (unspecified type of epoxy resin) without accelerator for 24 hours. Because epoxy resin is an oil-based embedding medium, it was supposed that the epoxy resin would soften the tissue like glycerol if the specimens were left in the resin long enough. In our pilot studies, nerve fascicles were immersed in resin for 6 hours, 12 hours, 24 hours, 2 days, and up to 1 week with a change of fresh resin every day. It was found that the tissue became softer with increasing immersion time and was most suitable for teasing after 4 days. However, the middle of the nerve fascicles immersed in resin over 4 days was still sometimes rigid and unsuitable for teasing probably because the old resin in the middle of the fascicle had polymerized. As resin without accelerator polymerizes very slowly but retains all the other physical and chemical properties of resin with accelerator, the specimens were immersed in resin without accelerator to retard resin polymerization. When the fascicle was softened, it was transferred to fresh resin with accelerator for 1 day. These procedures were performed on a rotator in order to let fresh resin replace the old resin as completely as possible. After these procedures, the specimens were soft and suitable for teasing. Softening in resin without accelerator requires at least 3 days and severely fibrotic nerves need softening in resin without accelerator for 1 week. Insufficient resin softening will make the tissue too rigid to tease and later lead to artefacts in teased fibres.

In a previous study (Dyck and Lais, 1970), the perineurium was peeled off and the nerve fascicles separated into small strands before infiltration in resin. We tried this method because it was hoped that the tissue would soften better and faster, but found that many artefacts (eg, myelin breaks) were produced in the single teased fibres. Careful examination of the small strands after osmication under a dissecting microscope showed that these artefacts were present in the fibres before teasing individual fibres. This finding indicated that these artefacts were produced during the separation of the fascicle into small strands before tissue softening.

Selection of epoxy resin

Resin is used not only as an embedding medium for later LM and EM studies but also as a medium to "soften" nerve fascicles to facilitate teasing single fibres. Thus water soluble or hydrophilic acrylic resins, such as JB4 resin, methacrylate resin and histocryl resin, are not suitable for this study (refer to **Catalogue 6 of Agar Accessories for Microscopy**). However, oil-based epoxy resins can be used to soften tissue. Araldite (Spencer and Thomas, 1970), epoxy (Dyck and Lais, 1970) and epoxy resin (Smith *et al.*, 1982) were used in the previous studies. Araldite is a type of epoxy resin. Two kinds of Araldite are commercially available: one is Araldite CY212 resin, which is generally referred to as epoxy resin or epoxy; and the second is Araldite 502 resin (refer to **Catalogue 4 of TAAB Laboratories**). Although the specific type of epoxy resin used was not detailed in the previous studies (Dyck and Lais, 1970; Smith *et al.*, 1982; Spencer and Thomas *et al.*, 1970), it is reasonable to speculate that Araldite CY212 or a resin similar to Araldite CY212 was used. Araldite CYC212 consists of resin, dodecenyl succinic anhydride (DDSA), dibutyl phthalate and DMP-30 CY212 (refer to **Catalogue 4 of TAAB Laboratories**). The composition and physical and chemical characteristics of Araldite are similar to those of **TAAB** resin (refer to **Catalogue 4 of TAAB Laboratories**), which is commonly used in

our laboratory for LM (Table 2-3) and can also be used for EM. Both TABB resin and Araldite have high viscosity and take a long time to infiltrate and soften the tissue. Routine embedding of peripheral nerves using TAAB resin takes 2 days in our laboratory (Cash and Blumbergs, 1995). In the pilot studies, single fascicles were not sufficiently soft for teasing if they were immersed in TAAB resin for less than 1 week. Furthermore, TAAB resin is too sticky for teasing.

Table 2-3. Recipe for TAAB resin (grams)

Total	**10.13**	**20.27**	**30.40**	**40.54**
MNA	3.16	6.31	9.47	12.63
DDSA	1.57 (4.73)	3.15 (9.46)	4.72 (14.19)	6.29 (18.92)
RESIN	5.27 (10.00)	10.54 (20.00)	15.81 (30.00)	21.08 (40.00)
DMP-30	0.13	0.27	0.40	0.54

MNA: Methyl nadic anhydride

DDSA: Dodecenyl succinic anhydride

RESIN: TAAB embedding resin

DMP-30: 2,4,6-TRI (Dimethylaminomethyl) phenol

Table 2-4. Recipe for Spurr resin

Total	**10.1ml**	**20.2ml**	**30.3ml**	**40.4ml**
NSA	6.5ml	13ml	19.5ml	26ml
ERL	2.5ml (9ml)	5ml (18ml)	7.5ml (27ml)	10ml (36ml)
DER	1ml (10ml)	2ml (20ml)	3ml (30ml)	4ml (40ml)
DMAE	0.1ml	0.2ml	0.3ml	0.4ml

NSA: Nonenyl succinic anhydride

ERL: Vinyl cyclohexene dioxide

DER: Diglycidyl ether of polypropylene glycol, epoxy equivalent 310-330

DMAE: 2, Dimethylaminoethanol

Spurr Resin has very low viscosity. It enables specimens normally difficult to infiltrate to be successfully embedded (refer to **Catalogue 6 of Agar Accessories for Microscopy**). Spurr resin is commonly used in our laboratory for EM (table 2-4) and also can be used for LM. Routine embedding of peripheral nerves using Spurr resin takes only 3 hours. Single

fascicles are usually soft and suitable for isolating individual myelinated fibres 4 days after they are immersed in Spurr resin. Furthermore the low viscosity of Spurr resin facilitates the teasing. Therefore, Spurr resin was selected for this study.

Fibre hardening

In previous studies (Dyck and Lais, 1970; Smith *et al.*, 1982; Spencer and Thomas, 1970), the soft teased fibres were hardened in a mould which was filled with fresh resin. We tried this method of hardening single fibres in pilot studies, but found that single fibres usually wouldn't keep the straight shape they had on the mounting slide but curved and twisted during the resin polymerization. A slight change in the straight shape of fibres would lead to difficulties in orientation. In order to keep a straight shape the teased fibres must be hardened before embedding in resin blocks.

Resin polymerization

The duration and temperature of resin polymerization are critical. In our lab, Spurr resin normally takes 5 to 6 hours to polymerize in a 73°C oven. However, resin teased fibres still remain soft and movable after 24 hours in the 73°C oven. This may be because the small volume of resin within and around individual nerve fibres takes a longer time to polymerize. After 3 days in the 73°C oven, the small volume of resin is partially polymerized and teased fibres stick to the slide firmly and maintain their shape. However, resin teased nerve fibres must not be left in the 73°C oven for more than 1 week because over-polymerization of the resin will make adequate staining of the fibre difficult later. As will be further discussed, plastic sections of single teased fibres are difficult to stain with toluidine blue, uranyl and lead. Resin hardening in a low temperature (45°C) oven for a longer time (1 week) overcomes this problem.

Marking specific sites of the teased fibres

No marker fibres were used in the previous studies (Dyck and Lais, 1970; Smith *et al.*, 1982; Spencer and Thomas, 1970). The thickness of teased fibres is only around 10 μm and it is very difficult to cut cross sections at sites of interest on the teased fibres without specific markers. If the fibre is serially transversely sectioned from one end to another, thousands of sections would need to be examined. The visibility of single fibres in the resin block (see Fig. 2-3D and G) inspired us to use short single resin teased fibres from the same fascicle to mark the specific sites of interest on the teased fibres. Such markers do not damage the original teased fibres and are of the same density, which is important in the process of sectioning. During sectioning, keeping the marker fibres parallel to the blade of the knife also helps in getting true cross sections.

The importance of using carbon-coated slides

Plain or gelatin coated slides were used at an early stage of this study. When the resin polymerized, the fibres and the resin block stuck to the slide firmly and it was impossible to separate the resin block from the glass slide without damaging the fibres. The use of the carbon-coated slide enables the separation of the resin block from the slide and the fibres are left undamaged in the resin block.

Staining of plastic sections

Dyck and Lais (1970) viewed thick sections of the teased fibre under a phase-contrast microscope. Spencer and Thomas (1970) and Smith *et al.* (1982) did not describe the light microscopy of plastic sections. In our laboratory, routine semithin (0.5 to 1 μm) plastic sections of peripheral nerves are stained with toluidine blue for 15 to 20 seconds on a 120°C hot plate for examination under the light microscope. In pilot studies, semithin transverse sections of single teased nerve fibres were stained with toluidine blue for 15 seconds. The

fibres in these sections were very pale and could hardly be distinguished under the light microscope. The increase in the thickness of the sections from 0.5 μm to 2 μm did not improve the staining. The reason for the pale staining is not clear. A possible reason is that the repeated resin polymerization (4 times for cross sections and 3 times for longitudinal sections) may make it difficult for the dye to infiltrate the section. This hypothesis was tested in two ways. The first was to increase the duration of staining and the second was to change the constituents of the toluidine blue staining solution.

The staining time was progressively increased from 15 seconds to 30 seconds, 1 minute, and then at 1 minute intervals up to 20 minutes on a 120°C hot plate. Better contrast of the fibres was obtained with the increase of staining time from 15 seconds to 10 minutes. But the contrast obtained by different staining periods from 11 minutes up to 20 minute was not significantly different, and the staining deposit increased with the prolongation of staining time probably due to the rapid evaporation and boiling of the staining solution. In order to avoid boiling the staining solution and decrease the evaporation of the staining solution, the staining temperature was decreased from 120°C to 98°C. It was found that the contrast obtained by staining at 120°C for 10 minutes was similar to that at 98°C for 10 minutes.

Routinely, 1000 ml toluidine blue solution contains 10 g toluidine blue and 10 g borax. Borax is used to "open the resin" to facilitate infiltration of the specimen by the dye. However, increasing the amount of borax in the staining solution was not successful and the staining of sections with modified toluidine blue solution (10 g toluidine blue and 20 g borax) for 8 minutes at 120°C was similar to that of sections stained with routine toluidine blue solution for 10 minutes at 98°C except that there was more staining deposit in the former. Therefore 10 minute staining using the routine toluidine blue solution at 98°C was selected to stain fibres in transverse sections. In the same way, 8 minute staining of

toluidine blue at 98°C or 5 minute at 120°C was determined to be the best compromise in the preparation of the longitudinal sections.

Loss of some of the components of MFs during the long period of processing, especially during tissue softening, might also contribute to the pale staining. This requires further investigation and is beyond the scope of this thesis.

2.4 EXAMPLES OF APPLICATION OF NEW TECHNIQUE IN THE INTERPRETATION OF TEASED NERVE FIBRE ABNORMALITIES

Four human sural nerve biopsies examined in the Neuropathology Section of the Institute of Medical and Veterinary Science (IMVS), Adelaide, were selected for this study, including 1 postmortem control nerve, 1 surgical biopsied nerve from a patient with sensory neuropathy with mitochondrial abnormalities, 1 surgical biopsied nerve from a patient with uraemic neuropathy, and 1 postmortem biopsied nerve from a patient with IgM anti-GM1 neuropathy (table 2-5). Sural nerve biopsies and nerve preparations for conventional studies were performed according to the standard methods (Cash and Blumbergs, 1995), which are described in Appendix A. The clinical features and conventional pathologic findings of these nerves are detailed in Appendix B.

Table 2-5. Summary of clinical features of the nerves used in this study

Nerve	Side	Age	Sex	Biopsy	Diagnosis
1	left	44	F	postmortem	suicide drowning, depression
2	left	56	M	surgical	sensory neuropathy with mitochondrial abnormalities
3	right	45	M	surgical	uraemic neuropathy
4	left	44	F	postmortem	anti-GM1 neuropathy

Single MFs were easily teased in resin after the nerve fascicles were softened in resin. Teased fibres were classified according to Dyck *et al.* (1993*a*) and Kalichman *et al.* (1999). Fibres with less than 5 internodes were excluded from this study except for fibres showing typical features of Wallerian degeneration (Dyck *et al.*, 1993*a*) or non-specific change in which the nodes of Ranvier are difficult to identify (Kalichman *et al.*, 1999).

Step cross sections were performed through a segment at least 3000 μm in length in each fibre. Cross sections were performed on 100 fibres and longitudinal sections on 6 fibres.

2.4.1 Condition A (Dyck classification)

Dyck Criteria: Teased fibre of normal appearance, ignoring criteria of internode length and of internode diameter. Myelin is not more irregular than in most MF internodes of the control. This judgement assumes that the observer is aware that myelin regularity varies with the preparation used, the species, the nerve assessed, and age. The average thickness of myelin of the internode with the thinnest myelin is 50% or more of that of the internode with the thickest myelin. No paranodal or internodal segmental demyelination is seen (Dyck *et al.*, 1993*a*).

Eighteen teased fibres from the postmortem control nerve showing normal external appearance as described above (condition A; Dyck *et al.*, 1993*a*) were transversely sectioned. All 18 fibres had approximately equally long internodal segments and the length of the shortest internode was more than 50% of that of the longest internode within the one fibre (Fig. 2-5). Cross sections revealed that the thickness of the myelin sheath in compact myelin regions remained the same along the length of the fibres (eg, L2, 4, 9, 10, 11, 13, 15, 16, 19, 21, 23, 25, and 28–32 in Fig. 2-5) and that the variation in axonal diameter in these regions was very small. The axonal diameter at SLCs (eg, L1, 3, 5–8, 12, 14, 17, 20, 22, 24, 26, 27 and 33 in Fig. 2-5) was smaller than that at compact myelin regions and varied considerably. For example, axonal diameter in L24 and L27 is significantly smaller than that in L5 in Fig. 2-5. Simple myelin infolding was occasionally found in the cross sections through externally normal regions (eg, Level 21 in Fig. 2-5). Complex myelin infolding or outfolding was not found. Complex myelin splitting, active myelin degeneration, abnormal axonal compaction and axonal degeneration were not detected in the cross sections. Schwann cell nuclei were usually found in cross sections in the middle of the internodes (eg, L14 in Fig. 2-5).

Four teased fibres from the patient with sensory neuropathy with mitochondrial abnormalities and 2 fibres from the patient with uraemic neuropathy showing the normal external appearance of condition A (Dyck *et al.*, 1993*a*) and approximately equally long internodes (the length of the shortest internode > 50% of the longest internode) were transversely sectioned. Cross sections of these fibres revealed similar features to those found in the fibres from the postmortem control nerve.

Five fibres showing the normal external appearance of condition A (Dyck *et al.*, 1993*a*) and excessive irregularity of internodal length (the length of the shortest internode < 50% of the longest internode) from the patient with sensory neuropathy with mitochondrial abnormalities were also transversely sectioned. Myelin infolding and/or outfolding were found in 4 fibres (eg, L36 in Fig. 2-6). Myelin debris in Schwann cell cytoplasm was found in cross sections through externally normal sites in 4 fibres (eg, L23 in Fig. 2-6). Myelin debris in Schwann cell cytoplasm was never found in the cross sections of the shortest internode and was usually present in the cross sections of the internodes adjoining the shortest internodes (eg, L23 and L39 in Fig. 2-6).

Summary

Teased nerve fibres with the external appearance of condition A (Dyck *et al.*, 1993*a*) and regular internodal length show normal internal structure on cross sections and can be classified as normal fibres.

Teased fibres with the external appearance of condition A (Dyck *et al.*, 1993*a*) and excessive irregularity of internodal length may show various abnormal changes on cross sections.

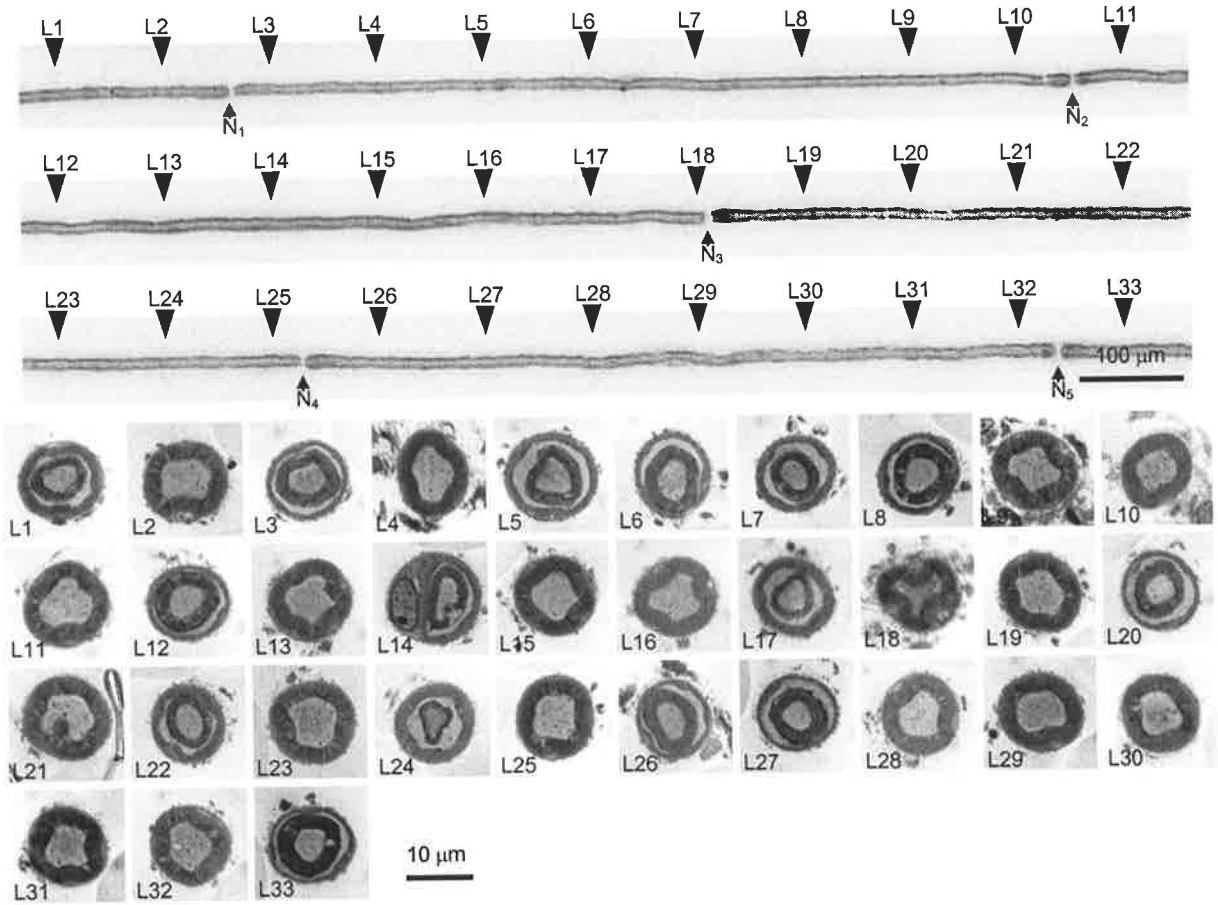

Figure 2-5. Light micrographs. The 3 upper panels show part of an externally normal teased fibre from the postmortem control sural nerve. The teased fibre was digitized using a Quantimet 500MC Image System. The thickness of myelin sheaths is regular within and between internodes. The nodes of Ranvier are indicated by arrows (N_1 to N_5). The length of the internodes is regular, 792 µm in the first internode (N_1–N_2), 755 µm in the second internode (N_2–N_3), 719 µm in the third internode (N_3–N_4), and 709 µm in the fourth internode (N_4–N_5). The 4 lower panels are transverse sections through the designated sites of the teased fibres at regular intervals of 100 µm. Cross sections were stained with toluidine blue and digitized using an Olympus DP11 Microscope Digital Camera System. The thickness of myelin sheaths in compact myelin regions (L2, 4, 9, 10, 11, 13, 15, 16, 19, 21, 23, 25, 28, 29, 30, 31 and 32) remains the same along the length of the fibres and the variation of axonal diameter in these regions is very small. SLCs are present at 15 levels (L1, 3, 5, 6, 7, 8, 12, 14, 17, 20, 22, 24, 26, 27 and 33). The axonal diameter at SLC regions is smaller than that at compact myelin regions. The axonal diameter at different SLCs varies considerably. For example, the axonal diameters in L24 and L27 are significantly smaller than that in L5. Simple myelin infolding is present at L21. A Schwann cell nucleus is present at L14 in the middle of the second internode. L18 is a cross section through the paranodal region and the axon is of fluted shape.

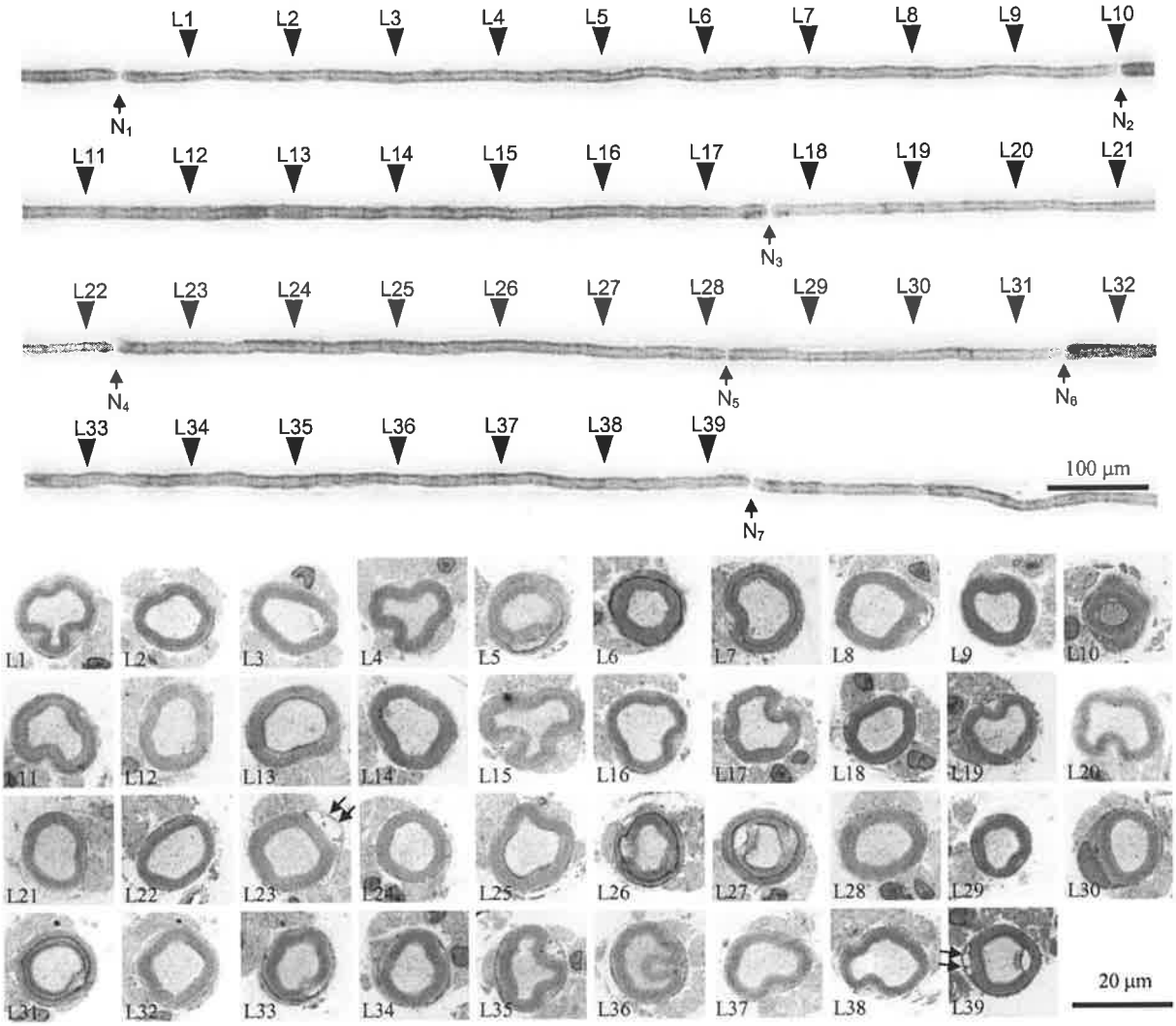

Figure 2-6. Light micrographs. The 4 upper panels show a teased fibre from the sensory neuropathy with mitochondrial abnormalities. The nodes Ranvier are indicated by arrows (N_1–N_7). The internodal lengths are irregular, 970 µm for the 1st internode (N_1–N_2), 758 µm for the 2nd internode N_2–N_3), 467 µm for the 3rd internode (N_3–N_4), 590 µm for the 4th internode (N_4–N_5), 329 µm for the 5th internode (N_5–N_6) and 795 µm for the 6th internode (N_6–N_7). The length of the shortest internode (N_5–N_6, 329µm) is less than 50% of the longest internode (N_1–N_2, 970 µm). Externally, the two short internodes (N_3–N_4 and N_5–N_6) are thinner than others, but more than 50% of the thickest internode (N_2–N_3 and N_4–N_5). The four lower panels show 39 cross sections through the designated sites at regular intervals of 100 µm. The compact myelin sheath thickness and the axonal diameter are not significantly different in the different internodes. SLCs are only present in 20% (7/39) cross sections (L5, 6, 7, 26, 27, 31 and 39). The section in L10 with a compacted axon and relatively thick myelin sheath is through a MYSA region. Myelin debris in Schwann cell cytoplasm is found in L23 and L29 (double arrows). L30 is through a Schwann cell nucleus. A simple myelin infolding is present in L36. The teased fibre and the cross sections were digitized using the Quantimet 500MC Image Analysis System.

2.4.2 Condition B (Dyck classification)

Dyck criteria: Teased fibres with excessive irregularity, wrinkling, and folding of myelin but with the other features of condition A. This judgement assumes that the observer is familiar with the degree of myelin regularity considering species, nerve, site, and age (Dyck *et al.*, 1993*a*).

Eighteen fibres showing the external appearance of condition B and approximately equally long internodes (the length of the shortest internode > 50% of that of the longest internode) from the sensory neuropathy with mitochondrial abnormalities were transversely sectioned. In 6 fibres, cross sections showed similar features to those found in fibres with external appearances of condition A and regular internodal length. In 12 fibres, myelin infolding and/or myelin outfolding (eg, L6 and L21 in Fig. 2-7) were present in the cross sections. Redundant myelin folding may be present in cross sections through externally irregular sites (eg, L6 in Fig. 2-7), externally normal sites (eg, L21 in Fig. 2-7) or externally visible myelin folding site (eg, L18-40μm in Fig. 2-7). Step sectional studies revealed the evolution from myelin indentation to myelin infolding (eg, L21 to L21-8μm in Fig. 2-7). Myelin debris in Schwann cell cytoplasm was found in cross sections through externally normal sites in 8 fibres (eg, L16 and L24 in Fig. 2-7). Myelin debris in Schwann cell cytoplasm and redundant myelin folding was found in cross sections of the same internode (eg, L24 and L21 in the internode between N_3–N_4 in Fig. 2-7) or in cross sections of different or adjoining internodes (eg, L16 in the internode between N_2–N_3 and 6 in the internode between N_1–N_2 in Fig. 2-7). Axonal compaction and enlargement of the adaxonal space were not noted in cross sections of these fibres.

Cross section studies were performed on 15 fibres showing the external appearance of condition B and approximately equally long internodes (the length of the shortest internode

> 50% of that of the longest internode) from the uraemic neuropathy. In 3 fibres, transverse sections showed similar features to those found in the fibres with external appearances of condition A (Dyck *et al.*, 1993*a*) and regular internodal length. In 10 fibres, cross sections showed various abnormalities, including complex myelin splitting and/or degeneration in 10 fibres (eg, L1 in Fig. 2-8), enlargement of adaxonal space in 10 fibres (eg, L3 and L5 in Fig. 2-8), axonal compaction at various sites along the fibre in 12 fibres (eg, L1 and L2 in Fig. 2-8), and myelin redundant folding in 8 fibres (eg, L2 in Fig. 2-8). In 2 large fibres, cross sections showed normal internal structure except abnormal variation of axonal calibre along the length of the fibre (Fig. 2-9).

Cross section studies were also performed on 3 fibres showing external appearance of condition B and excessive irregularity of internodal length (the length of the shortest internode < 50% of that of the longest internode) from the sensory neuropathy with mitochondrial abnormalities. A considerable variation in the shape of the fibres in cross sections along the length of the fibre was noted in all 3 fibres. Variation of the shape of MFs is present in different internodes (eg, L6 vs L16 in Fig. 2-10) or within a short segment of the same internode (eg, L15 vs L16 in Fig. 2-10). Myelin infolding and/or outfolding (eg, L16 and L17 in Fig. 2-10) were found in all three fibres, and redundant myelin folding was often found in association with active myelin splitting or degeneration (eg, L17 in Fig. 2-10). There was no consistent relationship between the internodal length and the average axonal diameter in these fibres on morphometry. Table 2-5 shows the internodal lengths and axonal diameters of different internodes of a single teased fibre illustrated in Fig. 2-10.

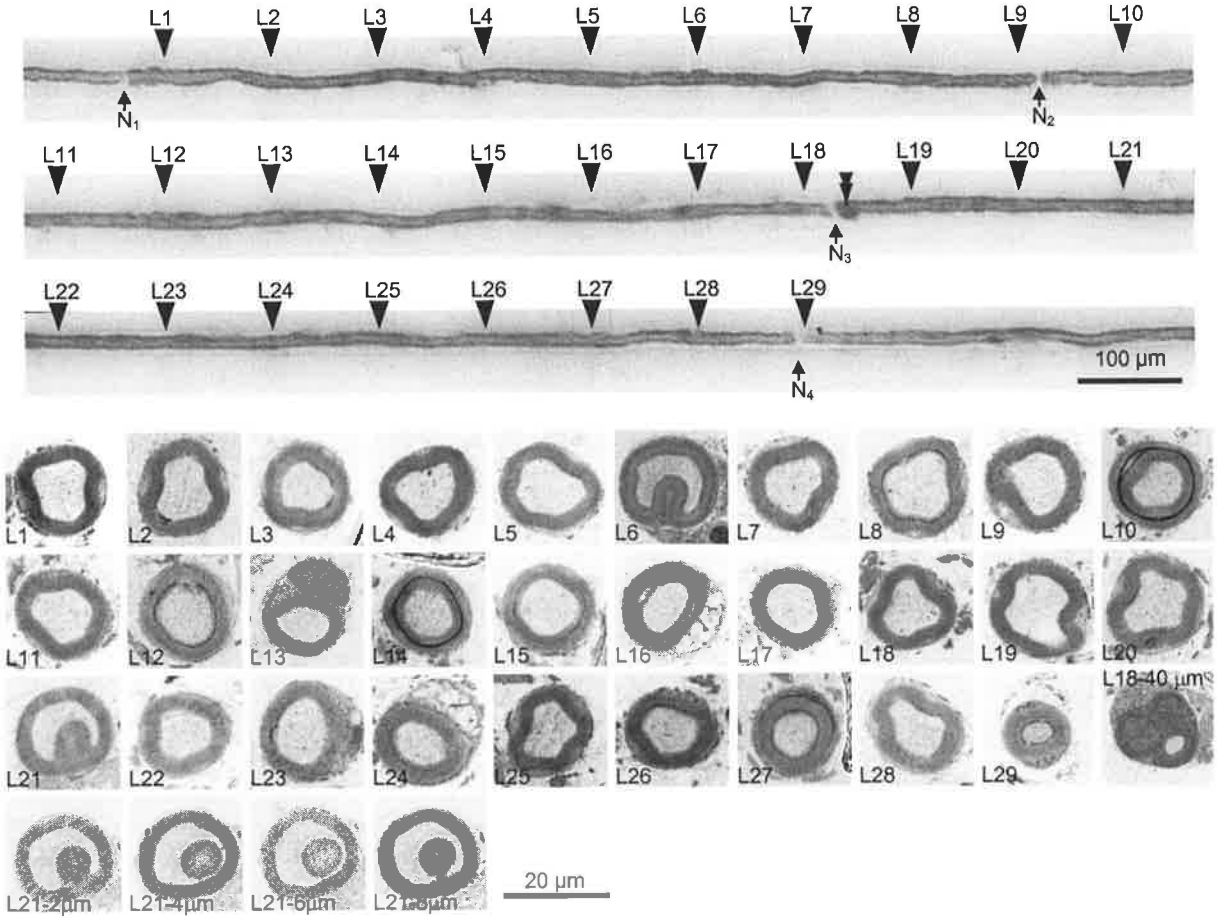

Figure 2-7. Light micrographs. The three upper panels show part of a teased fibre with consecutive and approximately equally long internodes, and myelin irregularity and myelin outfolding (double arrowheads) from the sensory neuropathy with mitochondrial abnormalities. The nodes of Ranvier are indicated by arrows (N_1 to N_4). The three middle panels show cross sections through designated sites at regular intervals of 100 µm. In cross sections, the myelin sheath is of the same thickness in compact myelin regions of the same and different internodes. Myelin infolding is seen at an externally irregular site (L6) and externally normal site (L21). L21-2µm to L21-8µm are step sections at intervals of 2 µm. The evolution from myelin indentation to infolding is clearly seen here. L18-40µm is a cross section through the externally visible paranodal myelin outfolding. A Schwann cell nucleus is seen in the L13 cross section. L29 is through a MYSA paranodal region. Myelin debris in Schwann cell cytoplasm is seen in cross sections through externally normal sites (L16 and L24). In 28 levels through the internodal regions (L1–28), SLCs are present at only 4 levels (L10, L14, L16 and L27). Axonal compaction and enlargement of adaxonal space are not present in the cross sections. Bar = 100 µm for the teased fibre. Bar = 20 µm for cross sections. Plastic cross sections were stained with toluidine blue. The teased fibres and cross sections were digitized using a Quantimet 500MC Image System.

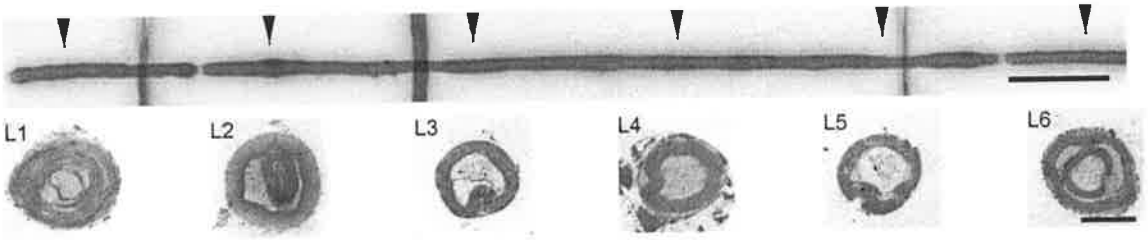

Figure 2-8. Light micrographs. The upper panel is part of a teased fibre showing excessive myelin irregularity from the uraemic neuropathy. The lower panel shows transverse sections through specified sites of the teased fibre at regular intervals of 200 μm. Cross sections show various morphological abnormalities: in L1, there is complex myelin splitting surrounding a contracted axon; in L2, there is myelin infolding; in L3 and L5, there are enlargements of the periaxonal spaces; L4 appears normal; and in L6, a SLC is seen. Bar = 100 μm for the teased fibre. Bar = 20 μm for cross sections. Plastic cross sections were stained with toluidine blue. The teased fibre and cross sections were digitized using the Quantimet 500MC Image Analysis System.

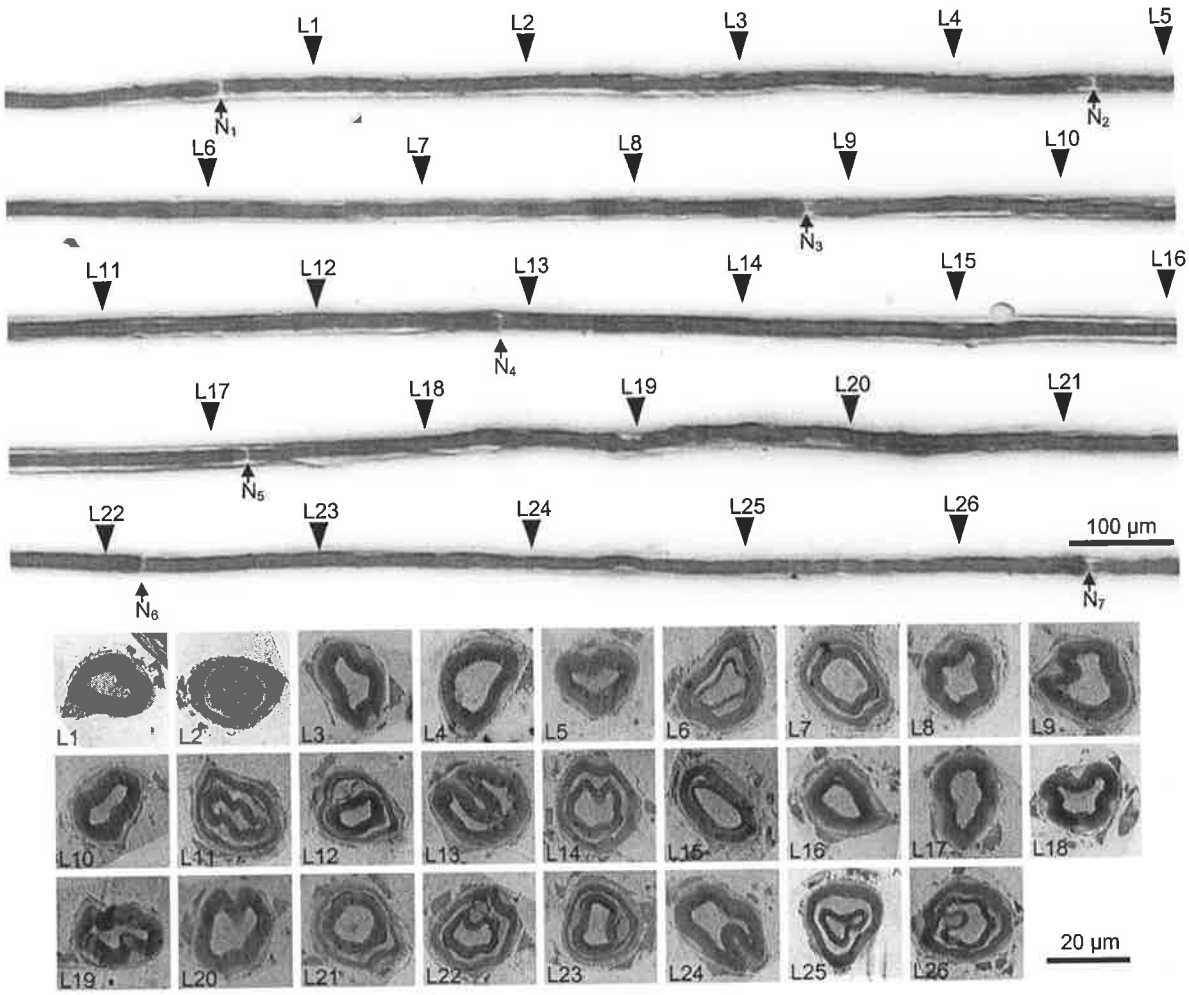

Figure 2-9. Light micrographs. The 5 upper panels are a teased nerve fibre showing external appearance of myelin irregularity from the uraemic neuropathy. The length of the internodes is regular, 820 µm in the first internode (N_1–N_2), 828 µm in the second internode (N_2–N_3), 812 µm in the third internode (N_3–N_4), 861 µm in the fourth internode (N_4–N_5), 1000 µm in the fifth internode (N_5–N_6), and 889 µm in the third internode (N_6–N_7). The 3 lower panels are cross sections of the teased fibre through designated sites at regular intervals of 200 µm. Considerable variation of axonal calibre is seen within the same internode (L19 vs L20) and between neighbouring internodes (L4 vs L5). Teased fibre and cross sections were digitized using the Quantimet 500MC Image Analysis System.

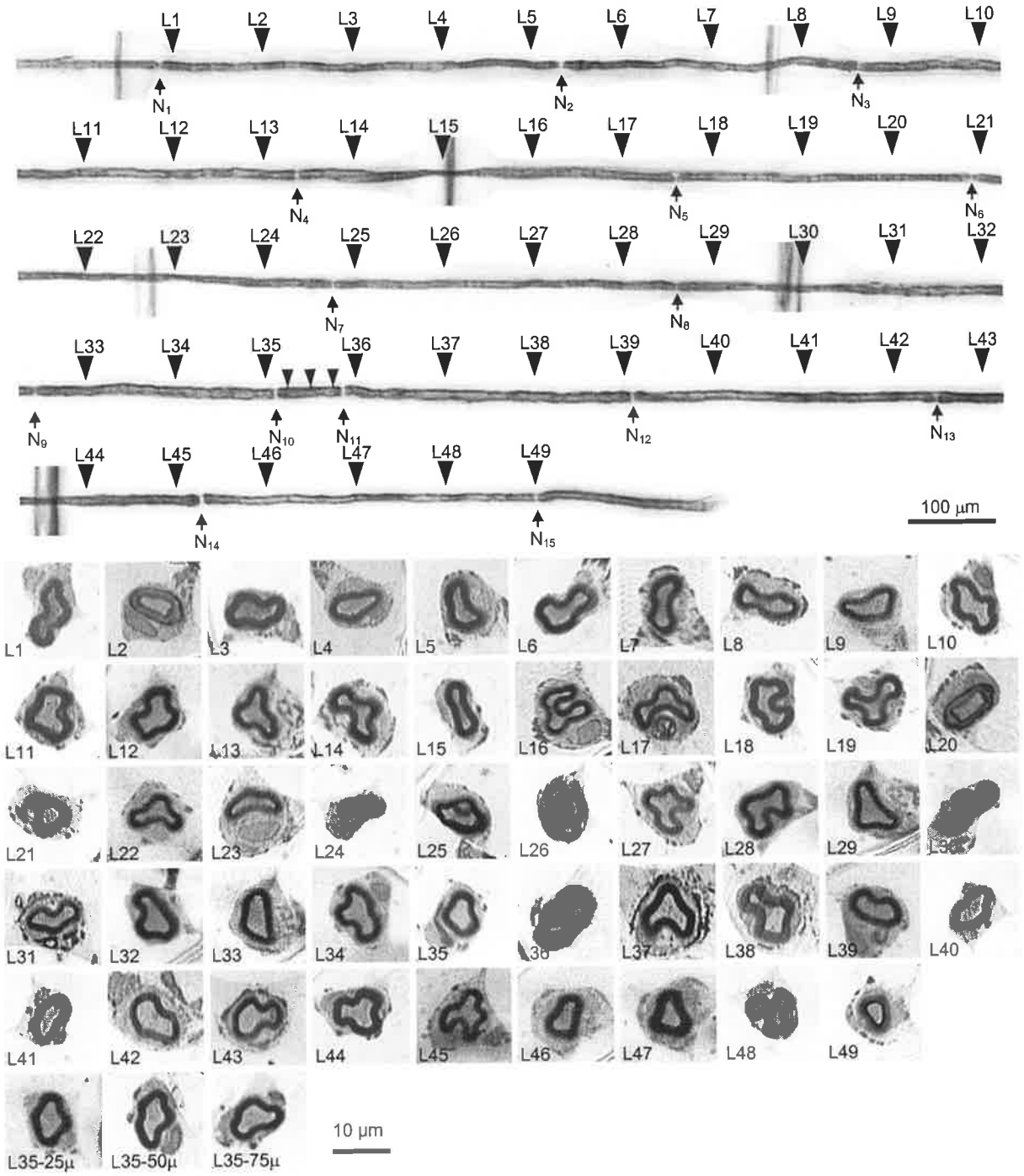

Figure 2-10. The 5 upper panels are a teased nerve fibre showing myelin irregularity and excessive irregularity of internodal lengths from the sensory neuropathy with mitochondrial abnormalities. The shortest internode (N_{10} to N_{11}) is 74 µm in length, only 15.7% of the longest internode (N_3 to N_4, 474 µm) (table 2-3). The five middle panels show cross sections of the fibre at regular intervals of 100 µm, and the lowest panel shows 3 cross sections through the shortest internode beginning 25 µm after L35 at regular intervals of 25 µm. The shape of the fibre on cross sections varies considerably along its length. Indented myelin (L16), myelin outfolding (L26) and outfolding with myelin degeneration (L17) are found. The axonal diameter of the shortest internode (mean ± SD = 4.34 ± 0.11 µm) is not significantly different from that of the longest internode (mean ± SD = 4.44 ± 0.30 µm).

Table 2-5. Internodal length and average axonal diameter of each internode in Fig. 2-10

Internode	1	2	3	4	5	6	7	8	9	10	11	12	13	14
IL (μm)	448	330	474	423	331	384	385	384	268	74	324	339	279	374
Da (μm)	3.60	3.97	4.41	3.18	3.76	3.16	3.72	4.44	4.31	4.34	4.32	4.09	4.70	3.29
SDDa	0.26	0.41	0.30	0.64	0.31	0.43	0.59	0.43	0.63	0.11	0.65	0.98	0.39	0.40

Abbreviations: IL = internodal length; Da = average axonal diameter of each internode; SDDa = standard deviation of axonal diameter.

Summary

Most teased nerve fibres with the external appearance of myelin irregularity show various abnormalities on cross sections although some of these teased nerve fibres (33.3% in the sensory neuropathy with mitochondrial abnormalities and 20% in the uraemic neuropathy) have similar internal structure on cross sections to those found in the teased fibres with normal external appearance and are classified as normal.

In the fibres from the sensory neuropathy with mitochondrial abnormalities, myelin debris in Schwann cell cytoplasm is the typical abnormality and the axon is relatively normal, suggesting primary damage to the myelin or the Schwann cell.

In the fibres from the uraemic neuropathy, axonal compaction and enlargement of the adaxonal space are found in regions with intact myelin sheaths suggesting a primary abnormality of the axon. Abnormal variation of axonal calibre in cross sections along the length of the fibre also support this concept.

2.4.3 Condition C (Dyck classification)

Dyck criteria: Teased fibre with a region or regions of paranodal or internodal segmental demyelination with or without myelin ovoids or balls in the cytoplasm of the associated Schwann cells. Thickness of myelin of the internode with the thinnest myelin is 50 percent or more of that of the internode with the thickest myelin. Myelin of internodes may be regular or irregular. In demyelination, as judged by the high-dry objective of the light microscope (Dyck's terminology, a magnification of ×400 used in this study), no myelin can be recognized. Paranodal demyelination implies that the node of Ranvier can be identified and that the nodal gap is increased beyond that seen in normal fibres. In internodal demyelination the entire internode is demyelinated (Dyck *et al.*, 1993*a*).

According to the criteria described above, fibres of condition C can be sub-classified into two groups: internodal demyelination and paranodal demyelination.

Teased fibres showing internodal demyelination with no visible myelin sheath at × 400 magnification were not common in this study. Only 2 resin teased fibres of this type were obtained from the sensory neuropathy with mitochondrial abnormalities. Due to early technical difficulties transverse sections of the "unmyelinated" internodes were not obtained.

Eight teased fibres showing paranodal demyelination from the IgM anti-GM1 neuropathy were cross sectioned. The external appearance of the internodal regions of these fibres was normal. A total of 34 demyelinated paranodal-nodal-paranodal regions from the 8 fibres were studied. The axons at all of the demyelinated paranodal regions were enclosed by a thin myelin sheath even though it was sometimes not visible under the LM (eg, L17-70μm in Fig. 2-11 and L1-60μm in Fig. 2-12). Electron microscopy confirmed the presence of a

thin residual myelin sheath although in some fibres there was complete loss of the myelin lamellae with only residual basal lamella and collagen (eg, Fig. 2-11). Active myelin degeneration was found in demyelinated paranodal regions and the degeneration became more severe close to the nodes of Ranvier (eg, L8-10μm to L8-90μm and L17-10μm to L17-90μm in Fig. 2-11). Electron microscopy confirmed myelin degeneration at the paranodal region (eg, Fig. 2-11). Axon compaction and/or axonal degeneration were found in cross sections through or close to 60/68 demyelinated paranodes (each PNP consisting of 2 paranodes and 1 node of Ranvier). Axon compaction became more severe close to the nodes of Ranvier (eg, L8-10μm to L8-90μm and L17-10μm to L17-90μm in Fig. 2-11). Compacted axons were usually displaced to one side resulting in enlargement of the adaxonal space (eg, L8-30μm, L8-70μm and L35-80μm in Fig. 2-11). Axonal compaction and enlargement of the adaxonal space were also found in externally normal internodal regions (eg, L17 and L26 in Fig. 2-11, L8-20μm to L8-80μm in Fig. 2-12). The myelin sheaths in these regions were better preserved. Axonal diameter was irregular in the internodal regions. Within one internode, the axon may be compacted (eg, L8 in Fig. 2-12) or normal (eg, L6 in Fig. 2-12). In 8/68 demyelinated paranodal regions, swollen axons were found in association with thin myelin sheaths and enlargement of the adaxonal space (eg, L1-60μm and L1-80μm in Fig.2-11). The axonal calibre in these regions (eg, L1-60μm and L1-80μm in Fig.2-12) was significantly larger than that of neighbouring internodal regions (eg, L4 and L6 in Fig. 2-12).

Six teased fibres showing paranodal demyelination from the IgM anti-GM1 neuropathy were longitudinally sectioned. Longitudinal sections through 9 demyelinated PNP regions were examined under LM. Irregularity of axonal calibre, enlargement of the adaxonal space and myelin splitting and degeneration were found in the demyelinated PNP regions similar to the findings in the transverse sections (Fig. 2-13).

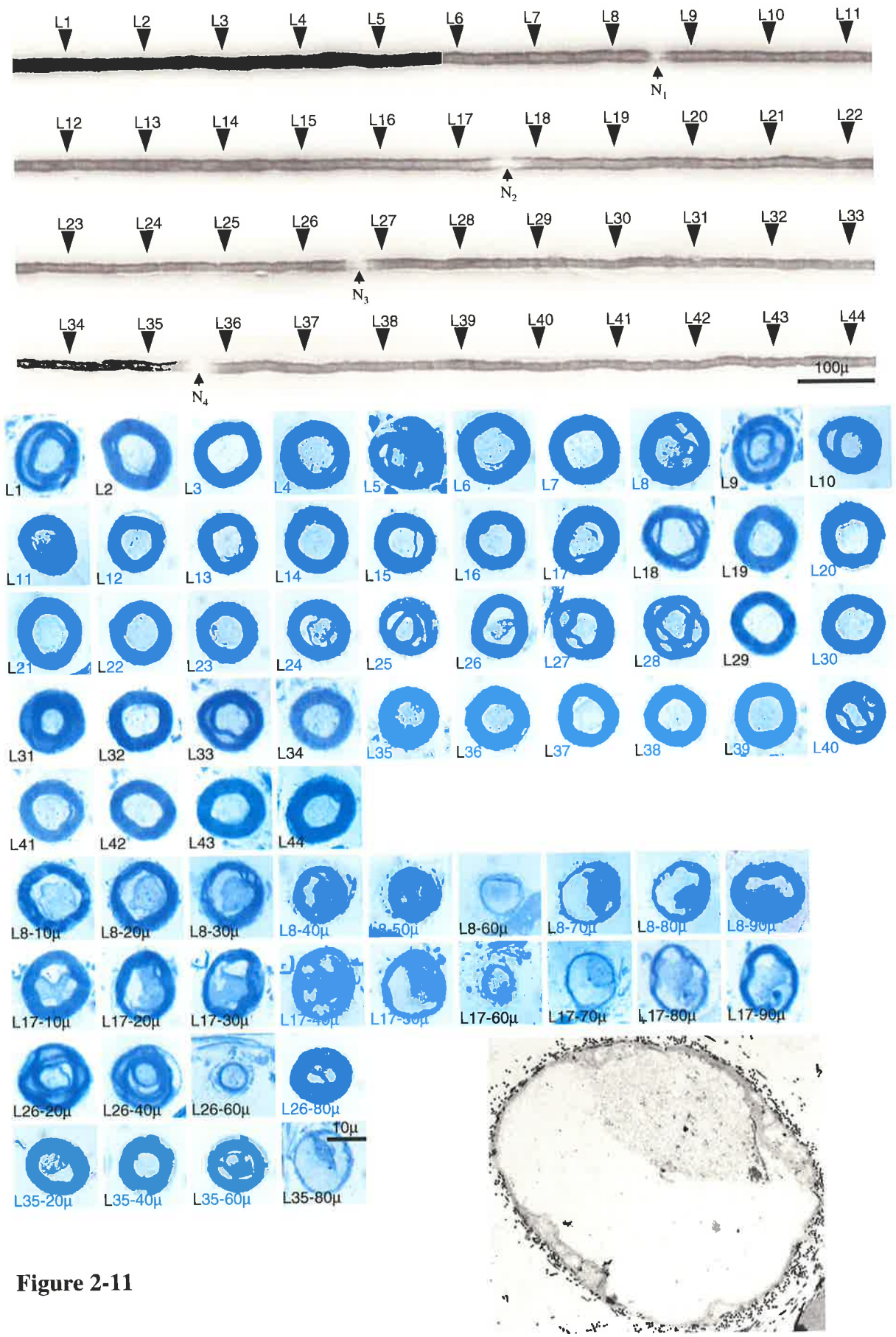
L1 L2 L3 L4 L5 L6 L7 L8 L9 L10 L11
N1
L12 L13 L14 L15 L16 L17 L18 L19 L20 L21 L22
N2
L23 L24 L25 L26 L27 L28 L29 L30 L31 L32 L33
N3
L34 L35 L36 L37 L38 L39 L40 L41 L42 L43 L44
N4
100µ
L1 L2 L3 L4 L5 L6 L7 L8 L9 L10
L11 L12 L13 L14 L15 L16 L17 L18 L19 L20
L21 L22 L23 L24 L25 L26 L27 L28 L29 L30
L31 L32 L33 L34 L35 L36 L37 L38 L39 L40
L41 L42 L43 L44
L8-10µ L8-20µ L8-30µ L8-40µ L8-50µ L8-60µ L8-70µ L8-80µ L8-90µ
L17-10µ L17-20µ L17-30µ L17-40µ L17-50µ L17-60µ L17-70µ L17-80µ L17-90µ
L26-20µ L26-40µ L26-60µ L26-80µ
10µ
L35-20µ L35-40µ L35-60µ L35-80µ

Figure 2-11

Figure 2-11. The four upper panels show a teased fibre from the IgM anti-GM1 neuropathy. The nodes of Ranvier are indicated by arrows (N_1 to N_4). The teased fibre was digitized using the Quantimet 500MC Image System. Except for paranodal demyelination, the external appearance of the fibre is normal. Panels 5 to 9 are cross sections through designated internodal sites at regular intervals of 100 μm. A Schwann cell nucleus is seen at L5. Axon compaction and enlargement of the adaxonal space are present in L17, L26 and L37. The myelin sheaths are preserved in the internodal regions. Panel 10 shows step sections through the demyelinated PNP region between L8 and L9 at regular intervals of 10 μm. Axonal compaction is present in the paranodal regions and is more severe close to the node of Ranvier. Myelin splitting and degeneration is also present in association with axonal compaction, and is more severe close to the node of Ranvier. Panel 11 shows step cross sections through the demyelinated PNP region between L17 and L18 at regular intervals of 10 μm. L17-60μ is sectioned through the node of Ranvier. Axonal degeneration (L17-10μ to L17-50μ) and compaction (L17-70μ), and myelin splitting and degeneration are noted. The right lower picture is an electron micrograph (×5000) adjacent to the semithin plastic section of L17-70μ. The axon is compacted and displaced to one side of the fibre resulting in enlargement of the adaxonal space. No myelin lamellae are seen and only the basal lamella and collagen are present. Panel 12 shows step sections through the demyelinated PNP region between L26 and L27 at regular intervals of 20 μm. Myelin splitting and axonal compaction are present. Panel 13 shows steps sections through the demyelinated PNP regions at regular intervals of 20 μm between L35 and L36. Axonal compaction in association with enlargement of adaxonal space and preservation of the myelin sheath is present at L35-20μ. Severe axonal compaction and an abnormally thin sheath are seen in L35-80μ. Semithin plastic sections were stained with toluidine blue and digitized using the Olympus DP11 Microscope Digital camera system.

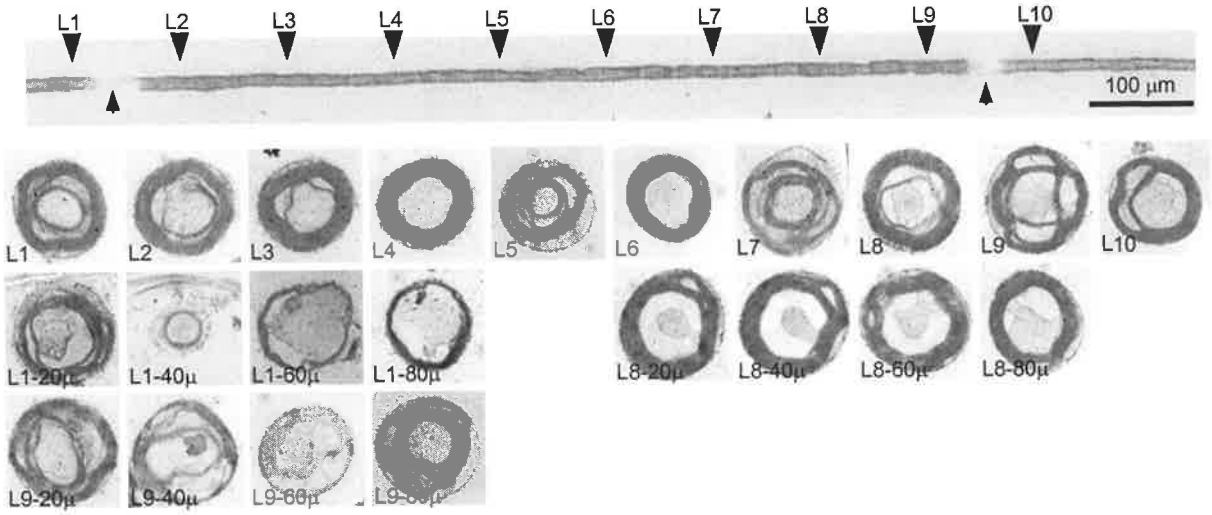

Figure 2-12. Light micrographs. The upper panel is part of a teased fibre from the IgM anti-GM1 neuropathy. The teased fibre was digitized using the Quantimet 500MC Image system. No myelin is seen under LM with a final magnification of ×400 (arrows). The internodal regions are externally normal. The three lower panels show cross sections at designated sites of the fibre. L1-40µ is sectioned through the 1st node of Ranvier. L1-20µ, through the paranodal region to the left of L1-40µ, shows myelin splitting and degeneration, axonal compaction and enlargement of the adaxonal space. L1-60µ and L1-80µ, through the paranodal region to the right of L1-20µ, show thin myelin sheaths, enlarged axons and enlargement of the adaxonal space. The axonal calibre in L1-60µ and L1-80µ is larger than that through the externally normal internodal region (L4 and L6). Myelin splitting is also seen in cross sections through the externally normal internodal region (L2, L3, L5 and L8). Axonal compaction is present in the internodal region (L8 to L9), and the myelin sheath at L8-20µ to L8-80µ is relatively intact. Step cross sections through the second demyelinated PNP region (L9-20µ to L9-80µ) show complex myelin splitting and degeneration in association with axonal compaction and degeneration. Cross section were stained with toluidine blue and digitized using the Olympus DP11 Microscope Digital Camera System.

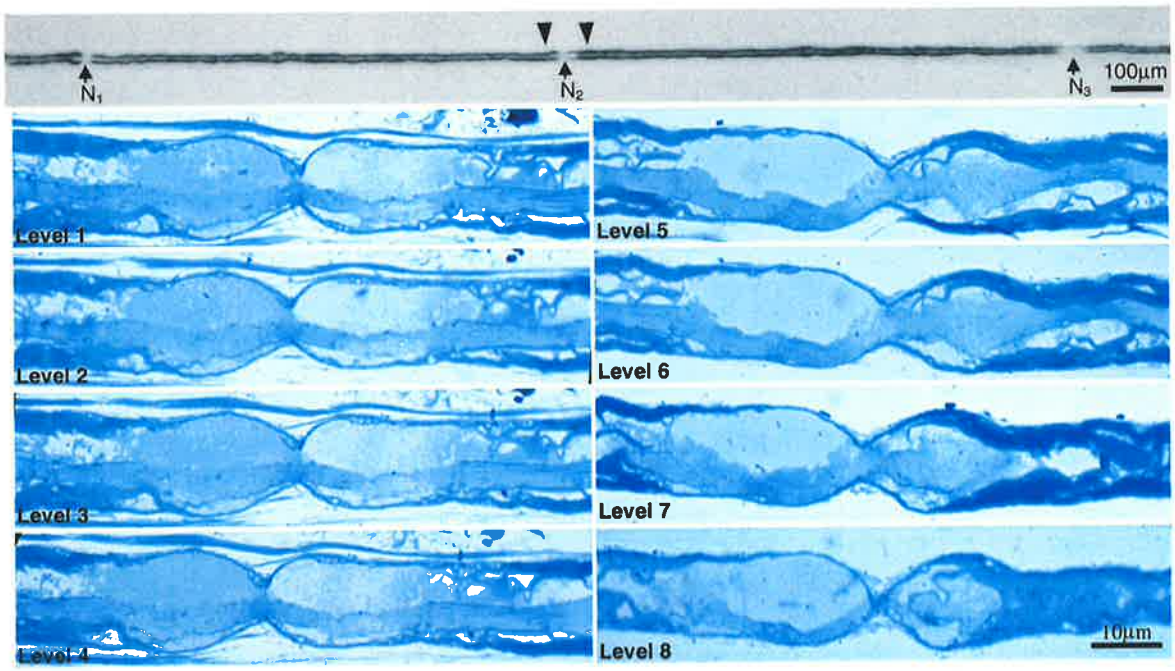

Figure 2-13. Light micrographs. The upper panel is part of a teased fibre from the anti-GM1 neuropathy. Three nodes of Ranvier are indicated by arrows (N_1, N_2 and N_3). Paranodal demyelination is present at the 2nd and 3rd nodes of Ranvier. The lower panels show 8 serial longitudinal sections of this fibre through the segment between the two arrowheads. There is loss of the normal paranodal architecture and the severely compacted irregular axon is enclosed by a very thin myelin sheath. There is a large space between the axon and the myelin sheath. 0.5 μm plastic longitudinal sections stained with toluidine blue. The teased fibre and the longitudinal sections were digitized using the Olympus DP11 Microscope Digital Camera System.

Summary

Both cross and longitudinal section studies of single teased fibres from the IgM anti-GM1 neuropathy demonstrated thin myelin sheaths in paranodal demyelination regions. The thin sheath consisted of residual myelin lamellae and sometimes only of residual basal lamina and collagen. In demyelinated paranodal regions, the axon was usually compacted and sometimes enlarged or swollen. Axonal compaction was also found in externally normal internodal regions, tended to be more severe close to the nodes of Ranvier and irregular in outline. Myelin sheaths in externally normal internodal regions may be relatively well preserved or degenerated. Well-preserved myelin sheaths in association with compacted axons suggests that the axon may be the primary site of damage.

2.4.4 Condition E (Dyck classification)

Dyck Criteria: Teased strand of nerve tissue with linear rows of myelin ovoids and balls at the same stage of degeneration (Dyck *et al.*, 1993*a*). MFs with this external appearance are undergoing axonal degeneration (Dyck *et al.*, 1993*a*).

Fourteen teased fibres showing axonal degeneration were transversely sectioned, including 2 fibres from the sensory neuropathy with mitochondrial abnormalities and 12 fibres from the uraemic neuropathy. Cross sections at different sites revealed various stages of degeneration (Fig. 2-14 and 2-15). The myelin sheath may be relatively preserved in some segments (eg, L3 in Fig. 2-15), and in other segments myelin may be completely lost (eg, L1 and L2 in Fig. 2-15). Axon swelling (eg, L4 in Fig. 2-15) and axon compaction (eg, L5 in Fig. 2-15) may be present in different segments of the same fibre.

Summary

Both axon and myelin may be at the different stages of degeneration in myelinated fibres showing axonal degeneration.

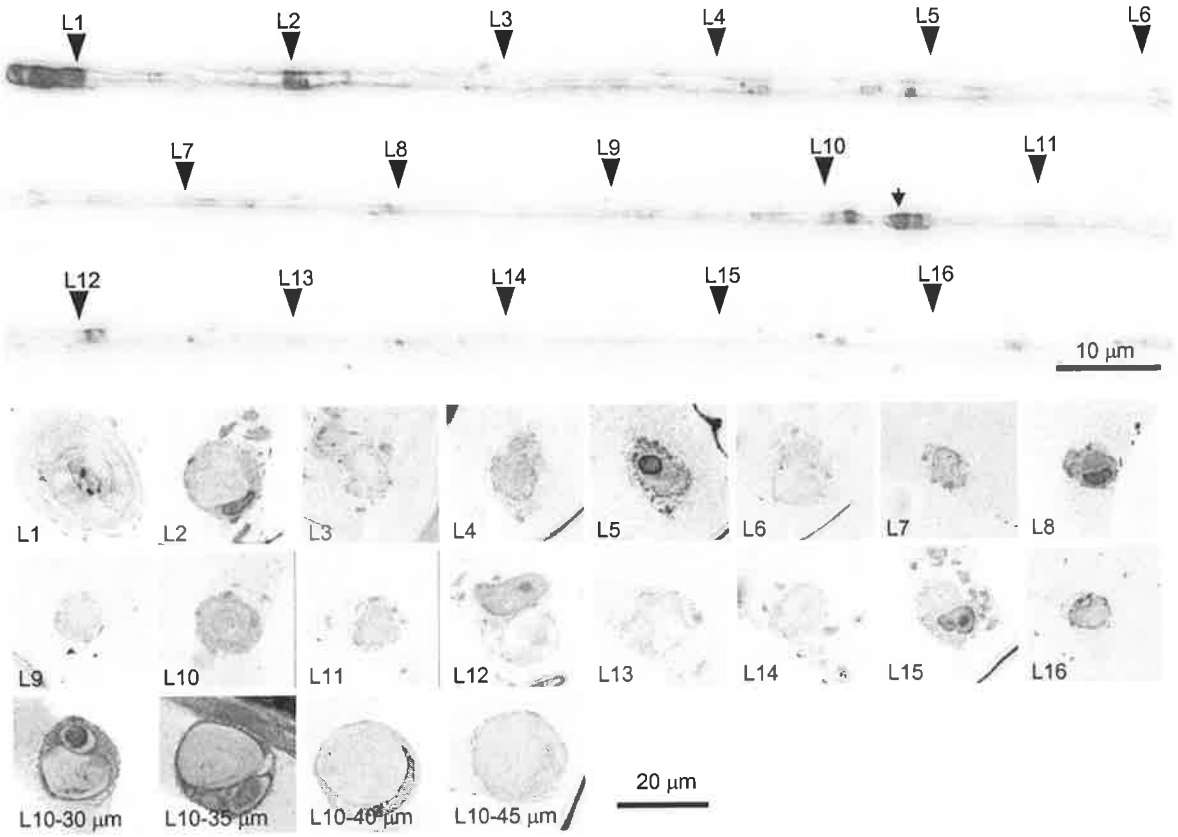

Figure 2-14. Light micrographs. The three upper panels are of a fibre showing Wallerian degeneration from the sensory neuropathy with mitochondrial abnormalities. The two middle panels show cross sections through designated sites (arrowheads) of the fibre at regular intervals of 200 µm. The lowest panel shows step cross sections beginning 30 µm after L10 (arrow). Various stages of myelin and axon degeneration can be seen in the cross sections.

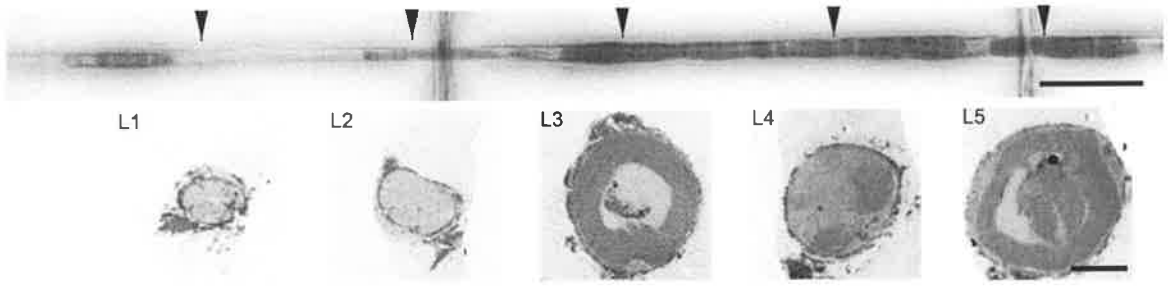

Figures 2-15. Light micrographs. The upper panel is part of a teased myelinated nerve fibre from the uraemic neuropathy, showing axonal degeneration. The lower panel shows transverse sections through specified sites at regular intervals of 200 µm. Transverse sections through L1, 2 and 4 show nearly naked axons with considerable variation of axonal calibre. The cross section at L3 shows an intact myelin sheath surrounding the axon displaying severe degenerative changes. In L5, there is degeneration of the myelin sheath surrounding an otherwise normal compacted axon. The teased fibre and cross sections were digitized using the Quantimet 500MC Image system. Bar = 100 µm for teased fibre, bar = 10 µm for transverse sections.

2.4.5 Condition F (Dyck classification)

Dyck Criteria: Teased fibre without region or regions of segmental demyelination but with excessive variability of myelin thickness among internodes. Thickness of myelin of the internodes with the thinnest myelin is less than 50 percent of that of the internode with the thickest myelin. Myelin of internodes may be regular or irregular (Dyck *et al.*, 1993*a*).

MFs showing the external appearance of condition F as described above are thought to indicate remyelinated fibres (Dyck *et al.*, 1993*a*). The internodal length of the thinly myelinated internodes (remyelinated internodes) is not defined (Dyck *et al.*, 1993*a*). In the illustrations (p541, Dyck *et al.*, 1993*a*) the length of the shortest internode with the thin myelin sheath is less than 50% of the that of the neighbouring externally normal internodes. In practice, thinly myelinated internodes may be abnormally short or of the same internodal length as the neighbouring normal internodes. In order to distinguish these two types, teased fibres with external appearance of condition F were sub-classified into two groups: one with approximately equally long internodes (the length of the thinly myelinated internode > 50% of that of the longest externally normal internode) and the other with excessive irregularity of internodal length (the length of the thinly myelinated internode < 50% of that of the longest internode).

Three teased fibres showing the external appearances of condition F and approximately equally long internodes from the postmortem control nerve were transversely sectioned. In cross sections, the myelin sheaths through the thinly myelinated internodes (eg, L1–4 and L12–19 in Fig. 2-16) were thinner than those of the neighbouring externally normal internodes (eg, L5–11 and L20–31 in Fig. 2-16). In cross sections through the thinly myelinated internodes, indented myelin was occasionally noted (eg, L3 in Fig. 2-16), but complex myelin infolding or outfolding were not detected. Morphometric data revealed that

the average axonal diameter of the thinly myelinated internodes was significantly smaller than that of neighbouring externally normal internodes in 2 fibres (eg, Table 2-6 and Fig. 2-16) and was not significantly different from that of the neighbouring externally normal internodes in 1 fibre. The axons were normal in cross sections of both externally normal internodes and the thinly myelinated internodes. Enlargement of the adaxonal space and myelin debris in Schwann cell cytoplasm were not detected in cross sections of both normal or thinly myelinated internodes.

One fibre of condition F with approximately equally long internodes from the sensory neuropathy with mitochondrial abnormalities was transversely sectioned. Cross sections through the thinly myelinated internodes showed thin myelin sheaths. Complex myelin splitting and active myelin degeneration were not detected. Surprisingly, quantitative studies revealed that the average axonal diameter of the thinly myelinated internodes was larger than that of neighbouring externally normal internodes (Table 2-7 and Fig. 2-17). Myelin debris in Schwann cell cytoplasm was not detected in the cross sections. Abnormal axonal compaction associated with enlargement of the adaxonal space was not found.

Five fibres showing the external appearance of condition F and excessive irregularity of internodal length from the sensory neuropathy with mitochondrial abnormalities were transversely sectioned. In 2 fibres, the sum of the internodal length of the shortest internode and its two adjoining internodes was similar to the sum of two adjacent externally normal internodes. For example, in Fig. 2-18 the 3rd internode (N_3-N_4) is the shortest and the sum of the internodal length of the 2nd, 3rd and 4th internodes (1402 μm) is equal to that of the 1st and 5th internodes (1400 μm). Focal myelin thickenings were present in the paranodal regions adjoining the shortest internode in 4 fibres (eg, small arrowhead in Fig. 2-18 and L3 in Fig. 2-19). Cross section studies revealed redundant myelin infolding or outfolding in the

paranodal focal myelin thickenings (eg, L6-150μ in Fig. 2-18 and L3 in Fig. 2-19) and in 1 fibre the redundant myelin fold was associated with active myelin splitting and degeneration (L3 in Fig. 2-19). Indented myelin or redundant myelin folding was also found in cross sections through externally normal regions (eg, L6 and L12 in Fig. 2-19). Myelin debris in Schwann cell cytoplasm was found in cross sections in 2 fibres (eg, L1 in Fig. 2-19). However, myelin debris in Schwann cell cytoplasm and redundant myelin folding in association with active myelin splitting and degeneration were not detected in the shortest and thinnest myelinated internodes. Because only 2 to 3 levels were obtained in each short and thinly myelinated internode in each fibre, it was not accurate to make a statistical comparison of axonal diameter between the small internode and the externally normal internodes. There was no obvious difference of axonal calibres between the small internodes and the externally normal internodes on visual inspection. Abnormal axonal compaction associated with enlargement of the adaxonal space was not detected in these five fibres.

Summary

MFs of condition F (Dyck *et al.*, 1993*a*) show thinner myelin sheaths on cross sections of the thinly myelinated internodes compared to those of the neighbouring externally normal internodes. The axon may be normal or smaller than that of the neighbouring externally normal internodes.

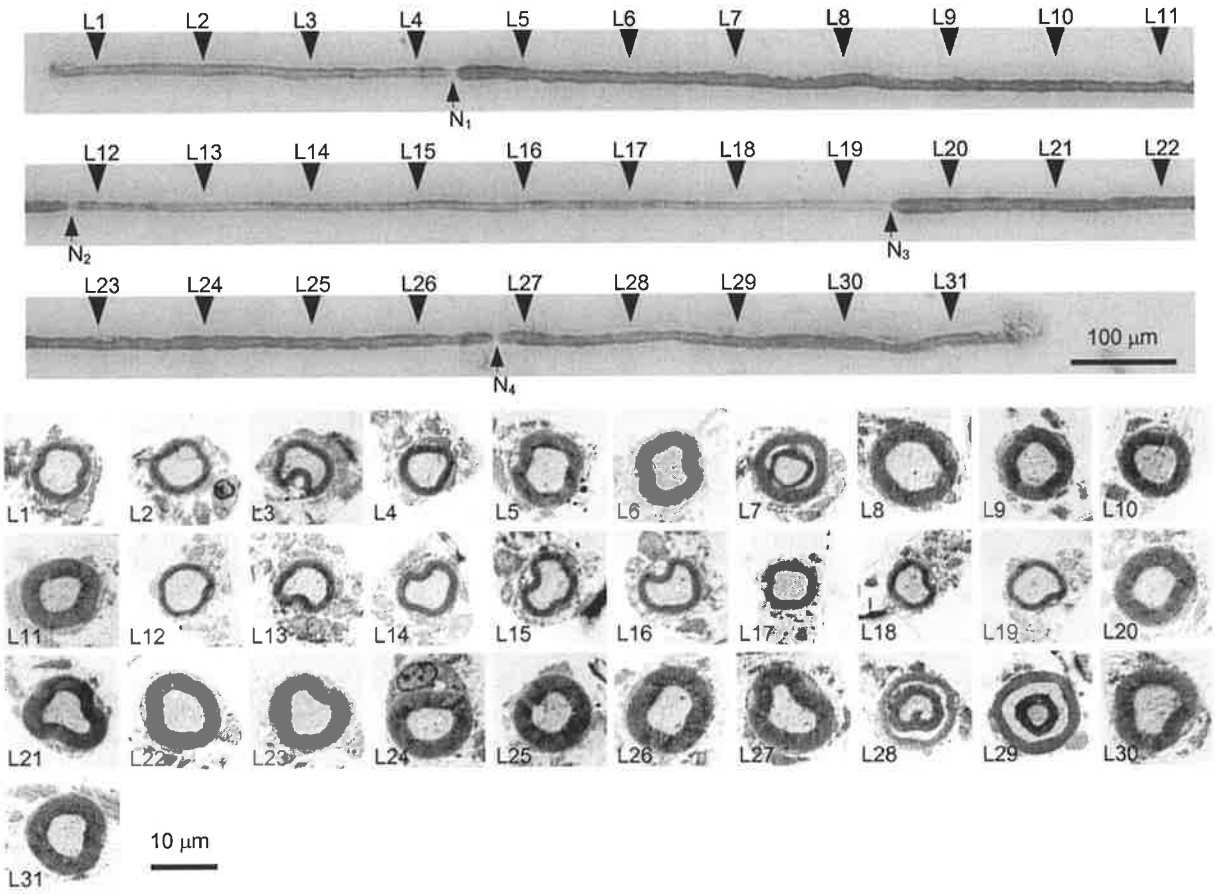

Figure 2-16. Light micrographs. The 3 upper panels show a teased fibre from the sensory neuropathy with mitochondrial abnormalities. Three whole consecutive internodes of approximately equal length are present with the 1st one (N_{1-2}, 1039 µm in length) showing an externally normal appearance, the 2nd one (N_{2-3}, 1075 µm in length) showing a thin myelin sheath, and the 3rd (N_{3-4}, 1022 µm in length) showing an externally normal appearance. Part of a thinly myelinated internode before the 1st node of Ranvier (N_1) and part of an externally normal internode after the 4th node of Ranvier (N_4) are also present. The four lower panels show transverse sections through specific sites at intervals of 100 µm. The axonal diameter (Da) at the compact myelin regions of the externally normal internodes (calculated from L5–6, L8–11, L20–27, and L30-31; mean ± SD = 8.29 ± 0.75 µm) is significantly larger than the axonal diameter of the thinly myelinated internodes (calculated from L1–4 and L12–19; mean ± SD = 7.68 ± 0.59 µm) (student *t* test, $P<0.05$).

Table 2-6. Axonal diameter at designated sites of the teased fibre in figure 2-16

Level	***1***	***2***	***3***	***4***	***5***	***6***	***7***	***8***	***9***	***10***	***11***
Da (µm)	8.47	7.98	7.19	7.34	8.60	7.65	5.97	10.16	8.02	8.02	7.61
Level	***12***	***13***	***14***	***15***	***16***	***17***	***18***	***19***	***20***	***21***	***22***
Da (µm)	8.30	7.46	7.87	7.99	7.99	6.98	6.65	7.90	8.24	7.93	8.58
Level	***23***	***24***	***25***	***26***	***27***	***28***	***29***	***30***	***31***		
Da (µm)	8.37	7.98	6.88	8.82	8.47	5.68	4.38	9.38	7.95		

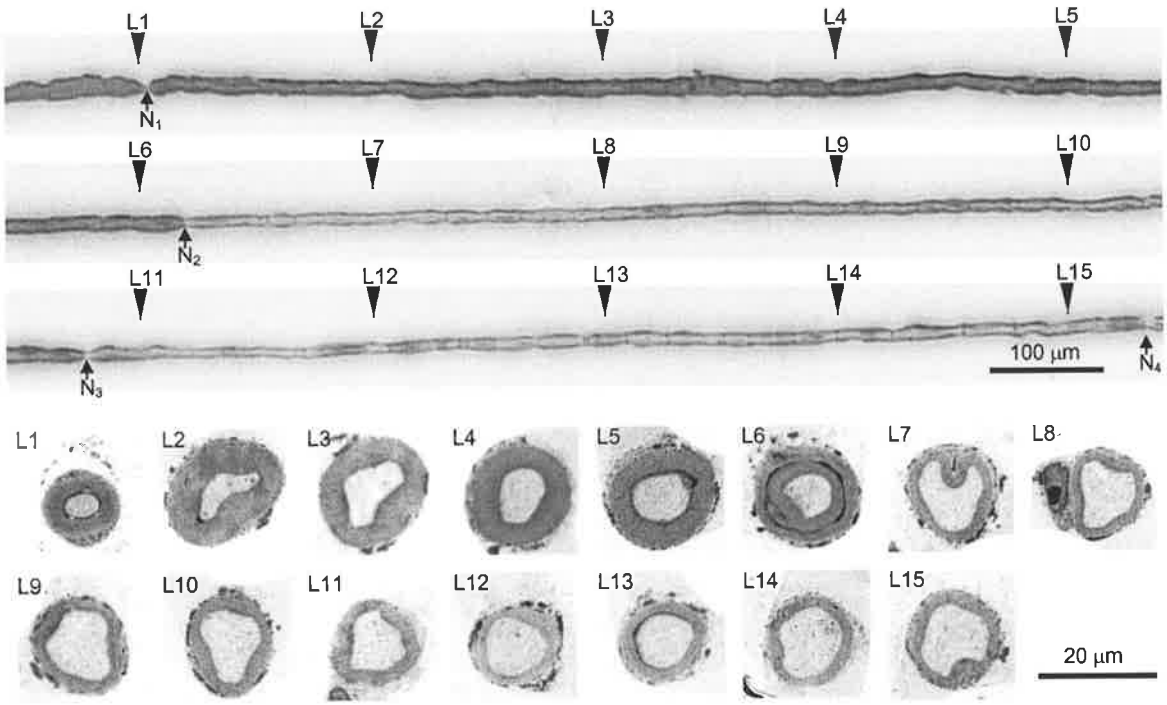

Figure 2-17. Light micrographs. The 3 upper panels show a teased nerve fibre with thinly myelinated internodes from the sensory neuropathy with mitochondrial abnormalities. Three consecutive internodes are present with the 1st internode (N_{1-2}, 968 µm in length) showing a normal external appearance and the 2nd (N_{2-3}, 915 µm in length) and the 3rd (N_{3-4}, 917 µm in length) showing a thin myelin sheath. The two lower panels show transverse sections through the specified sites at regular intervals of 200 µm. L1 is through a paranodal region. The axonal diameter (Da) is 8.1 ± 0.86 µm (mean ± SD) for the 1st internode (calculated from L2–6), 10.5 ± 0.52 µm for the 2nd internode (calculated from L7–10) and 10.1 ± 0.95 µm for the 3rd internode (calculated from L11–15). The axonal diameter of the 1st internode is significantly smaller than that of the 2nd or 3rd internode (student *t* test, $P<0.01$). If cross sections through SLCs are not taken into the calculation of average axonal diameter of internodes, the axonal diameter of the 1st internode is 8.3 ± 0.71 µm (calculated from L2–5, excluding the cross section through a SLC in L6), still significantly smaller than that of the 2nd internode ($P<0.01$) or the 3rd internode ($P<0.02$). In contrast, the total fibre diameter in cross sections (Ds) of the 1st internode (mean ± SD = 17.4 ± 0.81) is significantly larger than that of the 2nd internode (mean ± SD = 14.8 ± 0.94) ($P<0.01$) and that of the 3rd internode (mean ± SD = 14.3 ± 1.08) ($P<0.01$). The teased fibre and cross sections were digitized using the Quantimet 500MC Image Analysis System.

Table 2-7. Axonal diameter at designated sites of the teased fibre in figure 2-17

Level	2	3	4	5	6	7	8	9	10	11	12	13	14	15
Da (µm)	7.07	9.04	8.39	8.56	7.23	10.19	10.01	11.19	10.45	9.43	9.66	9.15	11.10	11.13
Ds (µm)	18.25	18.26	16.73	17.30	16.56	15.06	13.37	15.31	15.31	14.33	13.22	13.36	14.69	15.87

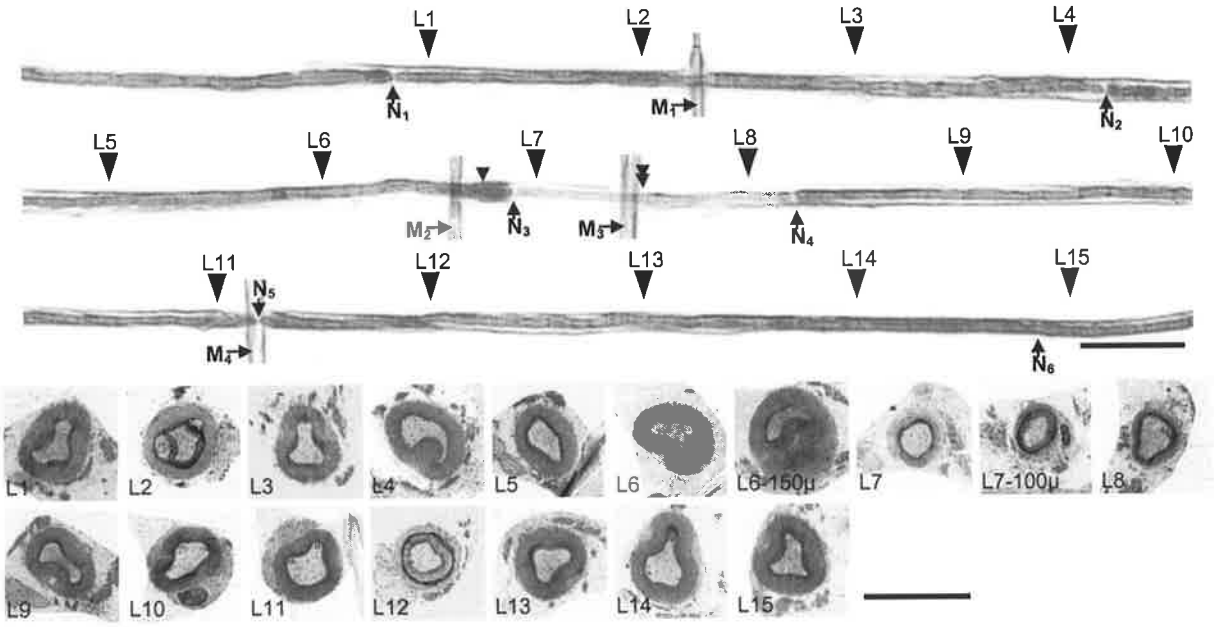

Figure 2-18. Light micrographs. The 3 upper panels show part of a teased nerve fibre showing the external appearance of condition F from the sensory neuropathy with mitochondrial abnormalities. The nodes of Ranvier are indicated by vertical arrows (N_1–N_6). The internodal length of this fibre is excessively irregular, 670 μm in the first internode (N_1–N_2), 542 μm in the second internode (N_2–N_3), 266 μm in the third internode (N_3–N_4), 594 μm in the fourth internode (N_4–N_5) and 730 μm in the fifth internode (N_5–N_6). The second internode (N_2–N_3) is the shortest and thinnest, and the sum of the internodal length of the 2nd, 3rd and 4th internodes (1402 μm) is equal to that of the 1st and 5th internodes (1400 μm). A focal paranodal myelin thickening is indicated by a small arrowhead. Four vertical marker fibres are indicated by horizontal arrows (M_1–M_4). L1 to L15 in the 2 lower panels are cross sections through designated sites (large arrowheads) of the teased fibre at regular intervals of 200 μm. Section L6-150μ (small arrowhead) which is located at 150 μm after L3 and 25 μm after M_3 is through the paranodal myelin thickening. Redundant myelin outfolding is present in L6-150μ. L7-100μ (double arrowheads) is a cross section through the edge of the 3rd marker. Cross sections L7, L7-100μ and L8 are through the 3rd internode. The myelin sheath thickness of the 3rd internode is obviously thinner than that of other internodes, but the axonal calibre of the 3rd internode is not significantly different from that of other internodes. The teased fibre and cross sections were digitized using the Quantimet 500MC Image Analysis System. Bar = 100 μm for the teased fibre. Bar = 20 μm for the cross sections.

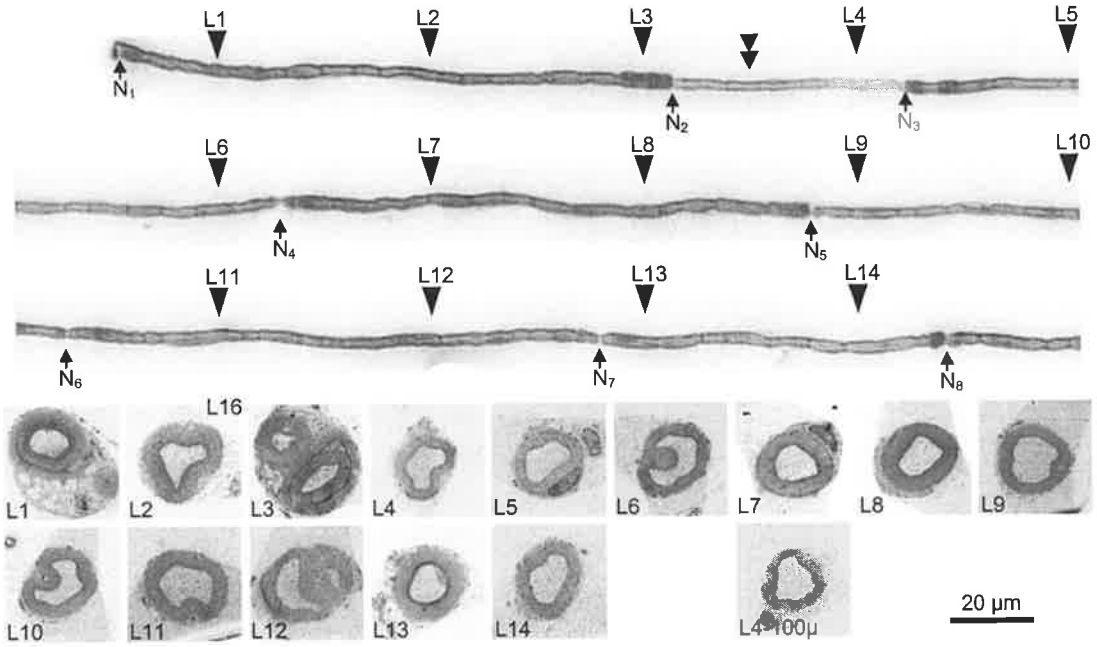

Figure 2-19. Light micrographs. The 3 upper panels show part of a teased nerve fibre with the external appearances of condition F from the sensory neuropathy with mitochondrial abnormalities. The nodes of Ranvier are indicated by vertical arrows (N_1–N_8). The internodal length of this fibre is excessively irregular, 519 μm in the first internode (N_1–N_2), 217 μm in the second internode (N_2–N_3), 416 μm in the third internode (N_3–N_4), 499 μm in the fourth internode (N_4–N_5), 301 μm in the fifth internode (N_5–N_6), 500 μm in the sixth internode (N_6–N_7) and 325 μm in the seventh internode (N_7–N_8). The second internode (N_2–N_3) is the shortest and thinnest. A paranodal myelin thickening is indicated at L3. The two lower panels are cross sections of the teased fibre through designated sites. Myelin debris in associated Schwann cell cytoplasm is clearly seen in L1 through an externally normal site. Cross section L3 is through the paranodal focal myelin thickening and shows redundant myelin outfolding and myelin splitting and degeneration. Redundant myelin outfolding (L12) and indented myelin (L6 and L10) are also seen in cross section through externally normal sites. Sections L4 and L4-100μ (small double arrowheads) are through the second (shortest and thinnest) internode. There is no obvious difference of axonal calibre between the second internodes and other internodes. The myelin thickness of the first internode (L2) and the fourth internode is thicker than that of the second (L4 and L4-100μ) and third (L5 and L6) internodes. The teased fibre and cross sections were digitized using the Quantimet 500MC Image Analysis System.

2.4.6 Non-specific change

Dyck *et al.* (1993*a*) didn't include this category in their classification system. However, teased fibres showing "unclassifiable changes" are often encountered in practice (Kalichman *et al.*, 1999). Pale fibres with unrecognizable nodes of Ranvier along the length of the fibre, short fibres and intertwined bundles of fibres were described by Kalichman *et al.* (1999) as unclassifiable teased fibres. As an experienced investigator should be able to obtain teased fibres of adequate length for diagnostic or research purposes and separate the intertwined bundles, only fibres, which showed the following external appearance, were classified as showing non-specific change in our study.

Criteria: A teased fibre with a minimum length of 3000 μm showing a very pale external appearance and nodes of Ranvier which can not be reliably identified along the length of the fibre.

Four teased fibres showing non-specific changes from the uraemic neuropathy were transversely sectioned. Cross section studies in 2 fibres revealed axons enclosed by thin pale myelin sheaths along the whole length of the fibres (eg, Fig 2-20). In another 2 fibres, cross section studies revealed bundles of unmyelinated axons joined together by collagens consistent with a band of Büngner (Fig. 2-21) (Personal communication PK Thomas, Royal Free Hospital, UK).

Summary

Teased nerve fibres with pale external appearance and non-recognisable nodes of Ranvier may represent thinly myelinated fibres or regenerating bands of Büngner.

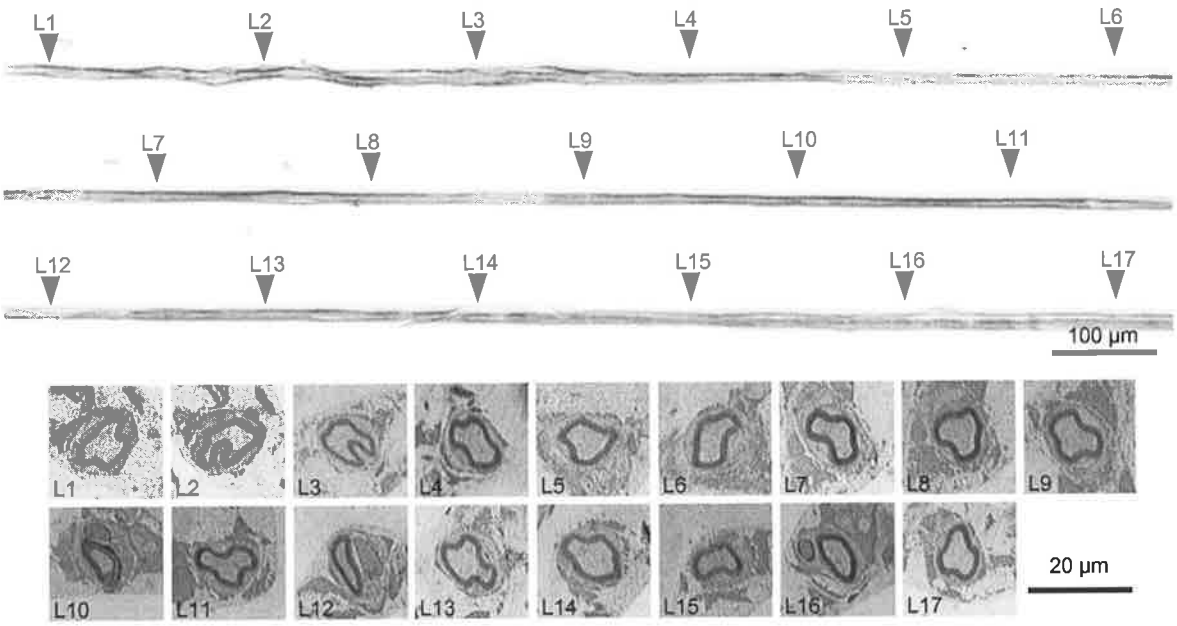

Figure 2-20. Light micrographs. The three upper panels show part of a teased fibre from the uraemic neuropathy. Nodes of Ranvier cannot be reliably recognized in the fibre. The two lower panels show cross sections of the fibre through designated sites at regular intervals of 200 µm. Cross sections show that a single axon is enclosed by a thin pale myelin sheath through the whole length of the fibre. Teased fibre and cross sections were digitized using the Quantimet 500MC Image Analysis System.

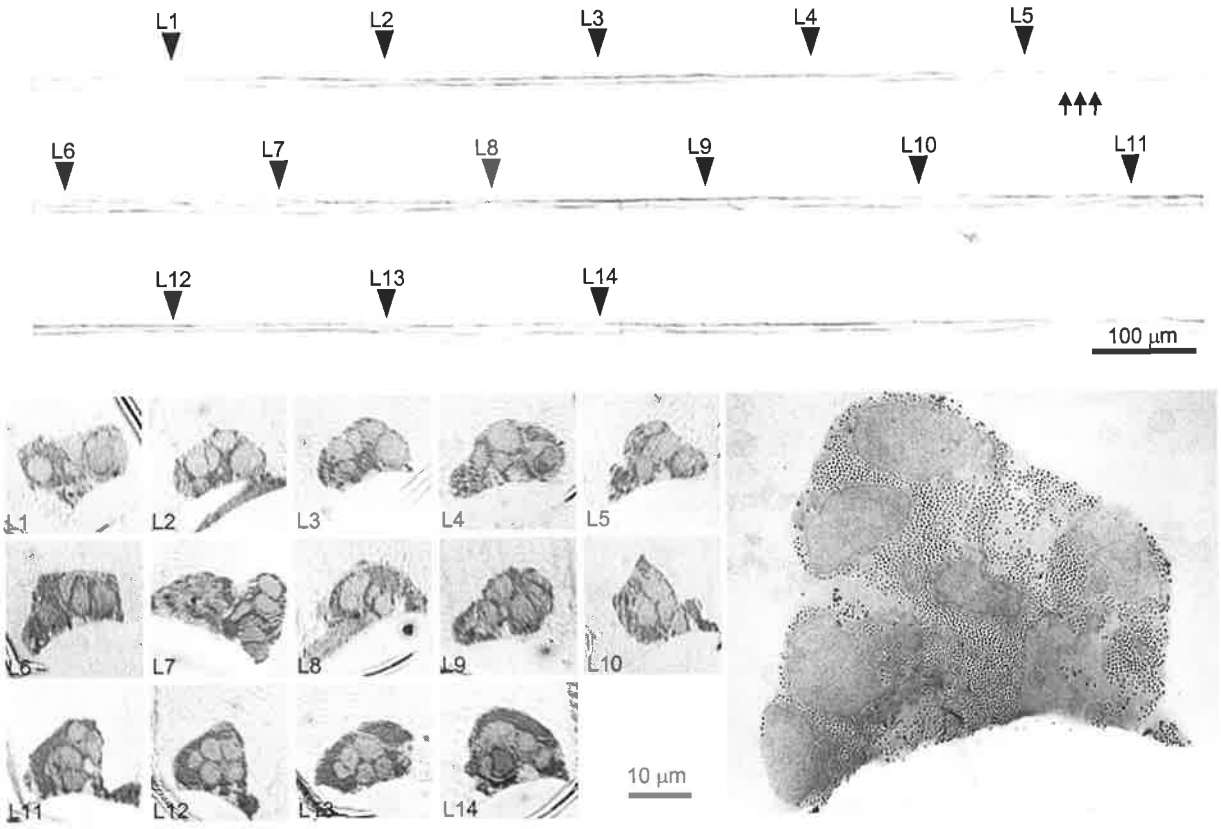

Figure 2-21. The three upper panels show a teased fibre from the uraemic neuropathy. Externally the fibre is so pale that in some areas the fibre looks discontinuous (arrows) and no nodes of Ranvier can be identified along the whole length of the fibre (non-specific change). The left lower panels are toluidine blue stained 0.5 µm plastic cross sections through specified sites of the fibre at regular intervals of 200 µm. The teased fibres and semithin plastic sections were digitized using the Quantimet 500 MC Image System. The lower right picture is an electron micrograph of a section taken 10 µm beyond the marker at L2 (×5000). The EM illustrates seven unmyelinated axons joined together by collagen consistent with a band of Büngner.

2.5 DISCUSSION

2.5.1 Advantages of the new technique

Techniques for the examination of transverse sections of isolated nerve fibres were first reported thirty years ago (Dyck and Lais, 1970; Spencer and Thomas 1970), but have not been much utilised. This may be due to the difficulties in technical reproduction and time-consuming nature of the work. Several problems are encountered with these previously described techniques. First, when placing the teased nerve fibres in a mould or dish containing fresh resin for the initial resin polymerization (Dyck and Lais, 1970; Smith *et al.*, 1982; Spencer and Thomas 1970), the teased fibres are easily twisted and damaged during the transfer from the slide to the mould, and the soft fibres tend to curve and twist during the resin polymerization creating difficulties in localizing specific sites and accurate cross sections. Second, it was also difficult to mark specific sites on the teased fibres in the mould for accurate correlation of external and internal structure. Although areas of interest in fibres embedded in an epoxy plate can be cut out of the resin and re-mounted in another epoxy block for sectioning (Dyck and Lais, 1970), this is not as effective as our modification. Sectioning even through a short length, such as 2-4 mm, and examining all the cross sections is very time-consuming and tedious. And it is also hard to localize specific sites for morphological and morphometric studies as shown in Figures 2-9, 2-15, 2-16, 2-17 and 2-18. Third, previous methods have been limited to one fibre per block. Our modification allows the simultaneous study of multiple fibres in a single block, which is especially suitable for quantitative studies.

We were unable to obtain longitudinal sections of single fibres using the previously described techniques (Dyck and Lais, 1970; Smith *et al.*, 1982; Spencer and Thomas, 1970) as it is virtually impossible to keep the teased fibres flat in a mould. Our technique overcomes this difficulty (Fig. 2-13). The technique described by Ochoa (1972) for

longitudinally sectioning single teased fibres is not as effective as our modification. Additionally longitudinal sections of single teased fibres of up to 150–200 μm in length could be obtained using the previous technique (Ochoa, 1972), while our technique enables to obtain longitudinal sections of more than 2000 μm in length.

Compared to the previous methods, this new refined technique has the following advantages. (1) Marker fibres facilitate the localization of specific points along the teased fibres for light and electron microscopic cross sectional studies. (2) Teased fibres are kept straight by hardening and fixing the fibres to glass slides which prevents movement during subsequent embedding and multiple resin polymerization. This is important for quantitative studies where true cross sections are required. (3) Carbon coating enables easy separation of the resin block from the slide without damaging the nerve fibres. (4) More than one teased fibre can be embedded in one resin block, enabling the study of multiple fibres simultaneously. (5) Longitudinal sections of individual teased fibres can be cut from the first resin block if required.

2.5.2 Correlation of external and internal structure of teased fibres

Systematic microscopic evaluation along the length of singly embedded fibres, with regard to the different conditions described by Dyck *et al.* (1993*a*), has not been undertaken previously. Our new technique provides new information to aid in the more accurate classification of teased nerve fibres.

Normal MFs

In teased fibres showing external appearance of condition A (Dyck *et al.*, 1993*a*) and regular internodal length, we found that the thickness of myelin sheaths and axonal calibres remain the same in cross sections along the length of the fibres. Simple myelin infolding or

outfolding may be present in the cross section occasionally. Myelin or axonal abnormalities are not detected in these fibres. Our findings confirm that teased fibres with these external appearances can be classified as normal fibres.

In teased fibres with external appearance of condition A (Dyck *et al.*, 1993*a*) and excessive irregularity of internodal length, myelin debris in associated Schwann cell cytoplasm was found in the cross sections of the fibres from the sensory neuropathy with mitochondrial abnormalities, indicating that most of these fibres were abnormal.

MFs with irregular myelin sheaths

The finding that the majority of teased fibres with myelin irregularity and regular internodal length showed various degrees of myelin and/or axonal abnormalities on cross sections suggests that Dyck condition B fibres (Dyck *et al.*, 1993*a*) with regular internodal length may be pathological. In a patient with uraemic neuropathy, which is a distal axonopathy, Dyck *et al.* (1971*b*) found that the frequency of teased fibres showing myelin irregularity decreased from 65% at the proximal (midcalf) level to 13% at the distal (ankle) level while the frequency of teased fibres showing demyelination or axonal degeneration increased from 18% at the proximal level to 76% at the distal level. They also found myelin irregularity in the internodes neighbouring demyelinated internodes (Dyck *et al.*, 1971*b*). Myelin irregularity was interpreted as the preliminary stage of axonal degeneration and secondary demyelination in uraemic neuropathy (Dyck *et al.*, 1971*b*).

Only myelin abnormalities were noted on the cross sections of teased fibres with irregular myelin sheaths and regular internodal length from the sensory neuropathy with mitochondrial abnormalities, indicative of primary myelin or Schwann cell damage. Both myelin and axonal abnormalities were found on cross sections of the fibres from the

uraemic neuropathy. However, myelin abnormalities were always detected in association with axonal abnormalities, while axonal compaction could be found associated with intact myelin sheath, indicative of a primary axonal damage. Therefore, the different abnormalities on cross sections of teased fibres with myelin irregularity from different neuropathies may be a clue to the underlying pathogenesis.

Transverse sections of teased fibres with irregular myelin sheaths and excessive irregularity of internodal length have not been studied in enough detail (only 3 fibres from the sensory neuropathy with mitochondrial abnormalities) to allow conclusions to be drawn. However, the active myelin splitting and degeneration, considerable variation of the shapes of fibres on cross sections, and variation of axonal calibre along the length of the fibres suggest that these fibres may be at a later stage of degeneration.

Paranodal demyelination

Cross section studies of condition C (Dyck *et al.*, 1993*a*) fibres showing paranodal demyelination have not previously been performed. Our cross and longitudinal section studies of teased fibres from the anti-GM1 neuropathy revealed the presence of a thin residual myelin sheath in most demyelinated paranodal regions although in some fibres there was complete loss of the myelin lamellae with only residual basal lamellae and collagen. Axonal compaction and enlargement of the adaxonal space in all demyelinated paranodal regions and some externally normal internodal regions suggests primary axonal damage in this case. In fibres with paranodal demyelination, the internodal myelin sheaths were smooth and regular without redundant myelin folding in the present anti-GM neuropathy in contrast to the excessive myelin irregularity reported in uraemic neuropathy (Dyck *et al.*, 1971*b*), suggesting a different mechanism of segmental demyelination. The epitope recognized by anti-GM1 antibodies, Gal(β1-3)GalNAc, has been localized to the

axolemmal surface of mature myelinated fibres in and around the nodes of Ranvier (Sheikh *et al.*, 1999*a*). Previous studies of anti-GM1 neuropathy also found structural abnormalities in the nodal and paranodal regions (Griffin *et al.*, 1996; Hafer-Macko *et al.*, 1996; Kaji *et al.*, 1993; Thomas *et al.*, 1991). These findings suggest that: (1) the pathologic changes begin in the nodal and paranodal regions of the myelinated nerve fibres at sites of GM1 ganglioside localised in the axolemma and progress to internodal regions; (2) paranodal demyelination in IgM anti-GM1 neuropathy is due to focal myelin degeneration which is probably secondary to axonal atrophy; (3) binding of IgM anti-GM1 antibodies to antigen(s) localized at the myelin-axon interface may lead to enlargement of the adaxonal space, axonal atrophy and segmental demyelination. Further studies are needed to test this hypothesis.

MFs showing axonal degeneration

Teased fibres showing linear rows of myelin ovoids or balls indicative of axonal degeneration (Dyck *et al.*, 1993*a*). Our studies have demonstrated that the breakdown of the axon and segmentation of the myelin may be at different stages along the length of the fibre. Relatively spared myelin sheaths associated with degenerated or atrophic axons in some regions may represent primary axonal damage in uraemic neuropathy.

MFs with thin myelin sheaths

In primary peripheral nerve cultures, myelination of segments of axonal processes results in local increases in axonal calibre (Pannese *et al.*, 1988; Windebank *et al.*, 1985). Consistent with the suggestion that demyelination or thin myelin sheath are associated with reduced axonal calibre (deWaegh and Brady, 1990; Martini *et al.*, 2001), we demonstrated that axonal diameter of thinly myelinated internodes was significantly smaller than that of neighbouring externally normal internodes in 2 of 3 examined fibres from the control nerve.

However, there was no obvious difference in axonal calibre between the short and externally normal internodes in 5 remyelinated fibres on visual inspection and the axonal diameter of thinly myelinated internodes with normal internodal length was significantly larger than that of the neighbouring external normal internode in 1 fibre from the sensory neuropathy with mitochondrial abnormalities. These findings suggest that there may be different types of axon-myelin interactions in different conditions. More detailed studies are required to clarify this question, such as investigation of neurofilament density and neurofilament phosphorylation in thinly myelinated internodes.

The definition of remyelination varies according to different researchers (Dyck *et al.*, 1993*a*; Kalichman *et al.*, 1999; Sima and Blaivas, 1997). However, it is generally recognized that excessive variability of myelin sheath thickness between internodes is commonly present in remyelinating fibres and that the intercalated internode is a pathologic hallmark of remyelinated fibres. Remyelination is defined by Dyck *et al.* (1993*a*) as excessive variability of myelin thickness between internodes, with the thinnest myelin being less than 50% of that of the internode with the thickest myelin (condition F). They also define focal myelin swellings (condition G) as the result of remyelination. Sima and Blaivas (1997) define segmental remyelination as a fibre showing two or more intercalated internodes surrounded by normally myelinated internodes. Kalichman *et al.* (1999) define remyelination as a fibre showing at least one abnormally short internode (length <60% of longest internode). According to Sima and Blaivas (1997) and Kalichman *et al.* (1999), myelin thickness in remyelinated internodes may be normal or decreased.

The term **intercalated internode** was first used by Renaut in 1881 to describe the short and thin internodes adjacent to the normal thicker and longer internodes in animals. He thought they were evidence that the nerve fibre grew not only from a central cell but also by the

addition of segments distally—a view which is no longer accepted. Intercalated internodes were studied in detail by Lubinska (1958) who found that a demyelinated internode was replaced by one or two shorter internodes and that intact segment of a partially demyelinated internode was always longer than one half of the length of the normal adjacent internode. When the length of several short regenerated internodes were added together, the sum equalled the length of the normal adjacent internodes (Lubinska, 1958). It is now commonly accepted that the intercalated internode is the result of remyelination after demyelination due to various causes and that an intercalated internode results from a demyelinated internode remyelinated by two or more Schwann cells (Dyck *et al.*, 1993*a*). Sima and Blaivas (1997) claim that the intercalated internode is a product of the repair process that follows paranodal demyelination.

In summary, we have provided a novel technique for correlating the external appearance with internal structure at specified sites along the length of individual teased nerve fibres. Detailed examination of transverse and longitudinal sections of single nerve fibres has provided new insight into the interpretation of teased nerve fibres and mechanism of pathological changes. Due to limitations of time, teased nerve fibres of different categories according to Dyck *et al.* (1993*a*) or other researchers (Kalichman *et al.*, 1999; Sima and Blaivas, 1997) will be the subject of further ongoing studies.

CHAPTER 3: Teased Nerve Fibre Studies in Human IgM Anti-MAG Paraproteinaemic Neuropathy

3.1 Introduction **105**

3.1.1 Anti-MAG IgM antibodies and peripheral neuropathy 105

3.1.2 Clinical manifestations in IgM anti-MAG neuropathy 108

3.1.3 Laboratory investigations 110

3.1.4 Pathology of IgM anti-MAG neuropathy 111

3.1.5 Experimental anti-MAG neuropathy 122

3.2 Materials and Methods **125**

3.2.1 Case report 125

3.2.2 Sural nerve biopsy and tissue preparation 125

3.3 Results **126**

3.3.1 Glycerinated teased nerve fibres 126

3.3.2 Correlative study of external appearance with multiple cross sections of single myelinated fibres teased in resin 127

3.3.3 Electron microscopy 134

3.4 Discussion **140**

3.4.1 Anti-MAG IgM monoclonal antibodies 140

3.4.2 Focal myelin thickenings in anti-MAG neuropathy 141

3.4.3 Demyelination in IgM anti-MAG neuropathy 143

3.5 Conclusion **146**

3.1 INTRODUCTION

Autoantibodies have been implicated as potential pathogenic agents in a variety of peripheral neuropathies, including inflammatory polyneuropathies and paraneoplastic neuropathies. The autoantibodies often react with carbohydrate antigens on cell surface glycoconjugates, including glycoproteins, glycolipids, and glycosaminoglycans. The monoclonal autoantibodies that react with neural glycoconjugates are almost always of the IgM class (Reviewed in Quarles and Weiss, 1999; Ropper and Gorson, 1998; Thomas and Willison, 1994). Nobile-Orazio *et al.* (1994) found high titers of IgM antibodies to one or more neural antigens in a large number of patients with peripheral neuropathy. Detailed investigations of the antigen-specificity of IgM paraproteins in patients with monoclonal gammopathy of unknown significance (MGUS) lead to the identification of anti-MAG, -P_0, -PMP22, -sulphatide, -ganglioside, -chondroitin sulphate, -neurofilament and –tubulin reactivity (Kelly *et al.*, 1988; Nobile-Orazio *et al.*, 1987, 1990, 1994; Quarles and Weiss, 1999). MAG and the cross-reactive glycoconjugates P0 and sulfated-3-glucuronyl paragloboside (SGPG) are the most frequently involved antigens (Gosselin *et al.*, 1991; Latov *et al.*, 1988; Nobile-Orazio *et al.*, 1987, 1989, 1992, 1994).

In this chapter the basis for the focal myelin swellings and tomacula is explored by examining the internal structure of individual teased nerve fibres in human IgM anti-MAG paraproteinaemic neuropathy.

3.1.1. Anti-MAG IgM antibodies and peripheral neuropathy

MAG was the first identified target for monoclonal IgM antibodies in patients with demyelinating polyneuropathy and gammopathy (Braun *et al.*, 1982). The most convincing evidence for a causal relationship exists for IgM gammopathies with specificities directed against carbohydrate determinants of MAG. The mechanisms responsible for the

occurrence of anti-MAG antibodies are unknown, but low titers (1:200 or less) of the antibodies are commonly present in normal individuals (McGinnis *et al.*, 1988; Nobile-Orazio *et al.*, 1989), and B-cells capable of secreting anti-MAG antibodies are present at birth (Lee *et al.*, 1990), indicating that anti-MAG antibodies are common and early constituents of the human immune repertoire. They are therefore similar to 'natural autoantibodies' which exhibit low affinities and are non-pathogenic, in contrast to pathogenic autoantibodies which are generated by somatic mutation and affinity maturation in the course of a T-cell dependent immune response (Spitzer *et al.*, 1992; Van der Heijden *et al.*, 1991; Zouali, 1992). The affinities and avidities of these anti-MAG antibodies are significantly increased by the multivalent nature of the antibody-antigen interaction (Ogino *et al.*, 1994).

High titers of anti-MAG IgM antibodies are usually associated with a chronic slowly progressive, predominantly sensory or sensory motor, demyelinating neuropathy (Chassande *et al.*, 1998; Latov *et al.*, 1988; Nobile-Orazio *et al.*, 1994; van den Berg *et al.*, 1996). In 31 cases of neuropathy with IgM monoclonal gammopathy (25 with MGUS and 6 with Waldenström's macroglobulinaemia), Vital *et al.* (1989) found anti-MAG antibodies in 25 of 28 tested cases. In patients with neuropathy associated with benign IgM MGUS, high titers of IgM antibodies to MAG were found in 93% (27/29) of patients by Yeung *et al.* (1991), 56% (42/75) by Nobile-Orazio *et al.* (1994), and in 65% (26/40) by Chassande *et al.* (1998). It is presently estimated that over half of the patients with neuropathy in association with IgM MGUS have a progressive sensory, or sensorimotor, demyelinating neuropathy and monoclonal antibody that reacts with MAG (Latov *et al.*, 1995; Quarles, 1997; Ropper and Gorson, 1998). In most cases with IgM anti-MAG neuropathy, the light chain is kappa (Ellie *et al.*, 1996; Vital *et al.*, 1989; Yeung *et al.*, 1991). Anti-MAG IgM also predicts the development of neuropathy in asymptomatic patients with MGUS (Meucci *et al.*, 1999). On

the other hand, symptoms of peripheral neuropathy may precede the appearance of anti-MAG antibodies in serum (Valldeoriola *et al.*, 1993). In 3 of 33 cases, Ellie *et al.* (1996) found that the identification of the circulating monoclonal antibody was delayed 1-8 years after onset of symptoms. Using confocal microscopy, Gabriel *et al.* (1998) described the deposition of anti-MAG IgM on myelinated fibres prior to a detectable gammopathy. The titer of anti-MAG antibodies does not correlate with the severity of the neuropathy (Nobile-Orazio *et al.*, 1994).

Although initial studies did not find statistically significant differences in clinical and electrophysiologic parameters between paraproteinaemic neuropathy with and without anti-MAG antibodies (Gosselin *et al.*, 1991), recently reported series have shown a significant correlation between clinical, electrophysiologic and pathologic data of peripheral neuropathy and anti-MAG antibody activity in most cases (Chassande *et al.*, 1998; Ellie *et al.*, 1996; Nobile-Orazio *et al.*, 1994; Yeung *et al.*, 1991).

Although disease progression is slow in most cases with IgM anti-MAG neuropathy, nearly half the patients suffer from disability, and severe disability is more likely in patients with predominantly motor neuropathy (Chassande *et al.*, 1998; Ellie *et al.*, 1996; Steck *et al.*, 1999). In a long-term follow-up study, Nobile-Orazio *et al.* (2000) concluded that (i) the majority of patients with neuropathy and anti-MAG IgM have a favourable prognosis even after several years; (ii) current immune therapies, though temporarily effective in half of the patients, are associated with considerable side effects which limit their prolonged use and efficacy, suggesting that until more effective or safer therapies become available, they should probably be reserved for patients impaired in their daily life or in a progressive phase of the disease.

3.1.2. Clinical manifestations in IgM anti-MAG neuropathy

The onset of peripheral neuropathy associated with IgM MGUS is usually after the fourth decade with an average age around sixty and male predominance (Chassande *et al.*, 1998; Kelly, 1990; Nobile-Orazio *et al.*, 1994; Smith, 1994; Vital *et al.*, 1989; Yeung *et al.*, 1991). In 33 cases with neuropathy associated with anti-MAG IgM MGUS, the mean age at onset of the neurological symptoms was 67 years (range 46-81) with a sex ratio of 7.2 (M:F) (Ellie *et al.*, 1996).

Most patients describe the gradual onset and slow progression of symmetrical sensory symptoms and mild distal weakness. A relapsing-remitting form has only been reported in a few patients (Yeung *et al.*, 1991). Predominantly sensory neuropathies were reported in 100% (7/7) of patients by Kelly (1990), 62% (26/42) by Nobile-Orazio *et al.* (1994), 82% (27/33) by Ellie *et al.* (1996), and 77% (23/30) by Chassande *et al.* (1998) in neuropathies associated with IgM MGUS and anti-MAG activity. In 36 patients with neuropathy associated with benign IgM paraproteins, Yeung *et al.* (1991) observed a mixed sensorimotor neuropathy in 31 and a pure sensory neuropathy in 5 patients, and anti-MAG activity was present in 27 of tested 29 cases. A predominantly motor neuropathy occurs in a minority of patients (Ellie *et al.*, 1996).

Distal sensory disturbance is the most common presenting symptom and absent ankle jerks are the most common sign. Paraesthesia, including tingling and pricking sensations in the lower limbs, sensation of cold feet, bandlike sensations around the feet and ankles, and the feeling of sand underfoot are often the first symptoms in patients with predominantly sensory neuropathies. Pain is not a prominent symptom according to most reports. However, Yeung *et al.* (1991) reported significant pain in 12 of 36 cases, including distal

aching discomfort in the limbs, painful tingling paraesthesiae, and sometimes superimposed stabs of pain. Contact hyperalgesia was not a feature.

Tremor may be encountered in a variety of familial or acquired neuropathies. It is generally accepted to be a common feature in IgM paraproteinaemic neuropathy (Smith, 1994), and sometimes the presenting symptom (Yeung *et al.*, 1991). The tremor of IgM anti-MAG neuropathy is typically a coarse low frequency postural and action tremor (Bain *et al.*, 1996). Chassande *et al.* (1998) reported a postural tremor of the hands in 12 of 40 patients with IgM paraproteinaemic neuropathy. In 33 cases with anti-MAG IgM paraproteinaemic neuropathies, Ellie *et al.* (1996) found intention tremor in 16 and marked ataxia in 15 with a trend that these occurred more frequently in patients with motor symptoms. Smith *et al.* (Smith *et al.*, 1983; Smith, 1994) found hand tremor in 16 of 18 patients indicating that tremor and ataxia are common features in IgM paraproteinaemic neuropathy against MAG or peripheral myelin. Said *et al.* (1982) asserted that tremor in patients with demyelinating neuropathies was related to weakness. Dalakas *et al.* (1984) found the tremor associated with neuropathy had no relationship to weakness or loss of proprioception in 11 patients with CIDP or dysgammaglobulinemic polyneuropathy. However, a relationship between the severity of tremor or ataxia and the degree of loss of joint position sense was found by Smith (1994) in IgM paraproteinaemic neuropathy, while Yeung *et al.* (1991) found that tremor was frequently present in the absence of detectable joint position sense loss. It has been hypothesized that distorted mistimed peripheral sensory inputs reach a central processor (probably the cerebellum) which although intact, is misled into producing a postural and action tremor in certain parts of the body during movement (Bain *et al.*, 1996). Several studies have documented that tremor improves in patients treated with high doses of prednisone, immunosuppressants, or intravenous immunoglobulin infusion (Cook *et al.*, 1990; Dalakas and Engel, 1981; Dalakas *et al.*, 1984; Kelly, 1985; Smith, 1994).

Interestingly, apart from one case with 10-year history of steroid-responsive urticaria (Ellie *et al.*, 1996), no clinical CNS manifestations have been observed in several large studies of IgM MGUS (Chassande *et al.*, 1998; Ellie *et al.*, 1996; Nobile-Orazio *et al.*, 1994; Smith, 1994; Yeung *et al.*, 1991) although subclinical CNS involvement is suggested by electrophysiologic examination (Barbieri *et al.*, 1987; Léger et al, 1992) and antibodies bind to the glycolipids present in the CNS white matter *in vitro* (Léger *et al.*, 1992; Mendell *et al.*, 1985). Significant autonomic dysfunction is uncommon (Ellie *et al.*, 1996; Yeung *et al.*, 1991).

3.1.3 Laboratory investigations

Electrophysiological findings

In patients with neuropathy associated with IgM MGUS and anti-MAG activity, the electrophysiological studies generally indicate a predominantly demyelinating neuropathy with slowing of conduction velocity and prolonged distal latencies (Chassande *et al.*, 1998; Ellie *et al.*, 1996; Kelly, 1990; Nobile-Orazio *et al.*, 1994).

Characteristic marked distal accentuation of conduction slowing (Kaku *et al.*, 1994) and frequent absence of sensory potentials (Chassande *et al.*, 1998) are consistent with the distal sensory impairment. In an investigation of motor conduction parameters in neuropathies associated with anti-MAG antibodies and other types of demyelinating and axonal neuropathies, Trojaborg *et al.* (1995) found that patients with highest titers of anti-MAG antibodies had longer distal motor latency and slower motor conduction velocity than those with lower titers, acute or chronic inflammatory demyelinating polyneuropathy or hereditary neuropathy. Measures of distal motor latency correlated best with anti-MAG antibody titers. Barbieri *et al.* (1987) found that the P100 latency of the visual evoked potential was

increased bilaterally in 5 of 6 patients with peripheral neuropathy and anti-MAG antibody suggesting subclinical CNS involvement.

Cerebrospinal Fluid Findings

In 24 patients with IgM anti-MAG neuropathy, Ellie *et al.* (1996) found a raised protein level in 22 and normal cell count in all cases in cerebrospinal fluid (CSF). CSF protein was higher in patients with motor symptoms than with pure sensory symptoms. These authors also found that an increase in CSF protein was associated with higher disability and ataxia scores, and prolongation of median nerve distal latency. Increased protein levels and normal cell count have also reported by others (Smith et al, 1983; Yeung *et al.*, 1991).

3.1.4 Pathology of IgM anti-MAG neuropathy

Predominant demyelination with varying degrees of axonal loss are found in the majority of peripheral nerve biopsies from IgM anti-MAG paraproteinaemic neuropathy (Ellie *et al.*, 1996; Jacobs and Scadding, 1990; Jacobs, 1996; Melmed *et al.*, 1983; Mendell *et al.*, 1985; Vital *et al.*; 1989; Yeung *et al.*, 1991). Widening of myelin lamellae (WML) resulting from separation of the intraperiod line is generally accepted as the pathological hallmark of anti-MAG neuropathy (Ellie *et al.*, 1996; Jacobs and Scadding, 1990; Jacobs, 1996; Melmed *et al.*, 1983; Mendell *et al.*, 1985; Vital *et al.*, 1989; Yeung *et al.*, 1991). Hypermyelination of fibres in transverse sections and focal myelin thickenings on individual teased nerve fibres are reported in some cases (Jacobs and Scadding, 1990; Rebai *et al.*, 1989; Vital *et al.*, 1985; Vital *et al.*, 1989). It is not an inflammatory neuropathy although inflammatory cells have been reported in a few cases (Vital *et al.*, 1991).

Demyelination and remyelination

Demyelination and remyelination are usually the predominant morphological features in peripheral nerve biopsies from patients with neuropathy associated with IgM anti-MAG MGUS (Ellie *et al.*, 1996; Mendell *et al.*, 1985; Jacobs, 1996; Smith, 1994; Vital *et al.*, 1989; Yeung *et al.*, 1991), and in teased nerve fibre studies (Jacobs and Scadding, 1990; Rebai *et al.*, 1989; Sander *et al.*, 2000). Axons surrounded by abnormally thin myelin sheaths and concentric Schwann cell processes indicative of onion bulb formation are also encountered in some cases (Mendell *et al.*, 1985). In 3 patients with benign IgM paraproteinaemic neuropathy, features of segmental demyelination and remyelination were found in 65% of teased nerve fibres (Sander *et al.*, 2000).

Although segmental demyelination is reported in most documented cases, few papers have reported the fibre appearances in any detail. In assessing the possible role of anti-MAG antibody in causing demyelination, it is important to know whether demyelination is primary or secondary. Jacobs and Scadding (1990) reported the morphological changes in sural nerve biopsies from 2 patients with anti-MAG IgM neuropathy. In one, almost every teased fibre showed evidence of demyelination and remyelination and that the incidence of demyelination and remyelination was higher than expected from the appearances in transverse section of the nerve. Quantitative studies of transverse plastic sections in the same case showed that there were many fibres with low values of g-ratio (axonal diameter/total fibre diameter in the cross section) indicating axonal atrophy and segmental demyelination in this case was classified as secondary demyelination (Jacobs and Scadding, 1990). In the other the segmental demyelination was classified as chronic primary demyelination.

Mendell *et al.* (1985) performed a complete postmortem examination of the nervous system in a patient with IgM anti-MAG neuropathy and did not find any specific abnormalities in the CNS or the dorsal and ventral nerve roots. Specifically, there was no axonal degeneration, only rare thinly myelinated fibres, no evidence of Schwann cell proliferation in the dorsal and ventral roots and anti-MAG antibody was not deposited in the CNS. The sciatic nerve showed a marked loss of nerve fibres. A sural nerve biopsy two years earlier had shown severe loss of MFs and prominent Schwann cell proliferation with striking onion bulb formation. These results were interpreted as indicative of a primary axonal neuropathy with secondary demyelination and remyelination (Mendell *et al.*, 1985).

Axonal damage

Varying degrees of axonal damage are present in the majority of patients with anti-MAG IgM neuropathy (Ellie *et al.*, 1996; Jacobs and Scadding, 1990; Melmed *et al.*, 1983; Vital *et al.*, 1989; Yeung *et al.*, 1991). Loss of myelinated fibres, especially large diameter fibres, is found in most peripheral nerve biopsies (Ellie *et al.*, 1996; Gabriel *et al.*, 1998; Jacobs and Scadding, 1990; Meier *et al.*, 1984; Melmed *et al.*, 1983; Mendell *et al.*, 1985; Rebai *et al.*, 1989; Vital *et al.*, 1989; Yeung *et al.*, 1991), and confirmed by a few quantitative studies (Rebai *et al.*, 1989; Vital *et al.*, 1989). Severely constricted axons with enlarged periaxonal spaces also indicate axonal atrophy (Jacobs and Scadding, 1990). Loss of unmyelinated fibres was also noted in some cases (Jacobs and Scadding, 1990; Kanda *et al.*, 1998). Sequential sural nerve biopsies in one patient revealed that clinical deterioration is accompanied by greater axonal depletion (Melmed *et al.*, 1983) though the pathology is not always progressive (Mendell *et al.*, 1985). These findings confirm the importance of axonal damage in this disease and that progressive axonal damage may be associated with clinical deterioration and a poor prognosis.

Focal myelin thickenings and tomacula

Focal myelin thickenings and tomacula have been described in teased fibre studies in a few cases of anti-MAG IgM paraproteinaemic neuropathy (Jacobs and Scadding, 1990; Rebai *et al.*, 1989; Sander *et al.*, 2000). However, hypermyelination and redundant myelin folding are commonly encountered in transverse sections in neuropathies associated with IgM MGUS (Nardelli *et al.*, 1981; Vital *et al.*, 1985), especially with anti-MAG activity (Jacobs and Scadding, 1990; Rebai *et al.*, 1989; Sander *et al.*, 2000; Vital *et al.*, 1989). Rebai et al (1989) found tomacula in 32% of internodes in one case with IgM anti-MAG neuropathy. In 3 cases with IgM anti-MAG neuropathy, tomacula were present in over half of the teased nerve fibres, and the size of tomacula ranged from 10.3 μm to 18 μm (average 14.4 μm) in diameter and 39 to 49.7 μm (average 45.9 μm) in length (Sander *et al.*, 2000). The pathogenesis of tomacula in IgM anti-MAG neuropathy is not well understood. Based on conventional electron microscopy, it was suggested that external or internal redundant myelin loops and symmetric and disproportionately thick myelin sheaths contributed to the tomaculous appearance on teased nerve fibres (Jacobs and Scadding, 1990; Rebai *et al.*, 1989; Vital *et al.*, 1989). Jacobs and Scadding (1990) also suggested that the "bubbly" myelin appearance on teased fibres was due to extensive swelling of the adaxonal space.

Tomacula in human peripheral neuropathies

Focal myelin swellings in demyelinated internodes were first reported by Dayan *et al.* (1968) in teased fibres from familial globular neuropathy. They were then described in nerve fibres from patients with hereditary neuropathy with liability to pressure palsies (HNPP) (Behse *et al.*, 1972) due to segmental deletion of chromosome 17p11.12 (Chance *et al.*, 1993). The tomacula ranged in length from 40 to 250 μm (average 100 μm) and up to 40 μm in diameter and were present in about one fourth of the internodes, which usually showed remyelination or were otherwise normal in external appearance (Behse *et al.*, 1972).

The sausage-like myelin swellings were first termed tomacula by Madrid and Bradley in 1975 (Latin: tomaculum = sausage). Pellissier *et al.* (1987) defined tomaculous neuropathy as focal myelin swellings present in more than 25% of internodes, and found 10 cases of tomaculous neuropathy in 980 sural nerve biopsies. Verhagen *et al.* (1993) defined tomacula as myelin thickenings measuring more than 50% of the fibre diameter. Tomaculous myelin swellings are found in other neuropathies such as hereditary motor and sensory neuropathy type 1B (HMSN1B) due to P_0 gene mutation (Fabrizi *et al.*, 2000; Tachi *et al.*, 1997; Thomas *et al.*, 1994), hereditary motor and sensory neuropathy with outfolding myelin sheath (CMT4B) (Gabreëls-Festen *et al.*, 1990; Gambardella *et al.*, 1999; Ohnishi *et al.*, 1989; Schenone *et al.*, 1994) probably due to a gene mutation on chromosome 11q23 (Bolino *et al.*, 1996) or due to an unknown gene mutation (Gambardella *et al.*, 1999), dominantly HMSN of unknown aetiology (Umehara *et al.*, 1993), autosomal recessive HMSN I (Gabreëls-Festen *et al.*, 1992), Ehlers-Danlos syndrome (Schady and Ochoa, 1984), acute recurrent polyneuropathy (Joy and Oh, 1989), familial recurrent plexus neuropathy (Madrid and Bradley, 1975), IgM anti-MAG neuropathy (Jacobs and Scadding, 1990; Rebai *et al.*, 1989), and chronic inflammatory demyelinating neuropathy (Sander *et al.*, 2000).

The incidence, size and location of focal myelin swellings on teased fibres may be different in different neuropathies (Sander *et al.*, 2000). They may show regular contour or a granular profile (Table 3-1).

The pathogenesis of tomacula is not well understood. In HNPP, tomacula were suggested to result from redundant myelin folding (Behse *et al.*, 1972; Verhagen *et al.*, 1993). In 2 patients with recurrent familial brachial plexus neuropathy, 1 with pressure-sensitive neuropathy and 1 with chronic sensori-motor neuropathy, Madrid and Bradley (1975)

speculated that the sausage-like shape of tomacula might be due to: (1) focal hypermyelination from continuous spiral rotation of the Schwann cell membrane around the axon, (2) redundant myelin loop, (3) a second mesaxon, derived from branching of the original rotating Schwann cell process during myelination or remyelination, rotating parallel with the original mesaxon or passing in the opposite direction, (4) myelin lamellae from one Schwann cell passing across a node of Ranvier to cover the axon in the territory of the adjacent Schwann cell, ie transnodal myelination, (5) two Schwann cells co-operating in the formation of one myelin sheath, (6) disruption of myelin lamellae. Behse *et al.* (1972) also indicated that tomacula in HNPP resulted from redundant myelin foldings.

Table 3-1 Diameter and length of tomacula on teased nerve fibres (Sander *et al.*, 2000)

	NS	Age (y)		Diameter (μm)		Length (μm)	
		Mean	SD	Mean	SD	Mean	SD
HNPP	37	37.9	15.7	16.3	2	83.7	14.4
IgM PPN	3	64.3	14.2	14.4	3.9	45.9	5.8
CIDP	3	49	29.1	18.9	1.2	56.3	10
CMT1	4	28.4	24.4	14.1	3.5	77.4	16.1
CMT4B	4	4.9	0.9	11.2	1.6	44.4	5.7

NS = number of sural nerve biopsies; SD = standard deviation; HNPP = Hereditary neuropathy with liability to pressure palsies; IgM PPN = IgM anti-MAG paraproteinaemic polyneuropathy; CIDP = chronic inflammatory demyelinating polyneuropathy; CMT1 = Charcot-Marie-Tooth disease type 1; CMT4B = Charcot-Marie-Tooth disease type 4B.

Sander *et al.* (2000) studied tomacula using conventional LM, EM and teased nerve fibre techniques. They found that in HNPP focal hypermyelination (excessive number of myelin lamellae) and redundant myelin loops contributed to the tomaculous appearance on teased nerve fibres. Redundant myelin loops were the most frequent cause of tomacula formation and myelin breakdown was often seen in redundant myelin loops. The appearance of myelin sheath thickenings in CMT1 was similar to that seen in HNPP (Sander *et al.*, 2000).

Redundant myelin outfoldings or infoldings were also the mechanism of tomacula formation in IgM anti-MAG neuropathy, CIDP, CMT4B and CMT3 (Sander *et al.*, 2000).

Redundant myelin foldings on conventional transverse sections have been found in nearly all human hereditary or acquired neuropathies with tomacula on teased nerve fibres.

The subsequent evolution of tomacula is not well understood. In human inherited and acquired peripheral neuropathies, tomacula are usually found in association with varying degrees of demyelination and remyelination.

Widening of myelin lamellae (WML)

Widening of the periodicity of myelin lamellae, due to an increase in the distance separating the intraperiod line interfaces associated with the normal formation of the major dense line, is a distinctive finding in biopsies from neuropathy associated with IgM MGUS and anti-MAG activity (Ellie *et al.*, 1996; Quarles and Weiss, 1999; Steck *et al.*, 1999; Vital *et al.*, 1989; Yeung *et al.*, 1991).

Increased myelin periodicity in a human nerve biopsy was first reported in a case of metachromatic leucodystrophy by Webster in 1964 (cited in King and Thomas, 1984) and later in a case of IgG paraproteinaemia by Sluga in 1970 (cited in Jacobs, 1996). WML has been described in peripheral neuropathy and Waldenström's macroglobulinaemia (WM) (Julien *et al.*, 1978; Propp *et al.*, 1975; Vital *et al.*, 1975; Vital and Vallat, 1980), and peripheral neuropathy and IgM MGUS (Meier *et al.*, 1984); Melmed *et al.*, 1983; Nardelli *et al.*, 1981; Pollard *et al.*, 1985; Smith *et al.*, 1983; Steck *et al.*, 1983). Further studies showed that WML was present in most cases with neuropathy and anti-MAG activity. In 33 cases of benign IgM anti-MAG neuropathy, Ellie *et al.* (1996) described WML in peroneal

nerve biopsies in 32. Vital *et al.* (1997) found WML present all 8 cases of peripheral neuropathy with WM and anti-MAG activity.

The incidence of WML varies greatly from one case to another and may affect 80% of myelinated fibres in benign anti-MAG neuropathy (Jacobs and Scadding, 1990) and 88% of fibres in IgM anti-MAG neuropathy with indolent WM (Vital *et al.*, 1997). It is more commonly observed in the outermost layers of the myelin sheath in benign anti-MAG IgM neuropathy and IgM anti-MAG neuropathy with WM (Ellie *et al.*, 1996; King and Thomas, 1984; Lach *et al.*, 1993; Meier *et al.*, 1984; Melmed *et al.*, 1983; Pollard *et al.*, 1985; Vital *et al.*, 1985, 1989, 1997), but is also found in the inner myelin sheath (Vital *et al.*, 1997). The distribution of WML may be limited to the center of the myelin sheath or present throughout the myelin sheath (Jacobs, 1996; King and Thomas, 1984; Mendell *et al.*, 1985; Ritz *et al.*, 1999; Yeung *et al.*, 1991). The latter appearance is thought to result from transverse sections through the nodal region (King and Thomas, 1984). WML may be more common in the paranodal region than the internode in longitudinal sections (King and Thomas, 1984). At the paranodal region, WML is represented as an increased space between paranodal terminal loops in longitudinal sections (Jacobs, 1996; Jacobs and Scadding, 1990). The widened gap in the paranodal region may be continuous with internodal myelin of increased normal periodicity or terminate abruptly (Jacobs, 1996; Jacobs and Scadding, 1990; King and Thomas, 1984).

The mechanism of WML remains unclear. Apart from a single illustration from a case of metachromatic leucodystrophy reported by Webster in 1964 (cited in King and Thomas, 1984), WML has only been encountered in neuropathies with an immunological basis including neuropathy associated with MGUS or WM, and chronic progressive or relapsing idiopathic inflammatory polyneuropathy. The occurrence of WML in these neuropathies

has led to the suggestion that WML results from the incorporation of immunoglobulin into the myelin sheath (Propp *et al.*, 1975). WML found in experimental allergic neuritis (EAN) and Marek's disease in chicken (Lampert *et al.*, 1977), and myelinated tissue cultures exposed to sera from experimental allergic encephalomyelitis (EAE) (Bornstein and Raine, 1976) and EAN (Raine and Bornstein, 1979) have led to the suggestion that the "uniform separation of myelin lamellae" is primed with antibody before becoming susceptible to cell-mediated lysis (Lampert *et al.*, 1977). However, the production of widely spaced myelin by exposure of nerve to hypotonic solutions suggested that it might be a physicochemical change, perhaps due to binding of specific immunoglobulin, leading to overhydration (King and Thomas, 1984). Monaco *et al.* (1990) observed a correlation between the numbers of fibres with abnormally spaced myelin and the extent of deposition of terminal-complement complex. They supposed that the abnormally spaced myelin might be due to an influx of intracellular water after damage by the terminal-complement complex. Now it is commonly assumed that in IgM paraproteinaemic neuropathy the typical modification of myelin observed at the ultrastructural level is associated with deposition of IgM between the myelin lamellae (Quarles and Weiss, 1999), and this hypothesis is supported by the following findings. First, the distribution of WML at paranodes, Schmidt-Lanterman incisures, periaxonal regions and external mesaxons in anti-MAG neuropathy very precisely matches the distribution of MAG (Jacobs and Scadding, 1990). The location of WML at sites that do not correspond to recognized sites of MAG, including the outermost lamellae, external surface of the Schwann cell and compact myelin, may be associated with glycoconjugates that are also recognized by MAG antibodies (Gabriel *et al.*, 1996; Jacobs, 1996; Murray *et al.*, 1986; Ritz *et al.*, 1999). Second, IgM deposits are found in the regions of the wide spacing. An early study by Mendell *et al.* (1985) found positive immunostaining for anti-MAG antibody in deplasticized semithin sections corresponded to regions of myelin widening in adjacent ultrathin sections. Clumps of granular material, sometimes of

considerable size, were noticed in continuity with similar material at widened lamellae by routine electron microscopy (Jacobs, 1996; Jacobs and Scadding, 1990). Yeung *et al.* (1991) observed that in no instance was abnormal myelin spacing detected in the absence of IgM deposition. In accordance with this finding, immunoelectron microscopy also demonstrated selective deposition of IgM gammaglobulin exclusively in the areas of splitting of the myelin lamellae (Lach *et al.*, 1993). Confocal microscopy has also shown a correlation between the penetration and localization of IgM in myelinated fibres and the myelin widening (Ritz *et al.*, 1999). This notion is also supported by animal experiments. Passive transfer of human IgM anti-MAG paraproteins into chicks caused demyelination and remyelination with the typical ultrastructural feature of widening of the outer myelin lamellae intermediate line, consistent with the pathological findings in the peripheral nerve biopsy (Tatum, 1993). The report that widening of myelin lamellae was particularly prominent in patients with indolent WM in comparison to other patients with benign anti-MAG antibodies suggests that another mechanism is involved in modifying myelin structure in addition to the anti-MAG activity (Vital *et al.*, 1997). Similar wide spacing in CNS myelin has been found after implanting mouse hybridomas that produce IgM antibodies to three different glycolipids, galactocerebroside, sulfatide and ganglioside, into rat spinal cord (Rosenbluth *et al.* 1996; 1997), suggesting that the formation of expanded myelin does not depend only on antibodies to MAG but can also be mediated by IgM antibodies that react with other myelin components. It is therefore supposed that the intercalation of IgM antibody to the myelin lamellae results in permeability effects or changes in adhesion properties of myelin components, especially MAG, leading eventually to abnormal myelin spacing (Quarles and Weiss, 1999). However, the pathogenic mechanism whereby IgM antibodies reach their targets and induce WML is still unclear. Based on the observation that the production of WML by human anti-MAG antibodies in rabbit nerve was found to be dependent on the terminal complement complex (TCC) (Monaco *et al.*, 1995), it was

speculated that the widening is caused by intramyelin oedema due to the formation of transmembrane pores by the complement cascade, leading to activation of proteases and phospholipases causing subsequent vesiculation and further oedema (Quarles and Weiss, 1999). However, the finding that no TCC aggregates were seen associated with myelinated fibres by confocal microscopy suggests that the damage of myelinated fibres may not directly mediated by TCC (Ritz *et al.*, 1999). Damage of the blood-nerve barrier in IgM paraproteinaemic neuropathy (Kanda *et al.*, 1998) may be associated with the presence of TCC aggregates in blood vessels (Ritz *et al.*, 1999), permitting the entry of circulating antibodies into the endoneurium.

Antibody deposits in peripheral nerve biopsies

Binding of anti-IgM serum and anti-homologous light chain serum to myelin sheaths were found in 14 of 23 patients by direct immunofluorescence, and no obvious binding was found in the endoneurium (Vital *et al.*, 1989). Immunohistochemical studies demonstrated IgM in the vicinity of endoneurial vessels and on some of the myelinated fibres (Meier *et al.*, 1984). Confocal microscopy (Gabriel *et al.*, 1998; Ritz *et al.*, 1999) showed that MAG in Schmidt-Lanterman incisures and paranodal loops, as well as some additional molecules involving other HNK-1–containing components of the basement membrane of myelinating Schwann cells, were the major targets of the anti-MAG monoclonal IgM antibodies *in vivo*. These HNK-1–containing epitopes were present in fibronectin, L1, J1/tenascin (Martini, 1994*b*), some integrins (Pesheva *et al.*, 1987) or sulfoglucuronyl (Jungalwala, 1994), and chondroitin sulfate proteoglycans (Gowda *et al.*, 1989; Hoffman and Edelman, 1987). Binding of anti-MAG antibodies to compact myelin may be due to binding of the antibody to the HNK-1 epitope shared by P0 and PMP22 (Hammer *et al.*, 1993; Snipes *et al.*, 1993). Double immunostaining for IgM antibodies and MAG in paraproteinaemic polyneuropathy nerves revealed that MAG staining intensities ranging from weak to strong (compared to

control nerves or myelinated fibres devoid of IgM in paraproteinaemic polyneuropathy nerves) were associated with a thin ring of IgM deposits, suggesting reduced MAG expression. Myelinated fibres devoid of MAG staining were often associated with thick IgM deposits either at the periphery or in the entire thickness of the myelin sheath (Gabriel *et al.*, 1996).

Although binding of anti-MAG antibodies to myelin components of the CNS *in vivo* was suggested by some researchers due to the presence of abnormal visual evoked potentials with M-protein in the cerebrospinal fluid (Barbieri *et al.*, 1987), immunofluorescent staining showed no deposits in any portion of the CNS including the cerebral cortex, corpus callosum, cerebellum, pons, medulla, midbrain, and spinal cord. However, IgM antibodies bind to myelin components of the CNS *in vitro* (Mendell *et al.*, 1985).

3.1.5 Experimental anti-MAG neuropathy

By-passing the blood-nerve-barrier, Hays *et al.* (1987) found that serum obtained from three patients with neuropathy and MAG-positive IgM M-protein induced demyelination when injected into the feline sciatic nerve. Control sera from healthy individuals, patients with IgM M-protein but no neuropathy, or patients with neuropathy and IgM M-proteins not directed towards MAG either did not produce this effect at all or produced it to a much lesser degree. Willison *et al.* (1988) showed that intraneural injection of serum from patients with neuropathy and anti-MAG antibodies produced an extensive inflammatory, macrophage-mediated demyelination of feline peripheral nerve, while injection of sera from normal subjects failed to produce any demyelination. The pathogenetic role of MAG in the central nervous system was demonstrated by the injection of mouse monoclonal anti-MAG antibody together with guinea pig serum into mammalian optic nerves producing *in vivo* demyelination (Sergott *et al.*, 1988). In an investigation of the pathogenic role of anti-MAG

IgM and complement (C) in anti-MAG-associated polyneuropathy, Monaco *et al.* (1995) found that intraneural injection of terminal complement complex (TCC) into rabbit sciatic nerve produced the same morphological changes as injection with anti-MAG antibodies, including intramyelin oedema, myelin vesiculation and widening of myelin lamellae due to the separation of major dense line. In nerves treated with anti-MAG IgM myelin alterations were concurrent with activation of the rabbit's own complement with the formation of TCC. Conversely, in C6 deficient rabbits injected with anti-MAG IgM neither myelin alteration nor complement depletion were observed.

Early experiments of systemic transfusion of IgM anti-MAG paraproteins from patients failed to produce neuropathy in guinea pigs, rabbits and marmosets (Steck *et al.*, 1985) probably because there is interspecies variation in antibody recognition of the molecule. Tatum (1993) succeeded in establishing a passive transfer animal model in chickens by intraperitoneal injection of monoclonal IgM anti-MAG antibody from a patient with neuropathy. This model showed typical pathological features of the human syndrome, including segmental demyelination and remyelination with minimal inflammation, specific antibody binding to myelin and widening of the myelin lamellae. The preferential targetting of the antibody to the nodes of Ranvier and Schmidt-Lanterman incisures suggested that MAG might be the antigenic target *in vivo*.

Several observations highlight the importance of complement mediation in the experimental passive transfer of neuropathy with IgM anti-MAG paraproteins. First demyelination induced by intraneural injection only occurs with anti-MAG antibody which is supplemented with additional complement (Willison *et al.*, 1988) or with serum (Sergott *et al.*, 1988). Furthermore, complement deposition is co-localized on myelin sheaths with IgM deposition in the animal models (Hays *et al.*, 1987; Tatum *et al.*, 1993). Additionally,

antisera produced in rabbits against purified MAG do not inhibit myelin formation in cerebellar tissue cultures or demyelinate centrally or peripherally myelinated fibres in spinal cord DRG cultures (Seil *et al.*, 1981). The requirement for complement in the intraneural injection models suggests that cytotoxic mechanisms are also involved.

3.2 MATERIALS AND METHODS

3.2.1 Case report

A 74-year-old man presented with a 2-year history of peripheral neuropathy and severe tremor. On examination there was a coarse action and postural "flapping" tremor with rotatory elements that changed depending on the posture of the arms, typical of a neuropathic tremor. There was no leg tremor. Fine manual tasks were severely compromised by the tremor. There was distal muscle wasting and weakness. He was areflexic and had a degree of deafferentation with impaired joint position sense and vibration in the toes and fingers and a glove and stocking impairment of light touch. He walked with a sensory ataxia and bilateral foot drop. Electrophoresis confirmed IgM kappa paraproteinaemia, 14.7g/L (normal range: 0.6 – 3.0g/L). Further testing for underlying haematological malignancy including bone marrow analysis were all negative. Nerve conduction studies indicated a demyelinating neuropathy. The right median distal motor latency was greatly prolonged at 27.6 ms. The right ulnar distal motor latency was 13.7 ms. The peroneal nerves were not excitable. The amplitude of upper limb compound muscle action potentials was less than 1 mv. Conduction velocities in the right median and left ulnar nerves were 6m/sec and 13m/sec respectively. Anti-MAG IgM antibody titre was >100,000 BTU (Buhlman titre units) (normal upper limit 1000BTU, courtesy Professor J. Pollard, The University of Sydney).

3.2.2 Sural nerve biopsy and tissue preparation

Full thickness right sural nerve biopsy was performed and processed according to the standard methods (Cash and Blumbergs, 1995) for routine LM, EM, teased nerve fibre and morphometric studies as described above. Nerve fascicles for correlating external and internal structure along individual nerve fibres were processed according to the methods described in Chapter 2.

3.3 RESULTS

Routine morphologic findings under LM will be detailed in Appendix C. In summary, a demyelinating neuropathy with severe loss of myelinated fibres was found in the sural nerve biopsy and some fibres displayed focal myelin thickenings.

Morphometric studies revealed 982 myelinated nerve fibres in 0.41 mm^2 total transverse fascicular area with an average fibre density of 2395/mm^2. Fibre density ranges from 4080 to 6950 in age-matched control from the literature (Jacobs and Love, 1985). Histograms of fibre diameter and axonal diameter revealed a predominant loss of large myelinated fibres (Fig. 3-1). The myelinated fibre diameter (4.54 ± 1.74 μm, mean ± SD) and axonal diameter (3.03 ± 1.30 μm, mean ± SD) were significantly smaller than those of a 44-year-old postmortem control (fibre diameter, 7.41 ± 1.95 μm, mean ± SD; axonal diameter, 5.29 ± 2.85 μm, mean ± SD) (student *t* test, P<0.001).

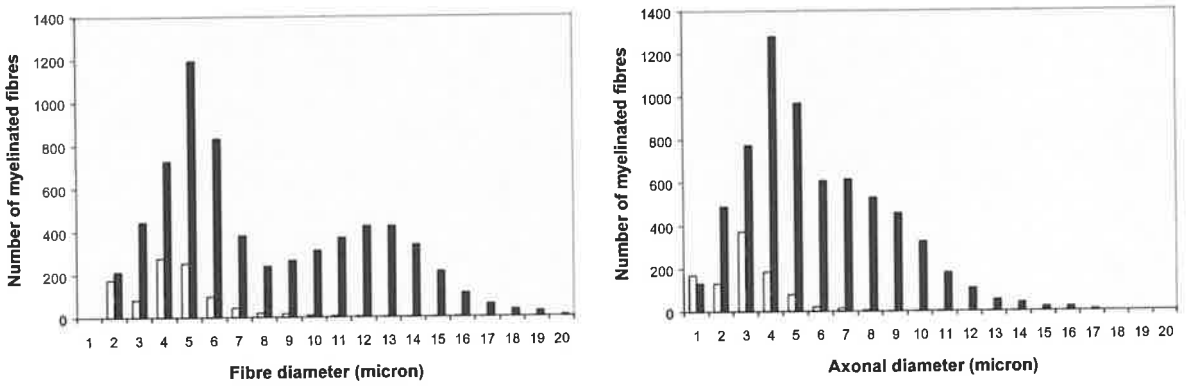

Figure 3-1. Comparison of histograms of fibre diameter (left) and axonal diameter (right) between this case (white column) and a postmortem control (black column) reveals severe loss of myelinated fibres, especially large diameter fibres.

3.3.1 Glycerinated teased nerve fibres

One hundred glycerinated teased fibres, ranging 15-25 mm in length and including at least 7 internodes in each fibre, were examined. Teased nerve fibres were classified according to generally accepted criteria (Dyck *et al.*, 1993*a*). Eighty-two (82%) showed demyelination

with extensive loss of myelin in both internodal and paranodal regions. Two teased fibres (2%) showed remyelination with internodes of variable length, one (1%) showed axonal degeneration and 15 (15%) were normal. Sixty-two (62%) fibres showed focal myelin swellings, which varied in size (20 – 130 μm in length) and shape (globular to sausage-like). Some fibres showed multiple myelin swellings. The large swellings, more than 50% of the fibre diameter, were classified as small tomacula (Verhagen *et al.*, 1993) and were present in 43 fibres (43%). All the focal myelin swellings were found in abnormal fibres showing demyelination and localised to both paranodal and internodal regions without predilection.

3.3.2 Correlative study of external appearance with multiple cross sections of single myelinated fibres teased in resin

Eleven single fibres teased in resin were examined. Ten fibres showed paranodal and/or internodal demyelination. One fibre showed a pale external appearance in which no nodes of Ranvier could be reliably recognized (non-specific change as described in Chapter 2). Five fibres had focal myelin thickening (s).

A total of 14 tomacula were identified in 5 of the 11 fibres. Four tomacula were present in each of 2 fibres, and the remaining 3 fibres had 3, 2 and 1 tomacula. Multiple transverse sections of these teased fibres were examined under LM and EM, and the cross sectional appearances were correlated with the external appearance of the teased fibres at corresponding points. Transverse sections through the 14 focal myelin thickenings showed various morphological appearances, including complex redundant myelin outfolding or infolding, multiple concentric myelin loops, enlargement of adaxonal space and complex splitting and degeneration of the myelin sheath. Redundant myelin outfolding (eg, L16 and L26 in Fig. 3-2, and L3 and L4 in Fig. 3-3) was the cause of swelling in 50% (7/14) of tomacula. The axon was small in 1 (L16 in Fig. 3-2) and of normal calibre compared to the

adjacent normal segments in 6 of the swellings (eg, L3 and L4 in Fig. 3-3). Serial sections through these 7 focal swellings revealed that 3 were also associated with degenerative changes in the redundant folds (eg, L17 and L25 in Fig. 3-2). Myelin debris in Schwann cell cytoplasm was also found adjacent to some of the swellings on serial cross sections suggesting that redundant myelin folds may be broken down by the Schwann cell (eg, L4 to L4-30μ in Fig.4-4). Myelin infolding was found in 2 swellings (eg L18-19 in Fig. 3-2) and in one of these the infolding was associated with enlargement of adaxonal space. One swelling was due to an increased number of concentric myelin loops surrounding a normal appearing axon (L3 in Fig. 3-5). Enlargement of the adaxonal space was found in 4 swellings, associated with a normal intact myelin sheath in 2 (eg, L21 in Fig. 3-2), with myelin outfolding and myelin degeneration in 1 (L17 in Fig. 3-2), and with myelin infolding alone in 1. Focal swellings in the same fibre may show similar (eg, L3 and L4 in Fig. 3-3) or different (eg, L16-22 and L25-26 in Fig. 3-2) internal abnormalities. Serial sections through two adjacent focal swellings revealed different abnormalities L18-19 and L21-22 in Fig. 3-2). The axonal calibre along the length of the fibre varied considerably in 4 of 5 fibres with focal myelin thickenings (eg, Fig. 3-2) and did not vary in 1 fibre (Fig. 3-5).

Abnormal myelin and/or axon morphological features were found in transverse sections of externally normal segments of the teased fibres. For example in Fig. 3-2, redundant myelin folding (L8-9), complex myelin splitting and degeneration (L11 and L14), enlargement of the adaxonal space with small axon (L8-9 and L15), and enlargement of the adaxonal space with normal axon (L10) were found in externally normal segments.

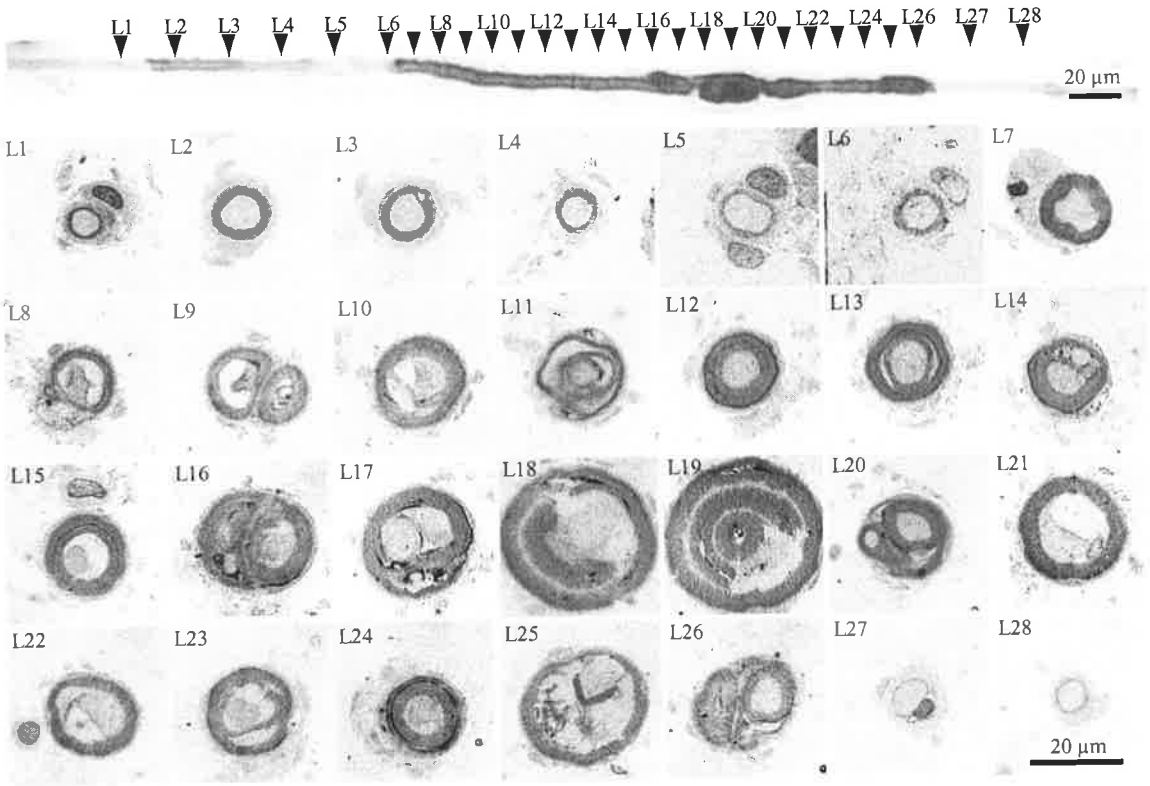

Figure 3-2. Light micrographs; teased fibre from the IgM anti-MAG neuropathy. The upper panel shows a fibre undergoing demyelination and 4 focal areas of myelin thickening (L16-17, L18-19, L21 and L25-26). Lower panels show LM transverse semithin plastic sections stained with toluidine blue through specific sites along the fibre as indicated by markers L1-28. The interval between two adjacent sections is 40 µm from L1 to L6 and L26 to L28, and 20 µm from L6 to L26. The myelin sheath is disproportionately thin in L1-4, and barely visible in L5-6 and L27-28 corresponding to the demyelinated appearance of the teased fibre. Sections L7-15 and L22-24, through the teased nerve fibre where the external appearance of the myelin is normal, show a normal appearance (L7, 12 and 13), normal myelin sheath with enlarged periaxonal space and small axon (L10, 15, 22 and 24), redundant myelin outfolding with myelin degeneration (L8-9), and complex myelin degeneration with or without enlarged periaxonal space (L11, 14, 23). Sections L16 and 17 through the first area of myelin thickening show redundant myelin outfolding with myelin degeneration and enlarged periaxonal space. Sections L18 and 19 through the small tomacula-like myelin thickening show redundant myelin folding. Section L20 through the junction of the second and third areas of myelin thickening shows myelin outfolding. Section L21 through the third focal swelling shows enlargement of periaxonal space with normal-like myelin sheath extending to section L22. Sections L25 and 26 through the fourth swelling show complex myelin degeneration and redundant myelin outfolding. Thin myelin sheaths are demonstrated in cross sections of areas of demyelination (eg, L1, L2, L5, L27 and L28).

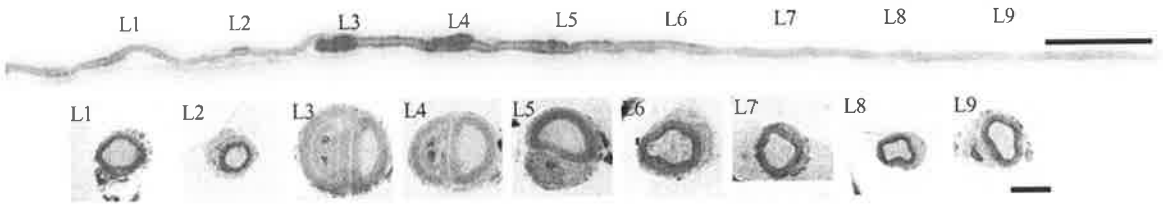

Figure 3-3. Light micrographs; teased fibre from the IgM anti-MAG neuropathy. The upper panel shows a resin teased fibre with two focal swellings (L3 and L4). The lower panel illustrates cross sections through different sites of the fibre. Two swelling areas show redundant myelin outfolding. Bar = 100μm for teased fibre. Bar = 10 μm for cross sections.

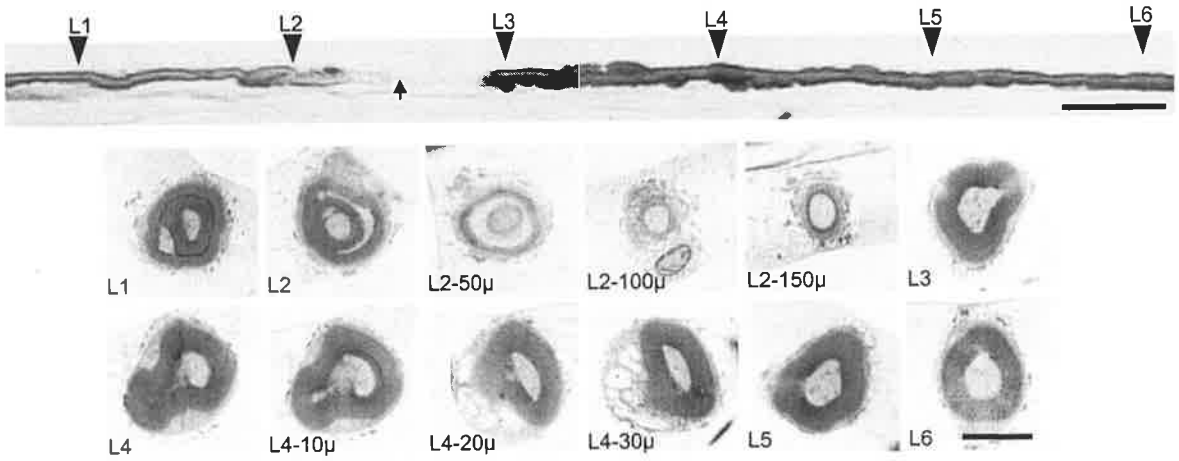

Figure 3-4. Light micrographs; teased fibre from the IgM anti-MAG neuropathy. The upper panel shows part of a teased fibre with paranodal demyelination (arrow) and focal myelin foldings. Two lower panels show cross sections of this fibre at designated sites. Very thin, pale myelin sheaths can be seen in transverse sections through the demyelinated paranodal regions (L2-40μ to L2-60μ). Step cross sections through the externally visible myelin folding site of the teased fibre reveal that the redundant myelin (L4 and L4-5μ) is associated with myelin breakdown products in the corresponding Schwann cell (L4-10μ and L4-15μ). Bar = 100 μm for teased fibre. Bar = 10 μm for cross sections.

Demyelinated paranodal and internodal segments in the teased fibres were also transversely sectioned. Cross sections revealed that axons in these regions were not completely naked. They were enclosed by thin and pale myelin sheaths (eg, L1, L5, L6, L27 and L28 in Fig. 3-2; L2-100μ and L2-150μ in Fig. 3-4; L3 and L4 in Fig. 3-6). The axonal calibre in the demyelinated internodal regions may be smaller than that of the externally normal segments (eg, L1 vs L7 in Fig. 3-2) or similar to the externally normal segments (eg, L5 vs L7 in Fig. 3-2). Enlargement of the adaxonal space was not detected in these regions.

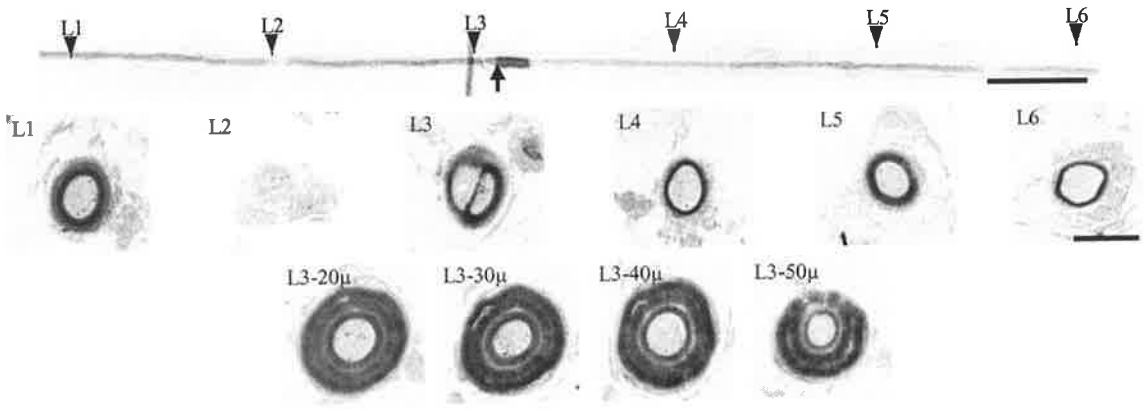

Figure 3-5. Light micrographs; teased fibre from the IgM anti-MAG neuropathy. The upper panel is part of a teased fibre showing segmental demyelination with a focal myelin swelling (arrow). The middle panel shows LM transverse semithin sections L1-6 with an interval of 200 μm between adjacent sections. Section L1 shows a normal myelin sheath and axon. Section L2 crosses a node of Ranvier. Section L3 through the edge of a marker fibre, and shows splitting of myelin sheath. Sections L4 and L6 across demyelinated segments reveal disproportionately thin myelin sheaths. The lower panel shows the internal structure of the focal swelling at level L3 in sections 10 μm apart beginning 20 μm from L3. Multiple myelin layers surround a normal appearing axon. Bar = 100μm for teased fibre. Bar = 10μm for transverse sections.

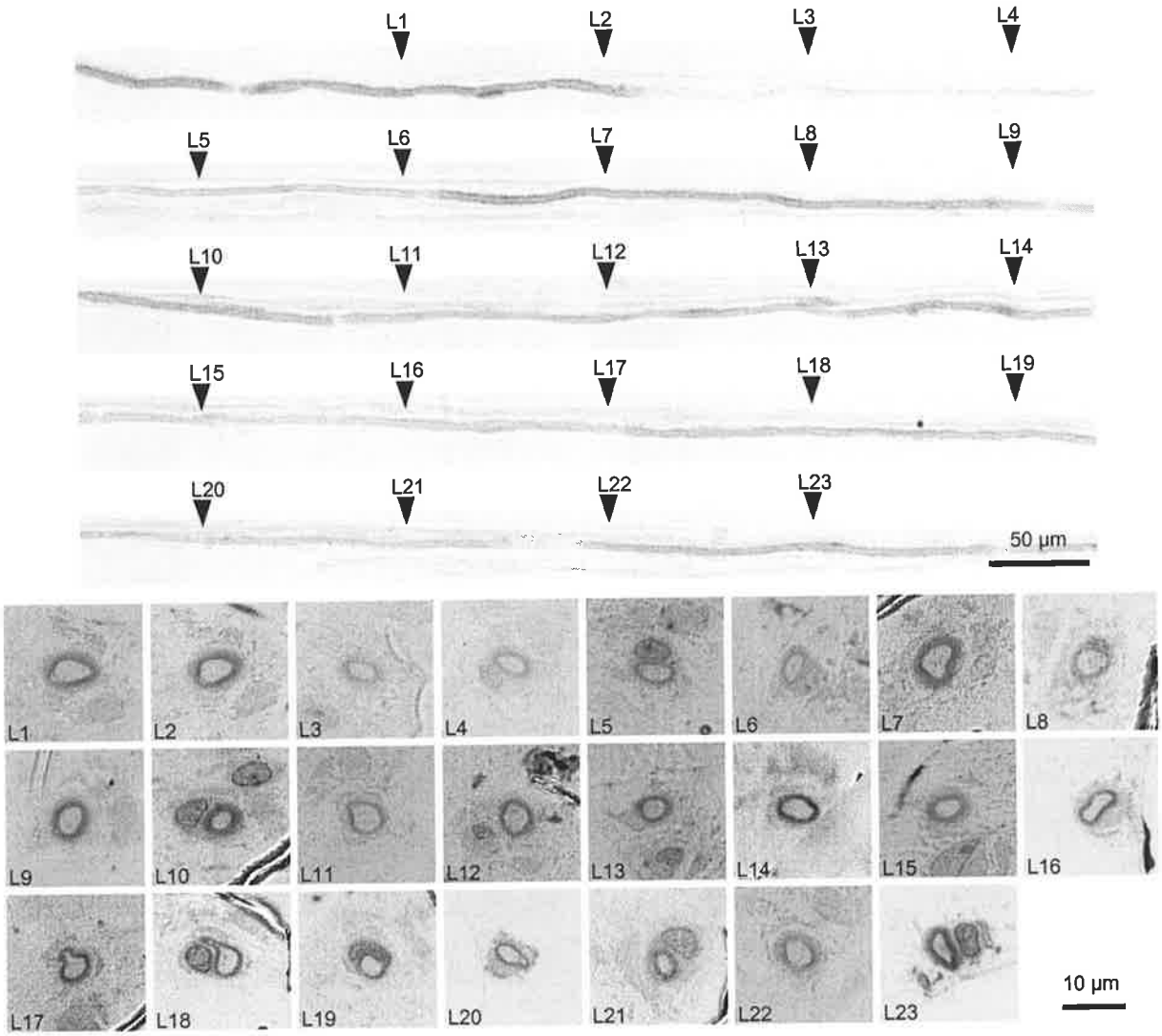

Figure 3-6. Light micrographs; teased fibre from the IgM anti-MAG neuropathy. The five upper panels show part of a teased fibre with a pale external appearance and no myelin sheath visible under LM at a magnification of × 400 in the segment indicated by L3 and L4. The three lower panels are cross sections of the teased fibre through designated sites at regular intervals of 100 µm. All cross sections show thin and pale myelin sheaths. The myelin sheaths in L3 and L4 are paler than those in other cross sections. The axonal calibre remains stable along the length of the fibre.

Cross section studies of the teased fibre with a "non-specific external appearance" revealed thin and pale myelin sheaths along the whole length of the fibre (Fig. 3-6).

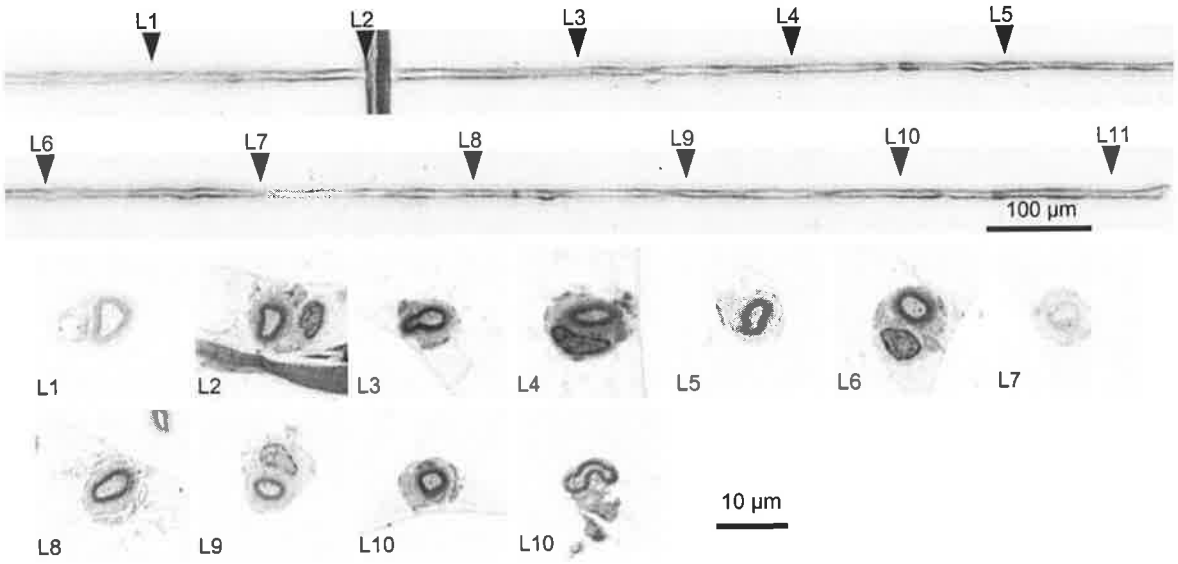

Figure 3-6. Light micrographs; teased fibre from the IgM anti-MAG neuropathy. The two upper panels show part of a teased fibre in which no nodes of Ranvier can be reliably recognized (non-specific change). The two lower panels are cross sections through designated sites of the fibre at regular intervals of 200 µm. L2 is at the edge of a marker fibre. All cross sections show a thin myelin sheath and the myelin sheaths in L1 and L7 are extra pale corresponding to the very pale external appearance of the teased fibre. Schwann cell nuclei are seen in L2, L4, L6 and L9. The axonal calibre remains stable along the length of the fibre.

3.3.3 Electron microscopy

Transverse sections

Electron microscopy confirmed severe loss of myelinated fibres, especially the large fibres. Many fibres had thin myelin sheaths compared to the axonal calibres. Some fibres had very thin myelin sheaths and were surrounded by Schwann cell processes with abundant cytoplasm and enlarged vesicular Schwann cell nuclei indicative of a very early stage of remyelination (Fig. 3-7). Large (> 1 μm) completely naked axons were not found. Occasional fibres were surrounded by multiple Schwann cell processes suggestive of early onion bulb formation (Fig. 3-8). Many fibres showed characteristic splitting of the intraperiod line in the external layers of the myelin lamellae resulting in widened myelin lamellae (WML). WML were also present in the center and the innermost part of the myelin sheaths in a few fibres, and occasionally involved the entire myelin sheath (Fig. 3-9). Enlargement of the periaxonal space was detected in a few fibres, and some of them had severely compacted axons (Fig. 3-10). Some axons were surrounded by excessive myelin sheaths showing redundant myelin infolding or outfolding. The redundant folding myelin sheaths could be of normal myelin lamella periodicity or show WML (Fig. 3-11). Various degrees of complex myelin splitting and degeneration with normal, compacted or degenerative axons were present in many fibres (Fig. 3-12). WML, redundant myelin folding, enlargement of periaxonal space, myelin degeneration and compacted or degenerative axons could be present simultaneously in one fibre or in different fibres. One hundred random myelinated fibres were quantitated under × 20,000 magnification. WML was found in 62 (62%) fibres. WML was in the periphery of myelin in 60 fibres, in the inner mesaxon in 3 fibres (2 also in the periphery), in the center of the myelin sheath in 2 fibres (1 also in the periphery), and nearly through all the myelin sheath in 1 fibre. Enlargement of periaxonal space was found in 34 (34%) fibres. Redundant myelin folding was found in 5 (5%) fibres.

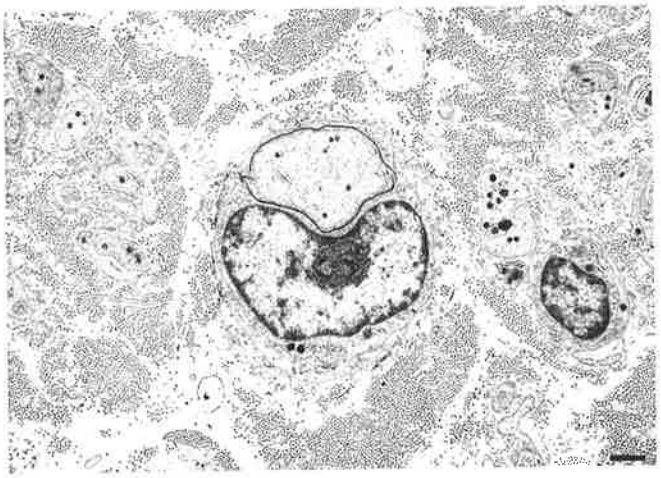

Figure 3-7. Electron micrograph shows a nerve fibre with a very thin myelin sheath surrounded by a Schwann cell with a vesicular nucleus indicative of a very early stage of remyelination. Bar = 1 μm

Figure 3-8. Electron micrograph shows a thinly myelinated nerve fibre was surrounded multiple Schwann cell processes indicative of early onion bulb formation.

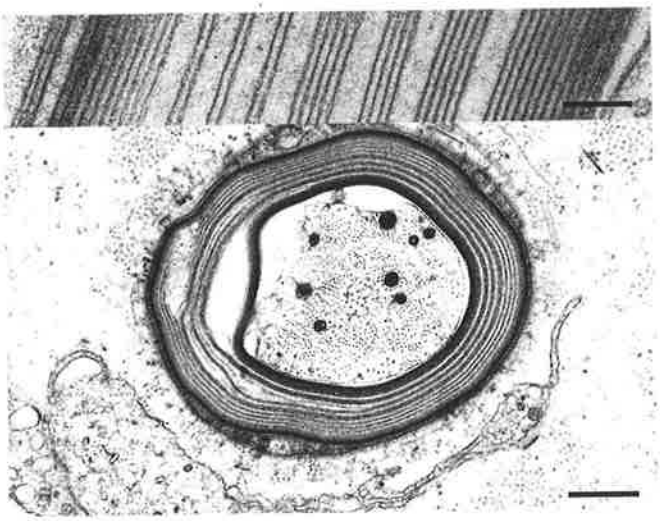

Figure 3-9. Electron micrograph of a cross section through a nerve fibre with enlarged adaxonal space and myelin splitting. WML involves nearly the entire myelin sheath (bar = 1 μm). Insert at the top of the picture shows WML at higher magnification (Bar = 0.1 μm).

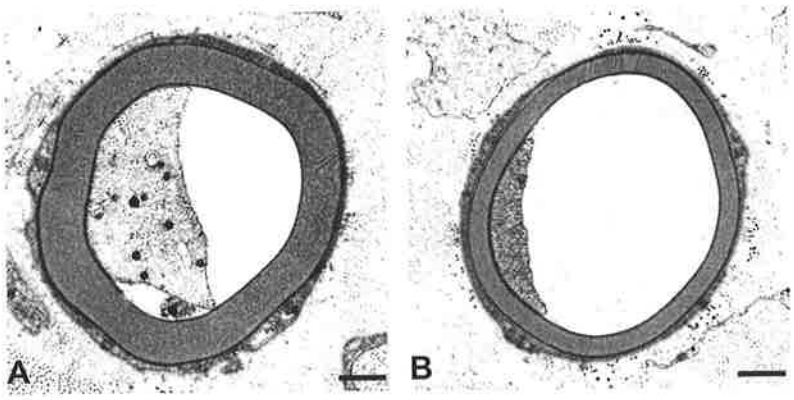

Figure 3-10. Electron micrographs show two myelinated fibres with intact myelin sheaths, enlarged periaxonal spaces and compacted axons (A, B). Bar = 1 μm

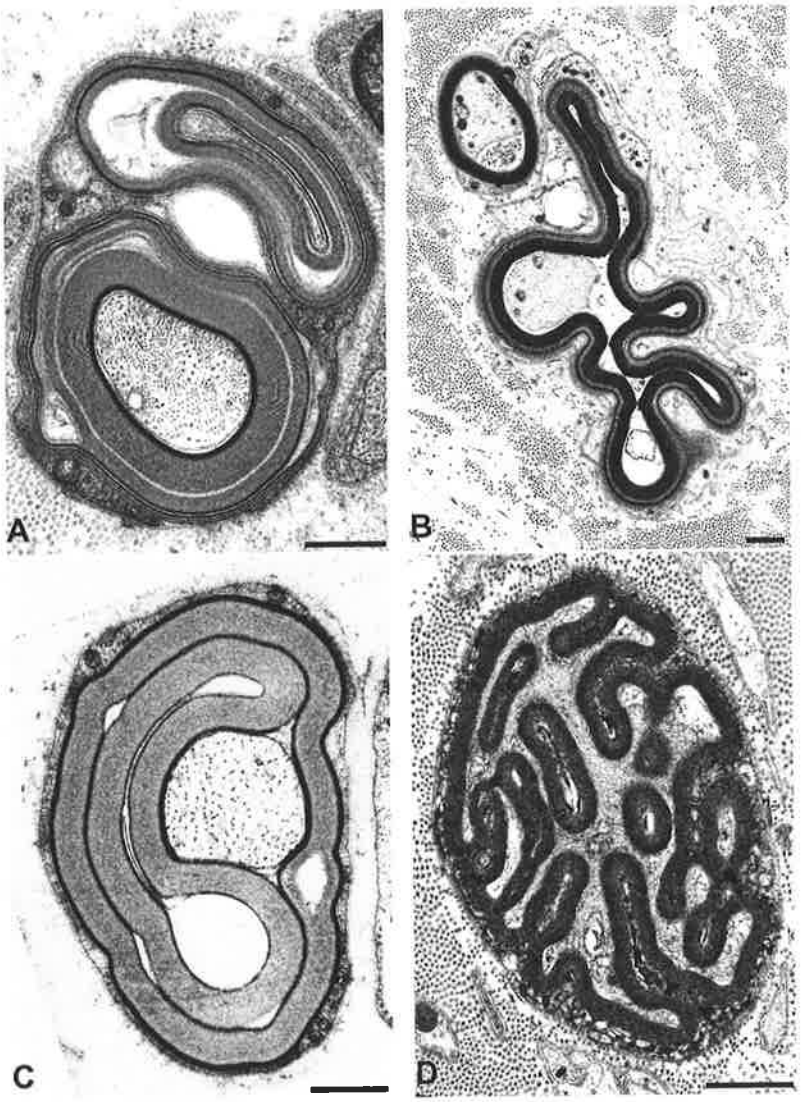

Figure 3-11. Electron micrographs show various patterns of myelin outfolding (A, B) and complex myelin infolding (C, D). WML can be clearly seen in the redundant folds of myelin (A, B). Bar = 1 μm

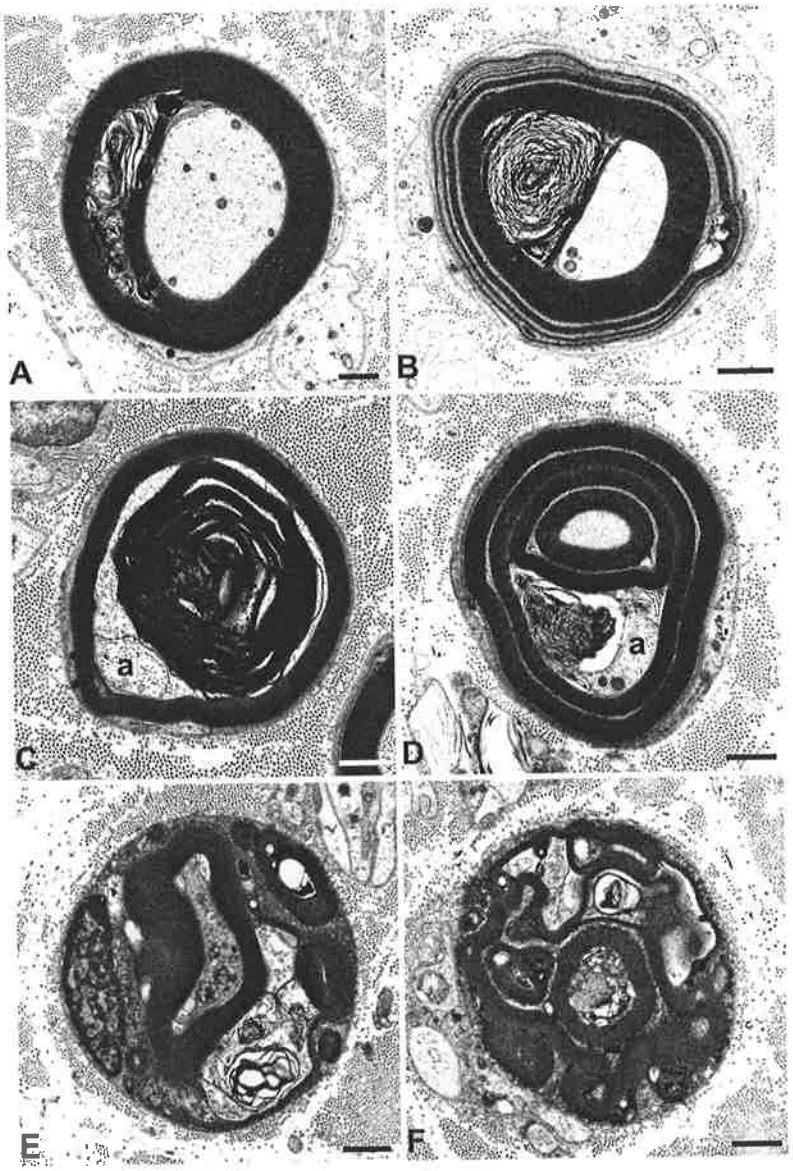

Figure 3-12. Electron micrographs showing various degrees of complex myelin splitting and degeneration. Myelin splitting with relatively normal axons is present in A and B. C shows a fibre with degenerate myelin surrounded by an externally intact myelin sheath and a severely compacted and displaced axon (a). D shows a fibre with redundant myelin folding, myelin degeneration and compacted axon (a). E and F show two fibres with myelin degeneration and complex myelin folding. Axons in these two fibres are also degenerate. Bar = 1 μm

Longitudinal sections

As in transverse sections, WML was usually found in the periphery of myelin sheaths, and sometimes extended from internodal regions to paranodal regions, leading to an increased space between the paranodal terminal loops (Fig. 3-13). It was noticed in a few paranodal-

nodal-paranodal regions that one side showed WML of the myelin sheath, while the other side showed normal periodicity of myelin lamellae. WML, localized to the center of the myelin sheath, was traced along the length of the fibre and was found to be in continuity with the Schmidt-Lanterman incisures (Fig. 3-14). Redundant myelin infolding and out folding were commonly encountered in longitudinal sections at both internodal and paranodal regions (Fig. 3-15–16). Sometimes redundant myelin infolding and outfolding loops were located just adjacent to each other (Fig. 3-15). WML and myelin degeneration were commonly found in the redundant folds of myelin.

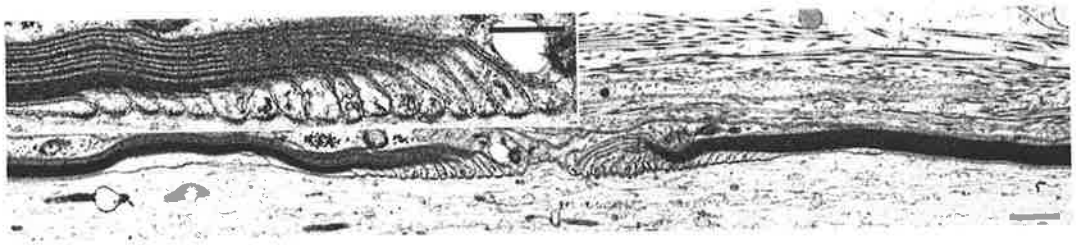

Figure 3-13. Electron micrograph of longitudinal section through a node of Ranvier (bar = 1 μm). WML is present to the left of the node of Ranvier, and extends from the internodal myelin to paranodal myelin. The periodicity of myelin lamellae at the right side of the node of Ranvier is normal. WML is clearly seen in the insert (left upper, bar = 0.5 μm).

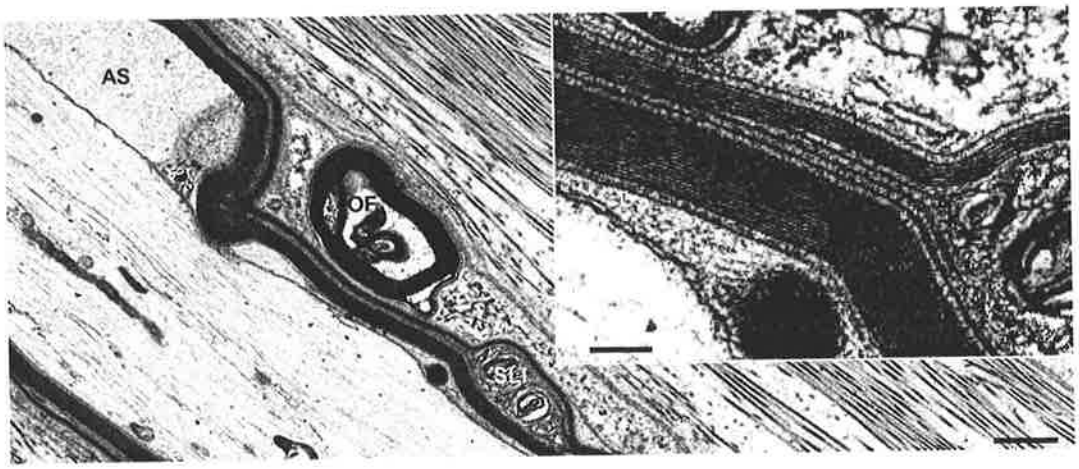

Figure 3-14. Electron micrograph showing enlargement of the adaxonal space (AS), redundant myelin outfolding with myelin degeneration (OF) and a Schmidt-Lanterman incisure (SCI) (bar = 1 μm). It clearly can be seen in the insert that WML in the center of the myelin sheath is a continuous expansion from the SLI (bar = 0.5 μm).

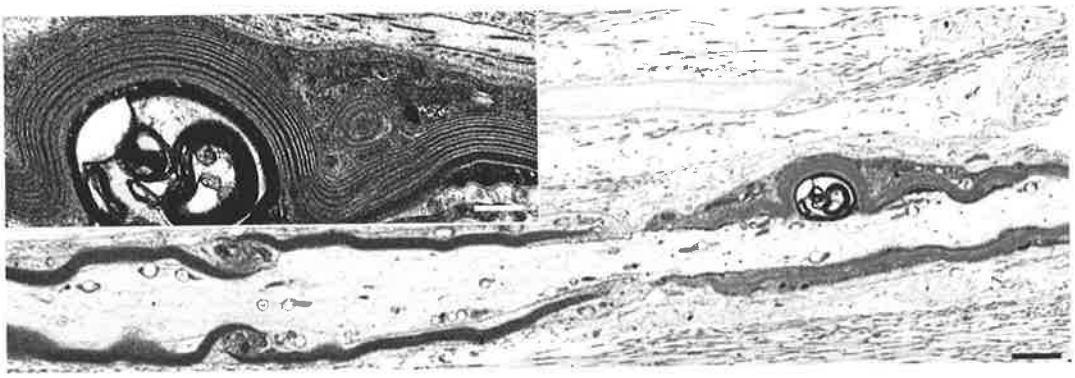

Figure 3-15. Electron micrograph of a longitudinal section through a node of Ranvier. A focal myelin swelling is present near the node of Ranvier (bar = 2 μm). Myelin degeneration is present in the focal myelin swelling, and the outer part shows WML (insert, bar = 0.5 μm).

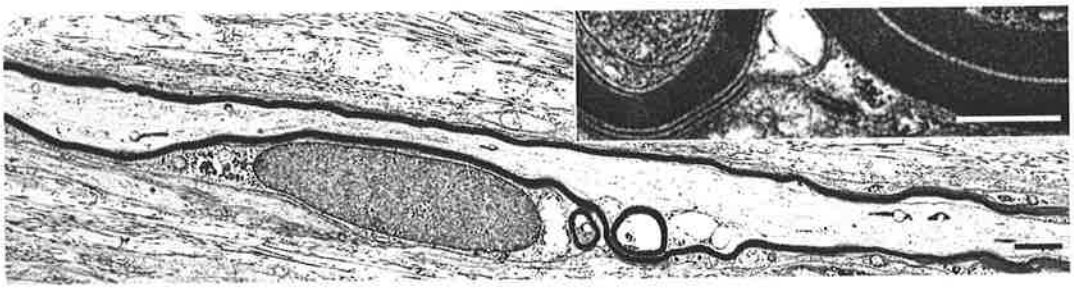

Figure 3-16. Electron micrograph of a longitudinal section through the internodal region of a myelinated fibre (bar = 2 μm). Outfolding and infolding myelin loops are located adjacent to each other. WML and myelin degeneration are present in the redundant myelin loops (insert, bar = 0.5 μm).

3.4 DISCUSSION

Focal myelin swellings and tomacula (myelin thickenings > 50% of fibre diameter as described by Verhagen *et al.*, 1993) have been described in the teased nerve fibres of IgM anti-myelin-associated glycoprotein (MAG) paraproteinaemic neuropathy (Jacobs and Scadding, 1990; Rebai *et al.*, 1989; Sander *et al.*, 2000) and focal hypermyelination of fibres in transverse sections of peripheral nerves has also been reported (Jacobs and Scadding, 1990; Lach *et al.*, 1993; Rebai *et al.*, 1989; Sander *et al.*, 2000; Vital *et al.*, 1989). The structure and mechanism of formation of focal myelin swellings and tomacula is not well understood. Demyelination/remyelination with axonal degeneration, widening of myelin lamellae and focal myelin thickenings found in this case are consistent with the typical pathological changes reported in IgM anti-MAG neuropathies (Vital *et al.*, 1989; Yeung *et al.*, 1991).

3.4.1 Anti-MAG IgM monoclonal antibodies

MAG was the first identified myelin target for monoclonal IgM antibodies in patients with demyelinating neuropathy and MGUS (Braun *et al.*, 1982). IgM anti-MAG antibodies from patients with peripheral neuropathy bind to the L2/HNK-1 carbohydrate epitope on MAG and other glycoconjugates, such as N-CAM, P0, PMP22, SGPG and sulfated glucuronic acid containing lactosaminyl paragloboside (SGLPG) (Ariga *et al.*, 1987; Burger *et al.*, 1990; 1992; Chou *et al.*, 1986; Hammer *et al.*, 1993; Ilyas *et al.*, 1990; Snipes *et al.*, 1993). The preferential binding of antibody to MAG may be because MAG contains multiple reactive oligosaccharide chains, whereas P0 and PMP22 only have a single oligosaccharide chain (Burger *et al.*, 1992, 1993), and MAG in non-compact myelin is more easily accessible to the antibody.

3.4.2 Focal myelin thickenings in anti-MAG neuropathy

Frequency and location of focal myelin thickening in teased nerve fibres

Although fibres with myelin sheaths of excessive thickness are commonly encountered in routine cross sections in neuropathies associated with anti-MAG IgM paraproteinaemia, focal myelin thickenings in teased myelinated nerve fibres have been reported in only a few cases (Jacobs and Scadding, 1990; Rebai *et al.*, 1989; Sander *et al.*, 2000). In 283 consecutive internodes from one case, Rebai *et al.* (1989) detected focal myelin swellings in 34% of internodes. Jacobs and Scadding (1990) noted only the very occasional tomaculous body in single fibres. In 3 patients, Sander *et al.* (2000) found that teased fibre preparations showed a high percentage of tomacula (52.7% of fibres), similar to our finding of tomacula in 62% of fibres teased in glycerol. As shown in the present case, tomacula are usually located in fibres showing demyelination/remyelination, and at both internodal and paranodal regions.

Structure of focal myelin thickenings

No previous study has focussed on the internal structure of tomacula in IgM anti-MAG neuropathy. Rebai *et al.* (1989) found redundant myelin loops (external and internal) and thick myelin sheaths on conventional electron microscopy in cases with focal myelin swellings in teased nerve fibres. Jacobs and Scadding (1990) suggested that the "bubbly" myelin in teased fibres was due to extensive swelling of the adaxonal space. These suggestions have been confirmed by our studies using the new teased nerve fibre technique. For the first time, we have demonstrated that myelin degeneration and multiple concentric myelin loops are also responsible for focal myelin thickenings and that these abnormalities may be present simultaneously in the same focal myelin thickening.

Mechanism of Tomacula Formation

The pathogenesis of focal myelin swellings and tomacula is not clear. The association of myelin thickening and the widening of myelin lamellae with IgM kappa deposition supports a pathogenic role for anti-MAG antibody in the formation of myelin swellings and tomacula (Lach *et al.*, 1993; Rebai *et al.*, 1989).

It has been suggested that this antibody binding to the L2/HNK-1 carbohydrate epitope, important in cell adhesion, may lead to the formation of tomacula and subsequent demyelination (Sander *et al.*, 2000). The presence of tomacula in fibres showing paranodal or internodal demyelination in the present case and in other reports (Jacobs and Scadding, 1990; Rebai *et al.*, 1989; Sander *et al.*, 2000) is in agreement with this view. Both in vitro and in vivo studies have supported the functional role of MAG in the maintenance of myelin and axon integrity (Schachner and Bartsch, 2000). Axonal atrophy and secondary segmental demyelination have been reported in IgM anti-MAG neuropathy (Jacobs and Scadding, 1990; Mendell *et al.*, 1985), and it has been suggested that axonal atrophy leads to focal redundancy and irregular folding of myelin sheaths leading to focal swellings (O'Neill and Gilliatt, 1987; O'Neill *et al.*, 1984). Tomacula and atrophic axons were also found in the peripheral nerve of adult MAG null mutant mice, and the tomacula attributed to outfolding of the myelin sheath due to axonal atrophy (Yin *et al.*, 1998). However, this does not explain focal excessive myelin in the absence of axonal atrophy. Although it was proposed that longitudinal movement of myelin along individual myelinated nerve fibres during the process of axonal atrophy led to the formation of tomacula (O'Neill and Gilliatt, 1987; O'Neill *et al.*, 1984), no evidence is available to support this hypothesis. In the present case, the finding of myelin infoldings and outfoldings in association with normal axons and externally normal internodes suggests that focal myelin swellings are the result of focal overproduction of myelin, which gradually increase in size. Animal studies suggest

that MAG has a functional role in inhibition of over-production of myelin (Li *et al.*, 1998). In IgM anti-MAG neuropathy, reduced MAG expression in myelin is often associated with thick IgM deposits (Gabriel *et al.*, 1996). Therefore it is reasonable to speculate that focal loss of MAG due to specific antibody binding leads to failure of inhibition of myelin formation and focal overproduction of myelin by the Schwann cell and tomaculum formation. The finding that myelin splitting and degeneration were commonly present in redundant myelin foldings indicates that these structures are not stable and tend to degenerate after a critical size reached, and is consistent with the finding in animal experiments that MAG functions in long-term maintenance of myelin integrity (Fruttiger *et al.*, 1995). Myelin debris in Schwann cell cytoplasm at the site of redundant myelin folds suggests that the Schwann cell which ensheaths the segment of the axon and generates the redundant myelin is also able to break down the redundant myelin. The enlargement of the adaxonal space in association with compaction of the axon in focal myelin swellings is consistent with disruption of normal myelin-axon relationships, and suggests that axonal structure may be focally modulated by MAG. Animal experiments suggest that MAG influences axonal calibre by modulating neurofilament phosphorylation (Yin *et al.*, 1998).

3.4.3 Demyelination in IgM anti-MAG neuropathy

As described in most peripheral nerve biopsies from the patients with IgM anti-MAG neuropathy (Ellie *et al.*, 1996; Mendell *et al.*, 1985; Jacobs, 1996; Smith, 1994; Vital *et al.*, 1989; Yeung *et al.*, 1991), demyelination was the predominant pathological process in the present case. Consistent with the finding of Jacobs and Scadding (1990), the incidence of segmental demyelination in teased nerve fibres was higher than might have been expected from the appearance in transverse section. In the present case, thin and pale myelin sheaths in cross sections through the demyelinated internodal and paranodal regions of the individual teased nerve fibres are consistent with the finding that no large completely naked

(demyelinated) axons were detected under EM. These results confirm the previous finding that very thin myelin sheaths may not be visible in teased nerve fibres under LM (Dyck *et al.*, 1993*a*) and suggest that if complete demyelination occurs, it is likely a transient phenomenon and completely demyelinated axons will be rapidly re-wrapped by new myelin lamellae.

The pathogenesis of demyelination in anti-MAG neuropathy is not well understood. MAG is a component of myelin. Autoantibodies against myelin component(s) may induce primary demyelination (Dyck *et al.*, 1993*a*). Binding of IgM anti-MAG antibodies to L2/HNK carbohydrate epitope shared by MAG and other glycoconjugates of PNS myelin, such as P_0 and PMP22, may contribute to the demyelination (Ariga *et al.*, 1987; Bollensen and Schachner, 1987; Bollensen *et al.*, 1988; Burger *et al.*, 1990, 1992; Chou *et al.*, 1986; Hammer *et al.*, 1993; Kruse *et al.*, 1984; McGarry *et al.*, 1983; Snipes *et al.*, 1993). On the other hand, MAG functions in myelin-axon relationships and can modulate axonal properties (Yin *et al.*, 1998; refer to Chapter 5). Segmental demyelination in a patient with IgM anti-MAG neuropathy was considered secondary to the axonal atrophy (Jacobs and Scadding, 1990). Distal axonopathy and secondary demyelination was also considered in another patient with IgM anti-MAG neuropathy (Mendell *et al.*, 1985). But these previous studies could not demonstrate axonal atrophy in teased fibres showing segmental demyelination (Jacobs and Scadding, 1990; Mendell *et al.*, 1985). Using the new teased nerve fibre technique, for the first time we have shown considerable variation of axonal calibre along the length of teased fibres showing segmental demyelination. Axonal compaction or axonal atrophy in externally normal segments of demyelinated teased fibres and axonal compaction or degeneration associated with well preserved myelin sheaths were present in our case and support the notion that the axon may be initially damaged in anti-MAG neuropathy and that demyelination is secondary to the axonopathy (Jacobs and

Scadding, 1990; Mendell *et al.*, 1985). This is also consistent with the recent finding that MAG functions in long term maintenance of axon-myelin relationships (Fruttiger *et al.*, 1995; Yin *et al.*, 1998). The feature of irregular axonal and myelin damage is consistent with autoantibody binding at different regions of the nerve fibre.

3.5 CONCLUSION

Tomacula and focal swellings are due to increased concentric multiple loops around the axon, redundant myelin infolding or outfolding, enlargement of the adaxonal space, myelin degeneration or a combination of these processes. It has also been shown that similar changes may be present in otherwise externally normal segments of teased fibres suggesting that these represent an early phase in the evolution of myelin swellings. The finding of axonal compaction in externally normal segments of teased fibres showing demyelination suggests that the primary damage is axonal and the demyelination secondary. The disturbances of myelin and myelin-axon relationships in this study are consistent with altered neural adhesion produced by anti-MAG antibodies targetting particularly vulnerable anatomical sites of the nerve fibres determined by the presence of MAG.

CHAPTER 4: Teased Nerve Fibre Studies in MAG Deficient Mice

4.1 Introduction **148**

4.2 MAG knockout mice and tomacula in experimental models **149**

4.2.1 Phenotype of MAG knockout neuropathy 149

4.2.2 MAG functions in maintenance of myelin-axon integrity in the PNS 149

4.2.3 MAG is essential in myelin formation and maintenance in the CNS 152

4.2.4 Studies of MAG and other myelin component(s) multiple knockout mice 153

4.2.5 Focal myelin swellings and tomacula in experimental models 156

4.3 Materials and Methods **159**

4.3.1 Animals 159

4.3.2 Nerve biopsies and tissue preparation 159

4.4 Results **160**

4.4.1 Glycerated Teased Nerve Fibre Studies 160

4.4.2 Correlative study of external appearance with multiple cross sections 161

4.4.3 Correlative study of external appearance with multiple longitudinal sections 165

4.4.4 Light microscopy 171

4.4.5 Electron microscopy 176

4.5 Discussion **181**

4.5.1 MAG is not essential for the initiation of myelination but functions in the long-term maintenance of myelin-axon integrity 181

4.5.2 Demyelination is not a feature in MAG-deficient mice 182

4.5.3 Focal myelin swellings and tomacula in MAG deficient mice 183

4.5.4 Comparison of experimental MAG knockout neuropathy and human IgM anti-MAG neuropathy 188

4.6 Conclusions **190**

4.1 INTRODUCTION

Although *in vitro* studies yielded major insights into the functional roles of MAG during myelination formation and the maintenance of myelin-axon interactions in the adult (**Chapter 1**), knowledge of its function *in vivo* was still lacking. Auto-antibodies against MAG can cause demyelinating peripheral neuropathy with various degrees of axonal damage (**Chapter 3**). Hereditary neuropathy due to MAG gene mutation has not been found. The generation of mice deficient in the expression of MAG by targeted disruption of the MAG gene via homologous recombination in embryonic stem cells allowed the study of the functional role of this molecule *in vivo* (Li *et al.*, 1994; Montag *et al.*, 1994). Knockout of the MAG gene ($MAG^{-/-}$) results in complete absence of MAG messenger RNA and MAG in both the CNS and PNS (Li *et al.*, 1994; Montag *et al.*, 1994). However, the other components of myelin in both the PNS and CNS are not different from those of wild-type littermates (Montag *et al.*, 1994). Heterozygous MAG-deficient ($MAG^{+/-}$) mice did not show any clinical and pathological phenotype (Fujita *et al.*, 1998; Montag *et al.*, 1994). Studies in homozygous MAG-deficient mice have provided new insights of functions of MAG in the formation and maintenance of myelin and in myelin-axon interactions.

In this chapter the myelin and axonal relationships within focal myelin swellings and tomacula of individual teased nerve fibres in MAG deficient mice are examined and compared with findings in human IgM anti-MAG neuropathy.

4.2 MAG KNOCKOUT MICE AND TOMACULA IN EXPERIMENTAL MODELS

4.2.1 Phenotype of MAG knockout mice

Homozygous MAG mutants displayed a subtle phenotype. No gross behavioural abnormalities were apparent (Li *et al.*, 1994; Montag *et al.*, 1994). The Water maze test (Morris, 1984; Morris *et al.*, 1982) demonstrated that the capabilities of $MAG^{-/-}$ mutants for coordinated movement and learning were not significantly different from wild-type littermates (Montag *et al.*, 1994). However, the bar-crossing test (Gerlai *et al.*, 1993) showed that mutant mice exhibited decreased locomotor activity and a mild and transient trunk tremor, suggesting that their finer motor coordination abilities were significantly affected by the mutation (Li *et al.*, 1994). Establishment of MAG-deficient lines by intercrossing homozygous MAG-deficient mice proved that both sexes are fertile (Montag *et al.*, 1994).

4.2.2 MAG functions in maintenance of myelin-axon integrity in the PNS

Role in PNS myelination

In MAG-deficient mutants, myelination in the PNS is similar to that observed in wild-type mice (Li *et al.*, 1994; Montag *et al.*, 1994). In the pectineus nerves of 4-day-old wild type and $MAG^{-/-}$ mice, the numbers of myelinated axon-Schwann cell units and axon-Schwann cell units acquiring the 1:1 ratio, but not yet myelinated, are indistinguishable (Montag *et al.*, 1994). In agreement with these findings, serial studies of sciatic nerves at different age also show that the number of myelinated fibres are comparable between $MAG^{-/-}$ and wild-type animals from postnatal 7 days to 9 months (Yin *et al.*, 1998).

The ultrastructure of compact myelin was unaffected in the PNS of MAG-deficient mutants (Li *et al.*, 1994; Montag *et al.*, 1994). X-ray diffraction studies showed the normal

periodicities of compact myelin lamellae in sciatic nerves (17.4 ± 0.01 nm in $MAG^{-/-}$ vs 17.4 ± 0.04 nm in $MAG^{+/+}$) (Li *et al.*, 1994).

Conflicting results have been reported concerning the Schwann cell periaxonal cytoplasmic collar and adaxonal space in MAG-deficient animals. Although loss of the periaxonal cytoplasmic collar and/or a dilated adaxonal space in some myelinated fibres in the PNS were reported (Li *et al.*, 1994), this was not confirmed (Montag *et al.*, 1994). An *in vitro* study showed that MAG-deficient Schwann cells myelinated neurites of co-cultured dorsal root ganglion (DRG) neurons with intact periaxonal cytoplasmic collar and periaxonal space (Carenini *et al.*, 1998).

Although MAG is not a crucial factor for myelin formation *in vivo* (Li *et al.*, 1994; Montag *et al.*, 1994), the analyses of adult and aged MAG null mutants reveal that MAG is a critical factor in the long-term maintenance of axon-myelin integrity, especially in the PNS (Fruttiger *et al.*, 1995; Yin *et al.*, 1998).

Degeneration and regeneration of myelinated fibres in the PNS

Degenerating MFs were first demonstrated in the peripheral nerves of 8- and 10-month-old $MAG^{-/-}$ mice (Fruttiger *et al.*, 1995). The incidence of degenerating MFs in postnatal 35 days to 16 months $MAG^{-/-}$ mice was significantly higher than in age-matched control mice (Yin *et al.*, 1998). Formation of onion bulbs, tomacula and decreased axonal calibre were demonstrated in the PNS of $MAG^{-/-}$ mice (Carenini *et al.*, 1997; Fruttiger *et al.*, 1995; Yin *et al.*, 1998). Probable regenerating sprouts were also noticed as unmyelinated fibres were ensheathed by Schwann cells, occasionally containing degenerate myelin and axonal debris (Fruttiger *et al.*, 1995). Fruttiger *et al* (1995) also reported the presence of onion bulbs, consisting of relatively large axons surrounded by multiple circumferentially oriented and

crescent-shaped Schwann cell processes each covered by basal lamina. Such structures are considered to originate as a result of repeated demyelination and remyelination-induced proliferation of Schwann cells (Dyck *et al.*, 1993*a*).

MAG modulates axonal properties in the PNS

The periaxonal localization of MAG suggests the potential function of MAG in axon-Schwann interaction (see above). Early studies in young MAG-deficient mice did not find morphological changes in the axon (Li *et al.*, 1994; Montag *et al.*, 1994). However, further studies indicate that MAG may exert a positive influence on the calibre of myelinated axons (Yin *et al.*, 1998). Morphometric studies showed that the calibre of axons surrounded by morphologically intact myelin in the sciatic nerves of $MAG^{-/-}$ mice of 3-month-old or over was significantly smaller than that of age-matched wild-type mice. Reduced axonal calibre correlated with reduced neurofilament spacing and a decrease of neurofilament phosphorylation (Yin *et al.*, 1998). Yin *et al.* (1998) suggested that MAG-deficient mice are a model for investigating mechanisms of axonal atrophy and degeneration and testing potential therapeutics that may delay or stop axonal atrophy associated with chronic diseases of myelin.

L-MAG is not essential for PNS myelination

The expression of L-MAG in the early stage of myelination in the PNS (Ishiguro *et al.*, 1991) suggests that L-MAG might be involved in myelin formation. However, myelin in the PNS appeared morphologically normal in mice deficient for L-MAG generated by introducing a stop codon into exon 13 of the MAG gene (Fujita *et al.*, 1998). Moreover, neither changes in periaxonal structures nor increased axonal degeneration was detected in 1-, 8-, 12-, and 16-month-old mutant animals. This finding suggests that L-MAG may not

be essential for the PNS, and that S-MAG may be sufficient to maintain the integrity of myelin and the axon in the PNS (Fujita *et al.*, 1998).

4.2.3 MAG is essential in myelin formation and maintenance in the CNS

A significant delay in the formation of compact myelin and hypomyelination were observed in the CNS in $MAG^{-/-}$ mice (Bartsch *et al.*, 1997; Li *et al.*, 1998; Montag *et al.*, 1994). The ultrastructure of compact myelin was unaffected in the CNS in $MAG^{-/-}$ mice (Bartsch *et al.*, 1995*b*; Li *et al.*, 1994; Montag *et al.*, 1994; Uschkureit *et al.*, 2000). However, oligodendrocyte cytoplasm (or cytoplasmic domain) was noted in some compact myelin sheaths (Li *et al.*, 1994; Montag *et al.*, 1994) of mutants but were absent in wild-type littermates (Montag *et al.*, 1994). In many of these sheaths, cytoplasm was restricted to terminal oligodendrocyte processes. These processes frequently correlated with a change in spiralling direction of myelin, suggesting that some axons in MAG-deficient mice are concentrically surrounded by more than one myelin sheath, double or multiple myelination (Bartsch *et al.*, 1995a; Montag *et al.*, 1994). The myelin sheaths displaced from the axon had a normal ultrastructure of compact myelin (Bartsch *et al.*, 1995a; Li *et al.*, 1998). Further investigations in the mechanism of the formation of multiple myelination will be beneficial for understanding the functional role(s) of MAG in the glia-axon signalling. Multiple myelination resulted in increased thickness of compact myelin in relation to axon diameter (Bartsch *et al.*, 1995*b*). A dying-back oligodendrogliopathy was noted in aged $MAG^{-/-}$ mice (Lassmann *et al.*, 1997).

Morphological and morphometric studies of CNS myelin revealed that the phenotype of L-MAG knockout mice was similar to that found in total MAG null mutants (Fujita *et al.*, 1998).

4.2.4 Studies of MAG and other myelin component(s) in double and triple knockout mice

Why does a decrease in the levels of MAG RNA *in vitro* impair myelination (Owens and Bunge, 1991), whereas a null mutation of the MAG gene *in vivo* does not (Li *et al.*, 1994; Montag *et al.*, 1994)? It has been suggested that compensatory mechanisms are available *in vivo* that are not available *in vitro* (Montag *et al.*, 1994). Schwann cells from MAG null mutants myelinate dorsal root ganglion neurons *in vitro* (Carenini *et al.*, 1998). Double or triple knockout mutants of MAG and other myelin components have been generated to investigate the possible involvement of other molecules in the formation and/or maintenance of myelin.

N-CAM and MAG double knockout mice

The neural cell adhesion molecule, N-CAM, was the first Ig-like cell adhesion molecule to be isolated and characterized in detail (Brackenbury *et al.*, 1977; Cunningham *et al.*, 1987). It is expressed by myelinating oligodendrocytes and Schwann cells. During development, its expression becomes confined to the axon-Schwann cell interface accompanied by the expression of MAG (Martini, 1994*a*; Martini and Schachner, 1986). In the spiral ganglia of wild type mice where nerve cell bodies are normally myelinated, MAG is not detectable in the perikaryal myelin but appears to be topographically replaced by N-CAM (Martini, 1994*b*). Expression of N-CAM is up-regulated at both protein and mRNA levels at those sites where MAG would normally be located in MAG-deficient mice (Montag *et al.*, 1994). N-CAM and MAG double knockout (*N-CAM*$^{-/-}$*MAG*$^{-/-}$) mice were generated by cross breeding the single mutants. The ultrastructure of myelin sheaths in peripheral nerves of N-CAM$^{-/-}$ mice or *N-CAM*$^{-/-}$*MAG*$^{-/-}$ mice was not affected, indicating that N-CAM is not required for the formation of morphologically intact myelin. However, degeneration of myelinated fibres started earlier in *N-CAM*$^{-/-}$*MAG*$^{-/-}$ mutants than in MAG$^{-/-}$ mice,

indicating a role for N-CAM in the maintenance of PNS myelin (Carenini *et al.*, 1997). N-CAM and MAG collaborate to function in the long-term maintenance of myelin integrity in the CNS (Schachner and Bartsch, 2000).

MAG and L1 double knockout mice

The neural adhesion molecule L1 is another candidate molecule that might compensate for the lack of MAG in MAG mutants. During development, L1 is expressed on fasciculating axons and Schwann cells at the onset of myelination, and becomes completely undetectable on both axons and Schwann cells when Schwann cells have made 1 and a half turns around the axon, at which time the Schwann cell expresses MAG (Martini *et al.*, 1994a; Martini and Schachner *et al.*, 1986). Anti-L1 antibodies interfere with the segregation and myelination of DRG neurites by co-cultured Schwann cells (Seilheimer *et al.*, 1989; Wood *et al.*, 1990). However, the analysis of 1-month-old $MAG^{-/-}L1^{-/-}$ mutants and control mice revealed a similar number of myelinated axons in the sciatic nerves of both genotypes (Haney *et al.*, 1996*b*).

MAG and P_0 double knockout mice

P_0 also belongs to neural cell adhesion molecule subfamilies of the immunoglobulin superfamily, and peripheral nerves of P_0-deficient mice display a severe dysmyelinating phenotype, confirming the view that P_0 mediates myelin formation and compaction (refer to section **2.6.1**). In 4-week-old $P_0^{-/-}MAG^{-/-}$, the dysmyelinating phenotype of the axon-Schwann cell units was very similar to that seen in the P_0-deficient single mutants, suggesting that MAG was not involved in the poor myelin compaction of P_0-deficient mice. However, peripheral nerves of older $P_0^{-/-}MAG^{-/-}$ mutants contained significantly more unmyelinated axons that had acquired a 1:1 relationship with Schwann cells than P_0 mutants of the similar age. These observations suggest a subtle role for MAG in the formation of

peripheral myelin, which becomes only apparent in the simultaneous absence of P_0 (Carenini *et al.*, 1999).

MAG and PLP double knockout mice

Proteolipid protein (PLP) is the major integral myelin component of CNS myelin, accounting for approximately 50% of myelin protein, but is also expressed by myelinating Schwann cells. However, in contrast to oligodendrocytes in the CNS, it is not incorporated into the myelin of Schwann cells in the PNS (Puckett *et al.*, 1987). The PLP gene is carried on the X-chromosome and encodes 2 isoforms, PLP and DM_{20} (Nave *et al.*, 1987; Yan *et al.*, 1993). PLP has 4 hydrophobic transmembrane domains, thus resembling channel proteins (Weimbs and Stoffel, 1992). PLP gene mutations in man cause Pelizaeus-Merzbacher disease (PMD), a central nervous system dysmyelinating disease typically characterized by nystagmus, delayed psychomotor development, spasticity and ataxia (Adams *et al.*, 1997). Most investigators have found that peripheral nerve function and structure is normal in patients with PMD. However, Garbern *et al.* (1997, 1999) reported a family with a mutation leading to absence of PLP and a demyelinating peripheral neuropathy. In $PLP^{-/-}$ mice, CNS myelin compaction is impaired and myelin lamellae are separated at the intraperiod dense line (Boison and Stoffel, 1994; Boison *et al.*, 1995). In $PLP^{-/-}MAG^{-/-}$ double mutants, the morphological abnormalities of the $PLP^{-/-}$ and $MAG^{-/-}$ single mutants are cumulative (Uschkureit *et al.*, 2000). The most striking feature is the early onset of axon degeneration in the CNS around postnatal day 40 (Uschkureit *et al.*, 2000), which starts in the $PLP^{-/-}$ mouse only at later stages of life (Griffiths *et al.*, 1998). These observations suggest that MAG functions in the maintenance of CNS axons in the absence of PLP.

MBP knockout mice and PLP, MBP and MAG double and triple knockout mice

Myelin basic proteins (MBPs) comprise 30-40% of CNS and 5-15% of PNS myelin proteins. The shiverer mouse, a naturally occurring null-mutant for MBP, is characterized by severe CNS hypomyelination, lack of major dense lines in myelin sheaths and premature death within 3 months (Rosenbluth, 1980*a*). PNS myelin does not show major abnormalities (Kirschner and Ganser, 1980; Rosenbluth, 1980*b*) except for an increased number of Schmidt-Lanterman incisures (Gould *et al.*, 1995). In $PLP^{-/-}MBP^{-/-}$ double and $PLP^{-/-}MBP^{-/-}MAG^{-/-}$ triple mutants, the CNS hypomyelination was not as severe and the lifespan of the double and triple mutants was prolonged (Uschkureit *et al.*, 2000).

4.2.5 Focal myelin swellings and tomacula in experimental models

Tomacula in MAG knockout mice

In MAG deficient mice, Yin *et al.* (1998) found tomacula were often located in paranodal regions and sometimes in internodal regions and the incidence of paranodal tomacula in the sciatic nerves increased from 57% at postnatal 3 months to 93% at postnatal 9 months (Yin *et al.*, 1998). In the paranodal tomacula, the focal excessive myelin was positioned asymmetrically around axons which showed dramatic focal reduction of calibre and neurofilament spacing (Yin *et al.*, 1998). These findings were interpreted as that paranodal tomacula in MAG deficient resulted from focal axonal shrinkage and folding of the myelin sheaths.

Focal myelin swellings were also found in paranodal regions but not in internodal regions in MAG and N-CAM double knockout mice (Carenini *et al.*, 1997). They were attributed to paranodal hypermyelination based on the symmetrical and disproportionately thick myelin sheaths (Carenini *et al.*, 1997). It was hypothesized that focal hypermyelination may cause mechanical axonal constriction and axonal degeneration (Carenini *et al.*, 1997).

Tomacula in PMP22 knockout mice

Tomacula were reported in heterozygous and homozygous PMP22 deficient mice (Adlkofer *et al.*, 1995; 1997). They were often located in paranodal regions and sometimes in internodal regions (Adlkofer *et al.*, 1995; 1997). In PMP22 homozygous deficient mice, tomacula were abundant at postnatal day 24 but were rarely found at postnatal week 10 at which time the fibres showed extensive segmental demyelination (Adlkofer *et al.*, 1995). PMP heterozygous mice developed an increasing number of tomacula over the first 10 weeks and tomacula were found in about 90% internodal segments at postnatal 5 months. Subsequently the frequency of tomacula decreased and the frequency of segmental demyelination increased (Adlkofer *et al.*, 1997). In heterozygous PMP22 deficient mice tomacula were attributed to focal hypermyelination (Adlkofer *et al.*, 1997).

Focal myelin swellings and tomacula in P_0 mutant mice

Focal myelin thickenings, which were termed "myelin ovoids", were found in 70% of paranodes in 4-month-old P_0 heterozygous deficient mice (Martini *et al.*, 1995*a*). These "myelin ovoids" were identified as complex and asymmetric myelin infoldings (Martini *et al.*, 1995*a*). In 1-year-old P_0 heterozygous deficient mice, teased nerve fibres showed extensive segmental demyelination, and the frequency of paranodal "myelin ovoids" was not documented (Martini *et al.*, 1995*a*).

Transgenic mice expressing a full length P_0 modified in the extracellular domain with a myc epitope tag (5'-CCATTGAGCAAAAGCTCATTTCTGAAGAGGACTTGAATG-3') showed a dysmyelinating peripheral neuropathy similar to CMT1B (Previtali *et al.*, 2000). Tomacula in these mice often originated from the paranodal regions and were due to redundant myelin foldings. The axon caliber is preserved underneath the tomacula (Previtali *et al.*, 2000).

Tomacula in neurofilament deficient quails

Focal myelin thickenings were found at both paranodal and internodal regions of otherwise externally normal teased nerve fibres of neurofilament deficient quails (Zhao *et al.*, 1993). They were thought to be the result of redundant myelin sheath due to the radial growth or maturation arrest of the axon (Zhao *et al.*, 1993).

4.3 MATERIALS AND METHODS

4.3.1 Animals

Mice deficient in MAG at the mRNA and protein levels resulting from disruption of the MAG gene (Li *et al.*, 1994) were provided by John Roder (Samuel Lunenfeld Research Institute, Mount Sinai Hospital, Canada) and maintained at the Walter & Eliza Hall Institute for Medical Research, Melbourne, Australia. Nineteen MAG gene knockout ($MAG^{-/-}$) mice of different ages and 14 age-matched control mice (Table 4-1) were used (Animal Ethics Committee, Institute of Medical and Veterinary Science, approval number 77/99).

Table 4-1 Control and mutant mice used in this study

Age (month)	$MAG^{+/+}$	$MAG^{-/-}$
0.5	2	2
1	2	2
4	4	5
9	3	5
20	3	5

4.3.2 Nerve Biopsies and Tissue Preparation

Mice were sacrificed by decapitation. Bilateral sciatic and posterior tibial nerves were immediately removed and immersed in 2.5% glutaraldehyde in 0.05 mol/l cacodylate buffer, keeping the natural shape of the nerve tissue without any stretching. Extreme care was taken in order to avoid nerve crushing and over stretching. Animal nerve tissues were then processed according to the methods described in chapter 2 except that the 1% osmium tetroxide for post-fixation was in 0.05 mol/l cacodylate buffer.

4.4 RESULTS

4.4.1 Glycerated Teased Nerve Fibre Studies

Fifty individual nerve fibres were prepared from the left posterior tibial nerve of every mouse and from the left sciatic nerve of 3 postnatal 9 months (P9m) mutants and 3 P9m control mice. Each fibre contained at least 5 internodes. Individual nerve fibres were classified according to Dyck *et al.* (1993*a*). Fibres showing segmental demyelination, remyelination or Wallerian degeneration constituted less than 4% of fibres in mutant and control mice. A striking finding in the teased nerve fibres from MAG-deficient mice was the presence of focal myelin thickenings (approximately 15-45 μm in length and 15-25 μm in maximum width). They were usually located at paranodal regions (paranodal myelin thickenings or paranodal tomacula) and occasionally (less than 2%) at sites close to the paranode (juxtaparanodal myelin thickenings or juxtaparanodal tomacula). Paranodal myelin thickenings were first detected in the mutants at age P1m. Their frequency increased significantly with age (R^2 = 0.85, P<0.05; Table 4-2). The size of paranodal myelin thickenings increased with age and after P4m most reached the criteria for tomacula, i.e. myelin thickenings > 50% of fibre diameter (Verhagen *et al.* 1993). Tomacula were present on only one side of a node of Ranvier (unilateral paranodal tomacula) or both sides of the node (bilateral paranodal tomacula). Occasional paranodal myelin thickenings were also noted in control after P9m of age, but the frequency was significant lower than that of age-matched mutants (Table 4-2).

Table 4-2. Frequency (%) of paranodal myelin thickenings in glycerol teased nerve fibres

Age (month)	Nerve	0.5	1	4	9	20
$MAG^{+/+}$	tibial	0	0	0.9±0.9	1.8±1.3	3.0±1.7
$MAG^{-/-}$	tibial	0	3.8±1.9*	15.1±3.9**	20.8±4.6**	28.4±5.3**
$MAG^{+/+}$	sciatic	–	–	0.7±0.2	–	–
$MAG^{-/-}$	sciatic	–	–	14.3±1.2**	–	–

Numbers represent mean ± SD of paranodal myelin thickenings on glycerol teased nerve fibres; *P<0.05; **P<0.01.

4.4.2 Correlative study of external appearance with multiple cross sections

Eighteen single myelinated fibers teased in resin from 2 P9m MAG-deficient mice (12 from one and 6 from another) and 14 fibers from 2 P20m mutants (6 from one and 8 from another) were transversely sectioned and the cross sectional appearance correlated with the external appearance of the teased fibers at corresponding points. A total of 83 paranodal tomacula were identified in these fibers, including 49 from the P9m mutants and 34 from the P20m mutant. Only one juxtaparanodal myelin thickening was identified in a fiber from the P20m mutant. Transverse sections through the 83 paranodal tomacula showed various morphological appearances, including complex myelin infolding or outfolding, symmetric and disproportionately thick myelin, and complex myelin splitting and degeneration.

Redundant myelin infolding (eg, L2 in Fig. 4-1) and outfolding (eg, L9 in Fig. 4-1) were often so complex (eg, L19 in Fig. 4-1) that they were hard to differentiate from each other. Redundant myelin folding, including infolding and outfolding, was the cause of swelling in 73.5% (36/49) of paranodal myelin thickenings from the P9m mutants and 50% (17/34) of paranodal myelin thickenings from the P20m mutant. Myelin splitting and degeneration were often noted in redundant folds of paranodal myelin (eg, L9 and L19 in Fig. 4-1).

Complex myelin splitting and degeneration without discernible redundant myelin folds were found in 24.5% (12/49) of paranodal myelin thickenings from the P9m mutants (e.g., L28 in Fig. 4-1) and in 47.1% (16/34) from the P20m mutant. The frequency of complex myelin splitting and degeneration in the P20m mutant was significantly higher than in the P9m mutants (Chi square test, $P<0.05$).

At sites of redundant myelin folding the axon was usually constricted. At some sites of focal paranodal myelin swellings, the axonal constriction was so severe that it was difficult to identify the axon.

Symmetric and disproportionately thick myelin (e.g., L2 in Fig. 4-2) was found in 1 of the 49 paranodal myelin thickenings from the P9m mutants (3.1%) and 1 of the 34 tomacula from the P20m mutant (2.9%).

Transverse sections through the juxtaparanodal myelin thickenings revealed myelin outfolding with an axon smaller than that present in neighbouring internodal compact myelin regions (L5 in Fig. 4-3).

Complicated redundant myelin folding in association with myelin splitting and degeneration were not detected in transverse sections through externally normal internodal regions, which did, however, show enlargement of the adaxonal space in some areas (eg, L15 in Fig. 4-1).

Five myelinated fibres from a P9m control and 10 from 2 P20m control mice were transversely sectioned. Simple myelin infolding was found in a paranode in one fibre from a P20m control. Complex redundant myelin folding, myelin splitting and myelin degeneration were not detected in either internodal and paranodal regions.

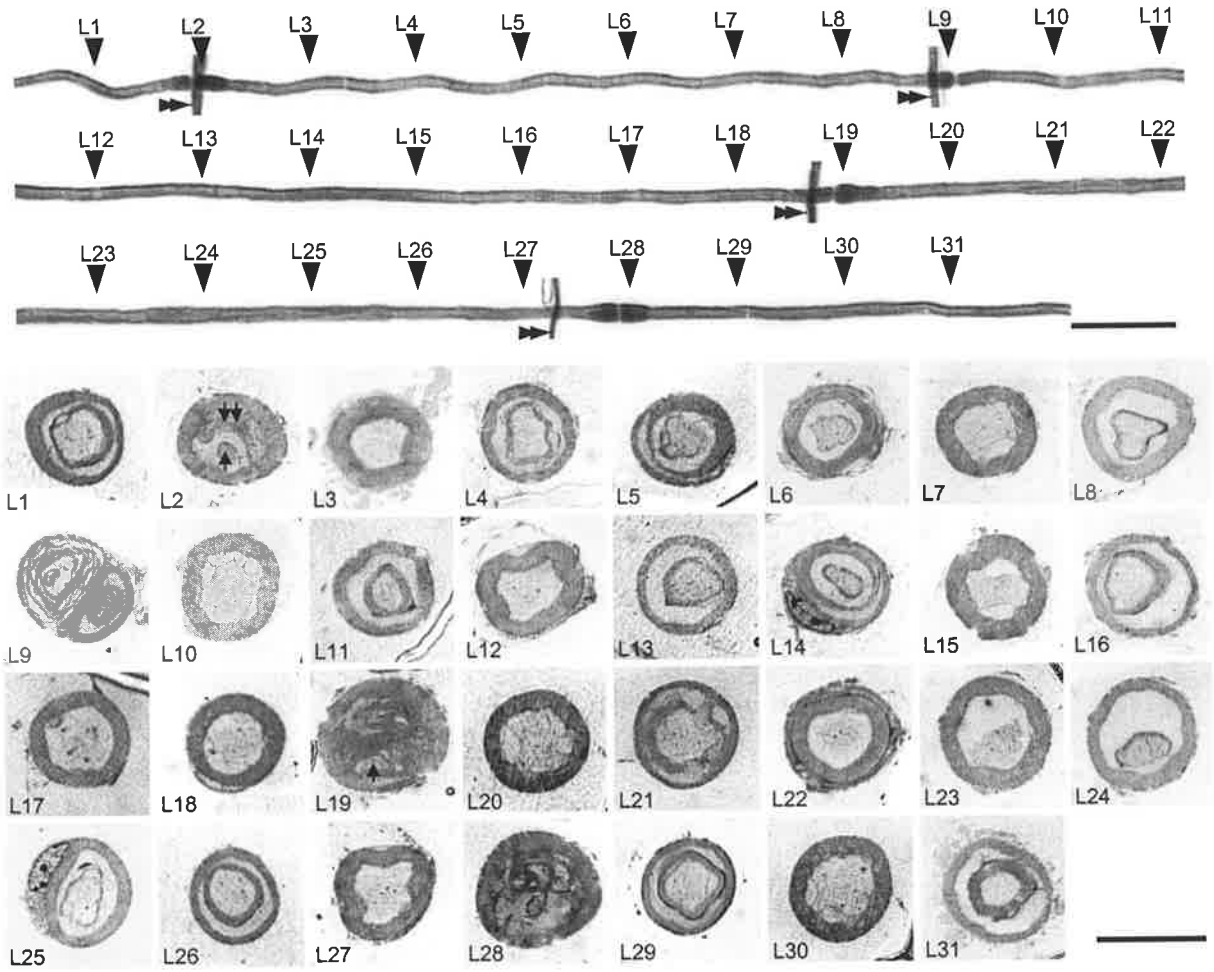

Figure 4-1. Light micrographs. The three upper panels show a single myelinated nerve fiber teased in resin from the P9m MAG-deficient mouse. Paranodal myelin thickenings are present in the fiber at L2, L9, L19 and L28. Four vertical marker fibers (double arrowheads) indicate specific sites for transverse sectional studies (bar = 100 μm). The four lower panels show semithin transverse plastic sections stained with toluidine blue through specific sites along the fiber as indicated by arrowheads, L1–31. The interval between two adjacent sections is 100 μm. Section L2 through the first paranodal myelin thickening shows myelin infolding (double arrows) with a small axon (arrow). Section L9 through the second paranodal myelin thickening shows myelin outfolding with complex myelin splitting in the outfolding myelin and a small axon (arrow). Section L19 through the third paranodal myelin thickening shows complex myelin folding in association with myelin degeneration and a constricted axon (arrow). Section L28 through the last paranodal myelin thickening shows complex myelin splitting and degeneration in association with a severely constricted axon (arrow). Cross sections through externally normal internodal regions show Schmidt-Lanterman incisures (L1, L4–6, L8, L11, L13–14, L16, L21, L24–26, L29 and L31), enlargement of adaxonal space (L15) and Schwann cell nuclei (L14 and L25). bar = 20 μm for transverse sections. Teased fibre and cross sections were digitized using the MC500 Image Analysis system.

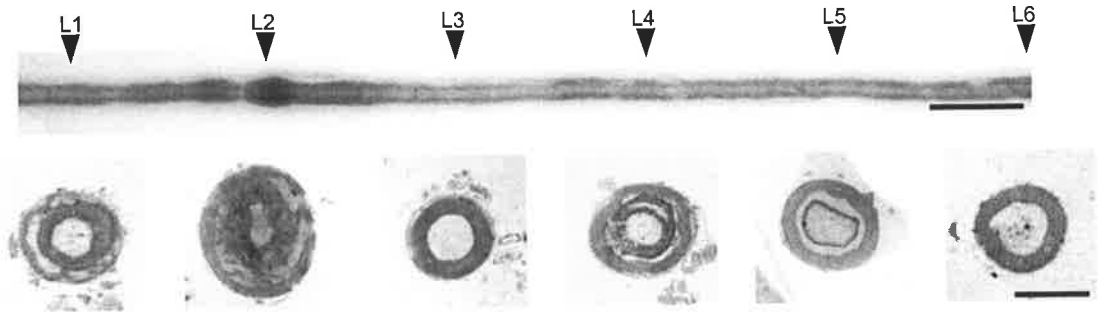

Figure 4-2. Light micrographs. The upper panel is a teased nerve fiber from a P20m MAG-deficient mouse (bar = 50 μm). A paranodal myelin thickening is indicated by L2. The lower panel shows semithin plastic sections stained with toluidine through specific sites along the fiber at a regular interval of 100 micra. Cross section through the paranodal myelin thickening (L2) shows symmetrical thick myelin with myelin splitting. Cross sections through externally normal internodal regions show Schmidt-Lanterman incisures (L1 and L4–5) and compact myelin (L3 and L6). bar = 10 μm for cross sections. Teased fibre and transverse sections were digitized using the Olympus DP11 Microscope Digital Camera System.

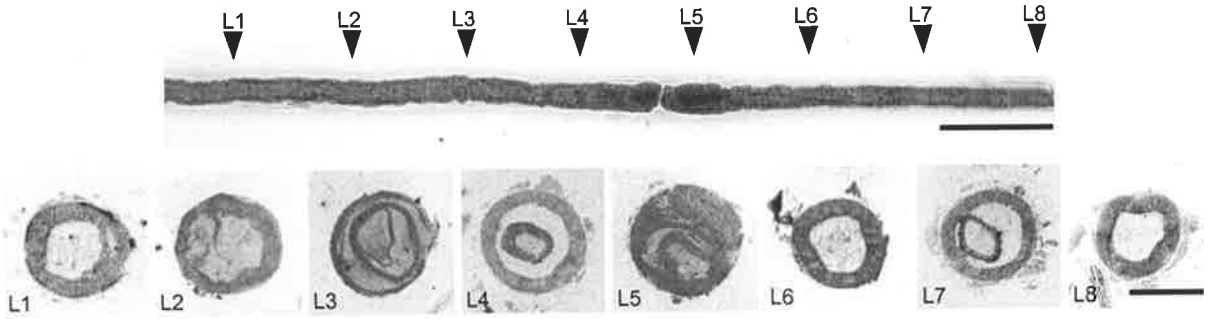

Figure 4-3. Light micrographs. The upper panel is a resin teased myelinated fibre from a P20m MAG-deficient mouse (bar = 50 μm). A juxtaparanodal myelin thickening is present (L5). The lower panel shows cross sections through specified sites of the teased fibre at an interval of 50 μm. Cross section through the juxtaparanodal myelin thickening (L5) shows complex myelin outfolding with a constricted axon that is smaller than that of the neighbouring internodal compact myelin region (L6). Myelin splitting is also present in the outfolded myelin. Transverse sections through externally normal internodal regions show compact myelin (L7 and L8), Schmidt-Lanterman incisures (L4 and L7), compact myelin with myelin splitting (L1 and L2), and a Schmidt-Lanterman incisure with myelin splitting (L3). bar = 10 μm for cross sections. Teased fibre and transverse sections were digitized using the Olympus DP11 Microscope Digital Camera System.

4.4.3 Correlative study of external appearance with multiple longitudinal sections

Twenty one single myelinated nerve fibers from 2 P9m MAG-deficient mice (14 fibers from one mutant and 7 from the other) and 73 single fibers from 3 P20m mutants were longitudinally sectioned. A total of 192 paranodal myelin thickenings, including 47 from the P9m mutants and 145 from the P20m mutants, were examined. One juxtaparanodal myelin thickening in a fiber from the P20m mutant was also longitudinally sectioned and examined.

Fig. 4-4 shows a longitudinal section through an externally normal PNP region of a fibre from a P20m control mouse. Redundant myelin folding (eg, left paranode in Fig. 4-5) was found in 70.2% (33/47) of paranodal myelin thickenings from the P9m mutants and 44.8% (65/145) of paranodal myelin thickenings from the P20m mutants. The frequency of redundant myelin folding in the P9m mutant was significantly higher than that in the P20m mutant (Chi square test, $P<0.01$). Serial sections through the complex myelin foldings revealed that these complex structures often showed complex multiple myelin infolding and outfolding (eg, Fig. 4-6), indicative of focal redundant production of myelin.

Complex myelin splitting and degeneration (eg, Fig. 4-7) were found in 29.8% (14/47) of paranodal myelin thickenings from the P9m mutants and 53.1% (77/145) of paranodal myelin thickenings from the P20m mutants. The frequency of paranodal myelin thickenings showing myelin splitting and degeneration in the P20m mutants was higher than that in the P9m mutants (Chi square test, $P<0.01$).

Symmetric and disproportionately thick myelin sheaths with myelin splitting (eg, right paranode in Fig 4-5) were found in 2.1% (3/145) of paranodal myelin thickenings from the P20m mutants, but not found in the paranodal myelin thickenings from the P9m mutants.

Within the one PNP region, paranodal tomacula may show the same (eg, Fig. 4-6) or different internal structure (eg, Fig. 4-5).

Serial longitudinal sections through the juxtaparanodal myelin thickening showed myelin outfolding with a focally compressed axon (Fig. 4-8). The paranodal myelin thickening close to this juxtaparanodal myelin thickening showed complex myelin folding (Fig. 4-8).

Longitudinal sections through externally normal paranodes revealed that 6/12 fibers from 2 P9m mutants, 14/32 fibres from the P20m mutants, 0/10 fibres from 2 P9m control mice, 2/27 from the P20m control mice showed myelin infolding at paranodes or juxtaparanodes (Fig. 4-9–10). Complex myelin splitting and degeneration were not detected in externally normal internodal regions.

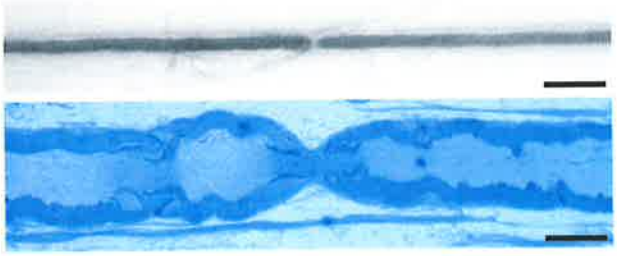

Figure 4-4. Light micrographs. The upper panel is part of a teased nerve fibre from the P20m control mice. A node of Ranvier is present at the center of the fibre (bar = 50 μm). The lower panel shows the normal longitudinal internal structure of the PNP region. The axonal calibre is reduced in the nodal and paranodal regions. 0.5 μm plastic section stained with toluidine blue (bar = 10 μm). Teased fibre and the longitudinal section were digitized using the Olympus DP11 Microscope Digital Camera System.

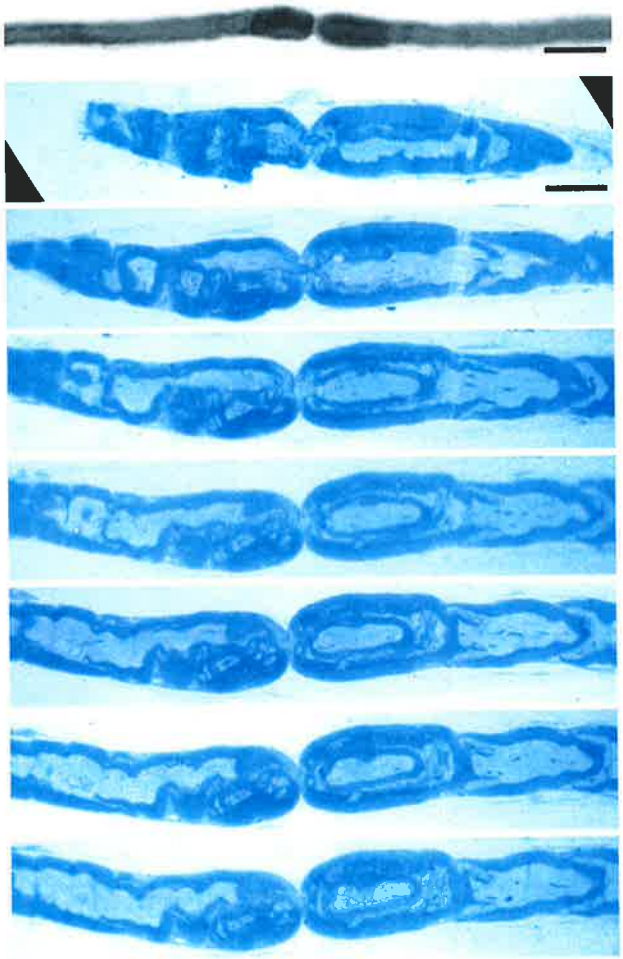

Figure 4-5. Light micrographs. The upper panel is part of a teased nerve fiber from the P20m mutant. Bilateral paranodal myelin thickenings are present at the center (bar = 20 μm). The seven lower panels are serial longitudinal sections through this region. The left paranodal tomaculum shows asymmetrical redundant myelin outfolding while the right paranodal tomaculum shows symmetrical thick myelin with a myelin splitting. 0.5 μm plastic section stained with toluidine blue (bar = 10 μm).

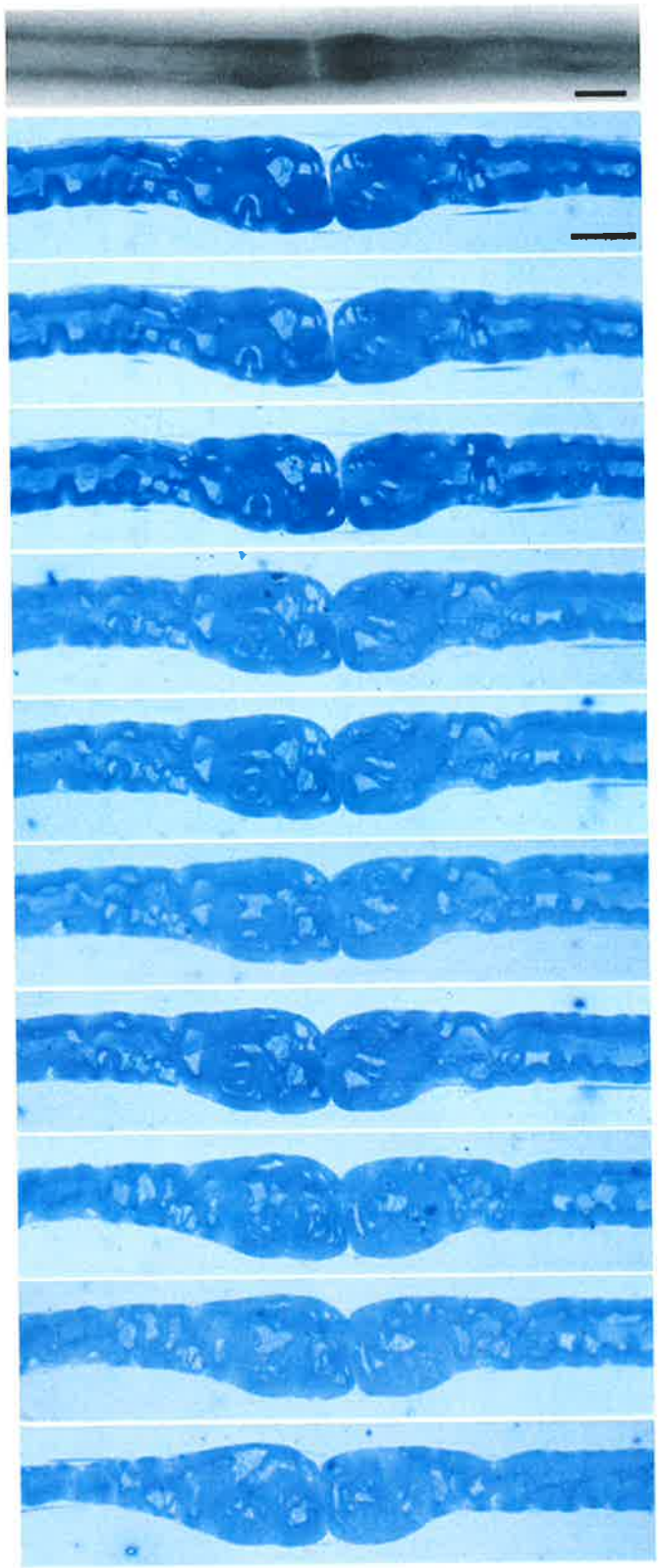

Figure 4-6. Light micrographs. The upper panel is part of a teased nerve fibre from the P20m mutant. Bilateral paranodal myelin thickenings are present in the fibre (bar = 10 μm). The ten lower panels are serial longitudinal sections through the teased nerve fibre. Both the paranodal myelin thickenings show complex myelin folding. 0.5 μm plastic section stained with toluidine blue (bar = 10 μm). Teased fibre and longitudinal sections were digitized using the Olympus DP11 Microscope Digital Camera System.

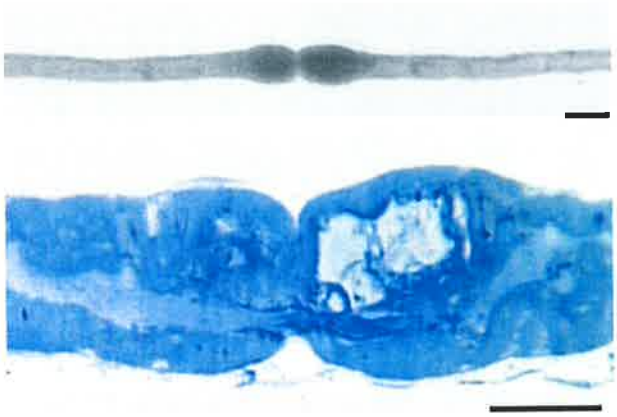

Figure 4-7. Light micrographs. The upper panel is part of a teased nerve fibre from a P9m MAG-deficient mouse. Bilateral paranodal tomacula are present in this fibre (bar = 20 μm). The lower panel is a longitudinal section through the bilateral tomacula. Myelin infolding in association with myelin splitting and degeneration is clearly seen in the longitudinal section. The axon is severely constricted and displaced to one side. 0.5 μm plastic section stained with toluidine blue (bar = 10 μm). Teased fibre and the longitudinal section were digitized using the MC500 Image Analysis System.

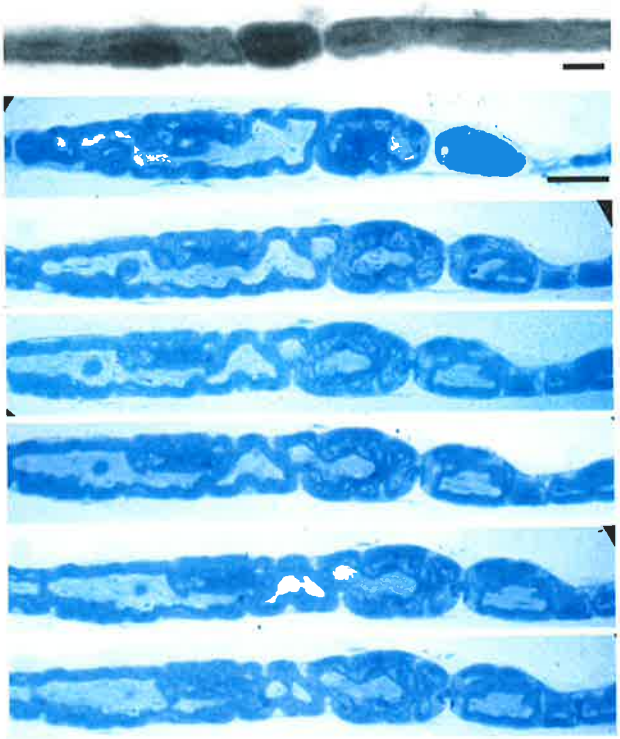

Figure 4-8. Light micrographs. The upper panel is part of a teased nerve fibre from the P20m mutant. A juxtaparanodal myelin thickening is present close to the paranodal myelin thickening at the left side of the node of Ranvier (bar = 20 μm). The six lower panels are serial longitudinal sections through the teased fibre. The paranodal myelin thickening shows complex myelin folding and myelin splitting. The juxtaparanodal myelin thickening consists of asymmetrical myelin outfolding around a focally compressed axon. 0.5 μm plastic sections stained with toluidine blue (bar = 10 μm)

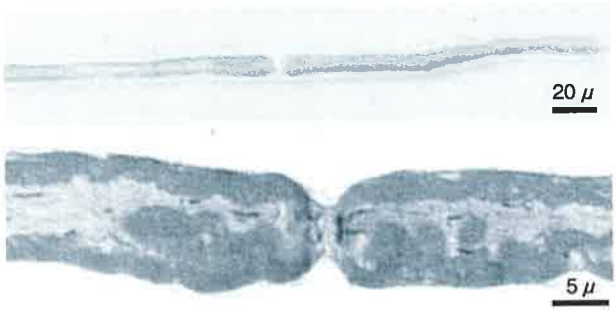

Figure 4-9. Light micrographs. The upper panel is part of a teased nerve fibre from the P9m mutant showing an externally normal PNP region. The lower panel is a longitudinal section through the teased nerve fibre. Myelin infoldings are present in both of paranodes. Half micron plastic section stained with toluidine blue. Teased fibre and the longitudinal section were digitized using the MC500 Image Analysis System.

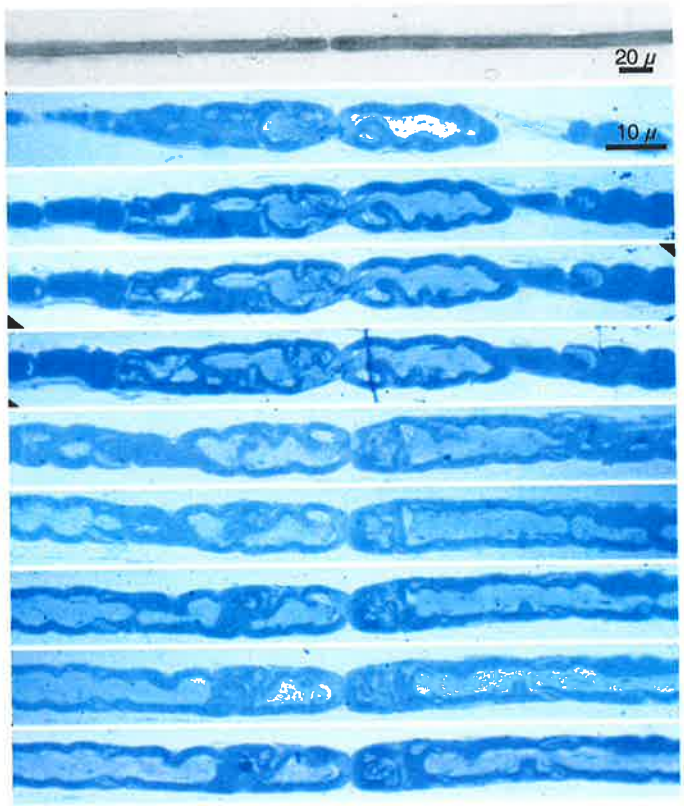

Figure 4-10. Light micrographs. The upper panel is part of a teased nerve fibre from the P20m mutant. An externally normal PNP region is present in the fibre. The nine lower panels are serial longitudinal sections through the teased fibre. The right paranode shows myelin infolding (panel 2–5) and myelin splitting and degeneration (panel 6–10). The left paranode shows paranodal and juxtaparanodal myelin infolding. 0.5 μm plastic sections stained with toluidine blue. Teased fibre and longitudinal sections were digitized using the Olympus DP11 Microscope Digital Camera System.

4.4.4 Light Microscopy

One-micron plastic sections of sciatic and posterior tibial nerves stained with toluidine blue were examined. MF density in MAG-deficient mice was comparable to that of controls from postnatal 0.5 month to 20 months, and there was no hypomyelination, suggesting that myelination was not delayed in MAG-deficient mice (Fig. 4-11). The appearance of MFs in the postnatal 0.5 month MAG-deficient mice did not differ significantly from age-matched control nerves. At P1m, sections of the MAG-deficient sciatic and posterior tibial nerves showed one to two degenerating fibres consisting of linear myelin ovoids. The frequency of degenerating fibres increased with age, but was still less than 1% of the total MFs even in the P20m MAG-deficient mice. Degenerating fibres were only occasionally detected in control mice at P20m of age and never more than two per section of the sciatic nerves. Compared with control sciatic nerves, Student's *t* test analysis found a statistically significant increase in the incidence of Wallerian degeneration in the sciatic nerves of P4m and older MAG-deficient mice (Table 4-3). MFs with disproportionately thin myelin sheaths compared to the axonal calibre, indicative of demyelination/remyelination, were very occasionally detected in semithin transverse sections in both mutant and control animals.

Table 4-3. Quantitative analysis of Wallerian degeneration in the sciatic nerves

Age (month)	0.5	1	4	9	20
$MAG^{+/+}$	0	0	0	0	0.67±0.58
$MAG^{-/-}$	0	1.5±0.71	4±1.2*	5±1.9*	5.4±2.1*

One micron plastic sections of right sciatic nerves from all the mutant and control mice were analysed at different time points. Numbers represent mean ± SD of degenerating MFs per total nerve cross section

*$P<0.01$ compared with the age matched control mice.

MFs with focal myelin thickenings were a characteristic finding in MAG-deficient mice. They were first occasionally detected in both sciatic and posterior tibial nerves of the MAG-

deficient mouse at P1m of age. The frequency and size of focal myelin thickenings increased with age. MFs with focal myelin thickenings in 0.1 mm^2 fascicular area of the right sciatic nerve of $MAG^{-/-}$ mice were counted at ×400 magnification using the Olympus DP11 Microscope Digital Camera System. The number of MFs with focal myelin thickenings per unit area was directly proportionately to the age (Fig. 4-12).

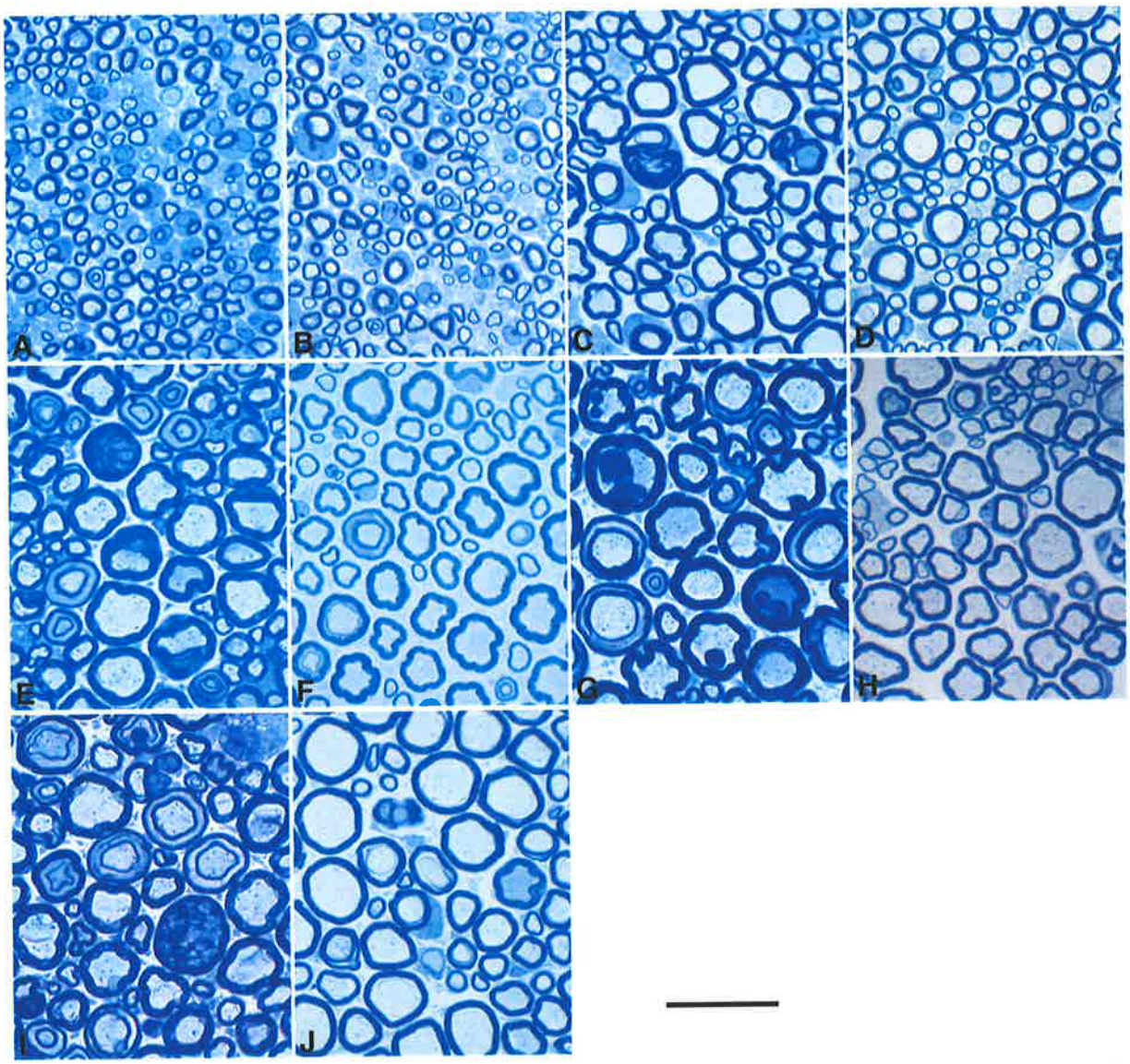

Figure 4-11. Light micrographs of sciatic nerves of MAG-deficient and age-matched control mice. There were no striking differences in myelinated fibre densities or the thickness of the myelin sheaths for most fibres between the two groups. In MAG-deficient mice older than P1m, some fibres had focal myelin thickening. Semithin plastic sections stained with toluidine blue and digitized using the Olympus DP11 Microscope Digital Camera system. Bar = 20 μm

A, P0.5m $MAG^{-/-}$; B, P0.5m $MAG^{+/+}$; C, P1m $MAG^{-/-}$; D, P1m $MAG^{+/+}$; E, P4m $MAG^{-/-}$; F, P4m $MAG^{+/+}$; G, P9m $MAG^{-/-}$; H, P9m $MAG^{+/+}$; I, P20m $MAG^{-/-}$; J, P20m $MAG^{+/+}$

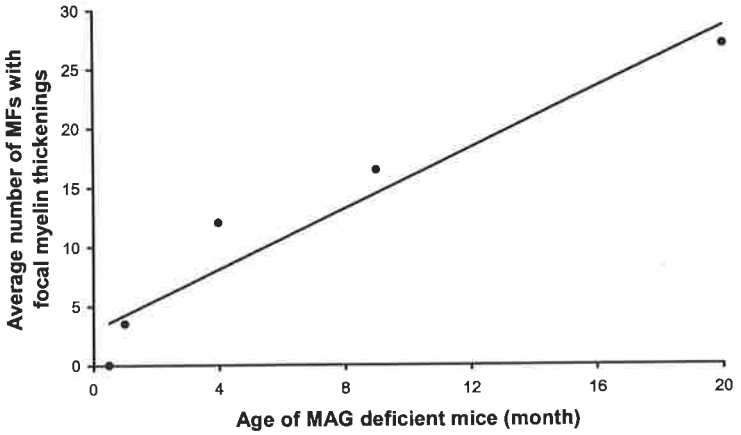

Figure 4-12. Average number of MFs with focal myelin thickenings in cross sections of right sciatic nerves of the MAG-deficient mice at different time points. The number of focal myelin thickenings is directly proportional to the age ($R^2 = 0.9$, $P<0.01$).

The focal myelin thickenings were due to asymmetrical myelin infolding, asymmetrical myelin outfolding, symmetric and disproportionately thick myelin, and complex myelin splitting and degeneration (Fig 5-13). Redundant myelin folds were the most common feature in young mutants. The structure of redundant myelin folds (including infolding and outfolding) was usually simple (eg, Fig 5-13A, E) in young mutants and tended to become increasingly complex in aged mutants (eg, Fig. 4-13C, G), especially in the mutants older than P9m. Complex redundant myelin folds were often associated with myelin splitting and degeneration (eg, Fig. 4-13H, I). Occasionally infolded or outfolded myelin loops partially enclosed the axon to form additional horseshoe-like myelin loops inside or outside the original myelin sheath (eg, Fig. 4-13D, J). Symmetric and disproportionately thick myelin sheaths (eg, Fig. 4-13K, L) accounted for a small number of the focal myelin thickenings in the mutants at all ages. MFs with focal myelin thickenings showing complex myelin splitting and degeneration were less in young mutants and became more frequent in aged mice. The axons in such fibres were usually severely compacted (eg, Fig. 4-13M, N, O). Occasionally fibres showed severe myelin splitting with large myelin vacuoles and compacted and displaced axons (Fig. 4-13P).

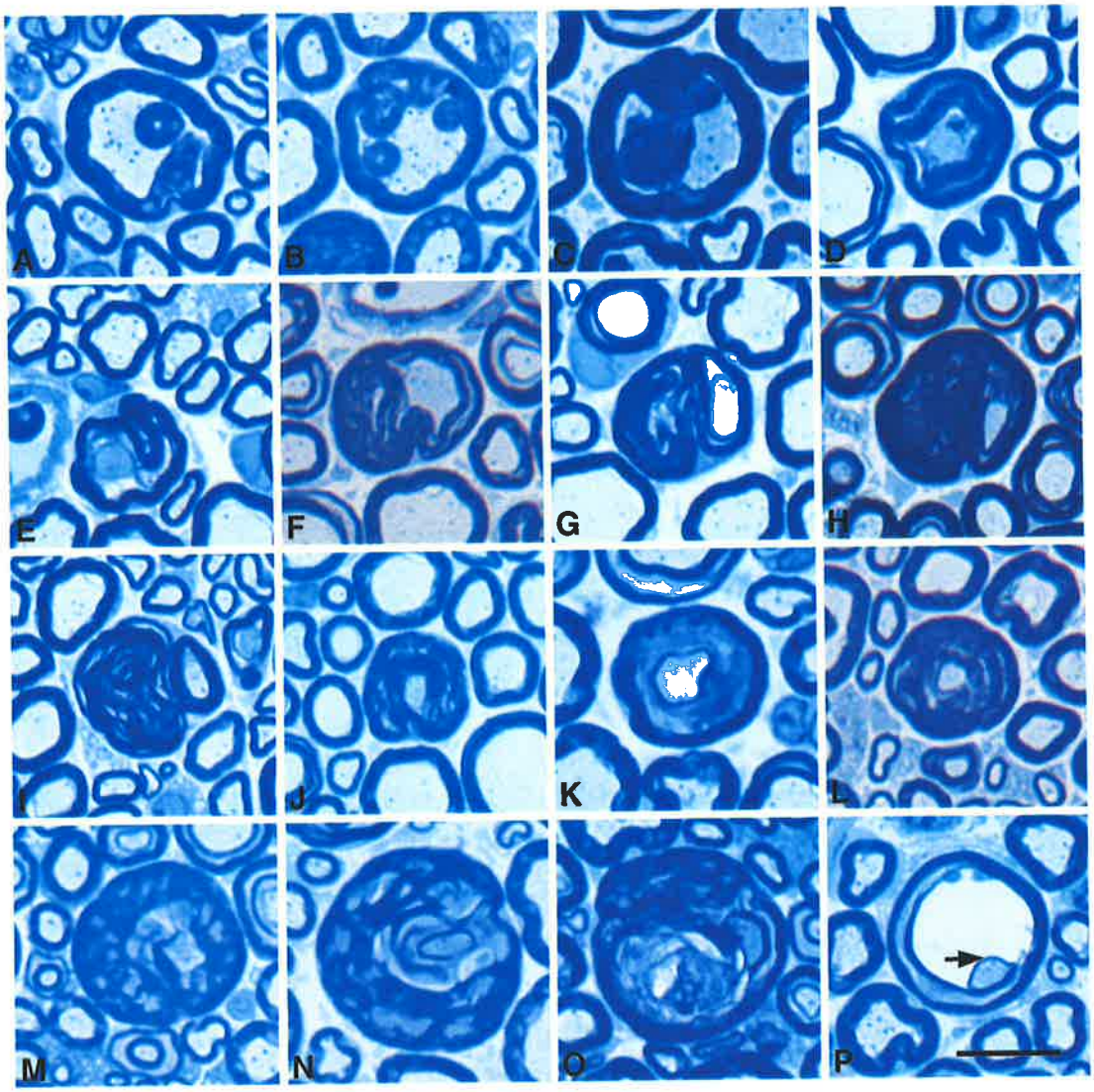

Figure 4-13. Various types of focal myelin thickenings in $MAG^{-/-}$ mice, including myelin infolding (A–D), myelin outfolding (E–J), symmetric and disproportionately thick myelin sheath (K and L), and excessive myelin with complex myelin splitting or degeneration (M–P). A, B and C show a possible sequence from simple myelin infolding to complex myelin infolding. In A and B, the axonal size and density seem normal. But in C, the axon is small and displaced by the focal redundant myelin folds, and seems high dense. Occasionally infolding partially enclose the axon to form an additional horseshoe-like myelin loop is formed within the original myelin sheath (D). E–I show a possible evolution from simple myelin outfolding (E) to spiral myelin outfolding (F, G), and to complicated folding in association with myelin splitting and degeneration (H, I). In J, the outfolding myelin forms an additional horseshoe myelin loop outside the original myelin sheath. The large fibre in P shows severe myelin splitting with a vacuole in the myelin sheath and displaced axon. The axon is surrounded by a thin layer of myelin (arrow) at the side opposite to the large vacuole. Semithin plastic sections stained with toluidine blue and digitized using the Olympus DP11 Microscope Digital Camera System. bar = 10 μm.

Under oil immersion (×1000), 60 to 100 MFs with focal myelin thickenings in cross sections of right sciatic nerves of the MAG-deficient mice were counted and classified into 3 groups: asymmetric myelin folding (including infolding and outfolding), symmetrical and disproportionately thick myelin, and complex splitting and degeneration (Fig. 4-14). The percentage of redundant myelin foldings decreased significantly with age (Fig5-14, R^2 = 0.87, P<0.05) while the percentage of complex myelin splitting and degeneration increased significantly with age (Fig. 4-14, R^2 = 0.88, P<0.05). The percentage of swellings with symmetric and disproportionately thick myelin sheaths was not related to the age.

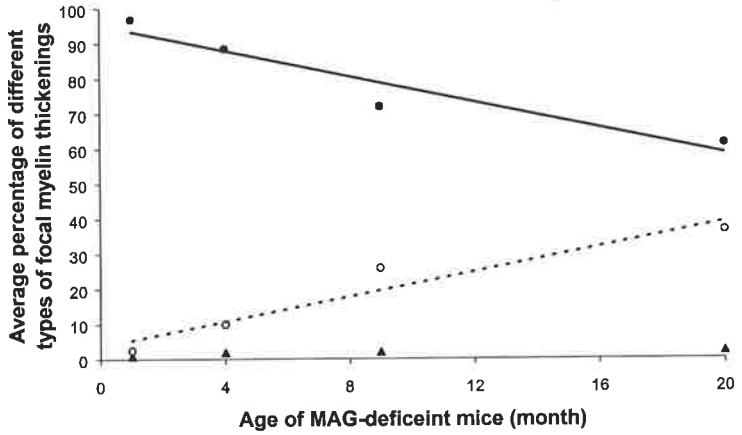

Figure 4-14. Average percentage of different types of focal myelin thickenings at different time points. Sixty to 100 MFs with focal myelin thickenings in cross sections of right sciatic nerves of each $MAG^{-/-}$ mouse were classified into 3 groups at ×1000 magnification. The percentage of fibres with redundant myelin foldings (filled circle) decreases with age (unbroken line, R^2 = 0.87, P<0.05) while the percentage of fibres with complex myelin splitting and degeneration (open circle) increases with age (broken line, R^2 = 0.88, P<0.05). Fibres with symmetric and disproportionately thick myelin (triangle) is not related to age.

Longitudinal section studies showed that focal myelin thickenings in MAG-deficient mice were located in paranodal regions. Longitudinal sections covering up to one thousand micra of internodal length did not find complex myelin infolding or outfolding in the internodal regions. Myelin fibres with simple myelin infolding or outfolding in paranodal regions were occasionally encountered in control mice, but complex myelin infolding or outfolding with myelin splitting and degeneration were not detected.

4.4.5 Electron Microscopy

Electron microscopy confirmed that myelination in the PNS of MAG-deficient mice was similar to that of age-matched wild-type mice. Myelin compaction and the periodicity of myelin lamellae of MAG-deficient mice appeared comparable to those of control mice as described by other researchers (Li *et al.*, 1994; Montag *et al.*, 1994). Similar to the findings of Montag *et al.* (1994), the periaxonal cytoplasmic collar in MAG-deficient mice was preserved, and the inner as well as the outer mesaxon of myelinating Schwann cells appeared normal in peripheral nerves (Fig. 4-15). The adaxonal space of about 12-14 nm width was well preserved in many fibres especially small myelinated fibres. Only a few small fibres had a very thin myelin sheath compared to the axonal diameter (Fig. 4-16). Occasional MFs surrounded by multiple Schwann cell processes suggestive of onion bulb formation were found in MAG knockout mice at P9m and older (Fig. 4-17). In the fibres with a large vacuole and displaced axon as described above under LM (Fig. 4-13P), EM showed that the vacuole was within the myelin and probably resulted from severe myelin splitting (Fig. 4-18). Besides focal myelin thickenings, some small myelinated fibres had redundant compacted myelin coursing away from the axon as described previously in the CNS of MAG-deficient mice (Li *et al.*, 1994; Montag *et al.*, 1994) (Fig. 4-19). Cross sections through nodes of Ranvier showed normal radiating Schwann cell microvilli in MAG-deficient mice (Fig. 4-20). Double or multiple myelination reported in the central nervous system of MAG-deficient mice (Montag *et al.*, 1994) was not found in the sciatic and posterior tibial nerves of MAG-deficient mice.

Nonmyelinated axon-Schwann cell units were the same in MAG-deficient and control mice (Fig. 4-21).

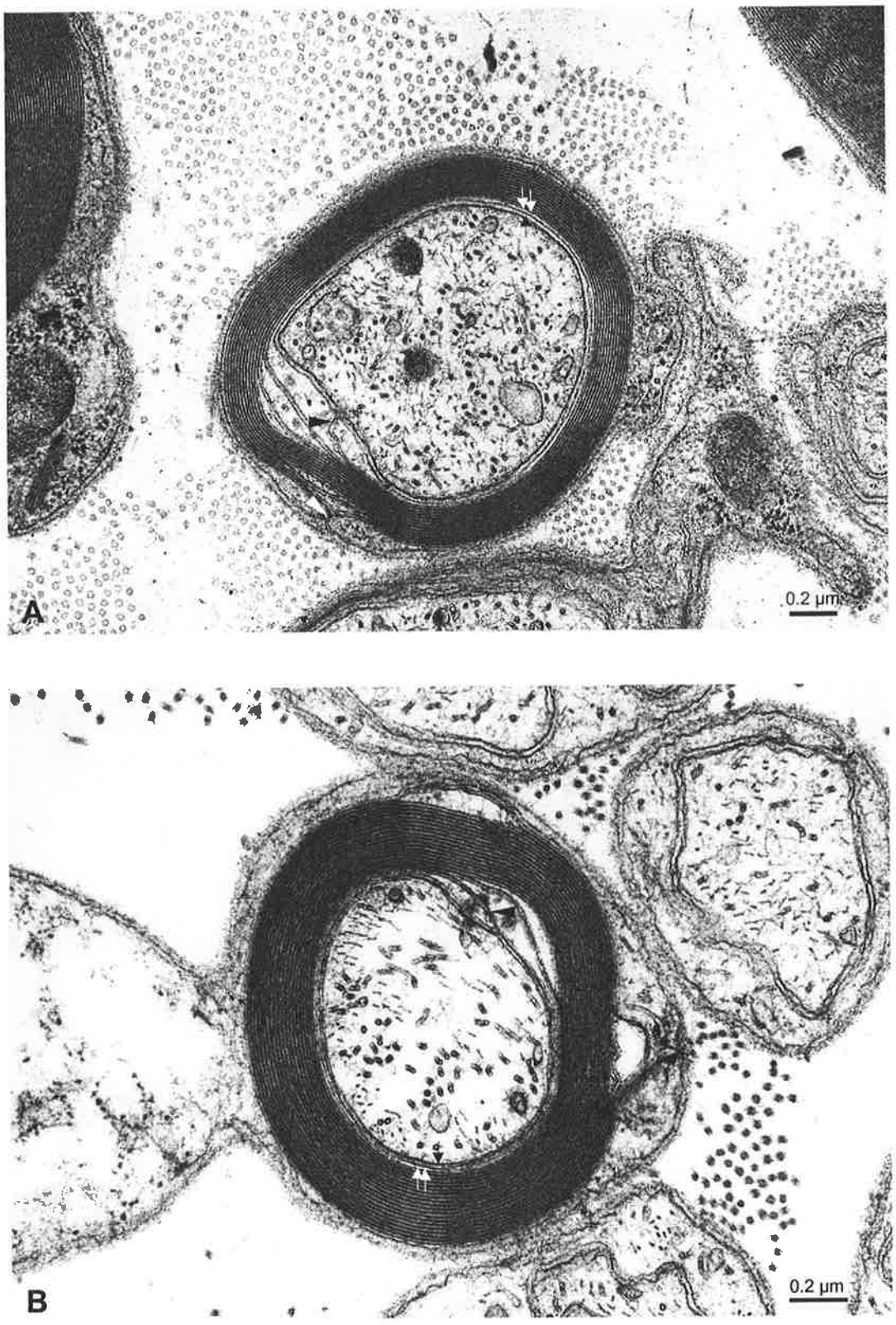

Figure 4-15. Electron micrographs of myelinated fibres from the right sciatic nerve (A) and posterior tibial nerve (B) of a P4m MAG-deficient mouse. The compaction of myelin lamellae is normal. The adaxonal space (black arrow) and the Schwann cell cytoplasmic collar (double white arrows) are well preserved. The inner mesaxon is indicated by the black arrowhead and the outer mesaxon by the white arrowhead.

Figure 4-16. Electron micrograph of sciatic nerve from a P4m MAG-deficient mouse. A myelinated fibre is surrounded by disproportionately thin myelin sheath.

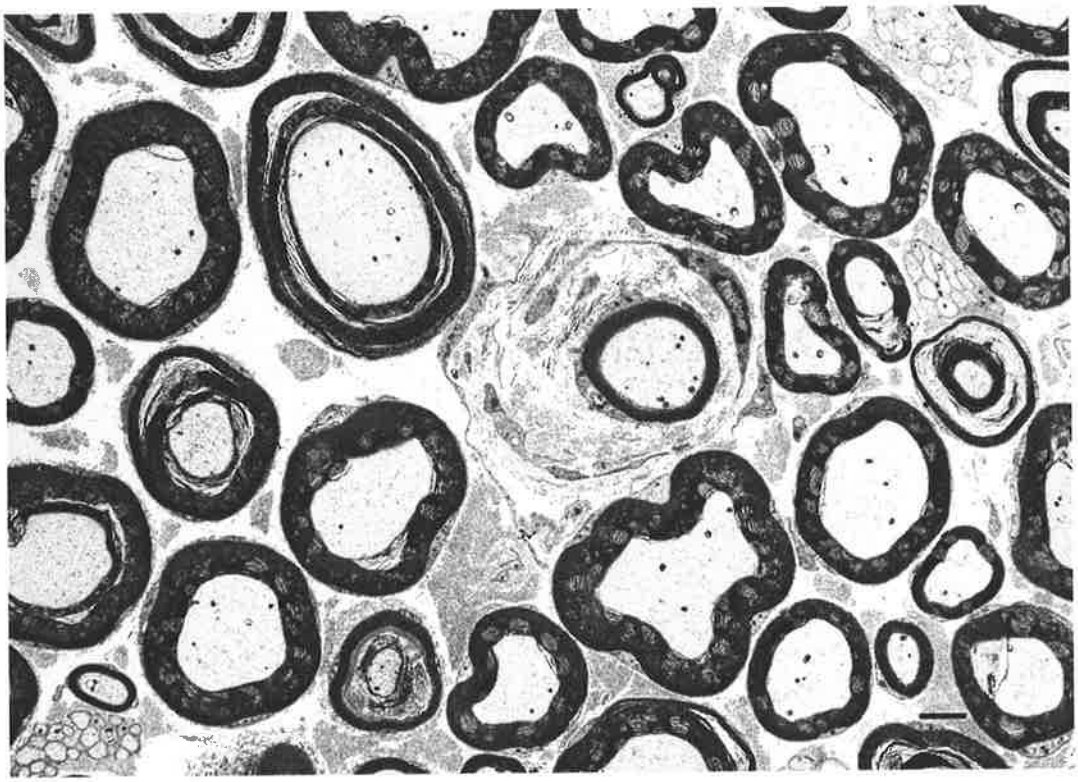

Figure 4-17. Electron micrograph of sciatic nerve from a P20m MAG-deficient mouse. A nerve fibre with thin myelin sheath is surrounded by multiple Schwann cell processes indicative of onion bulb formation. Bar = 2 μm

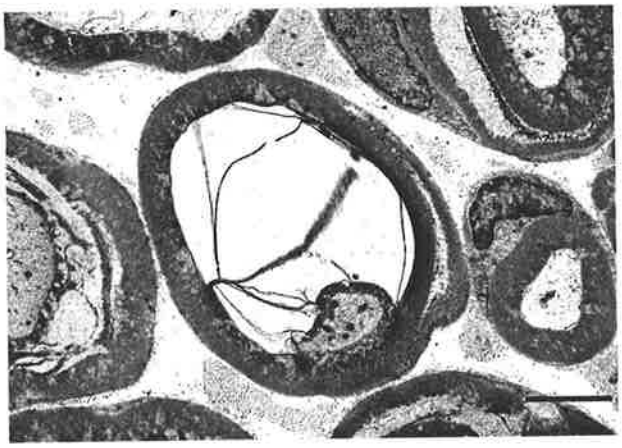

Figure 4-18. Electron micrograph of the sciatic nerve from the P20m MAG-deficient mouse. A MF shows a large vacuole in the myelin due to splitting of myelin. The axon is displaced to one side of the fibre and enclosed by myelin. Bar = 1 μm

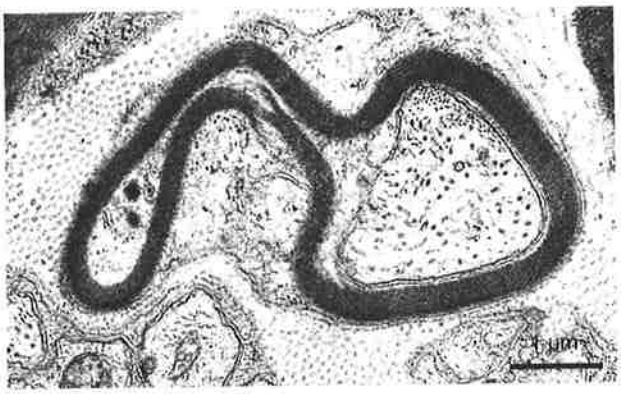

Figure 4-19. Electron micrograph of the sciatic nerve from a P4m MAG-deficient mouse. A small MF has redundant compact myelin coursing away from the axon.

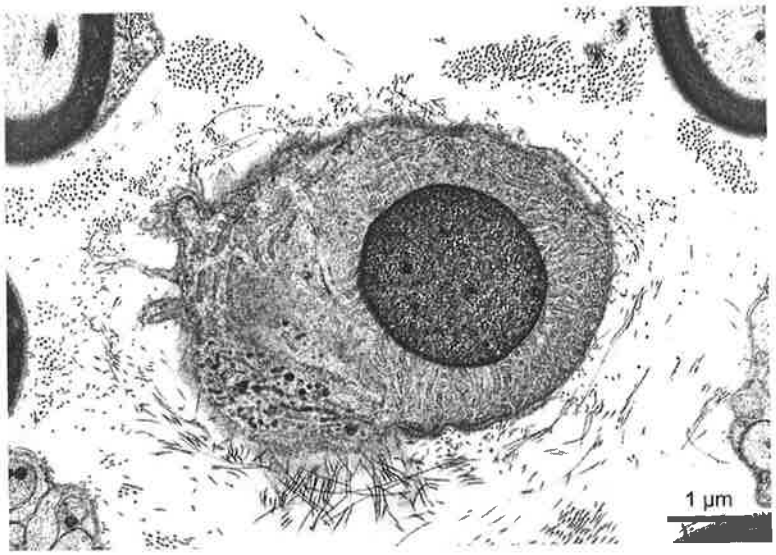

Figure 4-20. Cross section of the sciatic nerve of the P4m MAG-deficient mouse through the node of Ranvier shows the nodal axon is surrounded by a nodal gap filled with radiating Schwann cell microvilli.

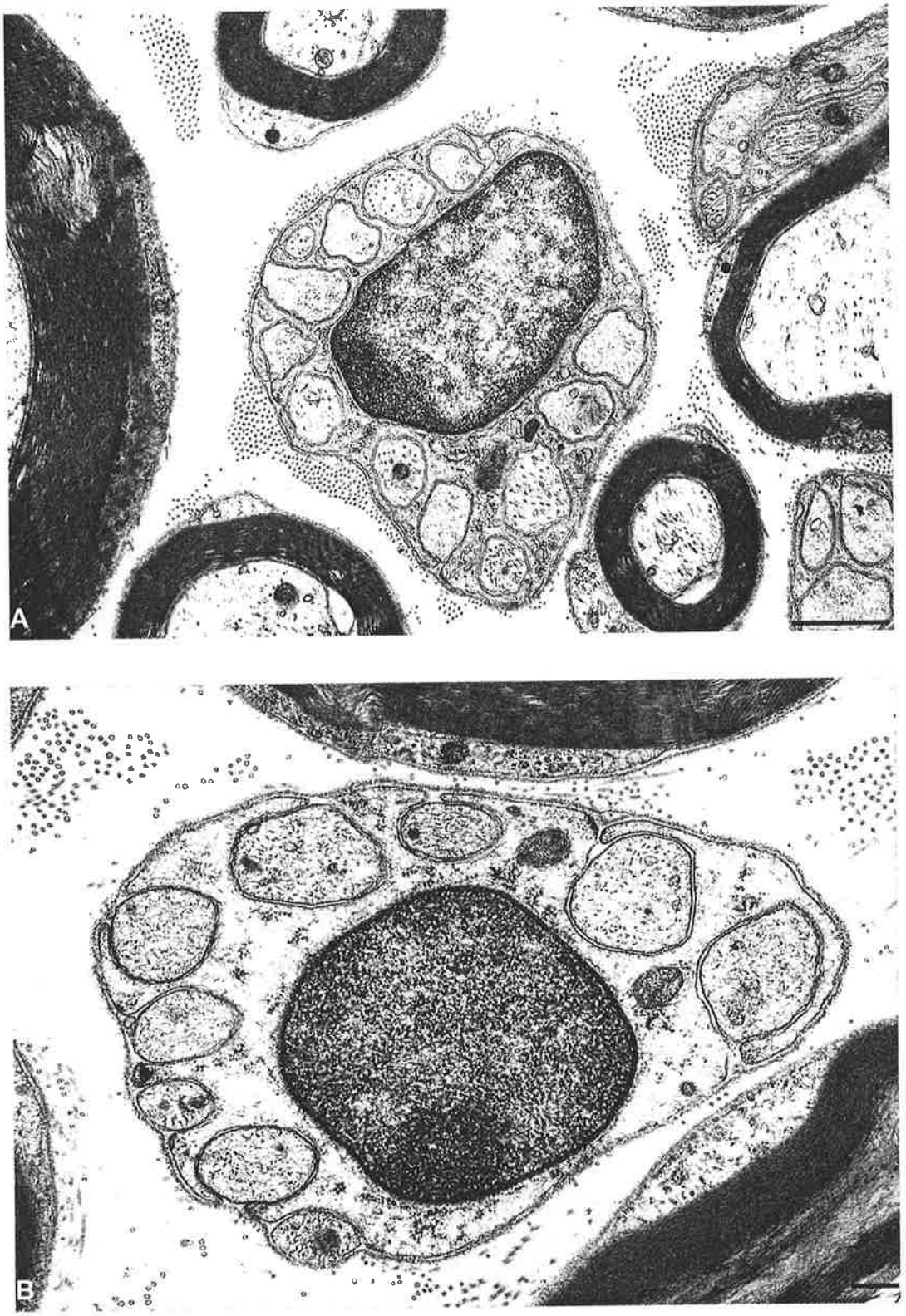

Figure 4-21. Electron micrographs show that the normal Schwann cell-unmyelinated fibre unit in MAG-deficient mice (A) is comparable to that of control mice (B). bar = 1 μm

4.5 DISCUSSION

4.5.1 MAG is not essential for the initiation of myelination but functions in the long-term maintenance of myelin-axon integrity

In development MAG is expressed at the tip of spirally turning loops of myelinating Schwann cell membrane (Martini and Schachner, 1986). In vitro studies suggested that MAG was involved in the formation of myelin (Owens and Bunge, 1991; Owens *et al.*, 1990). Thus a severe myelin deficiency was expected in mice lacking MAG. However, studies in MAG-deficient mice resulting from targeted disruption of the MAG gene found that the initiation and speed of myelination and the gross morphology were normal in the PNS (Li *et al.*, 1994; Montag *et al.*, 1994; Yin *et al.*, 1998). These findings suggest that MAG may not be involved in the initiation of myelin formation or that other components may substitute for MAG in the formation of myelin in the PNS. The mutant and control mice in this study showed the same overall pattern of myelination consistent with these previous findings (Li *et al.*, 1994; Montag *et al.*, 1994). At an early stage of myelination, no delay in sorting of larger calibre axons or onset in formation of a multilayered Schwann cell spiral around the axon was found. Myelin compaction, periodicity of myelin lamellae, width of the periaxonal space, myelin thickness and the inner cytoplasmic collar in the MAG-deficient mice were similar to those of control mice. Furthermore, Schwann cell-unmyelinated fibre units in the MAG-deficient mice were also indistinguishable from those of the control mice.

Because L1-, N-CAM-, MAG-deficient mice develop myelin of normal ultrastructure, it is evident that myelin molecules can fulfill functionally overlapping roles that ensure that myelination takes place even under conditions in which there is a deficiency in the normal molecular components of myelin (Martini and Carenini, 1998).

Degenerating MFs in the MAG-deficient mice were detected as early as P1m while they were only present in control mice at P20m of age. The frequency of fibres showing Wallerian degeneration in the MAG-deficient mice was higher than in age-matched controls. This finding is consistent with a previous report showing that the incidence of degenerating MFs in the PNS of MAG-deficient mice is significantly higher than in age-matched control mice from postnatal 35 days to 16 months (Yin *et al.*, 1998), suggestive of a functional role for MAG in the maintenance of myelin-axon integrity.

4.5.2 Demyelination is not a feature in MAG-deficient mice

Segmental demyelination is a predominant pathologic feature in experimental PMP2 deficient mice (Adlkofer *et al.*, 1995, 1997), experimental P_0 deficient mice (Martini, 1999; Martini *et al.*, 1995*a*; Shy *et al.*, 1997), and human hereditary neuropathies due to mutations of the gene(s) encoding PMP22 and P_0 (Kamiguchi *et al.*, 1998; Keller and Chance, 1999; Mezei *et al.*, 1993; Nelis *et al.*, 1999; Thomas *et al.*, 1997). But this is not the case in MAG-deficient mice. In the present study, teased nerve fibres from MAG-deficient mice did not show an increased frequency of segmental demyelination compared to the age-matched control mice from postnatal 15 days to 20 months. Previous studies also did not find an increased frequency of segmental demyelination in teased fibre preparations in young (8 weeks) and aged (9 months) MAG-deficient mice compared to age-matched controls (Carenini *et al.*, 1997; Yin *et al.*, 1998).

This is in contrast to the predominant segmental demyelination in teased fibre preparations in human IgM anti-MAG neuropathy in the present (**Chapter 3**) and previous studies (Jacobs and Scadding, 1990; Rebai *et al.*, 1989; Sander *et al.*, 2000). This may be because the demyelination in IgM anti-MAG neuropathy is due to binding of IgM anti-MAG antibodies to the L2/HNK carbohydrate epitope shared by other glycoconjugates in the PNS,

including N-CAM, P_0, PMP22, SGPG and SGLPG (Ariga *et al.*, 1987; Burger *et al.*, 1990; 1992; Chou *et al.*, 1986; Hammer *et al.*, 1993; Ilyas *et al.*, 1990; Snipes *et al.*, 1993), or it may be secondary to axonal damage as suggested previously (Jacobs and Scadding, 1990; Mendell *et al.*, 1985) and the present study (**Chapter 3**).

The absence of segmental demyelination in MAG deficient mice suggests that other proteins can substitute for MAG during development and that this compensatory mechanism is no longer available in the mature myelinated fibre affected by IgM anti-MAG antibodies leading to segmental demyelination. The finding of segmental demyelination in N-CAM and MAG double null mutant mice (Carenini *et al.*, 1997) supports this hypothesis. The peripheral nerves of N-CAM deficient mice appeared normal throughout the investigated ages from postnatal 4weeks to 26 weeks, while MAG and N-CAM double null mutants showed segmental demyelination from postnatal 8 weeks (Carenini *et al.*, 1997).

4.5.3 Focal myelin swellings and tomacula in MAG deficient mice

Tomacula are present in young MAG-deficient mice and increase with age

MFs with focal myelin thickenings are a prominent abnormality in MAG-deficient mice. Yin *et al.* (1998) reported excessive myelin thickness on cross sections of peripheral nerves as early as postnatal 5 weeks. In the present study, myelin thickenings were first detected on cross and longitudinal sections in the MAG-deficient mouse at P1m of age and focal myelin thickenings were detected in teased nerve fibres simultaneously, suggesting that tomacula start to form in young MAG-deficient mice.

The frequency of focal myelin thickenings increased significantly with age from P0.5m to P20m in the present study and from P3m to P9m in the study by Yin *et al.* (1998), suggesting that focal myelin thickening is an age-related pathologic feature in MAG-

deficient mice rather than a transient morphologic phenomenon as described in PMP gene knockout mice (Adlkofer *et al.*, 1995).

Tomacula are located in paranodal and juxtaparanodal regions

Teased nerve fibre and conventional longitudinal section examinations showed that most focal myelin thickenings were located at paranodes and only a few were present at juxtaparanodal regions. Internodal myelin focal thickenings were not detected in this study in contrast to the previous study by Yin *et al.* (1998). Focal myelin swellings were also found in paranodal regions but not in internodal regions in MAG and N-CAM double knockout mice (Carenini *et al.*, 1997). Paranodal tomacula or myelin thickenings in MAG deficient mice were found in otherwise externally normal teased fibres in the present study and a previous study (Yin *et al.*, 1998).

Paranodal abnormalities have been described in certain myelin mutations, including PMP22 deficient mice (Adlkofer *et al.*, 1995, 1997) and mice heterozygously deficient for P_0 (Martini *et al.*, 1995*a*) and transgenic mice expressing a mutant P_0 (Previtali *et al.*, 2000). It is therefore possible that the highly organized paranodal structures, including the complicated axon-Schwann cell apposition in the paranodal network (Gatzinsky, 1996; Gatzinsky *et al.*, 1997), are particularly susceptible to molecular alterations, leading to abnormal myelin folding and axonal constriction. However, tomacula in human IgM anti-MAG neuropathy were found in both internodal and paranodal regions in previous studies (Jacobs and Scadding, 1990; Rebai *et al.*, 1989; Sander *et al.*, 2000) and in this study (**Chapter 3**), suggesting differences in the mechanism of tomacula formation according to location on the nerve fibre.

Redundant folding myelin is the basis of tomacula formation in MAG deficient mice

There has been no previous study of transverse or longitudinal sections of tomacula in teased fibres of MAG-deficient mice. This study utilising our new technique shows for the first time that most paranodal tomacula result from redundant myelin infolding or outfolding. The redundant myelin folding is usually simple in young mutants, but in aged MAG-deficient mice redundant folding is complex with myelin splitting and degeneration. Tomacula with complex myelin splitting and degeneration increase with age. This evolution indicates that redundant folds of myelin are not stable and tend to degenerate with age, consistent with the notion that MAG functions in the longterm maintenance of myelin integrity (Fruggiter *et al.*, 1995).

Myelin loop invagination is the earliest change in most focal myelin thickenings in MAG-deficient mice. Focal redundant myelin may result from either focal overproduction of myelin or focal axonal atrophy. Tomacula described in MAG and N-CAM double knockout mice (Carenini *et al.*, 1997) and in heterozygous PMP22 knockout mice (Adlkofer *et al.*, 1997) were attributed to paranodal hypermyelination based on the symmetrical distribution of redundant myelin around paranodal axons. However, asymmetrical excessive myelin thickenings were also commonly found in these mutants (Adlkofer *et al.*, 1997; Carenini *et al.*, 1997). It has been suggested that paranodal redundant foldings in MAG-deficient mice were due to axonal shrinkage based on asymmetrical distribution of redundant myelin folds and reduced axonal calibre in association with reduced neurofilament spacing and reduced neurofilament phosphorylation (Yin *et al.*, 1998). Tomacula or focal myelin thickenings were detected as early as postnatal 1 month in the present study and postnatal 5 weeks in a previous study (Yin *et al.*, 1998). We did not find any subjective difference of axonal calibre between MAG-deficient and control mice at P1m of age. Quantitative studies by Yin *et al.* (1998) also did not find a reduction of axonal calibre in MAG-deficient mice at

postnatal 5 weeks. The finding that paranodal tomacula occur before any reduction of axonal calibre is contrary to the notion that redundant myelin folding results from axonal atrophy (Yin *et al.*, 1998). Furthermore, focal excessive volume of myelin cannot be explained using the longitudinal slippage of myelin because neither loss of myelin in the internodal regions nor paranodal myelin retraction was detected in the present study and previous studies (Carenini *et al.*, 1997; Yin *et al.*, 1998). A focal overproduction of myelin seems to be the suitable explanation of focal redundant myelin folding. Focal hypermyelination may cause mechanical axonal constriction and axonal degeneration as suggested by Carenini *et al.* (1997) in MAG and N-CAM double knockout mice.

Overproduction of myelin may lead to an excessive number of myelin lamellae concentrically surrounding the axon, resulting in a symmetric excessively thick myelin sheath without myelin folding (Fig. 4-22). This type of focal myelin thickening constitutes a small proportion of tomacula in MAG deficient mice, but were commonly found in heterozygous PMP22 knockout mice (Adlkofer *et al.*, 1997) and MAG and N-CAM double knockout mice (Carenini *et al.*, 1997).

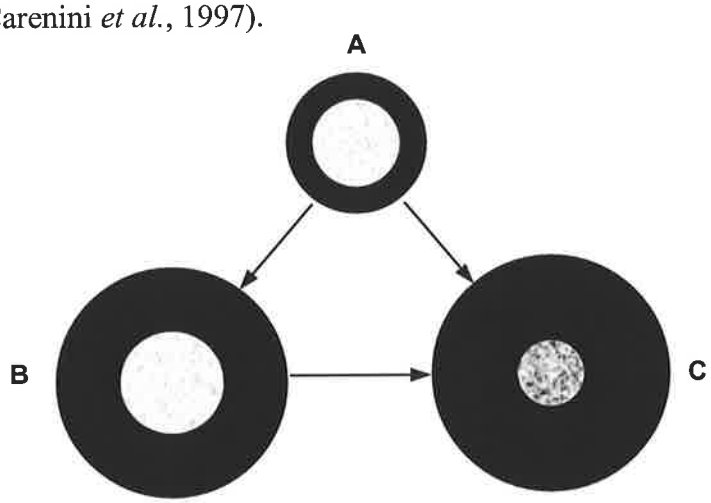

Figure 4-22. Diagram showing focal overproduction of myelin leading to symmetric excessively thick myelin sheath. **A** shows a normal myelin sheath and axon. **B** shows an increased number of myelin lamellae concentrically surrounding the axon leading to an excessively thick myelin sheath. The axon is not compressed and has the same density as the normal axon. **C** shows increased number of myelin lamellae in association with axonal compression. **C** may be derived from **B** or directly from **A**.

Excess myelin may lead to invagination of the myelin sheath to form myelin infolding or exvagination to produce myelin outfolding. The increase in the circumference of the myelin sheaths leads to the evolution from simple to complex myelin folding (Fig. 2-23). The axon may be normal or compacted. Tomacula of this type are the main type found in MAG deficient mice and most human hereditary and acquired tomaculous neuropathies (Sander *et al.*, 2000) and animal tomaculous neuropathy (Hill *et al.*, 1996). The excess myelin is unstable and degenerates with increasing size as the animal ages so that the tomacula in old MAG deficient mice show complex myelin splitting and degeneration. This speculation with the previous hypothesis that paranodal tomacula in MAG deficient mice were due to focal axonal shrinkage and resultant myelin outfolding (Fig. 2-24, Yin *et al.*, 1998).

The extracellular domain of MAG has been shown to bind to gangliosides and glycoproteins on the axolemma (Collins *et al.*, 1997; De Bellard and Filbin, 1999; Strenge *et al.*, 1999; Yang *et al.*, 1996). The cytoplasmic domains interact with S100β protein (Kursula *et al.*, 1999, 2000) and bind directly to tubulin of the microtubules (Kursula *et al.*, 2001). These findings suggest that MAG links the myelinating Schwann cell and the axon. The circumference of normal myelin sheath (or the innermost myelin lamella) may be determined, at least in part, by this linkage. Loss of MAG may lead to disruption of this myelin-axon adhesion and redundant myelin folding.

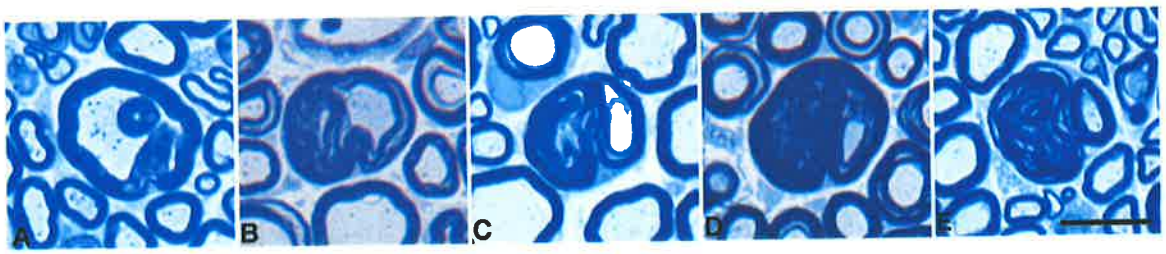

Figure 2-23. Light micrographs. ***A–E*** show the evolution from simple to complex redundant myelin folding in MAG deficient mice. The complex redundant folds often show myelin splitting and degeneration (***C–D***). The axon calibre may be preserved (***A***) or compacted (***D–E***). Bar = 10 μm.

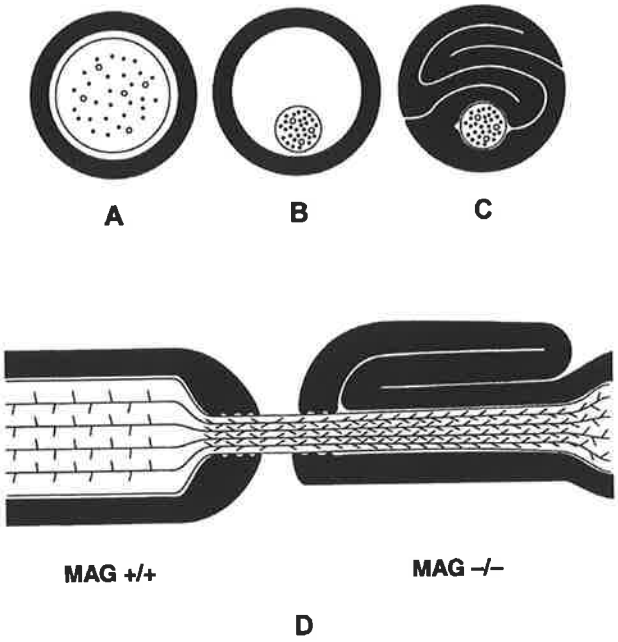

Figure 4-24. Diagrams showing the hypothesized mechanism of tomacula formation by Yin *et al* (1998) in MAG-deficient mice. A–C. Relationship between axonal calibre and myelin sheath in transverse section of normal fibre (A). In MAG-deficient nerves, paranodal axonal calibres shrink (B) and result in myelin sheath outfolding and collapse, and tomacula formation (C). In normal paranodal regions, increased NF spacings correlate with large axonal calibre. In $MAG^{-/-}$ paranodal regions surrounded by tomacula, NF spacings and axonal calibres are similar to those in nodal regions (D). Copied from Yin *et al.* (1998).

4.5.4 Comparison of experimental MAG knockout neuropathy and human IgM anti-MAG neuropathy

Based on the previous studies by others (reviewed in **Chapter 3** and **4**) and our studies, the clinical manifestations, electrophysiological findings and pathological findings of experimental MAG knockout neuropathy are different to those of human IgM anti-MAG neuropathy (table 4-4).

Further studies using our new teased nerve fibre technique combined with immunohistochemical staining (including confocal microscopy) and immunoelectron microscopy to localize specific molecules, such as N-CAM and P_0, along the length of individual teased nerve fibres will be helpful to test the hypothesis that there is a

redistribution of some adhesion molecules in MAG deficient mice to compensate the function of MAG.

Table 4-4. Comparison of clinico-pathological findings between human IgM anti-MAG and experimental MAG knockout neuropathies

	IgM anti-MAG neuropathy	**MAG knockout neuropathy**
Clinical features	Sensorimotor or sensory neuropathy often associated with tremor	Normal
Electrophysiology	Demyelination	Normal
Pathological findings		
Demyelination	Present	Absent
Onion bulb	Yes	Very occasional in aged mutant
WML	Yes	No
Tomacula	Located at both internodal and paranodal regions of MFs showing and/or remyelination	Located only at paranodal regions of MFs with otherwise externally normal appearance
Axonal atrophy	Yes	In mature mutants

WML, widening of myelin lamellae

4.6 CONCLUSIONS

1. Paranodal myelin thickenings or tomacula are the characteristic feature in MAG knockout mice. They are already present in P1m mutants and progressively increase in size and number with age.
2. Paranodal tomacula are the result of redundant myelin folding. These redundant myelin foldings are not stable with increasing complexity and tend to degenerate with age.
3. Demyelination is not a feature in MAG knockout mice.
4. The absence of segmental demyelination in MAG deficient mice suggests that other proteins can substitute for MAG during myelin development.

CHAPTER 5: Future Directions

The teased nerve fibre technique described in this thesis provides a new method for better interpreting the external appearance of teased nerve fibres and studying Schwann cell-axon relationships along the length of individual MFs. This technique will be useful in the diagnosis, classification and investigation of the pathogenesis of neuropathies. Preliminary applications of this technique have produced new insights into the pathological changes seen in peripheral nerve biopsies and demonstrated the usefulness of the technique (Cai *et al.*, 2001*ab*; **Chapter 2, 3, 4**). Further studies will extend the application of the technique to a range of experimental and human peripheral neuropathies.

The term demyelination, as used in this thesis, refers to degeneration of the myelin of a paranode (paranodal demyelination) or an internode (internodal or segmental demyelination). According to Dyck *et al.* (1993*a*) and Thomas *et al.* (1997), primary demyelination is caused by abnormalities affecting the Schwann cells or myelin, such as immune damage of myelin, pressure induced myelin damage, or faulty composition of myelin, and secondary demyelination is caused by axonal damage, especially axonal atrophy. Secondary segmental demyelination due to axonal atrophy is thought to be the more common type of change seen in sural nerve biopsies (Dyck *et al.*, 1993*a*; King, 1994; Thomas *et al.* 1997). The distinction between primary and secondary demyelination may be important in treatment and may affect prognosis. However it is difficult to distinguish primary from secondary demyelination in practice (Bosboom *et al.*, 2001; Uncini *et al.*, 1999).

We found the following: (i) axonal atrophy in association with enlargement of the adaxonal space in segments with preserved myelin is suggestive of secondary demyelination, eg Fig. 3-2 in IgM anti-MAG neuropathy and Fig. 2-11 to Fig. 2-13 in IgM anti-GM1 neuropathy;

(ii) excessive myelin irregularity with normal axons on transverse sections is suggestive of primary myelin or Schwann damage, eg myelin debris in Schwann cell cytoplasm in sensory neuropathy with abnormal mitochondria (**section 2.4.2**); and (iii) axonal atrophy in association with normal myelin on transverse sections of teased nerve fibres is suggestive of primary axonal or neuronal damage, eg uraemic neuropathy in **section 2.4.2**.

It has been suggested that in IgM anti-MAG neuropathy there may be both primary demyelination and secondary demyelination due to axonal atrophy (Jacobs and Scadding, 1990; Mendell *et al.*, 1985). We have demonstrated for the first time axonal atrophy in segments with intact myelin sheaths using our new teased nerve fibre technique (**Chapter 3**) supporting the concept that secondary demyelination may occur in anti-MAG neuropathy. However, in MAG deficient mice, axonal atrophy is characteristically present in the nerves of aged mutants but is not associated with segmental demyelination (see **Chapter 4**).

Future studies will extend our observations on the myelin-axon relationships in various neuropathies. In particular, we will focus on the mechanism of axonal atrophy in IgM anti-MAG neuropathy and the absence of demyelination in MAG knockout neuropathy. It has been suggested that MAG can modulate neurofilament phosphorylation (Yin *et al.*, 1998). We hypothesize that the molecular components of myelin and the axon in MAG knockout neuropathy may be re-distributed or organized differently and that these molecular changes may compensate for the loss of function of MAG in MAG knockout neuropathy. Immunostaining (LM and EM) of individual teased MFs will be used to study the distribution of myelin components (N-CAM, P_0, PMP22, MBP) and axonal components (NF, MT, ion channels) in anti-MAG and MAG knockout neuropathies.

These techniques will be applied to the study of a wide range of peripheral neuropathies. Further studies will select teased nerve fibres of different categories from human peripheral neuropathies due to known aetiologies and experimental neuropathies to test the above findings.

Bibliography

Abo T, Balch CM: A differentiation antigen of human NK and K cells identified by a monoclonal antibody (HNK-1). *J Immunol* 1981; 127:1024-9.

Adams RD, Victor M, Ropper AH: The inherited metabolic diseases of the nervous system, in Adams RD, Victor M, Ropper AH (eds): *Principles of Neurology*. McGraw-Hill, 1997, vol6th, pp 928-991.

Adlkofer K, Martini R, Aguzzi A, Zielasek J, Toyka KV, Suter U: Hypermyelination and demyelinating peripheral neuropathy in Pmp22-deficient mice. *Nat Genet* 1995; 11:274-80.

Adlkofer K, Frei R, Neuberg DHH, Zielasek J, Yoyka KV, Suter U: Heterozygous peripheral myelin protein 22-deficient mice are affected by a progressive demyelinating tomaculous neuropathy. *J Neurosci* 1997; 17:4662-71.

Agrawal HC, Noronha AB, Agrawal D, Quarles RH: The myelin-associated glycoprotein is phosphorylated in the peripheral nervous system. *Biochem Biophys Res Commun* 1990; 169:953-8.

Aguayo AJ, harron L, Bray GM: Potential of Schwann cells from unmyelinated nerves to produce myelin: A quantitative ultrastructural and autoradiographic study. *J Neurocytol* 1976; 5:565-73.

Allt G, Ghabriel MN, Sikri K: Lysophosphatidyl choline-induced demyelination. A freeze fracture study. *Acta Neuropathol (Berl)* 1988; 75:456-64.

Angata T, Varki A: Cloning, characterization, and phylogenetic analysis of siglec-9, a new member of the CD33-related group of siglecs. Evidence for co-evolution with sialic acid synthesis pathways. *J Biol Chem* 2000*a*; 275:22127-35.

Angata T, Varki A: Siglec-7: a sialic acid-binding lectin of the immunoglobulin superfamily. *Glycobiology* 2000*b*; 10:431-8.

Anzini P, Neuberg DHH, Schachner M, Nelles E, Willecke K, Zielasek J, Toyka KV, Suter U, Martini R: Structural abnormalities and deficient maintenance of peripheral nerve myelin in mice lacking the gap junction protein connexin32. *J Neurosci* 1997; 17:4545-51.

Ariga T, Kohriyama T, Freddo L, Latov N, Saito M, Kon K, Ando S, Suzuki M, Hemling ME, Rinehart KL, Kusunoki S, Yu RK: Characterization of sulfated glucuronic acid containing glycolipids reacting with IgM M-proteins in patients with neuropathy. *J Biol Chem* 1987; 262:848-53.

Arquint M, Roder J, Chia LS, Down J, Wilkinson D, Bayley H, Braun P, Dunn R: Molecular cloning and primary structure of myelin-associated glycoprotein. *Proc Natl Acad Sci USA* 1987; 84:600-4.

Arroyo EJ, Xu YT, Zhou L, Messing A, Peles E, Chiu SY, Scherer SS: Myelinating Schwann cells determine the internodal localization of Kv1.1, Kv1.2, Kvbeta2, and Caspr. *J Neurocytol* 1999; 28:333-47.

Arroyo EJ, Scherer SS: On the molecular architecture of myelinated fibers. *Histochem Cell Biol* 2000; 113:1-18.

Attia J, Tropak M, Johnson PW, Newerly-Abranow W, Pawson T, Roder JC, Dunn RJ: Modulated adhesion: a proposal for the role of myelin-associated glycoprotein in myelin wrapping. *Clin Chem* 1989; 35:717-20.

Ayers MM, Anderson RM: Onion bulb neuropathy in the trembler mouse: a model of hypertrophic interstitial neuropathy (Dejerine-Sottas) in man. *Acta Neuropathol (Berl)* 1973; 25:54-70.

Ayers MM, Anderson R: Development of onion bulb neuropathy in the Trembler mouse. Comparison with normal nerve maturation. *Acta Neuropathol (Berl)* 1975; 32:43-59.

Baas PW, Deitch JS, Black MM, Banker GA: Polarity orientation of microtubules in hippocampal neurons: uniformity in the axon and nonuniformity in the dendrite. *Proc Natl Acad Sci USA* 1988; 85:8335-9.

Baechner D, Liehr T, Hameister H, Altenberger H, Grehl H, Suter U, Rautenstrauss B: Widespread expression of the peripheral myelin protein-22 gene (pmp22) in neural and non-neural tissue during murine development. *J Neurosci Res* 1995; 42:733-41.

Bain PG, Britton TC, Jenkins IH, Thompson PD, Rothwell JC, Thomas PK, Brooks DJ, Marsden CD: Tremor associated with benign IgM paraproteinaemic neuropathy. *Brain* 1996; 119:789-99.

Balice-Gordon RJ, Bone LJ, Scherer SS: Functional gap junctions in the Schwann cell myelin sheath. *J Cell Biol* 1998; 142:1095-104.

Barbieri S, Nobile-Orazio E, Baldini L, Fayoumi Z, Manfredini E, Scarlato G: Visual evoked potentials in patients with neuropathy and macroglobunemia. *Ann Neurol* 1987; 22:663-6.

Barton DE, Arquint M, Roder J, Dunn R, Francke U: The myelin-associated glycoprotein gene: Mapping to human chromosome 19 and mouse chromosome 7 and expression in quivering mice. *Genomics* 1987; 1:107-12.

Bartoszewicz ZP, Noronha AB, Fujita N, Sato S, Bo L, Trapp BD, Quarles RH: Abnormal expression and glycosylation of the large and small isoforms of myelin-associated glycoprotein in dysmyelinating quaking mutants. *J Neurosci Res* 1995; 41:27-38.

Bartsch S, Montag D, Schachner M, Bartsch U: Increased number of unmyelinated axons in optic nerves of adult mice deficient in the myelin-associated glycoprotein (MAG). *Brain Res* 1997; 762:231-4.

Bartsch U, Kirchhoff F, Schachner M: Immunohistological localization of the adhesion molecules L1, N-CAM, and MAG in the developing and adult optic nerve of mice. *J Comp Neurol* 1989; 284:451-62.

Bartsch U, Bandtlow CE, Schnell L, Bartsch S, Spillmann AA, Rubin SP, Hillenbrand R, Montag D, Schwab ME, Schachner M: Lack of evidence that myelin-associated glycoprotein is a major inhibitor of axonal regeneration in the CNS. *Neuron* 1995*a*; 15:1375-81.

Bartsch U, Montag D, Bartsch S, Schachner M: Multiply myelinated axons in the optic nerve of mice deficient for the myelin-associated glycoprotein. *Glia* 1995*b*; 14:115-22.

Behse F: Morphometric studies on the human sural nerve. *Acta Neurol Scand (Suppl.)* 1990; 132:1-38.

Behse F, Buchthal F, Carlsen F, Knappeis GG: Hereditary neuropathy with liability to pressure palsies. *Brain* 1972; 95:777-94.

Bergoffen J, Scherer SS, Wang S, Oronzi Scott M, Bone LJ, Paul DL, Chen K, Lensch MW, Chance PF, Fischbeck KH: Connexin mutations in X-linked Charcot-Marie-Tooth disease. *Science* 1993; 262:2039-42.

Berthold C-H: Morphology of normal peripheral axons, in Waxman SG (ed): *Physiology and Pathobiology of Axons*. New York, Raven Press, 1978, pp 3-63.

Berthold C-H, Rydmark M: Morphology of normal peripheral axons, in Waxman SG, Kocsis JD, Stys PK (eds): *The axon: structure, function and pathophysiology*. New York, Oxford, 1995, pp 13-48.

Bird TD, Ott J, Giblett ER: Evidence for linkage of Charcot-Marie-Tooth neuropathy to the Duffy locus on chromosome 1. *Am J Hum Genet* 1982; 34:388-94.

Bjartmar C, Yin X, Trapp BD: Axonal pathology in myelin disorders. *J Neurocytol* 1999; 28:383-95.

Blatt C, Weiner J, Sutcliffe JG, Nesbitt MN, Simon MI: Chromosomal mapping of murine brain-specific genes. *J Neurochem* 1985; 40:583a

Boison D, Stoffel W: Disruption of the compacted myelin sheath of axons of the central nervous system in proteolipid protein-deficient mice. *Proc Natl Acad Sci USA* 1994; 91:11709-13.

Bolino A, Brancolini V, Bono F, Bruni A, Gambardella A, Romeo G, Quattrone A, Devoto M: Localization of a gene responsible for autosomal recessive demyelinating neuropathy with focally folded myelin sheaths to chromosome 11q23 by homozygosity mapping and haplotype sharing. *Hum Mol Genet* 1996; 5:1051-4.

Bollensen E, Schachner M: The peripheral myelin glycoprotein P0 expresses the L2/HNK-1 and L3 carbohydrate structures shared by neural adhesion molecules. *Neurosci Lett* 1987; 82:77-82.

Bollensen E, Steck AJ, Schachner M: Reactivity with the peripheral myelin glycoprotein P0 in serum from patients with monoclonal IgM gammopathy and polyneuropathy. *Neurology* 1988; 38:1266-70.

Bornstein MB, Raine CS: The initial structural lesion in serum-induced demyelination in vitro. *Lab Invest* 1976; 35:391-401.

Bosboom WMJ, van den Berg LH, Franssen H, Giesbergen PCLM, Flach HZ, van Putten AM, Veldman H, Wokke JHJ: Diagnostic value of sural nerve demyelination in chronic inflammatory demyelinating polyneuropathy. *Brain* 2001; 124:2427-2438.

Brackenbury R, Thiery J-P, Rutishauser U, Edelman GM: Adhesion among neural cells of the chick embryo. I. An immunological assay for molecules involved in cell-cell binding. *J Biol Chem* 1977; 252:6835-40.

Brandt R: Cytoskeletal mechanisms of axon outgrowth and pathfinding. *Cell Tissue Res* 1998; 292:181-9.

Braun PE, Frail DE, Latov N: Myelin-associated glycoprotein is the antigen for a monoclonal IgM in polyneuropathy. *J Neurochem* 1982; 39:1261-5.

Braun PE, Horvath E, Edwards AM: Two isoforms of myelin-associated glycoprotein accumulate in quaking mice: only the large polypeptide is phosphorylated. *Dev Neurosci* 1990; 12:286-92.

Bray D, Bunge MB: Serial analysis of microtubules in cultured rat sensory axons. *J Neurocytol* 1981; 10:589-605.

Bray GM, Rasminsky M, Aguayo AJ: Interactions between axons and their sheath cells. *Annu Rev Neurosci* 1981; 4:127-62.

Brockes JP, Raff MC, Nishiguchi DJ, Winter J: Studies on cultured rat Schwann cells. III. Assays for peripheral myelin proteins. *J Neurocytol* 1980; 9:67-77.

Brockes JP, Fryxell KJ, LemkeG.E.: Studies on cultured Schwann cells: the induction of myelin synthesis, and the control of their proliferation by a new growth factor. *J Exp Biol* 1981; 95:215-30.

Brunden KR, Windebank AJ, Poduslo JF: Catabolic regulation of the expression of the major myelin glycoprotein by Schwann cells in culture. *J Neurochem* 1990; 54:459-66.

Buchthal F, Carlsen F, Behse F: Schmidt-Lanterman clefts: A morphometric study in human sural nerves. *Amer J Anat* 1987; 180:156-160.

Bunge MB, Williams AK, Wood PM: Neuron-Schwann cell interaction in basal lamina formation. *Dev Biol* 1982; 92:449-60.

Bunge MB: Schwann cell regulation of extracellular matrix biosynthesis and assembly, in Dyck PJ, Thomas PK, Griffin JW, Low PA, Poduslo JF (eds): *Peripheral neuropathy*. 1993, vol3rd, pp 299-316.

Bunge RP: Tissue culture observations relevant to the study of axon-Schwann cell interactions during peripheral nerve development and repair. *J Exp Biol* 1987; 132:21-34.

Bunge RP, Bunge MB, Bates M: Movements of the Schwann cell nucleus implicate progression of the inner (axon-related) Schwann cell process during myelination. *J Cell Biol* 1989; 109:273-84.

Bunge RP: Expanding roles for the Schwann cell: ensheathment, myelination, trophism and regeneration. *Curr Opin Neurobiol* 1993; 3:805-9.

Burger D, Simon M, Perruisseau G, Steck AJ: The epitope(s) recognized by HNK-1 antibody and IgM paraprotein in neuropathy is present on several N-linked oligosaccharide structures on human P0 and myelin-associated glycoprotein. *J Neurochem* 1990; 54:1569-75.

Burger D, Perruisseau G, Simon M, Steck AJ: Comparison of the N-linked oligosaccharide structure of the two major human myelin glycoproteins MAG and P0: assessment and

relative occurence of oligosaccharide structures by serial lectin affinity chromatography of 14C-glycopeptides. *J Neurochem* 1992; 58:383-8.

Burger D, Pidoux L, Steck AJ: Identification of the glycosylated sequons of human myelin-associated glycoprotein. *Biochem Biophys Res Commun* 1993; 197:457-464.

Cai Z, Cash K, Thompson PD, Blumbergs PC. Accuracy of sampling methods in morphometric studies of human sural nerves. *Journal of Clinical Neuroscience* 2002; 9:181-6.

Carenini S, Montag D, Cremer H, Schachner M, Martini R: Absence of the myelin-associated glycoprotein (MAG) and the neural cell adhesion molecule (N-CAM) interferes with the maintenance, but not with the formation of peripheral myelin. *Cell Tissue Res* 1997; 287:3-9.

Carenini S, Montag D, Schachner M, Martini R: MAG-deficient Schwann cells myelinate dorsal root ganglion neurons in culture. *Glia* 1998; 22:213-20.

Carenini S, Montag D, Schachner M, Martini R: Subtle roles of neural cell adhesion molecule and myelin-associated glycoprotein during Schwann cell spiralling in P0-deficient mice. *Glia* 1999; 27:203-12.

Cash K, Blumbergs PC: Neuromuscular Tissue, in Woods AE, Ellis RC (eds): *Laboratory Histopathology: A complete reference*. Edinburgh, Churchill Livingstone, 1995, pp 7.3.1-7.3.25

Cavanagh JB, Jacobs JM: Some quantitative aspects of diphtheritic neuropathy. *Br J Exp Pathol* 1964; 45:309-22.

Chance PF, Alderson MK, Leppig KA, Lensch MW, Matsunami N, Smith B, Swanson PD, Odelberg SJ, Disteche CM, Bird TD: DNA deletion associated with hereditary neuropathy with liability to pressure palsies. *Cell* 1993; 72:143-51.

Chassande B, Leger JM, Younes-Chennoufi AB, Bengoufa D, Maisonobe T, Bouche P, Baumann N: Peripheral neuropathy associated with IgM monoclonal gammopathy: correlation between M-protein antibody activity and clinical clinical/electrophysiological features in 40 cases. *Muscle Nerve* 1998; 21:55-62.

Chopra JS, Hurwitz LJ: Internodal length of sural nerve fibres in chronic occlusive vascular disease. *J Neurol Neurosurg Psychiatry* 1967; 30:207-14.

Chou DKH, Ilyas AA, Evans JE, Costello C, Quarles RH, Jungalwala FB: Structure of sulfated glucuronyl glycolipids in the nervous system reacting with HNK-1 antibody and some IgM paraproteins in neuropathy. *J Biol Chem* 1986; 261:11717-25.

Cole JS, Messing A, Trojanowski JQ, Lee VM: Modulation of axon diameter and neurofilaments by hypomyelinating Schwann cells in transgenic mice. *J Neurosci* 1994; 14:6956-66.

Collins BE, Yang LJ, Mukhopadhyay G, Filbin MT, Kiso M, Hasegawa A, Schnaar RL: Sialic acid specificity of myelin-associated glycoprotein binding. *J Biol Chem* 1997; 272:1248-55.

Cook D, Dalakas MC, Galdi A, Biondi D, Porter H: High-dose intravenous immunoglobulin in the treatment of demyelinating neuropathy associated with monoclonal gammopathy. *Neurology* 1990; 40:212-4.

Cornish AL, Freeman S, Forbes G, Ni J, Zhang M, Cepeda M, Gentz R, Augustus M, Carter KC, Crocker PR: Characterization of siglec-5, a novel glycoprotein expressed on myeloid cells related to CD33. *Blood* 1998; 92:2123-32.

Crocker PR, Clark EA, Filbin M, Gordon S, Jones Y, Kehrl JH, Kelm S, Le Douarin N, Powell L, Roder J, Schnaar RL, Sgroi DC, Stamenkovic I, Schauer R, Schachner M, van den Berg TK, van der Merwe PA, Watt SM, Varki A: Siglec: a family of sialic-acid binding lectins. *Glycobiology* 1998; 8:V-VI

Cunningham BA, Hemperly JJ, Murray BA, Prediger EA, Brackenbury R, Edelman GM: Neural cell adhesion molecule: structure, immunoglobulin-like domains, cell surface modulation, and alternative RNA splicing. *Science* 1987; 236:799-806.

D'Eustachio P, Colman DR, Salzer JL: chromosomal location of the mouse gene that encodes the myelin-associated glycoproteins. *J Neurochem* 1988; 50:589-93.

D'Urso D, Brophy PJ, Staugaitis SM, Gillespie CS, Frey AB, Stempak JG, Colman DR: Protein zero of peripheral nerve myelin: biosynthesis, membrane insertion, and evidence for homotypic interaction. *Neuron* 1990; 2:449-60.

D'Urso D, Müller HW: Ins and outs of peripheral myelin protein-22: mapping transmembrane topology and intracellular sorting. *J Neurosci Res* 1997; 49:551-62.

Dalakas M, Engel WK: Polyneuropathy with monoclonal gammopathy: studies of 11 patients. *Ann Neurol* 1981; 10:45-52.

Dalakas MC, Teravainen H, Engel WK: Tremor as a feature of chronic relapsing and dysgammaglobulinemic polyneuropathies. Incidence and management. *Arch Neurol* 1984; 41:711-4.

Dayan AD, Graveson GS, Robinson PK, Woodhouse MA: Globular neuropathy. *J Neurol Neurosurg Psychiatry* 1968; 31:552-60.

De Bellard ME, Filbin MT: Myelin-associated glycoprotein, MAG, selectively binds several neuronal proteins. *J Neurosci Res* 1999; 56:213-8.

de Waegh SM, Brady ST: Altered slow axonal transport and regeneration in a myelin-deficient mutant mouse: the trembler as an in vivo model for Schwann cell-axon interactions. *J Neurosci* 1990; 10:1855-65.

de Waegh SM, Brady ST: Local control of axonal properties by Schwann cells: Neurofilaments and axonal transport in homologous and heterologous nerve grafts. *J Neurosci Res* 1991; 30:201-12.

de Waegh SM, Lee VM, Brady ST: Local modulation of neurofilament phosphorylation, axonal caliber, and slow axonal transport by myelinating Schwann cells. *Cell* 1992; 68:451-463.

Ding Y, Brunden KR: The cytoplasmic domain of myelin protein P0 interacts with negatively charged phospholipid bilayers. *J Biol Chem* 1994; 269:10764-70.

Dong Z, Brennan N, Liu Y, Yarden Y, Lefkowitz G, Mirsky R, Jessen KR: Neu differentiation factor is a neuron-glia signal and regulates survival, proliferation, and maturation of rat Schwann cell precursors. *Neuron* 1995; 15:585-596.

Dyck PJ, Lofgren EP: Method of fascicular biopsy of human peripheral nerve for electrophysiologic and histologic study. *Mayo Clin Proc* 1966; 41:778-84.

Dyck PJ, Lofgren EP: Nerve biopsy. Choice of nerve, method, symptoms, and usefulness. *Med Clin North Am* 1968; 52:885-93.

Dyck PJ, Lambert EH: Lower motor and primary sensory neuron diseases with peroneal muscular atrophy. I. Neurologic, genetic, and electrophysiologic findings in hereditary polyneuropathies. *Arch Neurol* 1968; 18:603-18.

Dyck PJ, Lais AC: Electron microscopy of teased nerve fibers: method permitting examination of repeating structures of same fiber. *Brain Res* 1970; 23:418-24.

Dyck PJ, Lambert EH, Nichols PC: Quantitative measurement of sensation related to compound action potential and number and sizes of myelinated and unmyelinated fibers of sural nerves in health, Friedreich's ataxia, hereditary sensory neuropathy, and tabes dorsalis, in Remond A (ed): *Handbook of Electroencephalography and Clinical Neurophysiology*. Amsterdam, Elsevier, 1971*a*, pp 83-118.

Dyck PJ, Johnson WJ, Lambert EH, O'Brien PC: Segmental demyelination secondary to axonal degeneration in uremic neuropathy. *Mayo Clin Proc* 1971*b*; 46:400-31.

Dyck PJ, Lais AC, Karnes JL, Sparks M, Hunder H, Low PA, Windebank AJ: Permanent axotomy, a model of axonal atrophy and secondary segmental demyelination and remyelination. *Ann Neurol* 1981; 9:575

Dyck PJ, Karnes J, Lais A, Lofgren EP, Stevens JC: Pathologic alterations of the peripheral nervous system of humans, in Dyck PJ, Thomas PK, Lambert EH, Bunge R (eds): *Peripheral neuropathy* . Philadelphia, WB Saunders, 1984, vol2nd, pp 760-870.

Dyck PJ, Karnes JL, Lambert EH: Longitudinal study of neuropathic deficits and nerve conduction abnormalities in hereditary motor and sensory neuropathy type 1. *Neurology* 1989; 39:1302-8.

Dyck PJ, Giannini C, Lais A: Pathologic alterations of nerves, in Dyck PJ, Thomas PK, Griffin J, Low P, Poduslo J (eds): *Peripheral Neuropathy*. Philadelphia, WB Saunders, 1993*a*, vol3rd, pp 514-95.

Dyck PJ, Chance P, Lebo R, Carney JA: Hereditary motor and sensory neuropathies, in Dyck PJ, Thomas PK, Lambert EH, Bunge RP (eds): *Peripheral neuropathy*. Philadelphia, WB Saunders, 1993*b*, vol3rd, pp 1094-136.

Edwards AM, Braun PE, Bell JC: Phosphorylation of myelin-associated glycoprotein in vivo and in vitro occurs only in the cytoplasmic domain of the large isoform. *J Neurochem* 1989; 52:317-20.

Ellie E, Vital A, Steck A, Boiron JM, Vital C, Julien J: Neuropathy associated with "benign" anti-myelin-associated glycoprotein IgM gammopathy: clinical, immunological, neurophysiological findings and response to treatment in 33 cases. *J Neurol* 1996; 243:34-43.

Ellisman MH, Porter KR: Microtrabecular structure of the axoplasmic matrix: visualization of cross-linking structures and their distribution. *J Cell Biol* 1980; 87:464-79.

Fabrizi GM, Taioli F, Cavallaro T, Rigatelli F, Simonati A, Mariani G, Perrone P, Rizzuto N: Focally folded myelin in Charcot-Marie-Tooth neuropathy type 1B with Ser49Leu in the myelin protein zero. *Acta Neuropathol (Berl)* 2000; 100:299-304.

Fahrig T, Landa P, Pesheva P, Kuhn K, Schachner M: Characterization of binding properties of the myelin-associated glycoprotein to extracellular matrix constituents. *EMBO J* 1987; 6:2875-83.

Fannon AM, Sherman DL, Ilyina-Gragerova G, Brophy PJ, Friedrich VLJ: Novel E-cadherin-mediated adhesion in peripheral nerve: Schwann cell architecture is stabilized by autotypic adherens junctions. *J Cell Biol* 1995; 129:189-202.

Figlewicz DA, Quarles RH, Johnson D, Barbarash GR, Sternberger NH: Biological demonstration of the myelin-associated glycoprotein in the peripheral nervous system. *J Neurochem* 1981; 37:749-758.

Filbin MT, Walsh FS, Trapp BD, Pizzey JA, Tennekoon GI: Role of myelin P0 protein as a homophilic adhesion molecule. *Nature* 1990; 344:2

Fischbeck KH, Abel A, Lin GS, Scherer SS: X-linked Charcot-Marie-Tooth disease and connexin32. *Ann NY Acad Sci* 1999; 883:36-41.

Floyd H, Ni J, Cornish AL, Zeng Z, Liu D, Carter KC, Steel J, Crocker PR: Siglec-8. A novel eosinophil-specific member of the immunoglobulin superfamily. *J Biol Chem* 2000; 275:861-6.

Fraher JP: A quantitative study of anterior root fibres during early myelination. *J Anat* 1972; 112:99-124.

Fraher JP: The growth and myelination of central and peripheral segments of ventral motoneurone axons. A quantitative ultrastructural study. *Brain Res* 1976; 105:193-211.

Fraher JP: Quantitative studies on the maturation of central and peripheral parts of individual ventral motoneuron axons. I. Myelin sheath and axon calibre. *J Anat* 1978; 126:509-533.

Fraher JP: Axon-myelin relationships in rat cranial nerves III, IV, and VI: A morphometric study of large- and small-fibre classes. J Comp Neurol. *J Comp Neurol* 1989; 286:384-390.

Fraher JP: Myelin-axon relationships in the rat phrenic nerve: Longitudinal variation and lateral asymmetry. *J Comp Neurol* 1992; 323:551-7.

Frail DE, Braun PE: Two developmentally regulated messenger RNAs differing in their coding region may exist for the myelin-associated glycoprotein. *J Biol Chem* 1984; 259:14857-62.

Frail DE, Webster HD, Braun PE: Developmental expression of the myelin-associated glycoprotein in the peripheral nervous system is different from that in the central nervous system. *J Neurochem* 1985; 45:1308-10.

Frei R, Motzing S, Kinkelin M, Schachner M, Koltzenburg M, Martini R: Loss of distal axons and sensory Merkel cells and features indicative of muscle denervation in hindlimbs of P0-deficient mice. *J Neurosci* 1999; 19:6058-67.

Friede RL, Samorajski T: Relation between the number of myelin lamellae and axon circumference in fibers of vagus and sciatic nerves of mice. *J Comp Neurol* 1967; 130:223-32.

Friede RL, Samorajski T: Myelin formation in the sciatic nerve of the rat. A quantitative electron microscopic, histochemical and radioactive study. *J Neuropathol Exp Neurol* 1968; 27:546-71.

Friede RL, Samorajski T: The clefts of Schmidt-Lantermann: a quantitative electron microscopic study of their structure in developing and adult sciatic nerves of the rat. *Anat Rec* 1969; 165:89-102.

Friede RL: Control of myelin formation by axon caliber (with a model of the control mechanism). *J Comp Neurol* 1972; 144:233-252.

Friede RL, Beuche W: Combined scatter diagrams of sheath thickness and fibre calibre in human sural nerves: changes with age and neuropathy. *J Neurol Neurosurg Psychiatry* 1995; 48:749-56.

Fruttiger M, Montag D, Schachner M, Martini R: Crucial role for the myelin-associated glycoprotein in the maintenance of axon-myelin integrity. *Eur J Neurosci* 1995; 7:511-5.

Fujita N, Kemper A, Dupree J, Nakayasu H, Bartsch U, Schachner M, Maeda N, Suzuki K, Popko B: The cytoplasmic domain of the large myelin-associated glycoprotein isoform is needed for proper CNS but not peripheral nervous system myelination. *J Neurosci* 1998; 18:1970-8.

Fullerton PM, Gilliatt RW, Lascelles RG, Morganhughes JA: The relation between fibre diameter and internodal length in chronic neuropathy (abstract). *J Physiol (Lond)* 1965; 178:26

Gabreëls-Festen AAWM, Joosten EMG, Gabreels FJM, Stegeman DF, Vos AJM, Busch HFM: Congenital demyelinating motor and sensory neuropathy with focally folded myelin sheaths. *Brain* 1990; 113:1629-43.

Gabreëls-Festen AAWM, Gabreels FJM, Jennekens FGI, Joosten EMG, Janssen-van Kempen TW: Autosomal recessive form of hereditary motor and sensory neuropathy type I. *Neurology* 1992; 42:1755-61.

Gabriel JM, Erne B, Miescher GC, Miller SL, Vital A, Vital C, Steck AJ: Selective loss of myelin-associated glycoprotein from myelin correlated with anti-MAG antibody titre in demyelinating paraproteinaemic polyneuropathy. *Brain* 1996; 119:775-87.

Gabriel JM, Erne B, Bernasconi L, Tosi C, Probst A, Landmann L, Steck AJ: Confocal microscopic localization of anti-myelin-associated glycoprotein autoantibodies in a patient with peripheral neuropathy initially lacking a detectable IgM gammopathy. *Acta Neuropathol (Berl)* 1998; 95:540-6.

Gal A, Mucke J, Theile H, Wieacker PF, Ropers HH, Wienker TF: X-linked dominant charcot-Marie-Tooth disease: suggestion of linkage with a cloned DNA sequence from the proximal Xq. *Hum Genet* 1985; 70:38-42.

Gambardella A, Bono F, Muglia M, Valentino P, Quattrone A: Autosomal recessive hereditary motor and sensory neuropathy with focally folded myelin sheaths (CMT4B). *Ann N Y Acad Sci* 1999; 883:47-55.

Garbay B, Heape AM, Sargueil F, Cassagne C: Myelin synthesis in the peripheral nervous system. *Prog Neurobiol* 2000; 61:267-304.

Garbern JY, Cambi F, Tang XM, Sima AA, Vallat JM, Bosch EP, Lewis R, Shy M, Sohi J, Kraft G, Chen KL, Joshi I, Leonard DG, Johnson W, Raskind W, Dlouhy SR, Pratt V, Hodes ME, Bird T, Kamholz J: Proteolipid protein is necessary in peripheral as well as central myelin. *Neuron* 1997; 19:205-18.

Garbern JY, Cambi F, Lewis R, Shy M, Sima A, Kraft G, Vallat J.M., Bosch EP, Hodes ME, Dlouhy S, Raskind W, Bird T, Macklin W, Kamholz J: Peripheral neuropathy caused by proteolipid gene mutations. *Ann NY Acad Sci* 1999; 883:351-365.

Garcia ML, Cleveland DW: Going new places using an old MAP: tau, microtubules and human neurodegenerative disease. *Curr Opin Cell Biol* 2001; 13:41-48.

Gatzinsky KP: Node-paranode regions as local degradative centres in alpha-motor axons. *Microsc Res Tech* 1996; 34:492-506.

Gatzinsky KP, Persson GH, Berthold C-H: Removal of retrogradely transported material from rat lumbosacral alpha-motor axons by paranodal axon-Schwann cell networks. *Glia* 1997; 20:115-126.

Geisler N, Vandekerckhove J, Weber K: Location and sequence characterization of the major phosphorylation sites of the high molecular mass neurofilament proteins M and H. *FEBS Lett* 1987; 221:403-7.

Gerlai R, Friend W, Becker L, O'Hanlon D, Marks A, Roder J: Female transgenic mice carrying multiple copies of the human gene for S100 beta are hyperactive. *Behav Brain Res* 1993; 55:51-9.

Ghabriel MN, Allt G: The role of Schmidt-Lanterman incisures in Wallerian degeneration. I. A quantitative teased fibre study. *Acta Neuropathol (Berl)* 1979*a*; 48:83-93.

Ghabriel MN, Allt G: The role of Schmidt-Lanterman incisures in Wallerian degeneration. II. An electron microscopic study. *Acta Neuropathol (Berl)* 1979*b*; 48:95-103.

Ghabriel MN, Allt G: Schmidt-Lanterman incisures. I. A quantitative teased fibre study of remyelinating peripheral nerve fibres. *Acta Neuropathol (Berl)* 1980; 52:85-95.

Ghabriel MN, Allt G: Incisures of Schmidt-Lanterman. *Prog Neurobiol* 1981; 17:25-58.

Giese KP, Martini R, Lemke G, Soriano P, Schachner M: Disruption of the P0 gene in mice lead to hypomyelination, abnormal expression of recognition molecules, and degeneration of myelin and axons. *Cell* 1992; 71:565-76.

Gortzen A, Schluter S, Veh RW: Schmidt-Lanterman's incisures--the principal target of autoimmune attack in demyelinating Guillain-Barre syndrome? *J Neuroimmunol* 1999; 94:58-65.

Gosselin S, Kyle RA, Dyck PJ: Neuropathy associated with monoclonal gammopathies of undertermined significance. *Ann Neurol* 1991; 30:54-61.

Gould RM, Byrd AL, Barbarese E: The number of Schmidt-Lantermann incisures is more than doubled in shiverer PNS myelin sheaths. *J Neurocytol* 1995; 24:85-98.

Gowda DC, Margolis RU, Margolis RK: Presence of the HNK-1 epitope on poly(N-acetyllactosaminyl) oligosaccharides and identification of multiple core proteins in the chondroitin sulfate proteoglycans of brain. *Biochemistry* 1989; 28:4468-4474.

Griffin JW, Drucker N, Benzaquen M, Charnes LR, Fahnestock KE, Stocks EA: Schwann cell proliferation and migration during paranodal demyelination. *J Neurosci* 1987; 7:682-699.

Griffin JW, Kidd G, Trapp BD: Interactions between axons and Schwann cells, in Dyck PJ, Thomas PK, Griffin J, Low P, Poduslo J (eds): *Peripheral Neuropathy*. Philadelphia, WB Saunders, 1993, vol3rd, pp 317-30.

Griffin JW, Li CY, Macko C, Ho TW, Hsieh ST, Xue P, Wang FA, Cornblath DR, McKhann GM, Asbury AK: Early nodal changes in the acute motor axonal neuropathy pattern of the Guillain-Barre syndrome. *J Neurocytol* 1996; 25:33-51.

Griffiths I, Klugmann M, Anderson T, Yool D, Thomson C, Schwab MH, Schneider A, Zimmermann F, McCulloch M, Nadon N, Nave KA: Axonal swellings and degeneration in mice lacking the major proteolipid of myelin. *Science* 1998; 280:1610-3.

Grinspan JB, Marchionni MA, Reeves M, Coulaloglou M, Scherer SS: Axonal interactions regulate Schwann cell apoptosis in developing peripheral nerve: neuregulin receptors and the role of neuregulins. *J Neurosci* 1996; 16:6107-18.

Gupta SK, Poduslo JF, Mezei C: Temporal changes in PO and MBP gene expression after crush-injury of the adult peripheral nerve. *Mol Brain Res* 1988; 464:133-41.

Gupta SK, Poduslo JF, Dunn R, Roder J, Mezei C: Myelin-associated glycoprotein gene expression in the presence and absence of Schwann cell-axonal contact. *Dev Neurosci* 1990; 12:22-33.

Gupta SK, Pringle J, Poduslo JF, Mezei C: Induction of myelin genes during peripheral nerve remyelination requires a continuous signal from the ingrowing axon. *J Neurosci Res* 1993; 34:14-23.

Gutrecht JA, Dyck PJ: Quantitative teased-fiber and histologic studies of human sural nerve during postnatal development. *J Comp Neurol* 1970; 138:117-29.

Hafer-Macko C, Hsieh ST, Li CY, Ho TW, Sheikh K, Cornblath DR, Mckhan GM, Asbury AK, Griffin JW: Acute motor axonal neuropathy: an antibody-mediated attack on axolemma. *Ann Neurol* 1996; 40:635-44.

Hall SM, Williams PL: Studies on the "incisures" of Schmidt and Lanterman. *J Cell Sci* 1970; 6:767-91.

Hammer JA, O'Shannessy DJ, De Leon M, Gould R, Zand D, Daune G: The immunoreactivity of PMP-22, P0 and other 19 to 28 kDa glycoprotein in peripheral nerve myelin of mammals and fish with HNK-1 and related antibodies. *J Neurochem* 1993; 35:558

Haney C, Snipes GJ, Shooter EM, Suter U, Garcia C, Griffin JW, Trapp BD: Ultrastructural distribution of PMP22 in Charcot-Marie-Tooth disease type 1A. *J Neuropathol Exp Neurol* 1996*a*; 55:290-99.

Haney CA, Li C, Yin X, Soriano P, Roder J, Trapp BD: Analysis of L1/NCAM double knockout mice. *Soc Neurosci Abstr* 1996*b*; 22:584

Hartung HP, Pollard JD, Harvey GK, Toyka KV: Immunopathogenesis and treatment of the Guillain-Barre syndrome. Part I. *Muscle Nerve* 1995*a*; 18:137-155.

Hartung HP, Pollard JD, Harvey GK, Yoyka KV: Immunopathogenesis and treatment of the Guillain-Barre syndrome. Part II. *Muscle Nerve* 1995*b*; 18:154-64.

Hayasaka K, Himoro M, Sato W, Takada G, Uyemura K, Shimizu N, Bird TD, Conneally PM, Chance PF: Charcot-Marie-Tooth neuropathy type 1B is associated with mutations of the myelin P0 gene. *Nat Genet* 1993; 5:

Hays AP, Latov N, Takatsu MSWH: Experimental demyelination of nerve induced by serum of patients with neuropathy and an anti-MAG IgM M-protein. *Neurology* 1987; 37:242-56.

Hildebrand C, Hann R: relation between myelin sheath thickness and axon size in spinal cord white matter thickness and axon size in spinal cord white matter of some vertebrate species. *J Neurol Sci* 1978; 38:421-34.

Hill BD, Prior H, Blakemore WF, Black PF: A study of the pathology of a bovine primary peripheral myelinopathy with features of tomaculous neuropathy. *Acta Neuropathol (Berl)* 1996; 91:545-8.

Hirokawa N, Glicksman MA, Willard MB: Organization of mammalian neurofilament polypeptides within the neuronal cytoskeleton. *J Cell Biol* 1984; 98:1523-36.

Hiscoe HB: Distribution of nodes and incisures in normal and regenerated nerve fibers. *Anat Rec* 1947; 99:447

Ho ST, Yu HS: Ultrastructural changes of the peripheral nerve induced by vibration: an experimental study. *Br J Ind Med* 1989; 46:157-64.

Ho TW, McKhann GM, Griffin JW: Human autoimmune neuropathies. *Annu Rev Neurosci* 1998; 21:187-226.

Hoffman PN, Griffin JW: The control of axonal caliber, in Dyck PJ, Thomas PK, Griffin JW, Low PA, Poduslo JF (eds): *Peripheral neuropathy*. Philadelphia, W.B. Saunders, 1993, vol3rd, pp 389-402.

Hoffman S, Edelman GM: A proteoglycan with HNK-1 antigenic determinants is a neuron-associated ligand for cytotactin. *Proc Natl Acad Sci USA* 1987; 84:2523-7.

Hsieh ST, Kidd GJ, Crawford TO, Xu Z, Lin WM, Trapp BD, Cleveland DW, Griffin JW: Regional modulation of neurofilament organization by myelination in normal axons. *J Neurosci* 1994; 14:6392-401.

Hudson L: Molecular biology of myelin proteins in the central and peripheral nervous systems. *Semin Neurosci* 1990; 2:487-96.

Hynes RO: Integrins: a family of cell surface receptors. *Cell* 1987; 48:549-554.

Ilyas AA, Chou DKH, Jungalwala FB, Costello C, Quarles RH: Variability in the structural requirements for binding of human monoclonal anti-myelin-associated glycoprotein immunoglobulin M antibodies and HNK-1 to sphingoglycolipids antigen. *J Neurochem* 1990; 55:594-601.

Ishiguro H, Sato S, Fujita N, Inuzuka T, Nakano R, Miyatake T: Immunohistochemical localization of myelin-associated glycoprotein isoforms during the development in the mouse brain. *Brain Res* 1991; 563:288-92.

Jacobs JM, Love S: Qualitative and quantitative morphology of human sural nerve at different ages. *Brain* 1985; 108:897-924.

Jacobs JM, Scadding JW: Morphological changes in IgM paraproteinaemic neuropathy. *Acta Neuropathol (Berl)* 1990; 80:77-84.

Jacobs JM: Morphological changes at paranodes in IgM paraproteinaemic neuropathy. *Microsc Res Tech* 1996; 34:544-53.

Jessen KR, Mirsky R, Lorgan L: Axonal signals regulate the differentiaition of non-myelin-forming Schwann cells: an immunohistochemical study of galactocerebroside in transected and regenerating nerves. *J Neurosci* 1987; 7:3362-9.

Jessen KR, Mirsky R: Schwann cells: early lineage, regulation of proliferation and control of myelin formation. *Curr Opin Neurobiol* 1992; 2:575-81.

Jessen KR, Brennan L, Morgan L, Mirsky R, Kent A, Hashimoto Y, Gavrilovic J: The Schwann cell precursor and its fate: a study of cell death and differentiation during gliogennesis in rat embryonic nerves. *Neuron* 1994; 12:509-27.

Jessen KR, Mirsky R: Developmental regulation in the Schwann cell lineage. *Adv Exp Med Biol* 1999; 468:3-12.

Joy JL, Oh SJ: Tomaculous neuropathy presenting as acute recurrent polyneuropathy. *Ann Neurol* 1989; 26:98-100.

Julien J, Vital C, Vallat J.M., Lagueny A, Deminiere C, Darriet D: Polyneuropathy in Waldenstrom's macroglobulinemia. Deposition of M component on myelin sheaths. *Arch Neurol* 1978; 35:423-5.

Jungalwala FB: Expression and biological functions of sulfoglucuronyl glycolipids (SGGLs) in the nervous system--a review. *Neurochem Res* 1994; 19:945-57.

Kaar GF, Fraher JP: The development of alpha and gamma motoneuron fibres in teh rat. I. A comparative ultrastructural study of their central and peripheral myelination. *J Anat* 1985; 141:77-88.

Kaji R, Oka N, Tsuji T, Mezaki T, Nishio T, Akiguchi I, Kimura J: Pathological findings at the site of conduction block in multifocal motor neuropathy. *Ann Neurol* 1993; 33:152-8.

Kaku DA, England JD, Sumner AJ: Distal accentuntion of conduction slowing in polyneuropathy associated with antibodies to myelin-associated glycoprotein and sulphated glucuronyl paragloboside. *Brain* 1994; 117:941-7.

Kalichman MW, Chalk CH, Mizisin AP: Classification of teased nerve fibers for multicenter clinical trials. *J Peripher Nerv Syst* 1999; 4:233-44.

Kamiguchi H, Hlavin ML, Yamasaki M, Lemmon V: Adhesion molecules and inherited diseases of the human nervous system. *Annu Rev Neurosci* 1998; 21:97-125.

Kanda T, Usui S, Beppu H, Miyamoto K, Yamawaki M, Oda M: Blood-nerve barrier in IgM paraproteinemic neuropathy: a clinicopathologic assessment. *Acta Neuropathol (Berl)* 1998; 95:184-92.

Keller MP, Chance PF: Inherited neuropathies: from gene to disease. *Brain Pathol* 1999; 9:327-41.

Kelly JJ Jr.: The electrodiagnostic findings in polyneuropathies associated with IgM monoclonal gammopathies. *Muscle Nerve* 1990; 13:1113-7.

Kelly JJ, Adelman LS, Berkman E, Bhan I: Polyneuropathies associated with IgM monoclonal gammopathies. *Arch Neurol* 1988; 45:1355-9.

Kelly JJ Jr: Peripheral neuropathies associated with monoclonal proteins: a clinical review. *Muscle Nerve* 1985; 8:138-50.

Kelm S, Pelz A, Schauer R, Filbin MT, Tang S, de Bellard M, Schnaar RL, Mahoney JA, Hartnell A, Bradfield P, Crocker PR: Sialoadhesin, myelin-associated glycoprotein and CD22 define a new family of sialic acid-dependent adhesion molecules of the immunoglobulin superfamily. *Curr Biol* 1994; 4:965-72.

Kelm S, Schauer R: Sialic acids in molecular and cellular interactions. *Int Rev Cytol* 1997; 175:137-240.

Kikly KK, Bochner BS, Freeman SD, Tan KB, Gallagher KT, D'Alessio KJ, Holmes SD, Abrahamson JA, Erickson-Miller CL, Murdock PR, Tachimoto H, Schleimer RP, White JR: Identification of SAF-2, a novel siglec expressed on eosinophils, mast cells, and basophils. *Allergy Clin Immunol* 2000; 105:1093-100.

King RHM: Diseases of peripheral nerve, in Adams D, Graham DG (eds): *An Introduction to Neuropathology*. Singapore, Groff Nuttall, 1994.

King RHM, Thomas PK: The occurrence and significance of myelin with unusually large periodicity. *Acta Neuropathol (Berl)* 1984; 63:319-29.

Kirchhoff F, Hofer HW, Schachner M: Myelin-associated glycoprotein is phosphorylated by protein kinase C. *J Neurosci Res* 1993; 36:368-81.

Kirschner DA, Ganser AL: Compact myelin exists in the absence of basic protein in the shiverer mutant mouse. *Nature* 1980; 283:207-10.

Krajewski K, Turansky C, Lewis R, Garbern J, Hinderer S, Kamholz J, Shy ME: Correlation between weakness and axonal loss in patients with CMT1A. *Ann N Y Acad Sci* 1999; 883:490-2.

Krajewski KM, Lewis RA, Fuerst DR, Turansky C, Hinderer SR, Garbern J, Kamholz J, Shy ME: Neurological dysfunction and axonal degeneration in Charcot-Marie-Tooth disease type 1A. *Brain* 2000; 123:1516-27.

Kruse J, Mailhammer R, Wernecke H, Faissner A, Sommer I, Goridis C, Schachner M: Neural cell adhesion molecules and myelin-associated glycoprotein share a common carbohydrate moiety recognized by monoclonal antibodies L2 and HNK-1. *Nature* 1984; 311:153-5.

Kunemund V, Jungalwala F, Fischer G, Chou DKH, Keilhauer G, Schachner M: The L2/HNK-1 carbohydrate of neural cell adhesion molecules is involved in cell interactions. *J Cell Biol* 1988; 106:213-23.

Kursula P, Tikkanen G, Lehto V-P, Nishikimi M, Heape AM: Calcium-dependent interaction between the large myelin-associated glycoprotein and S100beta. *J Neurochem* 1999; 73:1724-32.

Kursula P, Lehto VP, Heape AM: S100beta inhibits the phosphorylation of the L-MAG cytoplasmic domain by PKA. *Brain Res Mol Brain Res* 2000; 76:407-10.

Kursula P, Lehto V-P, Heape AM: The small myelin-associated glycoprotein binds to tubulin and microtubules. *Brain Res Mol Brain Res* 2001; 87:22-30.

Lach B, Rippstein P, Atack D, Afar DE, Gregor A: Immunoelectron microscopic localization of monoclonal IgM antibodies in gammopathy associated with peripheral demyelinative neuropathy. *Acta Neuropathol (Berl)* 1993; 85:298-307.

Lai C, Brow MA, Nave KA, Noronha AB, Quarles RH, Bloom FE, Milner RJ, Sutcliffe JG: Two forms of 1B236/myelin-associated glycoprotein, a cell adhesion molecule for postnatal neural development, are produced by alternative splicing. *Proc Natl Acad Sci USA* 1987*a*; 84:4337-41.

Lai C, Watson JB, Bloom FE, Sutcliffe JG, Milner RJ: Neural protein 1B236/myelin-associated glycoprotein (MAG) defines a subgroup of the immunoglobulin superfamily. *Immunol Rev* 1987*b*; 100:129-51.

Lampert PW, Garrett R, Powell H: Demyelination in allergic and Marek's disease virus induced neuritis. Comparative electron microscopic studies. *Acta Neuropathol (Berl)* 1977; 40:103-10.

Lascelles RG, Thomas PK: Changes due to age in internodal length in the sural nerve in man. *J Neurol Neurosurg Psychiatry* 1966; 29:40-44.

Lassmann H, Bartsch U, Montag D, Schachner M: Dying-back oligodendrogliopathy: a late sequel of myelin-associated glycoprotein deficiency. *Glia* 1997; 19:104-10.

Latov N, Hays AP, Sherman WH: Peripheral neuropathy and anti-MAG antibodies. *Crit Rev Neurobiol* 1988; 3:301-32.

Latov N: Pathogenesis and therapy of neuropathies associated with monoclonal gammopathies. *Ann Neurol* 1995; 37:S32-S42

Le Douarin NM, Dupin E: Cell lineage analysis in neural crest ontogeny. *J Neurobiol* 1993; 24:146-61.

LeBlanc AC, Poduslo JF, Mezei C: Gene expression in the presence or absence of myelin assembly. *Brain Res* 1987; 388:56-67.

LeBlanc AC, Poduslo JF: Axonal modulation of myelin gene expression in the peripheral nerve. *J Neurosci Res* 1990; 26:317-326.

Lee KW, Inghirami G, Sadiq SA, Thomas FP, Spatz L, Knowles DM, Latov N: B-cells that secrete anti-MAG or anti-GM1 antibodies are present at bith and anti-MAG antibody secreting B-cells are CD5+. *Neurology* 1990; 40:367

Lee MJ, Brennan A, Blanchard A, Zoidl G, Dong Z, Tabernero A, Zoidl C, Dent MAR, Jessen KR, Mirsky R: P0 is constitutively expressed in the rat neural crest and embryonic nerves and is negatively and positively regulated by axons to generate non-myelin-forming and myelin-forming Schwann cells, respectively. *Mol Cell Neurosci* 1997; 8:336-50.

Lee MK, Cleveland DW: Neuronal intermediate filaments. *Annu Rev Neurosci* 1996; 19:187-217.

Léger JM, Younes-Chennoufi AB, Zuber M, Bouche P, Jauberteau MO, Dormont D, Danon F, Baumann N, Brunet P: Frequency of central lesions in polyneuropathy associated with IgM monoclonal gammopathy: an MRI, neurophysiological and immunochemical study. *J Neurol Neurosurg Psychiatry* 1992; 55:112-5.

Lemke G, Axel R: Isolation and sequence of a cDNA encoding the major structural protein of peripheral myelin. *Cell* 1985; 40:501-8.

Lemke G: Molecular biology of the major myelin genes. *Trends Neurosci* 1986; 9:266-70.

Lemke G: The molecular genetics of myelination: An update. *Glia* 1993; 7:263-271.

Lenoir D, Battenberg M, Kiel M, Bloom E, Milner RJ: The brain-specific gene 1B236 is expressed postnatally in the developing rat brain. *J Neurosci* 1986; 6:522-30.

Li C, Tropak MB, Gerlai R, Clapoff S, Abramow-Newerly W, Trapp B, Peterson A, Roder J: Myelination in the absence of myelin-associated glycoprotein. *Nature* 1994; 369:747-50.

Li C, Trapp B, Ludwin S, Peterson A, Roder J: Myelin associated glycoprotein modulates glia-axon contact in vivo. *J Neurosci Res* 1998; 51:210-7.

LoPachin RL, Castiglia CM, Lehning E, Sauberman AJ: Effects of acrylamide on subcellular distribution of elements in rat sciatic nerve myelinated axons and Schwann cells. *Brain Res* 1993; 608:238-246.

Low PA: Hereditary hypertrophic neuropathy in the trembler mouse. Part 1. Histopathological studies: light microscopy. *J Neurol Sci* 1976*a*; 30:327-41.

Low PA: Hereditary hypertrophic neuropathy in the Trembler mouse. Part 2. Histopathological studies: Electron microscopy. *J Neurol Sci* 1976*b*; 30:343-68.

Lubinska L: The physical state of axoplasm in teased vertebrate nerve fibres. *Acta Biol Exp (Wars)* 1956; 17:135-142.

Lubinska L: Short internodes "intercalated" in nerve fibres. *Acta Biol Exp (Wars)* 1958; 18:117-36.

Lubinska L: Demyelination and remyelination in the proximal parts of regenerated nerve fibers. *J Comp Neurol* 1961; 117:275-89.

Madrid R, Bradley WG: The pathology of Neuropathies with focal thickening of the myelin sheath (Tomaculous Neuropathy). Studies of the formation of the abnormal myelin sheath. *J Neurol Sci* 1975; 25:415-48.

Marchionni MA, Goodearl ADJ, Chen MS, Bermincham-McDonogh O, Kirk C, Hendricks M, Danehy F, Misumi D, Sudhalter J, Kobayashi K: Glial growth factors are alternatively spliced erbB2 ligands expressed in the nervous system. *Nature* 1993; 362:312-8.

Martini R, Schachner M: Immunoelectron microscopic localization of neural cell adhesion molecules (L1, N-CAM, and MAG) and their shared carbohydrate epitope and myelin basic protein in developing sciatic nerves. *J Cell Biol* 1986; 103:2439-48.

Martini R: Myelin-associated glycoprotein is not detectable in perikaryal myelin of spiral ganglion neurons of adult mice. *Glia* 1994*a*; 10:311-4.

Martini R: Expression and functional roles of neural cell surface molecules and extracellular matrix components during development and regeneration of peripheral nerves. *J Neurocytol* 1994*b*; 23:1-28.

Martini R, Zielasek J, Toyka KV, Giese KP, Schachner M: Protein zero (P0)-deficient mice show myelin degeneration in peripheral nerves characteristic of inherited human neuropathies. *Nat Genet* 1995*a*; 11:281-6.

Martini R, Mohajeri MH, Kasper S, Giese KP, Schachner M: Mice doubly deficient in the genes for P0 and myelin basic protein show that both proteins contribute to the formation of the major dense line in peripheral nerve myelin. *J Neurosci* 1995*b*; 15:4488-95.

Martini R, Schachner M: Molecular bases of myelin formation as revealed by investigations on mice deficient in glial cell surface molecules. *Glia* 1997; 19:298-310.

Martini R, Carenini S: Formation and maintenance of the myelin sheath in the peripheral nerve: roles of cell adhesion molecules and the gap junction protein connexin 32. *Microsc Res Tech* 1998; 41:403-15.

Martini R: P0-deficient knockout mice as tools to understand pathomechanisms in Charcot-Marie-Tooth 1B and P0-related Dejerine-Sottas Syndrome. *Ann NY Acad Sci* 1999; 883:273-280.

Martini R: The effect of myelinating Schwann cells on axons. *Muscle Nerve* 2001; 24:456-66.

Mata M, Kupina N, Fink DJ: Phosphorylation-dependent neurofilament epitopes are reduced at the node of Ranvier. *J Neurocytol* 1992; 21:199-210.

May AP, Robinsin RC, Vinson M, Crocker PR, Jones EY: Crystal structure of the N-terminal domain of sialoadhesin in complex with 3'sialyllactose at 1.85 A resolution. *Mol Cell* 1998; 1:719-728.

McGarry RC, Helfand SL, Quarles RH, Roder J: Recognition of myelin-associated glycoprotein by the monoclonal antibody HNK-1. *Nature* 1983; 306:376-8.

McGinnis S, Kohriyama T, Yu RK, Pesce MA, Latov N: Antibodies to sulfated glucuronic acid containing glycosphingolipids in neuropathy associated with anti-MAG antibodies and in normal subjects. *J Neuroimmunol* 1988; 17:119-26.

Meier C, Vandevelde M, Steck A, Zurbriggen A: Demyelinating polyneuropathy associated with monoclonal IgM-paraproteimaemia. Histological, ultrastructural and immunocytochemical studies. *J Neurol Sci* 1984; 83:353-67.

Meier C, Parmantier E, Brennan A, Mirsky R, Jessen KR: Developing Schwann cells acquire the ability to survive without axons by establishing an autocrine circuit involving insulin-like growth factor, neurotrophin-3,and platelet-derived growth factor-BB. *J Neurosci* 1999; 19:3847-59.

Melmed C, Frail D, Duncan I, Braun P, Danoff D, Finlayson M, Stewart J: Peripheral neuropathy with IgM kappa monoclonal immunoglobulin directed against myelin-associated glycoprotein. *Neurology* 1983; 33:1397-1405.

Mendell JR, Sahenk Z, Whitaker JN, Trapp BD, Yates AJ, Griggs RC, Quarles RH: Polyneuropathy and IgM monoclonal gammopathy: studies on the pathogenetic role of anti-myelin-associated glycoprotein antibody. *Ann Neurol* 1985; 17:243-54.

Meucci N, Baldini L, Cappellari A, Di Troia A, Allaria S, Scarlato G, Nobile-Orazio E: Anti-myelin-associated glycoprotein antibodies predict the development of neuropathy in asymptomatic patients with IgM monoclonal gammopathy. *Ann Neurol* 1999; 46:119-22.

Meyer D, Birchmeier C: Distinct isoforms of neuregulin are expressed in mesenchymal and neuronal cells during mouse development. *Proc Natl Acad Sci USA* 1994; 91:1064-8.

Meyer D, Birchmeier C: Multiple essential functions of neuregulin in development. *Nature* 1995; 378:386-90.

Meyer D, Yamaii T, Garrett R, Riethmacher-Sonnenberg E, Kane D, Theill LE, Birchmeier C: Isoform-specific expression and function of neuregulin. *Development* 1997; 124:3575-86.

Mezei C: Myelination in the peripheral nerve during development, in Dyck PJ, Thomas PK, Griffin J, Low P, Poduslo J (eds): *Peripheral neuropathy*. Philadelphia, WB Saunders, 1993, vol3rd, pp 267-281.

Milner RJ, Lai C, Nave KA, Montag D, Farber L, Sutcliffe JG: Organization of myelin protein genes: myelin-associated glycoprotein. *Ann NY Acad Sci* 1990; 605:254-261.

Mirsky R, Jessen KR: Schwann cell development and the regulation of myelination. *Sem Neurosci* 1990; 2:423-436.

Mirsky R, Jessen KR: Schwann cell development, differentiation and myelination. *Curr Opin Neurobiol* 1996; 6:89-96.

Mirsky R, Jessen KR: The neurobiology of Schwann cells. *Brain Pathol* 1999; 9:293-311.

Monaco S, Bonetti B, Ferrari S, Moretto G, Nardelli E, Tedesco F, Mollnes TE, Nobile-Orazio E, Manfredini E, Bonazzi L: Complement-mediated demyelination in patients with IgM monoclonal gammopathy and polyneuropathy. *N Engl J Med* 1990; 322:649-52.

Monaco S, Ferrari S, Bonetti B, Moretto G, Kirshfink M, Nardelli E, Nobile-Orazio E, Zanusso G, Rizzuto N, Tedesco F: Experimental induction of myelin changes by anti-MAG antibodies and terminal complement complex. *J Neuropathol Exp Neurol* 1995; 54:96-104.

Montag D, Giese KP, Bartsch U, Martini R, Lang Y, Bluthmann H, Karthigasan J, Kirschner DA, Wintergerst ES, Nave K-A, Zielasek J, Toyka KV, Lipp H-P, Schachner M: Mice deficient for the myelin-associated glycoprotein show subtle abnormalities in myelin. *Neuron* 1994; 13:229-46.

Moos M, Tacke R, Scherer H, Teplow D, Fruh K, Schachner M: Neural adhesion molecule L1 as a member of the immunoglobulin superfamily with binding domains similar to fibronectin. *Nature* 1988; 334:701-3.

Morris RGM, Garrud P, Rawlins JNP, O'Keefe J: Place navigation impaired in rats with hippocampal lesions. *Nature* 1982; 297:681-3.

Morris RGM: Developments of a water-maze procedure for studying spatial learning in the rat. *J Neurosci Method* 1984; 11:47-60.

Mugnaini EK, Olsen KK, Schnapp B, Friedrich VL: Distribution of Schwann cell cytoplasm and plasmalemmal vesicles (caveolae) in peripheral myelin sheaths. An electron microscopic study with thin sections and freeze-fracturing. *J Neurocytol* 1977; 6:647-68.

Munday J, Kerr S, Ni J, Cornish AL, Zhang JQ, Nicoll G, Floyd H, Mattei M-G, Moore P, Liu D, Crocker PR: Identification, characterization and leucocyte expression of Siglec-10, a novel human sialic acid-binding receptor. *Biochem J* 2001; 355:489-97.

Murray N, Page N, Steck AJ: The human anti-myelin-associated glycoprotein IgM system. *Ann Neurol* 1986; 19:473-8.

Naef R, Suter U: Many facets of the peripheral myelin protein PMP22 in myelination and disease. *Microsc Res Tech* 1998; 41:359-71.

Nagafuchi A, Tsukita S, Takeichi M: Transmembrane control of cadherin-mediated cell-cell adhesion. *Semin Cell Biol* 1993; 4:175-81.

Nakagawa T, Chen J, Zhang Z, Kanai Y, Hirokawa N: Two distinct functions of carboxyl-terminal tail domain of NF-M upon neurofilament assembly: cross-bridge formation and longitudinal elongation of filaments. *J Cell Biol* 1995; 129:411-29.

Nardelli E, Pizzighella S, Tridente G, Rizzuto N.: Peripheral neuropathy associated with immunoglobulin disorders an immunological and ultrastructural study. *Acta Neuropathol (Berl)* 1981; 7:258-61.

Nave KA, Lai C, Bloom FE, Milner RJ: Splice selection in the proteolipid protein (PLP) gene transcript and primary structure of the DM-20 protein of central nervous system myelin. *Proc Natl Acad Sci* 1987; 84:5665-5669.

Nelis E, Haites N, Van Broeckhoven C: Mutations in the peripheral myelin genes and associated genes in inherited peripheral neuropathies. *Hum Mutat* 1999; 13:11-28.

Nicoll G, Ni J, Liu D, Klenerman P, Munday J, Dubock S, Mattei MG, Crocker PR: Identification and characterization of a novel siglec, siglec-7, expressed by human natural killer cells and monocytes. *J Biol Chem* 1999; 274:34089-95.

Nixon RA, Sihag RK: Neurofilament phosphorylation: a new look at regulation and function. *Trends Neurosci* 1991; 14:501-6.

Nobile-Orazio E, Marmiroli P, Baldini L, Spagnol G, Barbieri S, Moggio M, Polli N, Polli E, Scarlato G: Peripheral neuropathy in macroglubulinemia: incidence and antigen-specificity of M proteins. *Neurology* 1987; 37:1506-14.

Nobile-Orazio E, Francomano E, Daverio R, Barbieri S, Marmiroli P, Manfredini E, Carpo M, Moggio M, Legname G, Baldini L: Anti-myelin-associated glycoprotein IgM antibody titers in neuropathy associated with macroglobulinemia. *Ann Neurol* 1989; 26:543-50.

Nobile-Orazio E, Carpo M, Legname G, Meucci N, Sonnino S, Scarlato G: Anti-GM1 IgM antibodies in motor neuron disease and neuropathy. *Neurology* 1990; 40:1747-50.

Nobile-Orazio E, Barbieri S, Baldini L, Marmiroli P, Carpo M, Premoselli S, Manfredini E, Scarlato G: Peripheral neuropathy in monoclonal gammopathy of undetermined significance: prevalence and immunopathogenetic studies. *Acta Neurol Scand* 1992; 85:383-90.

Nobile-Orazio E, Manfredini E, Carpo M, Meucci N, Monaco S, Ferrari S, Bonetti B, cavaletti G, Gemignani F, Durelli, L.: Frequency and clinical correlates of anti-neural IgM antibodies in neuropathy associated with IgM monoclinal gammopathy. *Ann Neurol* 1994; 36:416-424.

Nobile-Orazio E, Meucci N, Baldini L, Di Troia.A., Scarlato G: Long-term prognosis of neuropathy associated with anti-MAG IgM M-proteins and its relationship to immune therapies. *Brain* 2000; 123:710-7.

O'Neill JH, Jacobs JM, Gilliatt RW, Baba M: Changes in the compact myelin of single internodes during axonal atrophy. *Acta Neuropathol (Berl)* 1984; 63:313-8.

O'Neill JH, Gilliatt RW: Adaption of the myelin sheath during axonal atrophy. *Acta Neuropathol (Berl)* 1987; 74:62-5.

Ochoa J, Danta G, Fowler TJ, Gilliatt RW: Nature of the nerve lesion caused by pneumatic tourniquet. *Nature* 1971; 233:265-266.

Ochoa J: Ultrathin longitudinal sections of single myelinated fibres for electron microscopy. *J Neurol Sci* 1972; 17:103-106.

Ogino M, Tatum.A.H., Latov N: Affinity studies of human anti-MAG antibodies in neuropathy. *J Neuroimmunol* 1994; 52:41-6.

Ohnishi A, Murai Y, Ikeda M, Fujita T, Furuya H, Kuroiwa Y: Autosomal recessive motor and sensory neuropathy with excessive myelin outfolding. *Muscle Nerve* 1989; 12:568-75.

Orr-Urtreger A, Trakhtenbrot L, Ben-Levy R, Wen D, Rechavi G, Lonai P, Yarden Y: Neural expression and chromosomal mapping of Neu differentiation factor to 8p12-p21. *Proc Natl Acad Sci USA* 1993; 90:1867-71.

Owens GC, Bunge RP: Evidence for an early role for myelin-associated glycoprotein in the process of myelination. *Glia* 1989; 2:119-28.

Owens GC, Boyd CJ, Bunge RP, Salzer JL: Expression of recombinant myelin-associated glycoprotein in primary Schwann cells promotes the initial investment of axons by myelinating Schwann cells. *J Cell Biol* 1990; 111:1171-82.

Owens GC, Bunge RP: Schwann cells infected with a recombinant retrovirus expressing myelin-associated glycoprotein anti-sense RNA do not form myelin. *Nueron* 1991; 7:565-575.

Pannese E, Ledda M, Matsuda S: Nerve fibers with myelinated and unmyelinated portion in dorsal spinal root. *J Neurocytol* 1988; 17:693-700.

Parmantier E, Cabon F, Braun C, D'Urso D, Muller HW, Zalc B: Peripheral myelin protein-22 is expressed in rat and mouse brain and spinal cord motoneurons. *Eur J Neurosci* 1995; 7:1080-8.

Patel N, Brinkman-Van der Linden E, Altmann SW, Gish K, Balasubramanian S, Timans JC, Peterson D, Bell MP, Bazan JF, Varki A, Kastelein RA: OB-BP1/siglec-6: a leptin- and sialic acid-binding protein of the immunoglobulin superfamily. *J Biol Chem* 1999; 274:22729-38.

Peles E, Salzer JL: Molecular domains of myelinated axons. *Curr Opin Neurobiol* 2000; 10:558-565.

Pellissier JF, Pouget J, de Victor B, Serratrice G, Toga M: Tomaculous neuropathy. A histopathological study and electroclinical correlates in 10 cases. *Rev Neurol (Paris)* 1987; 143:263-78.

Pesheva P, Horwitz AF, Schachner M: Integrin, the cell surface receptor for fibronectin and laminin, expresses the L2/HNK-1 and L3 carbohydrate structures shared by adhesion molecules. *Neurosci Lett* 1987; 83:303-6.

Pfister KK: Cytoplasmic dynein and microtubule transport in the axon: the action connection. *Mol Neurobiol* 1999; 20:81-91.

Poduslo J, Windebank AJ: Differentiation-specific regulation of Schwann cell expression of the major myelin glycoprotein. *Proc Natl Acad Sci USA* 1985; 82:5987-91.

Poduslo JF: Regulation of myelination: biosynthesis of the major myelin glycoprotein by Schwann cells in the presence and absence of myelin assembly. *J Neurochem* 1984; 42:493-503.

Poliak S, Gollan L, Martinez R, Custer A, Einheber S, Salzer JL, Trimmer JS, Shrager P, Peles E: Caspr2, a new member of the neurexin superfamily, is localized at the juxtaparanodes of myelinated axons and associates with K+ channels. *Neuron* 1999; 24:1037-47.

Pollard JD, McLeod JG, Feeney D: Peripheral neuropathy in IgM kappa paraproteinaemia: clincal and ultrastructural studies in two patients. *Clin Exp Neurol* 1985; 21:41-54.

Poltorak M, Sadoul R, Eilhauer G, Landa C, Fahrig T, Schachner M: Myelin-associated glycoprotein, a member of the L2/HNK-1 family of neural cell adhesion molecules, is involved in neuron-oligodendrocyte and oligodendrocyte-oligodendrocyte interaction. *J Cell Biol* 1987; 105:1893-9.

Previtali SC, Quattrini A, Fasolini M, Panzeri MC, Villa A, Filbin MT, Li W, Chiu SY, Messing A, Wrabetz L, Feltri ML: Epitope-tagged P(0) glycoprotein causes Charcot-Marie-Tooth-like neuropathy in transgenic mice. *J Cell Biol* 2000; 151:1035-46.

Probstmeier R, Fahrig T, Spiess E, Schachner M: Interactions of the neural cell adhesion molecule and the myelin-associated glycoprotein with collagen type I: involvement in fibrilogenesis. *J Cell Biol* 1992; 116:1063-70.

Propp RP, Means E, Deibel R, Sherer G, Barron K: Waldenstrom's macroglobulinemia and neuropathy. Deposition of M-component on myelin sheaths. *Neurology* 1975; 25:980-8.

Puckett C, Hudson L, Ono K, Friedrich V, Benecke J, Dubios-Dalcq M, Lazzarini RA: Myelin-specific proteolipid protein is expressed in myelinating Schwann cells but is not incorporated into myelin sheaths. *J Neurosci Res* 1987; 18:511-8.

Quarles RH, Everly JL, Brady RO: Evidence for the close association of a glycoprotein with myelin in rat brain. *J Neurochem* 1973*a*; 21:1177-91.

Quarles RH, Everly JL, Brady RO: Myelin-associated glycoprotein: a developmental change. *Brain Res* 1973*b*; 58:506-9.

Quarles RH, Barbarash GR, Figlewicz DA, Mcintyre LJ: Purification and partial characterization of the myelin-associated glycoprotein from adult rat brain. *Biochim Biophys Acta* 1983; 757:140-3.

Quarles RH: The spectrum and pathogenesis of antibody mediated neuropathies. *The Neuroscitist* 1997; 3:195-204.

Quarles RH, Weiss MD: Autoantibodies associated with peripheral neuropathy. *Muscle Nerve* 1999; 22:800-22.

Quattrini A, Nemni R, Fazio R, Iannaccone S, Lorenzetti I, Grassi F, Canal N: Axonal neuropathy in a patient with monoclonal IgM kappa reactive with Schmidt-Lantermann incisures. *J Neuroimmunol* 1991; 33:73-79.

Raine CS, Bornstein MB: Experimental allergic neuritis. Ultrastructure of serum-induced myelin aberrations in peripheral nervous system cultures. *Lab Invest* 1979; 40:423-32.

Ranscht B: Sequence of contactin, a 130-kD glycoprotein concentrated in areas of interneural contact, defines a new member of the immunoglobulin superfamily in the nervous system. *J Cell Biol* 1988; 107:1561-73.

Rebai T, Mhiri C, Heine P, Charfi H, Meyrignac C, Gherardi R: Focal myelin thickenings in a peropheral neuropathy associated with IgM monoclonal gammopathy. *Acta Neuropathol (Berl)* 1989; 79:226-32.

Riethmacher D, Sonnenberg-Riethmacher E, Brinkmann V, Yamaai T, Lewin GR, Birchmeier C: Severe neuropathies in mice with targeted mutations in the ErbB3 receptor. *Nature* 1997; 389:725-30.

Ritz MF, Erne B, Ferracin F, Vital A, Vital C, Steck AJ: Anti-MAG IgM penetration into myelinated fibers correlates with the extent of myelin widening. *Muscle Nerve* 1999; 22:1030-1037.

Robertson AM, King RHM, Muddle JR, Thomas PK: Abnormal Schwann cell/axon interactions in the Trembler-J mouse. *J Anat* 1997; 190:423-32.

Ropper AH, Gorson KC: Neuropathies associated with paraproteinemia. *N Engl J Med* 1998; 338:1061-7.

Rosenbluth J: Central myelin in the mouse mutant shiverer. *J Comp Neurol* 1980*a*; 194:639-48.

Rosenbluth J: Peripheral myelin in the mouse mutant shiverer. *J Comp Neurol* 1980*b*; 193:729-39.

Rosenbluth J, Liang WL, Liu Z, Guo D, Schiff R: Expanded CNS myelin sheaths formed in situ in the presence of an IgM antigalactocerebroside-producing hybridoma. *J Neurosci* 1996; 16:2635-41.

Rosenbluth J, Liang WL, Schiff R, Dou WK: Spinal cord dysmyelination induced in vivo by IgM antibodies to three different myelin glycolipids. *Glia* 1997; 19:58-66.

Rosenbluth J: A brief history of myelinated nerve fibers: one hundred and fifty years of controversy. *J Neurocytol* 1999; 28:251-62.

Ruoslahti E, Pierschbacher MD: New perspectives in cell adhesion and integrins. *Science* 1987; 238:491-7.

Rydmark M: Nodal axon diameter correlates linearly with internodal axon diameter in spinal roots of the cat. *Neurosci Lett* 1981; 24:247-50.

Rydmark M, Berthold C-H: Electron microscopic serial section analysis of nodes of Ranvier in lumbar spinal roots of the cat. A morphometric study of nodal compartments in fibres of different sizes. *J Neurocytol* 1983; 12:537-565.

Sadoul R, Fahrig T, Schachner M: Binding properties of liposomes containing the myelin-associated glycoprotein MAG to neural cell cultures. *J Neurosci Res* 1990; 25:1-13.

Sahenk Z, Chen L: Abnormalities in the axonal cytoskeleton induced by a connexin32 mutation in nerve xenografts. *J Neurosci Res* 1998; 51:174-84.

Sahenk Z, Mendell JR: Alterations in nodes of Ranvier and Schmidt-Lanterman incisures in Charcot-Marie-Tooth neuropathies. *Ann N Y Acad Sci* 1999; 883:508-512.

Sahenk Z, Chen L, Mendell JR: Effects of PMP22 duplication and deletions on the axonal cytoskeleton. *Ann Neurol* 1999; 45:16-24.

Said G, Bathien N, Gesaro P: Peripheral neuropathies and tremor. *Neurology* 1982; 32:480-5.

Saida K, Sumner AJ, Saida T, Brown MJ, Silberberg DH: Antiserum-mediated demyelination: relationship between remyelination and functional recovery. *Ann Neurol* 1980; 8:12-24.

Saida T, Saida K, Brown MJ, Silberberg DH: Peripheral nerve demyelination induced by intraneurial injection of experimental allergic encephalomyelitis serum. *J Neuropathol Exp Neurol* 1979; 38:-498

Salzer JL, Holmes WP, Colman DR: The amino acid sequence of the myelin-associated glycoproteins: Homology to the immunoglobulin gene superfamily. *J Cell Biol* 1987; 104:957-65.

Salzer JL, Pedraza L, Brown M, Struyk A, Afar D, Bell J: Structure and function of the myelin-associated glycoproteins. *Ann NY Acad Sci* 1990; 605:302-12.

Salzer JL: Clustering sodium channels at the node of Ranvier: Close encounters of the axon-glia kind. *Neuron* 1997; 18:843-6.

Sancho S, Magyar JP, Aguzzi A, Suter U: Distal axonopathy in peripheral nerves of PMP22-mutant mice. *Brain* 1999; 122:1563-77.

Sander S, Ouvrier RA, McLeod JG, Nicholson GA, Pollard JD: Clinical syndromes associated with tomacula or myelin swellings in sural nerve biopsies. *J Neurol Neurosurg Psychiatry* 2000; 68:483-8.

Sandri C, Van Buren JM, Akert K: Membrane morphology of the vertebrate nervous system. A study with freeze-etch technique. *Prog Brain Res* 1977; 46:1-384.

Sato S, Fujita N, Kurihara T, Kuwano R, Sakimura K, Takahashi Y, Miyatake T: cDNA cloning and amino acid sequence for human myelin-associated glycoprotein. *Biochem Biophys Res Commun* 1989; 163:1473-80.

Schachner M, Martini R: Glycans and the modulation of neural recognition molecule function. *Trends Neurosci* 1995; 18:183-191.

Schachner M, Bartsch U: Multiple functions of the myelin-associated glycoprotein MAG (siglec-4a) in formation and maintenance of myelin. *Glia* 2000; 29:154-165.

Schady W, Ochoa J: Ehlers-Danlos in association with tomaculous neuropathy. *Neurology* 1984; 34:1270-1.

Schauer R: Chemistry, metabolism, and biological functions of sialic acids. *Adv Carbohydr Chem Biochem* 1982; 40:131-234.

Schenone A, Abbruzzese M, Uccelli A, Mandich R, James R, Bellone E, Giunchedi M, Rolando S, Capello E, Mancardi GL: Hereditary motor and sensory neuropathy with myelin outfolding: clinical, genetic and neuropathological study of three cases. *J Neurol Sci* 1994; 122:20-7.

Scherer S: Axonal pathology in demyelinating disease. *Ann Neurol* 1999; 45:6-7.

Scherer SS, Wang DY, Kuhn R, Lemke G, Wrabetz L, Kamholz J: Axons regulate Schwann cell expression of POU transcription factor SCIP. *J Neurosci* 1994; 14:1930-42.

Scherer SS: Molecular specializations at nodes and paranodes in peripheral nerve. *Microsc Res Tech* 1996; 34:452-61.

Scherer SS: The biology and pathobiology of Schwann cells. *Curr Opin Neurol* 1997*a*; 10:386-97.

Scherer SS: Molecular genetics of demyelination: new wrinkles on an old membrane. *Neuron* 1997*b*; 18:13-6.

Scherer SS, Xu YT, Nelles E, Fischbeck KH, Willecke K, Bone LJ: Connexin32-null mice develop demyelinating peripheral neuropathy. *Glia* 1998; 24:8-20.

Scherer SS: Nodes, paranodes, and incisures: from form to function. *Ann N Y Acad Sci* 1999; 883:131-142.

Schneider-Schaulies J, von Brunn A, Schachner M: Recombinant peripheral myelin protein P0 confers both adhesion and neurite outgrowth-promoting properties. *J Neurosci Res* 1990; 27:286-297.

Schröder JM, Bohl J, Brodda K: Changes of the ratio between myelin thickness and axon diameter in the human developing sural nerve. *Acta Neuropathol (Berl)* 1978; 43:169-78.

Schröder JM, Himmelmann F: Fine structural evaluation of altered Schmidt-Lanterman incisures in human sural nerve biopsies. *Acta Neuropathol (Berl)* 1992; 83:120-133.

Schuller-Petrovic S, Gebhart N, Lassmann H, Rumpold H, Kraft D: A shared antigenic determinant between natural killer cells and nervous tissue. *Nature* 1983; 306:179-81.

Seil FJ, Quarles RH, Johnson D, Brady RO: Immunization with purified myelin-associated glycoprotein does not evoke myelination-inhibition or demyelinating antibodies. *Brain Res* 1981; 209:470-475.

Seilheimer B, Persohn E, Schachner M: Antibodies to the L1 adhesion molecule inhibit Schwann cell ensheathment of neurons in vitro. *J Cell Biol* 1989; 109:3095-103.

Sergott RC, Brown MJ, Lisak RP, Miller SL: Antibody to myelin-associated glycoprotein produces central nervous system demyelination. *Neurology* 1988; 38:422-6.

Shapiro L, Fannon AM, Kwong PD, Thompson A, Lehmann MS, Grubel G, Legrand JF, Als-Nielsen J, Colman DR, Hendrickson WA: Structural basis of cell-cell adhesion by cadherins. *Nature* 1995; 374:327-37.

Shapiro L, Doyle JP, Hensley P, Colman DR, Hendrickson WA: Crystal structure of the extracellular domain from P0, the major structural protein of peripheral nerve myelin. *Neuron* 1996; 17:435-49.

Sheetz MP, Martenson CH: Axonal transport: Beyond kinesin and cytoplasmic dynein. *Curr Opin Neurobiol* 1991; 1:393-8.

Sheikh KA, Deerinck TJ, Ellisman MH, Griffin JW: The distribution of ganglioside-like moieties in peripheral nerves. *Brain* 1999*a*; 122:449-60.

Sheikh KA, Sun J, Liu Y, Kawai H, Crawford TO, Proia RL, Griffin JW, Schnaar RL: Mice lacking complex gangliosides develop Wallerian degeneration and myelination defects. *Proc Natl Acad Sci USA* 1999*b*; 96:7532-7537.

Shy ME, Arroyo E, Sladky J, Menichella D, Jiang H, Xu W, Kamholz J, Scherer SS: Heterozygous P0 knockout mice develop a peripheral neuropathy that resembles chronic inflammatory demyelinating polyneuropathy (CIDP). *J Neuropathol Exp Neurol* 1997; 56:811-21.

Sima AAF, Blaivas M: Peripheral neuropathies, in Garcia JH, Budka H, McKeever PE, Sarnat HB, Sima AAF (eds): *Neuropathology: The Diagnostic Approach*. Mosby, 1997, pp 765-809.

Smith-Slatas C, Barbarese E: Myelin basic protein gene dosage effects in the PNS. *Mol Cell Neurosci* 2000; 15:343-354.

Smith IS, Kahn SN, Lacey BW, King RH, Eames RA, Whybrew DJ, Thomas PK: Chronic demyelinating neuropathy associated with benign IgM paraproteinaemia. *Brain* 1983; 106:169-95.

Smith IS: The natural history of chronic demyelinating neuropathy associated with benign IgM paraproteinaemia. A clinical adn neurophysiological study. *Brain* 1994; 117:949-57.

Smith KJ, Blakemore WF, Murray JA, Patterson RC: Internodal myelin volume and axon surface area: a relationship determining myelin thickness? *Journal of Neurol Sci* 1982; 55:231-46.

Snipes GJ, Suter U, Shooter EM: Human peripheral myelin protein-22 carries the L2/HNK-1 carbohydrate adhesion epitope. *J Neurochem* 1993; 61:1961-4.

Snipes GJ, Suter U: Molecular anatomy and genetics of myelin proteins in the peripheral nervous system. *J Anat* 1995; 186:483-94.

Spagnol G, Williams M, Srinivasan J, Golier J, Bauer D, Lebo RV, Latov N: Molecular cloning of human myelin-associated glycoprotein. *J Neurosci Res* 1989; 24:137-42.

Spencer PS, Thomas PK: The examination of isolated nerve fibres by light and electron microscopy, with observation on demyelination proximal to neuromas. *Acta Neuropathol (Berl)* 1970; 16:177-86.

Spitzer RE, Stitzel AE, Tsokos GC: Autoantibody to the alternative pathway C3/C5 convertase and its anti-idiotypic response: A study in affinity. *J Immunol* 1992; 148:137-41.

Stahl N, Harry J, Popko B: Quantitative analysis of myelin protein gene expression during development in the rat sciatic nerve. *Brain Res Mol Brain Res* 1990; 8:209-12.

Steck AJ, Murray N, Meier C, Page N, Perruisseau G: Demyelinating neuropathy and monoclonal IgM antibody to myelin-associated glycoprotein. *Neurology* 1983; 33:19-23.

Steck AJ, Murray N, Justafre JC, Meier C, Toyka KV, Heininger K, Stoll G: Passive transfer studies in demyelinating neuropathy with IgM monoclonal antibodies to myelin-associated glycoprotein. *J Neurol Neurosurg Psychiatry* 1985; 48:927-9.

Steck AJ, Erne B, Gabriel JM, Schaeren-Wiemers N: Paraproteinaemic neuropathies. *Brain Pathol* 1999; 9:361-8.

Sternberger NH, Quarles RH, Itoyama Y, Webster HD: Myelin-associated glycoprotein demonstrated immunocytochemically in myelin and myelin-forming cells of developing rat. *Proc Natl Acad Sci USA* 1979; 76:1510-4.

Stolinski C, Breathnach AS, Thomas PK: Distribution of particle aggregates in the internodal axolemma and axonal Schwann cell membrane in rodent peripheral nerve. *J Neurol Sci* 1985; 67:

Strenge K, Schauer R, Kelm S: Binding partners for the myelin-associated glycoprotein of N2A neuroblastoma cells. *FEBS Lett* 1999; 444:59-64.

Suter U, Moskow JJ, Welcher AA, Snipes G, Kosaras B, Sidman R, Buchberg A, Shooter E: A Leucine-to-proline mutation in the putative first transmembrane domain of the 22-kDa peripheral myelin protein in the trembler-J mouse. *Proc Natl Acad Sci USA* 1992*a*; 89:4382-6.

Suter U, Welcher AA, Ozcelik Y, Snipes G, Kosaras B, Francke U, Billings-Gagliardi S: Trembler mouse carries a point mutation in a myelin gene. *Nature* 1992*b*; 356:241-4.

Suter U, Snipes GJ, Schoener-Scott R, Welcher AA, Pareek S, Lupski JR, Murphy RA, Shooter EM, Patel PI: Regulation of tissue-specific expression of alternative peripheral myelin protein-22 (PMP22) gene transcripts by two promotors. *J Biol Chem* 1994; 269:25795-808.

Suter U, Snipes GJ: Biology and genetics of hereditary motor and sensory neuropathies. *Annu Rev Neurosci* 1995; 18:45-75.

Syroid DE, Maycox PR, Burrola PG, Liu N, Wen D, Lee K-F, Lemke G, Kilpatrick TJ: Cell death in the Schwann cell lineage and its regulation by neuregulin. *Proc Natl Acad Sci USA* 1996; 93:9229-9234.

Tachi N, Kozuka N, Ohya K, Chiba S, Sasaki K: Tomaculous neuropathy in Charcot-Marie-Tooth disease with myelin protein zero gene mutation. *J Neurol Sci* 1997; 153:106-9.

Tao-Cheng JH, Rosenbluth J: Nodal and paranodal membrane structure in complementary freeze-fracture replicas of amphibian peripheral nerves. *Brain Res* 1980; 199:249-65.

Tatum.A.H.: Experimental paraprotein neuropathy, demyelination by passive transfer of human IgM anti-myelin-associated glycoprotein. *Ann Neurol* 1993; 33:502-6.

Taylor V, Welcher AA, Program A, Suter U: Epithelial membrane protein-1, peripheral myelin protein 22 and lens membrane 20 define a novel gene family. *J Biol Chem* 1995; 270:28824-33.

Taylor V, Suter U: Epithelial membrane protein-2 and epithelial membrane protein-3: two novel members of the peripheral myelin protein 22 gene family. *Gene* 1996; 175:115-20.

Thomas FP, Trojaborg W, Nagy C, Santoro M, Sadiq SA, Latov N, Hays AP: Experimental autoimmune neuropathy with anti-GM1 antibodies and immunoglobulin deposits at the nodes of Ranvier. *Acta Neuropathol (Berl)* 1991; 82:378-83.

Thomas FP, Lebo RV, Rosoklija G: Tomaculous neuropathy in chromosome 1 Charcot-Marie-Tooth syndrome. *Acta Neuropathol (Berl)* 1994; 87:91-6.

Thomas PK, Young JZ: Internode lengths in the nerves of fishes. *J Anat* 1949; 83:336-51.

Thomas PK, Berthold C-H, Ochoa J: Microscopic anatomy of the peripheral nervous system, in Dyck PJ, Thomas PK, Griffin JW, Low PA, Poduslo JF (eds): *Peripheral neuropathy*. Philadelphia, WB Saunders, 1993, vol3rd, pp 28-91.

Thomas PK, Willison HJ: Paraproteinaemic neuropathy. *Baillieres Clin Neurol* 1994; 3:129-47.

Thomas PK, Landon DN, King RHM: Diseases of the peripheral nerves, in Graham DI, Lantos PL (eds): *Greenfield's Neuropathology*. London, Edward Arnold, 1997, vol6th, pp 367-487.

Trachtenberg JT, Thompson WJ: Schwann cell apoptosis at developing neuromuscular junctions is regulated by glial growth factor. *Nature* 1996; 379:174-7.

Trapp BD, Quarles RH: Presence of the myelin-associated glycoprotein correlates with alterations in the periodicity of peripheral myelin. *J Cell Biol* 1982; 92:877-82.

Trapp BD, Quarles RH: Immunocytochemical localization of the myelin-associated glycoprotein. Fact or artifact? *J Neuroimmunol* 1984; 6:231-49.

Trapp BD, Quarles RH, Griffin JW: Myelin-associated glycoprotein and myelinating Schwann cell-axon interaction in chronic B,B'-iminodipropionitrile neuropathy. *J Cell Biol* 1984*a*; 98:1272-8.

Trapp BD, Quarles RH, Suzuki K: Immunocytochemical studies of quaking mice support a role for the myelin-associated glycoprotein in forming and maintaining the periaxonal space and periaxonal cytoplasmic collar of myelinating Schwann cells. *J Cell Biol* 1984*b*; 99:594-606.

Trapp BD, O'Connell MF, Andrews SB: Ultrastructural immunolocalization of MAG and P0 proteins in cryosections of peripheral nerve. *J Cell Biol* 1986; 103:228

Trapp BD: Distribution of the myelin-associated glycoprotein and P0 protein during myelin compaction in quaking mouse peripheral nerve. *J Cell Biol* 1988; 107:675-85.

Trapp BD, Hauer P, Lemke G: Axonal regulation of myelin protein mRNA levels in actively myelinating Schwann cells. *J Neurosci* 1988; 81:3515-21.

Trapp BD: Myelin-associated glycoprotein: location and potential functions. *Ann NY Acad Sci* 1990; 605:29-43.

Trojaborg W, Hays AP, van den Berg L, Younger DS, Latov N: Motor conduction parameters in neuropathies associated with anti-MAG antibodies and other types of demyelinating and axonal neuropathies. *Muscle Nerve* 1995; 18:730-5.

Tropak MB, Johnson PW, Dunn RJ, Roder JC: Differential splicing of MAG transcripts during CNS and PNS development. *Mol Brain Res* 1988; 4:143-55.

Tsukita S, Usukura J, Ishikawa H: The cytoskeleton in myelinated axons: A freeze-etch replica study. *Neuroscience* 1980; 7:2135-47.

Tsukita S, Ishikawa H: The cytoskeleton in myelinated axons: Serial section study. *Biomed Res* 1981; 2:424-37.

Umehara H, Takenaga S, Nakagawa M, Takahashi K, Izumo S, Matsumuro K, Sakota S, Nishimura T, Yoshikawa H, Osame M: Dominantly inherited motor and sensory neuropathy with excessive myelin folding complex. *Acta Neuropathol (Berl)* 1993; 86:602-608.

Uncini A, De Angelis MV, Di Muzio A, Callegarini C, Ciucci G, Antonini G, Lugaresi A, Gambi D: Chronic inflammatory demyelinating polyneuropathy in diabetics: motor conductions are important in the differential diagnosis with diabetic polyneuropathy. *Clin Neurophysiol* 1999; 110:705-11.

Uschkureit T, Sporkel O, Stracke J, Bussow H, Stoffel W: Early onset of axonal degeneration in double (plp-/-mag-/-) and hypomyelinosis in triple (plp-/-mbp-/-mag-/-) mutant mice. *J Neurosci* 2000; 20:5225-33.

Uyemura K, Horie K, Kitamura K, Suzuki M, Uehara S: Developmental changes of myelin proteins in the chick peripheral nerve. *J Neurochem* 1979; 32:779-88.

Valldeoriola F, Graus F, Steck AJ, Munoz E, de la Fuente M, Gallart T, Ribalta T, Bombi AJ, Tolosa E: Delayed appearance of anti-myelin-associated glycoprotein antibodies in a patient with chronic demyelinating polyneuropathy. *Ann Neurol* 1993; 34:394-6.

van den Berg L, Hays AP, Nobile-Orazio E, Kinsella LJ, Manfredini E, Corbo M, Rosoklija G, Younger DS, Lovelace RE, Trojaborg W, Lange DE, Goldstein S, Delfiner JS, Sadiq SA, Sherman WH, Latov N: Anti-MAG and anti-SGPG antibodies in neuropathy. *Muscle Nerve* 1996; 19:637-43.

Van der Heijden RWJ, Bunschoten H, Hoek A, van Es J, Punter M, Osterhaus ADME, Uytdehaag FGCM: A human CD5+ B cell clone that secretes an idiotype-specific high affinity IgM monoclonal antibody. *J Immunol* 1991; 146:1503-8.

Verhagen WI, Gabreels-Festen AA, van Wensen PL, Joosten EM, Vingerhoets HM, Gabreels FJ, de Graaf R: Hereditary neuropathy with liability to pressure palsies: a clinical, electroneurophysiological and morphological study. *J Neurol Sci* 1993; 116:176-84.

Vital A, Vital C, Julien J, Baquey A, Steck AJ: Polyneuropathy associated with IgM monoclonal gammopathy: immunological and pathological study in 31 patients. *Acta Neuropathol (Berl)* 1989; 79:160-7.

Vital A, Latinville D, Aupy M, Dumas P, Vital C: Inflammatory demyelinating lesions in two patients with IgM monoclonal gammopathy and polyneuropathy. *Neuropathol Appl Neurobiol* 1991; 17:415-20.

Vital C, Henry P, Loiseau P, Julien J, Vallat J-M, Tignol J, Bonnaud E, Hendreville-Tablon M-A: Peripheral neuropathies i- Waldenstrom's disease. Histological and ultrastructural studies of 5 cases. *Ann Anat Pathol* 1975; 20:93-107.

Vital C, Vallat J-M: *Ultrastructural study of the human diseased peripheral nerve*, New York, Masson, 1980.

Vital C, Pautrizel B, Lagueny A, Vital A, Bergouignan FX, David B, Loiseau P: Hypermyelination in a case of peripheral neuropathy with benign IgM monoclonal gammopathy. *Rev Neurol (Paris)* 1985; 141:729-34.

Vital C, Vital A, Deminiere C, Julien J, Lagueny A, Steck AJ: Myelin modifications in 8 cases of peripheral neuropathy with Waldenstrom's macroglobulinemia and anti-MAG activity. *Ultrastruct Pathol* 1997; 21:509-16.

Vizoso AD, Young JZ: Internode length and fibre diameter in developing and regenerating nerves. *J Anat* 1948; 82:110-134.

Vuorinen VS, Röyttä M: Taxol-induced neuropathy after nerve crush: long-term effects on Schwann and endoneurial cells. *Acta Neuropathol (Berl)* 1990*a*; 79:653-62.

Vuorinen VS, Roytta M: Taxol-induced neuropathy after nerve crush: long-term effects on regenerating axons. *Acta Neuropathol (Berl)* 1990*b*; 79:663-71.

Watson DF, Nachtman FN, Kuncl RW, Griffin JW: Altered neurofilament phosphorylation and beta tubulin isotypes in Charcot-Marie-Tooth disease type 1. *Neurology* 1994; 44:2383-7.

Webster HD, Palkovits CG, Stoner GL: Myelin-associated glycoprotein: electron microscopic immunocytochemical localization in compact developing and adult central nervous system myelin. *J Neurochem* 1983; 41:1469-79.

Webster HD: Development of peripheral nerve fibers, in Dyck PJ, Thomas PK, Griffin J, Low P, Poduslo J (eds): *Peripheral Neuropathy*. Philadelphia, WB Saunders, 1993, vol3rd, pp 243-266.

Webster HF: Relationship between Schmidt-Lantermann incisures and myelin segmentation during Wallerian degeneration. *Ann NY Acad Sci* 1965; 122:29

Weimbs T, Stoffel W: Proteolipid protein (PLP) of CNS myelin: positions of free disulfide bonded, and fatty acid thioester-linked cysteine residues. Implications for the membrane topology of PLP. *Biochemistry* 1992; 31:12289-96.

Weinberg HJ, Spencer PS: Studies on the control of myelinogenesis. II. Evidence for neuronal regulation of myelin production. *Brain Res* 1976; 113:363-78.

Weiss DG, Seitz-Tutter D, Langford GM, Allen RD: The native microtubule as the engine for bidirectional organelle movements, in Smith RS, Bisby MA (eds): *Axonal Transport*. New York, Alan R. Liss, Inc, 1987, pp 91-111.

Weiss P, Hiscoe HB: Experimental on the mechanism of nerve growth. *J Exp Zool* 1948; 107:315-96.

Welcher AA, Suter U, De Leon M, Snipes GJ, Shooter EM: A myelin protein is encoded by the homologue of a growth arrest-specific gene. *Proc Natl Acad Sci USA* 1991; 88:9.

Westland K, Pollard JD: Proteinase-induced demyelination. *J Neurol Sci* 1987; 82:41-53.

Williams PL, Wendell-Smith CP: Some additional parametric variations between peripheral nerve fibre populations. *J Anat* 1971; 109:505-26.

Willians AF, Barclay AN: The immunoglobulin superfamily--domains for cell surface recognition. *Annu Rev Immunol* 1988; 6:381-405.

Willison HJ, Trapp BD, Bacher JD, Dalakas MC, Griffin JW, Quarles RH: Demyelination induced by intraneural injection of human antimyelin-associated glycoprotein antibodies. *Muscle Nerve* 1988; 11:1169-76.

Windebank AJ, Wood P, Bunge RP, Dyck PJ: Myelination determines the caliber of dorsal root ganglion neurons in culture. *J Neurosci* 1985; 6:1563-7.

Wood JG, Engel EL: Peripheral nerve glycoproteins and myelin fine structure during development of rat sciatic nerve. *J Neurocytol* 1976; 5:605-15.

Wood PM, Schachner M, Bunge RP: Inhibition of Schwann cell myelination in vitro by antibody to the L1 adhesion molecule. *J Neurosci* 1990; 10:3635-45.

Yan Y, Lagenaur C, Narayanan V: Molecular cloning of M6: Identification of a PLP/DM20 gene family. *Neuron* 1993; 11:31

Yang H, Xiao ZC, Becker B, Hillenbrand R, Rougon G, Schachner M: Role for myelin-associated glycoprotein as a functional tenascin-R receptor. *J Neurosci Res* 1999; 55:687-701.

Yang LJ, Zeller CB, Shaper NL, Kiso M, Hasegawa A, Shapiro RE, Schnaar RL: Gangliosides are neuronal ligands for myelin-associated glycoprotein. *Proc Natl Acad Sci USA* 1996; 93:814-8.

Yeung KB, Thomas PK, King RH, Waddy H, Will RG, Hughes RA, Gregson NA, Leibowitz S: The clinical spectrum of peripheral neuropathies associated with benign monoclonal IgM, IgG and IgA paraproteinaemia. Comparative clinical, immunological and nerve biopsy findings. *J Neurol* 1991; 238:383-91.

Yim SH, Toda K, Goda S, Quarles RH: Comparison of the phosphorylation of myelin-associated glycoprotein in cultured oligodendrocytes and Schwann cells. *J Mol Neurosci* 1995; 6:63-74.

Yin X, Crawford TO, Griffin JW, Tu P, Lee VMY, Li C, Roder J, Trapp BD: Myelin-associated glycoprotein is a myelin signal that modulates the center of myelinated axons. *J Neurosci* 1998; 18:1953-1962.

Young JZ: Surface tension and the degeneration of nerve fibers. *Nature* 1944; 154:521-2.

Zhang JQ, Nicoll G, Jones C, Crocker PR: Siglec-9, a novel sialic acid binding member of the immunoglobulin superfamily expressed broadly on human blood leukocytes. *J Biol Chem* 2000; 275:22121-6.

Zhao JX, Ohnishi A, Itakura C, Mizutani M, Yammamoto T, Hayashi H, Murai Y: Smaller number of large myelinated fibres and focal myelin thickening in mutant quails deficient in neurofilaments. *Acta Neuropathol (Berl)* 1993; 86:242-48.

Zielasek J, Martini R, Toyka KV: Functional abnormalities in P0-deficient mice resemble human hereditary neuropathies linked to P0 gene mutations. *Muscle Nerve* 1996; 19:946-52.

Zorick TS, Lemke G: Schwann cell differentiation. *Curr Opin Cell Biol* 1996; 8:870-6.

Zorick TS, Syroid DE, Arroyo E, Scherer SS, Lemke G: The transcription factors SCIP and Krox-20 mark distinct stages and cell fates in Schwann cell differentiation. *Mol Cell Neurosci* 1996; 8:129-45.

Zouali M: Development of human antibody variable genes in systemic autoimmunity. *Immunol Rev* 1992; 128:73-99.

APPENDIX A

Methods for sural nerve biopsies and processing for conventional studies

The sural nerve biopsies and nerve processing were performed according to a standard protocol (Cash and Blumbergs, 1995). The methods are described briefly below.

Under local anaesthesia, an incision of about 8 cm was made in the furrow just behind and above the lateral malleolus. The sural nerve was exposed and approximately 6 centimeters of nerve was excised and placed directly onto a sheet of dental wax. Extreme care was taken in the process of biopsy in order to avoid nerve crushing and stretching.

The nerve is further dissected on the dental wax with a razor blade. One 2mm specimen orientated in the transverse plane is placed in a blob of O.C.T. (Tissue Tek) on a piece of cork with a needle in one corner. This is plunged into isopentane pre-cooled by liquid nitrogen and frozen in an upright position and then stored in liquid nitrogen for frozen section. Five-micron cross sections are cut and stained with H&E for morphological studies. Two 2mm specimens are put into 10% formal-saline for no less than 4 hours, and then embedded in paraffin. Five-micron cross sections are cut for routine histological and immonohistochemical studies.

One 3 to 4 cm long specimen is secured at each end with cotton. A 5g stainless steel weight is attached to one end of the tissue which is suspended in 2.5% glutaraldehyde (in 0.05 *M* cacodylate buffer) for 1.5 hours. The nerve is then separated from the weight and dissected into smaller segments; 2mm for electron microscopy, 2mm oriented transversely for resin embedment and light microscopy, 4mm orientated longitudinally for resin embedment and light microscopy, and 15 to 20mm for teased nerve fibre studies.

Tissue preparation for conventional resin embedding and light microscopy

Blocks for resin embedding and light microscopy (LM) remain in glutaraldehyde overnight and are washed in 0.05 *M* sodium cacodylate buffer (PH 7.4) for at least half an hour with 5 changes of buffer. Then the specimens are processed as indicated in table A-1. Nerve specimens are finally embedded in TAAB resin. Semithin sections are cut at 1μm using a SORVALL JB-4 microtome (Porter-Blum) with glass knives and transferred to gelatin-coated microscope slides. Sections stained with 1% toluidine blue in 1% boric acid for 20 seconds on a 120^{0}C hot plate are used for morphologic study. Transverse sections, with no additional staining, are used for semi-automatic morphometric study of MFs under LM.

Table A-1. Resin processing schedule for light microscopy

Step	Solution required	Time
1	1% aqueous osmium tetroxide	24 hours
2	0.05 *M* sodium cacodylate buffer	½ hour with 5 changes of the buffer
3	70% ethanol	30 minutes
4	95% ethanol	30 minutes
5	100% ethanol	Three changes, each of 30 minutes
6	Propylene oxide	30 minute
7	Propylene oxide: TAAB resin (1:1)	1 hour
8	Propylene oxide: TAAB resin (1:3)	1 hour
9	TAAB resin	Two changes, each of 1 hour (under vacuum)
10	TAAB resin	Overnight (under vacuum)
11	Fresh TAAB resin	Three changes, each of 2 hours (under vacuum)
12	Embedded in TAAB resin	
13	polymerize at 73°C	overnight

Tissue preparation for conventional electron microscopy

Tissue blocks for electron microscopy remain in glutaraldehyde overnight and are washed in 0.05 *M* sodium cacodylate buffer. Then the specimens are processed as indicated in table

A-2. Nerve specimens are finally embedded in Spurr resin. Ultrathin sections are cut at 60-100nm using a SORVALL MT2-B Ultra-microtome (Porter-Blum) or LKB Bromma 8800 Ultrotome®III with a diamond knife, and double stained with uranyl acetate and lead for viewing in a Jeol electron microscope.

Table A-2 Resin processing schedule for electron microscopy

Step	Solution required	Time
1	1% Osmium fixation	60min
2	70% Uranyl acetate	15min
3	100% Methanol	30min
4	100% Methanol	30min
5	Preplan oxide (PO)	15min
6	PO: Spurr resin	1:1
7	Spurr resin	30min
8	Spurr resin embedding	overnight

Tissue processing for isolating individual MFs in glycerol

After a further half an hour fixation in glutaraldehyde, the portion for teasing nerve fibres is separated into fascicles. The fascicles are washed in 0.5 *M* sodium cacodylate buffer for at least half an hour with several changes of buffer. Then they are post-fixed in 1% aqueous osmium tetroxide for 2 hours, and washed in 0.5 *M* cacodylate buffer for at least 30 minutes with several changes of buffer. Fascicles for teasing MFs in glycerol are processed as indicated in table A-3. Individual MFs are isolated and examined according to standard methods (Cash and Blumbergs, 1995; Dyck et al., 1993).

Table A-3. Processing schedule for glycerol teased fibre preparations

Step	Solution required	Time
1	45% glycerol	Overnight at 45°C
2	66% glycerol	Overnight at 45°C
3	100% glycerol	Overnight at 45°C

Methods for semi-automatic morphometric studies of myelinated fibres

Morphometric studies of MFs are performed according to the method currently used in our laboratory (Cai et al., 2002). The Quantimet 500MC computer-assisted image analysis system (Leica-Cambridge, UK) is used for quantitation using software developed in our laboratory. Under low magnification, each fascicle is numbered, and then magnified on a video display using an oil immersion lens (100x), a 3.3x tube, and a Sony Charge Coupled Device (CCD) camera. A rectangular frame defines the measuring field on the video image and each measuring frame contains 202500 (405×500) pixels. The image of the nerve through the oil lens and the 3.3x tube is magnified 3018 times and each pixel equals 0.11mm along its edge. The measuring frame divides each fascicle into rectangular fields and beginning with the upper left corner of each fascicle, fibres in each measuring frame are only measured if the lowest pixel of the fibre is within the measuring frame. Otherwise, it is measured in an adjoining field. Each horizontal field is measured in sequence until more than half of the measuring frame is occupied by subperineurial space or perineurium, at which time the field is shifted one frame down and fields are counted in the opposite direction and so on until the whole fascicle has been examined. Artifacts produced in nerve biopsy and tissue preparation are excluded by operator interaction.

The image system receives a digitized image from the camera at 256 grey levels. The threshold is adjusted to capture only the dark grey myelin sheaths to generate binary images. The number of MFs within each field and the number of measuring frames within each fascicle are counted and stored on an Excel spreadsheet. For each identified MF, the area of the myelin sheath (Am) and the sum of perimeters (P) of external and internal edges of the myelin sheath are measured. The external edge of the myelin sheath is assumed to be the fibre perimeter on cross section, and the internal edge to be the axonal perimeter. The contours of the MFs on cross section are converted into myelin sheath areas and perimeter-

equivalent circles. The fibre diameter (Ds) and axonal diameter (Da) are assumed to be equivalent to the outer and inner diameter of the myelin sheath respectively (Figure A-1), and are determined mathematically from Am and P (Auer, 1994) using the following equations. All objects with a diameter less than 1 micron are excluded as all MFs in the peripheral nervous system are larger than 1 μm in diameter (Thomas *et al.*, 1993).

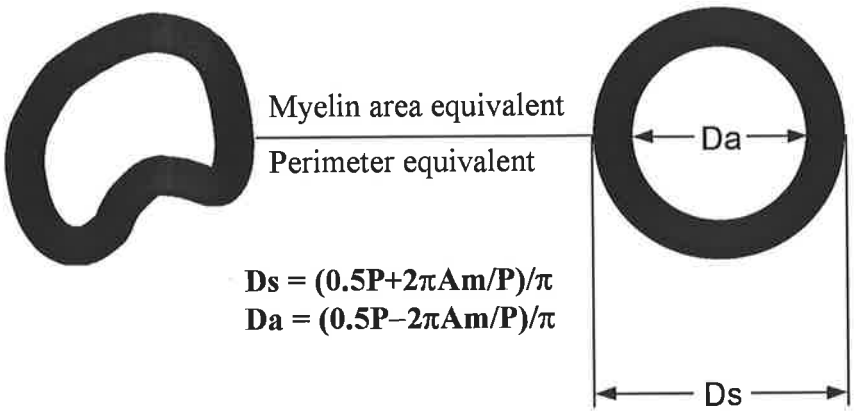

Figure A-1. Transformation of the shape of myelinated fibres on cross section for semi-automatic quantitation of myelinated fibres using Quantimet 500MC Image system.

Mathematical calculation of fibre diameter and axonal diameter

As: total fibre area on transverse section; **Aa**: axonal area on transverse section; **Am**: myelin sheath area on transverse section; **Po**: out perimeter of myelin sheath; **Pi**: inner perimeter of myelin sheath = axonal perimeter; **P** = Po + Pi.

$$As = As + Am$$

$$Am = As - As$$

$$= \pi Ds^2/4 - \pi Da^2/4$$

$$= \pi(Ds^2 - Da^2)/4$$

$$= \pi(Po^2/\pi^2 - Pi^2/\pi^2)/4$$

$$= (Po^2 - Pi^2)/4\pi$$

$$= (Po^2 - (P - Po)^2)/4\pi$$

$$= (2PPo - P^2)/4\pi$$

$$2PPo = 4\pi Am + P^2$$

$$Po = 0.5P + 2\pi Am/P$$

$$Ds = Po/\pi = (0.5P + 2\pi AmP)\pi$$

$$Da = Pi/\pi = (P\text{-}Po)/\pi = (P - (0.5P + 2\pi Am/P))/\pi = (0.5P - 2\pi Am/P)/\pi$$

APPENDIX B

Clinical data and conventional pathologic findings of the nerves used in chapter 2

Table B-1. Clinical data of the 4 nerves used in chapter 2

Nerve	Age	Sex	Clinical features	Electrophysiology
1	44	F	suicidal drowning, depression	not done
2	56	M	sensory neuropathy for 2 years	absent sural SNAPs
3	45	M	predominantly sensory neuropathy for years, Chronic renal failure, failed renal transplantation, renal dialysis	↓↓motor NCV ↓amplitude
4	44	F	progressive motor neuropathy with high titer IgM anti-GM1 antibodies for 4 months	Denervation and reinnervation

SNAP, sensory nerve action potential; NCV, nerve conduction velocity;

Table B-2. Pathological findings on conventional paraffin, frozen and plastic sections

Nerve	LMF	AD	Demy	Remy	EF	IC	Electron microscopy
1	–	–	–	–	–	–	–
2	+	+	+	++	+	+	mitochondrial crystalloids in Schwann cells and myelinated axons
3	++	++	+	+	+	+	compacted axon in many large MFs
4	+	+	+	++	+	+	compacted axon in some MFs

LMF, loss of myelinated nerve fibres; AD, axonal degeneration; Demy, demyelination; Remy, remyelination; IC, inflammatory cells; NA, not available

Table B-3. Classification of glycerinated teased nerve fibres

Nerve	NTNF	Normal	MI	Demy	Remy	AD	Non
1	60	50 (83.3%)	2 (3.3%)	3 (5%)	3 (5%)	0	2 (3.3%)
2	60	18 (30%)	5 (8.3%)	2 (3.3%)	27 (45%)	2 (3.3%)	6 (10%)
3	60	10 (16.7%)	8 (13.3%)	4 (6.7%)	19 (31.7%)	14 (23.3%)	4 (6.7%)
4	60	6 (10%)	3 (5%)	31 (51.7%)	16 (26.7)	2 (3.3%)	2 (3.3%)

NTNF, number of examined teased nerve fibres; MI, myelin irregularity; Demy, demyelination; Remy, remyelination; AD, axonal degeneration; Non, nonspecific change.

APPENDIX C

Light microscopic findings of the nerve used in chapter 3

Haematoxylin and eosin stained frozen and paraffin sections showed peripheral nerve in which the fascicular architecture was preserved. There was obvious decrease in the myelinated nerve fibre population throughout the fascicles. The blood vessel vessels and perineurium appeared normal. Paraffin sections stained with trichrome confirmed severe loss of myelinated fibres with endoneurial fibrosis. Congo red staining for amyloid deposition was negative. Occasional endoneurial macrophages and lymphocytes were seen with CD68 and CD45 immunostaining on paraffin sections. IgM and kappa light chain immunofluorescent staining of the myelin sheaths (Immunology Lab, IMVS).

Toluidine blue stained semithin plastic sections revealed 7 fascicles in a normal fascicular architecture, and showed severe loss of myelinated fibres, which varied considerably from one fascicle to another. In one fascicle, no intact myelinated fibres were found. In other fascicles, many fibres showed disproportionately thin myelin sheaths compared to axonal diameter indicative of demyelination and remyelination, and a few fibres showed axonal degeneration. Three to five fibres per × 400 magnified field displayed focal myelin thickenings.